

Topics in Electromobility and Related Applications



Mingming Liu

Hamilton Institute

National University of Ireland Maynooth

This dissertation is submitted for the degree of
Doctor of Philosophy

Supervisors: Prof. Robert Shorten

Prof. Seán McLoone

Head of Department: Prof. Ken Duffy

September 2015

To my wife, Yingqi Gu, and my parents

致我的妻子顾颖奇和我的父母

Declaration

I hereby declare that the material presented in this thesis, which I now submit for assessment on the programme of study leading to the award of Doctor of Philosophy from the Hamilton Institute is entirely my own works and has not been previously submitted for any other degree or qualification and has not been taken from the work of others save and to the extent that such work has been cited and acknowledged within the text of my work.

Mingming Liu
September 2015

Acknowledgements

First and foremost, I would like to express my deepest gratitude to my dear supervisors Prof. Robert Shorten and Prof. Seán McLoone, for your consistent support, understanding, encouragement, and inspiring guidance through the years of my PhD. You have always been good mentors and my best friends in my life. I would also appreciate your patience, selflessness, responsibility and fruitful discussions for every piece of work we have done together. Without your kind personality and brilliant wisdom, this thesis would not have been done. Seán, it would be my great fortune to know you at the beginning of my PhD. You are invaluable to me for opening my doors to research which I will never forget. Bob, thank you for giving me the opportunity working in the Hamilton Institute. Thank you as well for your tremendous efforts helping me grow as an independent research scientist during the last four years. Looking back, you always raise me up when I want to give up, and you always lead me to the right direction when I am frustrated, just like my father.

I would also like to acknowledge Dr. Seán Doherty, thank you for being my undergraduate supervisor and your strong recommendations for my PhD, without you I would have changed my career plan four years ago. Although you have not guided me till the end of my PhD, your valuable suggestions and positive attitude to life I would always remember.

In much of work I have done together with Dr. Paul McNamara, Prof. Emanuele Crisostomi, Prof. Seán McLoone and Prof. Robert Shorten. Thanks for your numerous help and detailed instructions on every paper we have done and every conference presentation I attended. You make me feel more confident on my way to research. Special thanks to Prof. Fabian Wirth and Prof. Martin Corless, for your inspired discussions and for making me appreciate the beauty of mathematics.

A number of people have also contributed a lot to my research, these co-authors and collaborators are also acknowledged, Dr. Wynita Griggs, Dr. Rodrigo Ordóñez-Hurtado, and Sonja Stüdli, for your willingness to help and sharing ideas with me. Thank you for solving my confusions through uncountable emails and video discussions. I should also send my sincere thanks to all staff members in Hamilton Institute, especially Rosemary and Kate, and all staff members in the Department of Electronic Engineering at Maynooth University,

for every moments we shared about life and work. Thanks for giving me a warm working atmosphere and such an enjoyable experience during my stay in Ireland.

During the past four years of my PhD, I was sponsored in part by Maynooth University under the Doctoral Teaching Scholarship (Sept. 2011 - Dec. 2012), and by Science Foundation Ireland under grant number 11/PI/1177 (Jan. 2013 - Present), their generous support is also highly acknowledged.

At last, I am grateful to my family. My parents, Xianfu Liu and Lianhua Wang, and my father-in-law Zhuhua Gu, and my mother-in-law, Rong Ma. Words cannot express how deeply your love to me in writing this thesis and all aspects of support, encouragement and selfless dedication through these years. Special thanks to my wife Yingqi Gu (Annie), for your consistent companion, support, and endless love with me in the past years. I would always remember those lovely, wonderful moments we have spent together in the world.

List of Publications

The following **journals/transactions** papers have been **submitted/published** during the course of my PhD.

1. "On global convergence of consensus with nonlinear feedback, the Lure problem, and some applications", *IEEE Transactions on Automatic Control*, 2015. **[submitted]**
Mingming Liu, Fabian Wirth, Martin Corless and Robert Shorten
2. "A Distributed and Privacy-Aware Speed Advisory System for Optimising Conventional and Electric Vehicles Networks", *IEEE Transactions on Intelligent Transportation Systems*, 2015. **[submitted]**
Mingming Liu, Rodrigo H. Ordóñez-Hurtado, Fabian Wirth, Yingqi Gu, Emanuele Crisostomi and Robert Shorten
3. "Plug-and-Play Distributed Algorithms for Optimized Power Generation in a Microgrid", in *IEEE Transactions on Smart Grid*, vol. 5, no. 4, pp. 2145-2154, 2014. **[published]**
Emanuele Crisostomi, Mingming Liu, Marco Raugi and Robert Shorten
4. "Enhanced AIMD-based Decentralized Residential Charging of EVs", in *Transactions of the Institute of Measurement and Control*, 2013. **[published]**
Mingming Liu, Seán McLoone
5. "Residential Electrical Vehicle Charging Strategies - the Good, the Bad and the Ugly", in *Special Issue on Electric Vehicles and Their Integration with Power Grid, Journal of Modern Power Systems and Clean Energy*, Springer, 2014. **[published]**
Mingming Liu, Paul McNamara, Robert Shorten and Seán McLoone

The following **conference** papers have been **submitted/published** during the course of my PhD.

1. "Intelligent Speed Advisory System for Electric Vehicles", *5th IFAC conference on Analysis and Design of Hybrid Systems*, 2015. **[submitted]**

-
- Mingming Liu, Rodrigo H. Ordóñez-Hurtado, Fabian Wirth, Yingqi Gu, Emanuele Crisostomi and Robert Shorten
2. "Distributed Consensus Charging for Current Unbalance Reduction", in *18th IFAC World Congress*, 2014. **[published]**
Mingming Liu, Paul McNamara, Robert Shorten and Seán McLoone
 3. "Optimal Distributed Consensus Algorithm for Fair V2G Power Dispatch in a Microgrid", in *IEEE International Electric Vehicle Conference*, 2014. **[published]**
Mingming Liu, Emanuele Crisostomi, Yingqi Gu and Robert Shorten
 4. "Optimised Consensus for Highway Speed Limits via Intelligent Speed Advisory Systems", in *IEEE International Conference on Connected Vehicles and Expo*, 2014. **[published]**
Yingqi Gu, Mingming Liu, Emanuele Crisostomi and Robert Shorten
 5. "Optimal Distributed Power Generation for Thermal and Electrical Scheduling in a Microgrid", in *4th IEEE/PES Innovative Smart Grid Technologies Europe*, 2013. **[published]**
Mingming Liu, Emanuele Crisostomi, Marco Raugi and Robert Shorten
 6. "Fair Charging Strategies for EVs Connected to a Low-Voltage Distribution Network", in *4th IEEE/PES Innovative Smart Grid Technologies Europe*, 2013. **[published]**
Mingming Liu, Paul McNamara and Seán McLoone
 7. "Applying a QoS-based Fleet Dimension Method to Reduce Fleet Emissions", in *IEEE International Conference on Connected Vehicles and Expo*, 2013. **[published]**
Mingming Liu, Wynita Griggs, Christopher King, Fabian Wirth, Paul Borrel and Robert Shorten
 8. "Investigation of AIMD based EV Charging Strategies for EVs Connected to a Low-Voltage Distribution Network", in *Intelligent Computing for Sustainable Energy and Environment*, Springer, pages 433-441, 2013. **[published]**
Mingming Liu, Seán McLoone
 9. "On-Off based Charging Strategies for EVs Connected to a Low Voltage Distribution Network", in *IEEE Asia-Pacific Power and Energy Engineering Conference*, 2013. **[published]**
Mingming Liu, Sonja Stüdli, Richard Middleton, Seán McLoone, Robert Shorten and Julio Braslavsky

Abbreviations

AIMD	Additive-Increase-Multiplicative-Decrease
CER	Commission for Energy Regulation
CHP	Combined Heat and Power
DER	Distributed Energy Resource
DG	Distributed Generator
DPF	Distributed Price Feedback
DSO	Distribution System Operator
EMS	Energy Management System
EV	Electric Vehicle
G2V	Grid-to-Vehicle
HIL	Hardware-In-the-Loop
HV	High-Voltage
ICEV	Internal Combustion Engine Vehicle
ISA	Intelligent Speed Advisory
ITS	Intelligent Transportation System
LV	Low-Voltage
MV	Medium-Voltage
QoS	Quality of Service
SAS	Speed Advisory System
SOC	State of Charge
SME	Small Medium Enterprise
TOU	Time-of-Use
TSO	Transmission System Operator
VPP	Virtual Power Plant
V2G	Vehicle-to-Grid
V2X	Vehicle-to-vehicle/infrastructure

Abstract

In this thesis, we mainly discuss four topics on Electric Vehicles (EVs) in the context of smart grid and smart transportation systems.

The first topic focuses on investigating the impacts of different EV charging strategies on the grid. In Chapter 3, we present a mathematical framework for formulating different EV charging problems and investigate a range of typical EV charging strategies with respect to different actors in the power system. Using this framework, we compare the performances of all charging strategies on a common power system simulation testbed, highlighting in each case positive and negative characteristics.

The second topic is concerned with the applications of EVs with Vehicle-to-Grid (V2G) capabilities. In Chapter 4, we apply certain ideas from cooperative control techniques to two V2G applications in different scenarios. In the first scenario, we harness the power of V2G technologies to reduce current imbalance in a three-phase power network. In the second scenario, we design a fair V2G programme to optimally determine the power dispatch from EVs in a microgrid scenario. The effectiveness of the proposed algorithms are verified through a variety of simulation studies.

The third topic discusses an optimal distributed energy management strategy for power generation in a microgrid scenario. In Chapter 5, we adapt the synchronised version of the Additive-Increase-Multiplicative-Decrease (AIMD) algorithms to minimise a cost utility function related to the power generation costs of distributed resources. We investigate the AIMD based strategy through simulation studies and we illustrate that the performance of the proposed method is very close to the full communication centralised case. Finally, we show that this idea can be easily extended to another application including thermal balancing requirements.

The last topic focuses on a new design of the Speed Advisory System (SAS) for optimising both conventional and electric vehicles networks. In Chapter 6, we demonstrate that, by using simple ideas, one can design an effective SAS for electric vehicles to minimise group energy consumption in a distributed and privacy-aware manner; Matlab simulation are give to illustrate the effectiveness of this approach. Further, we extend this idea to conventional vehicles in Chapter 7 and we show that by using some of the ideas introduced in Chapter

6, group emissions of conventional vehicles can also be minimised under the same SAS framework. SUMO simulation and Hardware-In-the-Loop (HIL) tests involving real vehicles are given to illustrate user acceptability and ease of deployment.

Finally, note that many applications in this thesis are based on the theories of a class of nonlinear iterative feedback systems. For completeness, we present a rigorous proof on global convergence of consensus of such systems in Chapter 2.

Contents

Abstract	ix
List of Figures	xv
List of Tables	xix
1 Introduction	1
1.1 Introduction	1
1.1.1 A Consensus Algorithm with Feedback	2
1.1.2 Grid Integration with EVs	4
1.1.3 Optimal Energy Management Strategies in Smart Grid	6
1.1.4 Distributed and Privacy-Aware Speed Advisory Systems	8
1.2 Research Objectives and Contributions	9
1.3 Thesis Outline	12
I A Consensus Algorithm with Feedback	14
2 Stability and Convergence Analysis	15
2.1 Introduction	15
2.2 Notation, Conventions and Preliminary Results	17
2.3 Consensus under Feedback	20
2.3.1 Local Stability Results	21
2.3.2 Global Stability Results	25
2.3.3 Switched Systems	28
2.4 Conclusions	28

II	Grid Integration with EVs	29
3	EV Charging Strategies in Low-Voltage Distribution Networks	30
3.1	Introduction	30
3.2	Problem Formulation	33
3.2.1	Notation	33
3.2.2	Plug-in Constraints	35
3.2.3	Power System Constraints	36
3.2.4	Types of Optimisation	36
3.3	Fairness based EV Charging Strategies	37
3.3.1	Uncontrolled Charging Strategy	38
3.3.2	Decentralised AIMD Algorithm	38
3.3.3	Distributed Price Feedback Algorithm	40
3.3.4	Ideal Centralised Instantaneous Charging	42
3.3.5	Distributed On-Off Charging	43
3.3.6	Centralised On-Off Charging	44
3.4	Enhanced Charging Strategies	44
3.4.1	Communication Topology and Infrastructure Requirements	45
3.4.2	Enhanced AIMD Charging Strategy	46
3.4.3	Price-adjusted Available Power	48
3.5	Valley-Filling based Charging Strategies	48
3.5.1	Optimal Decentralised Valley-Filling Charging	48
3.5.2	Centralised Load-Variance-Minimisation Charging	49
3.6	Cost Minimisation based Strategies	50
3.6.1	Decentralised Selfish Charging Strategy	50
3.6.2	Centralised Charging Cost Minimisation Strategy	50
3.7	Comparisons of ‘Continuous’ EV Charging Strategies	51
3.7.1	Simulation Setup	51
3.7.2	Evaluation of the Uncoordinated Charging Strategy	55
3.7.3	Evaluation of Continuous Fairness based Charging Strategies	55
3.7.4	Evaluation of Cost Minimisation Strategies	58
3.7.5	Evaluation of Valley-Filling Charging Strategies	58
3.8	Comparisons of On-Off EV Charging Strategies	58
3.8.1	Simulation Setup	64
3.8.2	Evaluation of On-Off Fairness based Charging Strategies	66
3.9	Discussion	66
3.10	Testbed Design	69

3.11	Conclusions	71
4	Using V2G for Ancillary Services	74
4.1	Introduction	74
4.2	Current Imbalance Reduction	76
4.2.1	Current Unbalance Factor	76
4.2.2	Current Balance Equation	76
4.2.3	Distributed Consensus Algorithm	78
4.2.4	Simulations	81
4.2.5	Results and Discussion	82
4.3	Optimal V2G Power Dispatch	87
4.3.1	Model and Algorithm	87
4.3.2	Utility Functions	88
4.3.3	Optimal Solution	90
4.3.4	Optimal Decentralised Consensus Algorithm for V2G	92
4.3.5	Simulations	93
4.3.6	Results and Discussion	96
4.4	Conclusions	102
III	Optimal Energy Management Strategies in Smart Grid	103
5	Optimal Algorithms for Energy Management	104
5.1	Introduction	104
5.2	Problem Statement and Preliminaries	106
5.2.1	Utility Minimisation	107
5.3	AIMD based Utility Optimisation Algorithms	108
5.3.1	AIMD	109
5.3.2	Utility Optimisation via Synchronised AIMD	110
5.3.3	Practical Implementation	114
5.3.4	Extensions for Thermal and Electrical Scheduling	115
5.4	Case Studies	117
5.4.1	Simulations for the Electrical Scheduling	117
5.4.2	Simulations for Thermal and Electrical Scheduling	120
5.5	Conclusions	127

IV	Distributed and Privacy-Aware Speed Advisory Systems	128
6	Intelligent Speed Advisory System for Electric Vehicles	129
6.1	Introduction	129
6.2	Related Work	130
6.3	Model and Algorithm	131
6.3.1	Cost Functions	131
6.3.2	Problem Statement	132
6.4	Experimental Results	135
6.5	Conclusions	138
7	Intelligent Speed Advisory System for Conventional Vehicles	139
7.1	Introduction	139
7.2	Problem Statement	140
7.3	Evaluation using SUMO Simulations	141
7.3.1	SUMO Simulations with a Fixed Number of Vehicles	141
7.3.2	SUMO Simulations with a Dynamic Number of Vehicles	142
7.3.3	Hardware-In-the-Loop (HIL) Emulation	146
7.4	Conclusions	149
8	Conclusions and Future Work	150
8.1	Summary	150
8.1.1	A Consensus Algorithm with Feedback	150
8.1.2	Grid Integration with EVs	151
8.1.3	Optimal Energy Management Strategies	152
8.1.4	Distributed and Privacy-Aware Speed Advisory Systems	153
8.2	Future Work	154
8.2.1	Grid Integration with EVs	154
8.2.2	Optimal Energy Management Strategies	154
8.2.3	Distributed and Privacy-Aware Speed Advisory Systems	155
	References	156

List of Figures

1.1	A Virtual Power Plant (VPP) is generally characterised by Distributed Energy Resources (DERs), including Combined Heat and Power (CHP) and wind/solar plants, storage systems, controllable and uncontrollable loads, Electric Vehicles (EVs), and is connected to other VPPs through the grid.	7
3.1	Schematic diagram of the distribution network	34
3.2	Decentralised AIMD smart charging communication topology	40
3.3	Flow chart of the distributed charging algorithm	43
3.4	Communication topology for the enhanced AIMD implementation	46
3.5	Average summer and winter residential power consumption profiles in Ireland as computed from smart meter trial data of 4225 customers [26]	53
3.6	Average residential power consumption profiles for 160 customers on January 23 rd 2010 [26]	53
3.7	Comparison of the minimum voltage profiles with different levels of EV penetration using uncontrolled charging. Red dashed line marks the minimum acceptable voltage level on the network.	56
3.8	Comparison of the power consumption at the main substation with different levels of EV penetration using uncontrolled charging. Red dashed line marks the maximum available power from the grid.	56
3.9	Comparison of the power consumption at the main substation with different charging strategies.	57
3.10	Comparison of the minimum voltage profile with different charging strategies. Red dashed line marks the minimum acceptable voltage level on the network.	57
3.11	Comparison of the loading conditions on transformer TR(2) with different charging strategies	60
3.12	Comparison of the charge rates in the same area [both connected to TR(2)] (a) Enhanced AIMD charging with price adjusted available power (b) Enhanced DPF charging with price adjusted available power	60

3.13	Diagram of the TOU electricity price	61
3.14	Comparison of the EV load when using CCCM and DSC with the price adjusted available power modification	61
3.15	Comparison of the optimal aggregated load profile obtained using CLVM and the iterative ODVF methods	63
3.16	Percentage obtained for CLVM and the iterative ODVF methods (in terms of MSE) with different numbers of iterations	63
3.17	Schematic diagram of the distribution network	65
3.18	Office building power consumption from 6am to 8pm	65
3.19	Comparison of the power utilisation	67
3.20	Comparison of the total power losses	67
3.21	Comparison of the minimum voltage profile	69
3.22	Schematic diagram for the hardware testbed	71
3.23	Comparisons of charging fairness on the testbed	72
3.24	Charging current and voltage of the first battery	72
4.1	Schematic diagram of the communication topology	80
4.2	Schematic diagram of the distribution network.	82
4.3	Active charge rates for EVs connected to phase one with $\eta = 0.5$ and $\mu = 0.01$. 83	
4.4	Active charge rates for EVs connected to phase one with $\eta = 0.8$ and $\mu = 0.01$. 83	
4.5	Total power consumptions on each phase compared with desired result with $\eta = 0.5$ and $\mu = 0.01$	84
4.6	Active charge rates for EVs connected to phase one with $\eta = 0.5$ and $\mu = 0.2$. 84	
4.7	Active power consumption on each phase with distributed consensus algorithm. 85	
4.8	Reactive power consumption on each phase with distributed consensus algo- rithm.	85
4.9	Comparison of current balance factor	86
4.10	Comparison of neutral current magnitude	86
4.11	Schematic diagram of the utility function	89
4.12	Schematic diagram of the optimisation framework [94]	90
4.13	Power topology of the microgrid network	95
4.14	Schematic diagram of the microgrid	95
4.15	Discharge rates of the EVs with V2G in operation	97
4.16	Fairness index of the ODC algorithm with V2G in operation	97
4.17	Power generation profiles of DGs	99
4.18	Comparison of demand and power generation with V2G and EV loads	99
4.19	Accumulative economical benefits for each EV in the scheme	100

4.20	Accumulative economical benefits for all EVs in the scheme	100
4.21	Economical benefits for the grid at each time slot	101
4.22	Accumulative economical benefits for the grid	101
5.1	DERs (on the left) must provide enough energy to satisfy the demand coming from the users (e.g., from industries and residential areas).	106
5.2	A scenario where a PhotoVoltaic (PV) plant, a wind plant and a CHP are required to provide a (static) power of 35 MW. The fair sharing solution is that all plants provide the same power.	111
5.3	Constraints on the plant sizes and availability of solar / wind.	112
5.4	A typical non-constant energy requirement.	112
5.5	Required and provided power (summing contributions of single plants) of scenario in Fig. 5.4.	113
5.6	Schematic topology of the tested network.	118
5.7	Comparisons of the distributed AIMD solution and the optimal centralised solution on electrical power balancing during the whole day	121
5.8	The detail of how AIMD shares the energy production.	121
5.9	Comparisons on the costs of the two algorithms	122
5.10	Comparisons on the communication costs of the two algorithms: with same step size, AIMD clearly outperforms the centralised approach.	122
5.11	Schematic topology of the tested network.	123
5.12	Electrical power generation by each DER.	125
5.13	Comparisons of the total power generation profile (both electrical and thermal) by applying different algorithms.	125
5.14	Comparisons of the costs by using the two algorithms.	126
5.15	Minimum and maximum voltage profiles in the network obtained with the two algorithms.	126
6.1	A typical individual cost function.	133
6.2	The cost functions for the 100 EVs.	136
6.3	Simulation results for the network of EVs: Algorithm 11 is applied until time 0.33 h, and then two different speeds (below and above the optimal one) are suggested in [0.33,0.66] h and [0.66, 1] h, respectively.	137
7.1	Curves for the CO ₂ emission profiles in Table 7.1.	143

7.2	Results of the SUMO simulation for the static case, before and after the activation of the algorithm at time step 500 s. Setup: 40 vehicles, of which 32 are of emission type R007 and 8 are of emission profile R021, and uniform distribution of types of vehicles.	144
7.3	Results of the SUMO simulation for the static case, before and after the activation of the algorithm at time step 500 s. Setup: 40 vehicles, with uniform distribution of emission profile among R016, R017, R018 and R019, and uniform distribution of types of vehicles.	145
7.4	Example for case 3: 500 time-step MA of CO ₂ emissions for a set of initial speeds in the range (40,60) [km/h].	146
7.5	Schematic of the HIL emulation platform.	147
7.6	Evolution of the overall CO ₂ emissions. The algorithm was turned on around time 300 s.	148
7.7	Evolution of some variables along the whole HIL simulation. Top: related speeds for the Prius (the 6th car), and Bottom: the related speeds for the 7h car (just behind the Prius). The algorithm was turned on around time 300 s.	149

List of Tables

3.1	A comparison of simulation results for various EV charging strategies (50% EV penetration)	59
3.2	ODVF computation time for different iteration counts (50% EV penetration).	62
3.3	CLVM computation times with different levels of EV penetration.	62
3.4	A comparison of simulation results for various temporal based EV charging strategies (50% EV penetration)	62
3.5	A comparison of simulation results for various on-off type of EV charging strategies (50% EV penetration)	68
5.1	Parameters of the utility functions	119
5.2	Parameters of the utility functions	124
7.1	Emission factors for some CO ₂ emission profiles reported in [14].	142
7.2	General results: total emissions per lane.	145

Chapter 1

Introduction

***Abstract:** This chapter introduces some basic concepts and presents the background information for the topics to be discussed in the thesis. It also highlights the research objectives and contributions of the work.*

1.1 Introduction

This thesis is motivated by problems that arise due to the deployment of Electric Vehicles (EVs) and the construction of the smart grid and smart transportation systems. To commence the thesis, we give a short background on some of the issues that arise due to these developments. This thesis is organised in four parts:

- Part I: A Consensus Algorithm with Feedback.
- Part II: Grid Integration with EVs.
- Part III: Optimal Energy Management Strategies in Smart Grid.
- Part IV: Distributed and Privacy-Aware Speed Advisory Systems.

In Part I, we describe a privacy-preserving consensus algorithm that we shall use throughout the thesis. In Part II, we describe several problems that arise when EVs integrate with grids. In Part III, we describe issues arising from microgrids. Finally we describe in Part IV, mobility related ideas for EV efficiency.

1.1.1 A Consensus Algorithm with Feedback

Literally, convergence to a common value is called the consensus or agreement problem [162]. Consensus problems have been studied for a long time in the field of computer science [145]. These problems are particularly of interest in the communities of control theory, distributed computation and optimisation [122, 136, 162], which usually require a target system could be operated at some consensus conditions. In recent years, a variety of consensus algorithms have been developed in a large volume of literature for cooperative control of multi-agent systems, see for instance, [135, 136, 139, 144, 162, 214]. At the heart of the algorithm design is to achieve agreement (consensus) on the states of the agents in a multi-agent system by using local (neighbour-to-neighbour) information exchange [160, 161]. Information flow in a system is usually considered under the assumptions of time-varying communication topologies to model the practical disturbance and uncertainty (e.g. delays and link failures) imposed on the deployed communication networks in the process of information exchange among agents [103, 195, 214]. For achieving consensus, each agent is usually required to update its own states in an iterative fashion based on other information received from its neighbours. Eventually, it is expected that these algorithms could drive the states of the agents to the consensus conditions in this manner. This idea can also be extended to deal with other consensus problems by adding a global feedback signal as a common input to all agents. Under this circumstance, the states of the agents can be designed to converge to a more desired consensus value as a function of the global feedback signal. Thus, a global objective can be considered while the consensus of the states of agents are still maintained. In the thesis, we call such algorithm a consensus algorithm with feedback.

Most recently, many consensus algorithms with feedback have been applied to solve problems in the context of smart grid and smart transportation systems. In smart grids, distributed consensus algorithms could be used to automatically distribute the power generation task among Distributed Generators (DGs), where the consensus variable could be chosen as the amount of power need to be generated by each DG. The consensus algorithm is used to drive the power dispatched by each DG to the same value (fairness) and the feedback signal is used to match the total power generation from DGs with the demand required. In addition, consensus algorithms can also be adopted for solving optimisation problems by choosing different variables for consensus. For instance, in [220] a consensus algorithm is applied to solve optimal economical dispatch problem in a smart grid. The philosophy behind the algorithm is to equalise the incremental cost of each generator such that the optimisation criterion is satisfied (i.e. the total generation cost of all power generators is minimised) and the feedback signal is chosen to make the demand constraint. Similar ideas have also been applied to solve the smart transportation related problems, especially from the perspective

of environmental benefits [94, 167]. It has been shown in [94] that by using the proposed consensus algorithm, a fleet of hybrid vehicles could be cooperated to regulate CO₂ emissions to a given level while maximising their overall driving range, where the fairness (consensus) of the algorithm refers to the emission target allocated to each vehicle must be equalised.

Compared to conventional centralised based solutions, which usually depend on many global information for coordination, consensus based distributed optimisation algorithms are more attractive as they only require local info exchange among agents and limited global information as a feedback signal. Under the appropriate setup, they can also easily handle time-varying communication topologies and reserve the privacy of each agent. In this spirit, many of the algorithms we shall discuss in the thesis (i.e., Chapters 4, 6 and 7) are based on a fundamental distributed consensus theory from the cooperative control literature [95].

In particular, we shall consider the following nonlinear system studied in [95]:

$$x(k+1) = P(k)x(k) + \mu(r - g(x(k)))e \quad (1.1)$$

where $x(k) \in \mathbb{R}^n$, $P(k)$ is a $n \times n$ row stochastic matrix, $e = [1 \ 1 \ \dots \ 1]^T$, μ and r are scalars while g is a scalar valued function. Equation (1.1) describes a consensus problem subject to an output constraint. It basically says that if consensus is achieved, it must be achieved subject to the equilibrium constraint $g(x^*) = r$. That is, at equilibrium

$$g(x^*) = r, \quad (1.2)$$

with $x_i^* = x_j^*$ for all $i, j \in \{1, 2, \dots, n\}$.

Known from [162] that a row stochastic matrix P operates on a vector $x \in \mathbb{R}^n$ such that

$$\max(x) - \min(x) \geq \max(Px) - \min(Px) \quad (1.3)$$

where $\max(x)$ and $\min(x)$ are defined as the maximum and minimum component in vector x , respectively. Since the addition of $(r - g(x(k)))e$ does not affect this contraction, intuition suggests that $x_i(k) - x_j(k) \rightarrow 0$ as k increases and eventually, the dynamics of (1.1) will be governed by the following scalar **Lure system**:

$$y(k+1) = y(k) + \mu(r - g(y(k))e), \quad (1.4)$$

with $x_i(k) \approx y(k)$ asymptotically for all i . Intuition further suggests, as long as (1.4) is stable, then so is (1.1). A plausibility argument along these lines, in support of (1.1), is given in [95]. However, no formal stability proof is given in that paper. This is the first problem that we shall mainly discuss in the thesis.

1.1.2 Grid Integration with EVs

In recent years, with government policies incentivising sustainable society developments, and rapid technological advances by the automotive industry, electric vehicles are increasingly being prioritised as a means of reducing pollution, combating climate change and improving energy security. Many countries have set ambitious target for EV penetration. The Irish Government, for example, has set a target of 10% for penetration of EVs in Ireland by 2020 [54]. China is targeting 20% - 30% EV penetration by 2030.

Electric vehicles can generally be classified as being either battery electric, battery and combustion engine hybrids or fuel cell based [118]. Among these, Battery Electric Vehicles (BEVs) and Plug-in Hybrid Electric Vehicles (PHEVs) can recharge the batteries from the external power grid and are collectively referred to as Plug-in EVs (PEVs). PHEVs have become a very popular topic for research and development since 2007 due to their potential to overcome the range anxiety adoption barrier associated with BEVs [171]. However, as battery capacities continue to grow BEVs are also likely to be widely adopted [89, 90].

From a power system perspective a major concern is that, as EV penetration increases, the extra demand due to EV charging will have a considerable impact on the design and operation of electrical power systems [119]. In [50, 60, 125, 156, 172, 200] it has been shown that the widespread adoption of EVs could negatively impact the distribution network if charging is not properly coordinated. Grid impacts of uncoordinated charging include, but are not limited to, increased voltage imbalance [156], increased grid losses [200], overloading [172], fluctuation of grid frequencies [199], and increased harmonic distortion [97]. In turn these effects result in a decrease in the operational efficiency of the grid and in the life span of electrical devices. It is also observed in these studies that in order to accommodate the extra EV charging loads it will be necessary for utilities to invest in and reinforce grid infrastructures in heavily loaded areas to accommodate both EV and household loads. Hence, it becomes important to develop modern smart grid infrastructure and flexible charging and discharging strategies to mitigate the impact of the role out of EVs on the grid [157, 163, 184].

To date, there have been many research studies focused on designing a variety of EV charging algorithms for different purposes. However, it is also shown that not every proposed solution in literature considers real grid constraints, e.g., [48, 192]. As a consequence, these algorithms are mostly helpful for modelling and theoretical analysis of the EV charging process, but not suitable for practical implementation. This is the second problem we shall consider in the thesis. In addition, it is observed that different charging algorithms are usually evaluated in its individual framework. However, this brings challenges for comparing the performance of different algorithms in a common framework, which is normally desirable to identify the characteristics of each approach for purposes of comprehensive assessment.

This is the third problem that we shall discuss in the thesis. Finally, it should be noted that although many existing works have evaluated the performance of algorithms through a variety of simulation studies, there are a few testbeds available for physically testing the charging algorithms, especially for those distributed algorithms that we shall discuss in the thesis. An interesting work in this direction can be seen in [13]. In this work, the circuit design for evaluation of the algorithms was based on a dedicated printed circuit board, which is usually time-consuming to design. Thus, a simple circuit design is more desirable for our purposes.

Another concern of the grid, due to an increasing number of EVs charging on the grid, is the load balancing issue. This issue would occur dramatically when there are uneven numbers of EVs charging on different phases in a three-phase power network. It has been shown that unbalanced power consumption on the grid can lead to challenges for grid operations, e.g., overheating of devices and increased power losses [66, 98]. At this stage, it should be remarked that many conventional methods, which include applying advanced power electronics devices and controllers, e.g., Static Synchronous Compensators (STATCOMS) [79, 181], and the Unified Power Flow Controller (UPFC) [69, 185], have been deployed to solve this issue. However, these existing methods represent an increasing expense for utilities as they seek to maintain or update supporting infrastructure in low power quality areas. In the meanwhile, there is a huge body of work, e.g., [17, 68, 86, 92, 183, 201], on using Vehicle-to-Grid (V2G) technologies on EVs to provide ancillary service to the grid. This technology is attractive since EVs in this context are regarded as a set of large and flexible batteries to support the power grid when needed. Clearly, this provides opportunities for developing charging/discharging methods for EVs to improve power quality (especially at critical times) as well. Thus, how to design the proper EV charging/discharging method for this purpose becomes the fourth problem that we shall discuss in the thesis.

In spirit of V2G, energy can be stored when the grid produces excess energy, and can be delivered back to the grid in times of need. EV owners see in this process the possibility of earning money by selling the V2G service to the grid when the EV is not needed. Also, this service can be provided without inconvenience for the owners, as they simply need EVs plugged into the grid constantly, even if it is fully charged. At the same time, utility companies see in this process the opportunity to actively use this service to regulate power dispatch of generators in an efficient, economical, and environmentally-friendly manner.

In fact, in a forthcoming scenario when a large share of energy will be provided from renewable sources, it will be possible to use ideas of V2G to mitigate the fluctuations of renewable energy by storing energy to EVs when it is in excess, and by recovering energy from the EVs when the renewable power generation is not enough to match the power load.

Note that nowadays most of the support for renewable energy is performed by switching on conventional power plant that are more expensive than solar/wind plant (as there are some fuel and carbon costs to be paid), and also less environmentally friendly in terms of produced CO₂, NO_x or other pollutants' emissions. In this context, note that some countries are already characterised by a high penetration level of energy produced from renewables, see for instance the case of Denmark, where wind plants alone provided more than 30% of the electricity production in 2012, and are planned to supply 50% of the overall demand by the year 2020 [123]. Also Denmark is currently trying to become a system based only on renewable energy by 2050 [127]. Recent works on V2G practices can be found in references [1, 70, 76, 153]. A recent work on the same topic [191] provides an overview of the optimality criteria that should be considered when planning V2G functionalities. In particular, it shows that V2G functionalities should be planned in a smart fashion, as taking electricity from vehicles in an indiscriminate fashion, could sometimes give rise to an environmental cost that might even exceed the environmental gain of using power generated from renewables (e.g., if the consequence of V2G services is that the EV owner has to take a polluting Internal Combustion Engine Vehicle (ICEV) because his/her EV no longer has sufficient energy for the next trip). This is the fifth problem that we shall tackle in the thesis.

1.1.3 Optimal Energy Management Strategies in Smart Grid

In many countries around the world, current conventional power systems are facing the problems of gradual depletion of fossil fuel resources, lower energy efficiency and environmental issues [29, 42, 124]. However, the emerging smart grid envisions enhancing the existing power system by integrating advanced sensor, communication and coordination devices into the grid [217] with a view to enhancing its performance.

An important objective of the smart grid is to perfectly balance supply and demand in the power network [5, 55, 138], and achieving such an objective with a high level of reliability when a large share of power is generated from renewable fluctuating resources is one of the current challenges in the power community. The main challenges in realising this aspiration arises because the power network is very large scale, and each node of the network should sense in real-time its required energy demand, and then try to balance this demand with the amount of produced energy [132]. Clearly, not only the generated power from renewable sources is stochastic, but the demand is also uncertain as it depends on the end-users' usage of electric appliances. Energy usage is also further affected by highly unpredictable factors, such as energy price, weather conditions (use of air conditioning/heating), and possibly also by an increasing penetration of electric transportation [193]. Thus, due to the large number

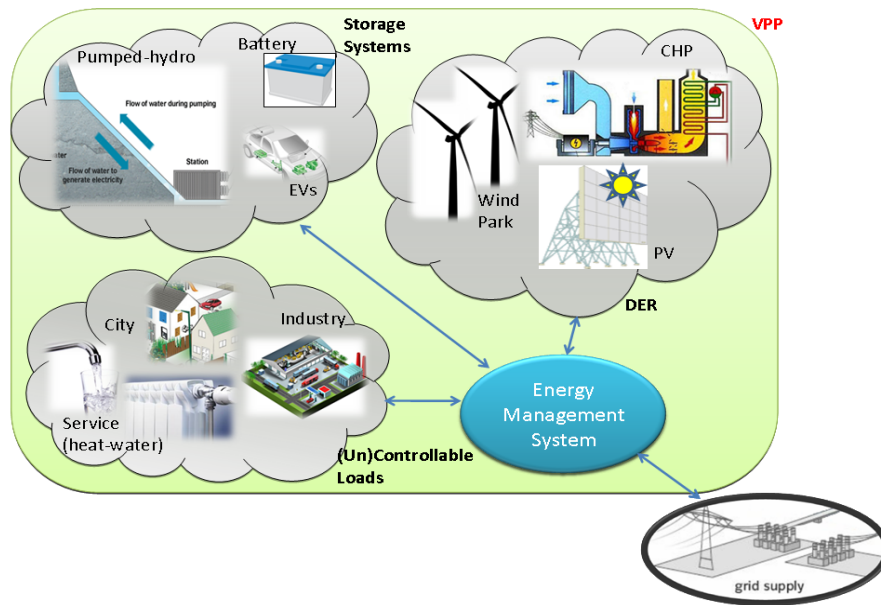


Fig. 1.1 A Virtual Power Plant (VPP) is generally characterised by Distributed Energy Resources (DERs), including Combined Heat and Power (CHP) and wind/solar plants, storage systems, controllable and uncontrollable loads, Electric Vehicles (EVs), and is connected to other VPPs through the grid.

of Distributed Energy Resources (DERs) and (aggregates of) end-users, the real-time power scheduling and balancing problem is currently an important and challenging area of research.

Recently, Virtual Power Plants (VPPs) are becoming viewed as a viable answer to the aforementioned scale and distributed nature of the power system network [9]. A Virtual Power Plant is defined as “a cluster of dispersed generator units, controllable loads and storage systems, aggregated in order to operate as a unique power plant” [117]. The term virtual refers to the fact that the VPP will be, in general, a multi-fuel, multi-location, and multi-owned power station. From a grid operator’s perspective, purchasing energy or ancillary services from a virtual power plant is equivalent to purchasing from a conventional station [138]. The idea of a VPP is illustrated in Figure 1.1.

Microgrids share similar features with VPPs, but usually the term VPP is used to emphasise the economic features of the structure, i.e., the ability to compete in the energy market against other VPPs. In addition, microgrids must be able to operate in a grid-connected mode, isolated mode, and in a transition between grid-connected and isolated modes [130]. One of the main advantages of microgrids and VPPs is that the energy demand will be primarily satisfied by the DERs belonging to the same cluster of users, thus generally avoiding long distance transport of energy and satisfying the small-distance producer-consumer paradigm [49].

In practice VPPs decompose the original complex fully centralised network into a number of distributed units, each one with its own central entity, called an Energy Management System (EMS), that performs the balancing task. Every time balancing is not achieved (e.g., the power generated within a VPP, plus that stored in available storage systems is not enough to fulfil the end-users' requirements), then the VPP buys energy from other VPPs, or from the smart grid in general, or can curtail some controllable loads (e.g., Direct Load Control, see [6]). Similarly, if more energy than required is produced, then the VPP tries to sell energy to other VPPs. The main task of the EMS is to achieve the aforementioned balance of produced/consumed energy. Although the size of a microgrid is much smaller than that of the whole smart grid, there is still the major problem of selecting which power generators to use, and in which proportion, to provide the required power. This management task is the sixth problem that we shall consider in the thesis, bearing in mind that DERs within the same VPP or microgrid do not compete among themselves to increase their earnings, as overall they constitute a single unique (virtual) power plant. In fact, the DERs cooperate to achieve a common goal, e.g., minimise the sum of the financial costs incurred by each DER to generate its share of power.

1.1.4 Distributed and Privacy-Aware Speed Advisory Systems

Vehicles have become the main mode of transport (even for short distances) in the world. Recently, they have turned into products with a high sophistication level in the current commercial market hand-in-hand with technological advancements, ranging from electric bikes made of smart/modern materials, provided with specialised gearing, powerful engines and advanced localisation/tracking systems, up to magnetic-levitation trains with speed records for terrestrial transportation. In spite of this, vehicular systems suffer from critical issues such as congestion management, safety concerns and control of pollutant emissions, among others.

In recent years, a wide variety of applications have been proposed to address these problems by adopting advanced communication, sensing and control technologies in Vehicular Ad-hoc Networks (VANETs) such as Vehicle-to-vehicle/infrastructure (V2X) communication systems, advanced on-board computing capabilities, Radio Frequency Identification (RFID), and Advanced Driver Assistance Systems (ADAS) [73, 143, 168]. These technologies can be used as an ancillary service providing various kinds of services to users in the framework of Intelligent Transportation Systems (ITS), concerning safety, commercial, or even entertainment purposes [61]. In some specific situations, they can be used to provide precise online road traffic information to drivers and therefore affect their driving behaviours to reduce congestion and avoid accidents [216].

A Speed Advisory System (SAS) can be regarded as a specific application of ADAS in VANETs. They are designed such that the drivers will “know” the speed limits on the road and thus suggest the proper speed to drivers to achieve various kinds of traffic objectives, such as enhancing driving safety [25]. However, to date little work has been done concerning the design of the SAS for vehicles networks (e.g., conventional vehicles and EVs), taking account of environmental and energy efficiency objectives from an optimisation perspective. This design task for both EVs and conventional vehicles is the last problem that we shall tackle in the thesis. In addition, the SAS should be designed to in a smart fashion to preserve the privacy of vehicle drivers. By privacy-preserving we mean that the states of agents may be revealed to other agents but other important information cannot be communicated directly to other agents (e.g. some drivers may not wish to reveal their fuel consumption information to other vehicles if sharing of information is a necessary procedure as required by such a SAS). Thus, how to design a SAS for optimising conventional and electric vehicles networks to achieve the aforementioned objectives in a distributed, flexible, and privacy-preserving manner becomes the last problem we shall deal with in the thesis.

1.2 Research Objectives and Contributions

Part I: A Consensus Algorithm with Feedback

We consider the nonlinear system described by (1.1). The research objective is to establish conditions on the function g for which global uniform asymptotic stability is assured, thereby giving a rigorous proof of convergence in the process. The general setup we study can be formulated as a special case of the systems studied in [121]. In this reference the authors prove local synchronisation results for a general class of nonlinear time-varying systems. In contrast to the assumptions of that paper we require fewer differentiability assumptions and state conditions which ensure global convergence.

The contribution of this part is to present a rigorous proof for the stability and convergence properties of system (1.1). This work is presented in Chapter 2 and the original paper has been submitted in [115].

Part II: Grid Integration with EVs

The research on this topic can be divided into two sections according to whether EVs are considered with or without V2G capabilities. In the first section, we consider a variety of G2V EV charging problems, and in the second section we propose two specific schemes for V2G implementations.

The objective in the first section is to present a common framework such that the performance of a wide variety of EV charging algorithms can be compared. In particular, we shall provide a comparative evaluation of a range of EV charging strategies within this framework using a realistic power system simulation testbed in Low-Voltage (LV) distribution networks and representative charging scenarios. Through this comparison, we aim at identifying the positive and negative characteristics of each EV charging approach and giving an overall assessment for implementing these approaches in practice. The contributions in the first section are listed as follows:

- A comprehensive literature review of EV charging strategies is presented from the perspective of the different actors in the power system.
- A common optimisation framework incorporating real grid constraints is presented. Several typical EV charging strategies, classified as either centralised and decentralised, and providing continuous or on-off based charging, are evaluated within the proposed optimisation framework on a distribution network using a dedicated power system simulation platform.
- A distributed wireless testbed for charging mobile phone batteries is demonstrated as a proxy for EVs.

The above works are presented in Chapter 3 and the original papers were published in [107, 108, 110, 114].

The objective in the second section is to harness the power of V2G technologies to provide flexible ancillary services to the grid. To illustrate these ideas, two specific V2G applications are designed in different scenarios.

In the first application, we apply V2G technologies on a group of EVs to alleviate current imbalance in a typical three-phase distribution network. In this application, we propose a distributed EV charging strategy to balance currents along the individual phases. To the best of our knowledge, this is the first time that a distributed control algorithm has been used to manage current imbalance issues via controlled EV charging. This work is presented in Chapter 4 and the original paper was published in [111].

In the second application, we model the V2G problem as an optimisation problem in the framework of microgrids with Distributed Generators (DGs). We aim to find the optimal trade-off between the economic convenience of using energy from renewables instead of energy from other more expensive power plants, and the inconvenience caused to the owner in terms of residual energy remaining in the EV. Also, we are interested in computing a

“fair” solution, where fairness is related to the fact that the same amount of energy should be taken from all EVs participating in the V2G programme (i.e. some EV owners might decide not to participate in such a programme to preserve the level of energy in their EVs). The contribution of this work is to apply an optimal decentralised consensus algorithm that solves the V2G problem in a fair manner, trying to achieve an optimal trade-off between power generation costs and inconvenience to the vehicle owner. This work is presented in Chapter 4 and the original paper was published in [105].

Part III: Optimal Energy Management Strategies in Smart Grid

In this topic, we consider the optimal energy management problem in a microgrid scenario with DGs. As stated previously, the main task of the EMS in a microgrid is to achieve balance of produced/consumed energy and to cooperate with DGs for efficient and economical power generation.

The objective of this topic is to design an algorithm that automatically shares the power generation task among the available DERs in a way that is fair and distributed. As we shall see later, the concept of fairness in this context will be with respect to a utility function, where utility will refer to financial costs for power generation. We shall achieve this objective by adopting Additive-Increase-Multiplicative-Decrease (AIMD) algorithms [28]. The contributions of this work are summarised as follows:

- A truly distributed solution is demonstrated for the power generation problem.
- A consensus-like modification of the conventional synchronised AIMD algorithm is presented to solve the utility minimisation problem for specific cost functions.
- The results are illustrated in a realistic power system simulation framework.

This work is presented in Chapter 5 and the original papers were published in [35, 106].

Part IV: Distributed and Privacy-Aware Speed Advisory Systems

In this topic, we consider the design of a Speed Advisory System (SAS), making use of Vehicle-to-vehicle/infrastructure (V2X) technologies, for optimising both electric and conventional vehicles networks in an Intelligent Transportation System (ITS) scenario.

The objective of this topic is to develop a SAS which allows groups of vehicles to collaborate in order to find the optimal speed at which the group should travel. We shall assume that vehicles can exchange information with their neighbours and can exchange limited information with the infrastructure via their equipped V2X technologies. We shall

show that one can design, using very simple ideas, an effective SAS, which can be used to minimise energy consumption of electric vehicles and emission generation of conventional vehicles, in a distributed manner that preserves the privacy of individual vehicles. The contributions on this topic are listed as follows:

- A consensus based distributed speed advisory system is proposed that optimally determines a recommended common speed for a given area in order that the group battery consumptions of EVs are minimised. The proposed algorithms achieve this in a privacy-aware manner; namely, individual vehicles do not reveal in-vehicle information to other vehicles or to infrastructure. Matlab simulations are given to illustrate the effectiveness of the proposed approach. This work is presented in Chapter 6 and the original papers were submitted in [112, 113].
- Some of the ideas from Chapter 6 are extended to minimise the group emissions of conventional vehicles. SUMO simulations are given to illustrate the efficacy of the algorithm, and Hardware-In-the-Loop (HIL) tests involving real vehicles are given to illustrate user acceptability and ease of the deployment. This work is presented in Chapter 7 and the original papers were submitted in [112, 113].

1.3 Thesis Outline

The rest of the thesis is organised as follows:

- **Chapter 2** gives a rigorous proof for the stability and convergence properties of a recently proposed consensus algorithm with output constraint.
- **Chapter 3** presents a comprehensive review of recent works on a variety of EV charging strategies. We model different EV charging problems in a common mathematical framework and describe different EV charging scenarios as optimisation problems having either temporal or instantaneous objectives with respect to different power system stakeholders. To compare the performances of these approaches, typical fairness and temporal based EV charging strategies are introduced and evaluated on a dedicated power system simulation platform. A few modifications to the algorithms are introduced to enhance the grid performance for algorithm implementations. Finally, detailed design procedures for an AIMD based battery charging testbed (hardware) are demonstrated.
- **Chapter 4** focuses on investigating different V2G schemes as an ancillary service to support the grid. Two V2G schemes are presented. The first scheme considers a

current imbalance problem in a distribution network. The second scheme discusses the optimal power dispatch of EVs in a microgrid scenario with fluctuating renewable energy generation.

- **Chapter 5** proposes an AIMD-like distributed approach to optimally share the power generation tasks for DERs in a microgrid scenario. The performance of the proposed approach is evaluated and compared to a centralised solution to show its effectiveness. As an extension, this solution is further modified to incorporate thermal constraints for double power balancing requirements.
- **Chapter 6** demonstrates a new design for a SAS, using ideas from Chapter 2, to optimise energy efficiencies for a group of EVs in a city centre scenario. Matlab simulations are given to illustrate the effectiveness of the proposed system.
- **Chapter 7** extends the works in Chapter 6 and applies some of the ideas of the SAS to minimising pollutant generation of conventional vehicles in an highway scenario. A variety of simulation studies are given, e.g., SUMO simulations and HIL tests, to evaluate the performance of the proposed system.
- **Chapter 8** concludes the thesis and discusses future research directions.

Part I

A Consensus Algorithm with Feedback

Chapter 2

Stability and Convergence Analysis

***Abstract:** In this chapter, we discuss the stability and convergence of a recently proposed consensus algorithm with output constraints. It is joint work with Fabian Wirth, Martin Corless and Robert Shorten and has been submitted to the IEEE Transactions on Automatic Control [115]. The algorithm is further extended for applications in Chapters 4, 6 and 7.*

2.1 Introduction

We consider nonlinear systems described by

$$x(k+1) = P(k)x(k) + \mu(r - g(x(k)))e \quad (2.1)$$

where $x(k) \in \mathbb{R}^n$, $P(k)$ is a $n \times n$ row stochastic matrix, $e = [1 \ 1 \ \dots \ 1]^T$, μ and r are scalars while g is a scalar valued function. Equation (2.1) describes a consensus problem subject to an output constraint. It basically says that if consensus is achieved, it must be achieved subject to the equilibrium constraint $g(x^*) = r$. That is, at equilibrium

$$g(x^*) = r, \quad (2.2)$$

with $x_i^* = x_j^*$ for all $i, j \in \{1, 2, \dots, n\}$.

Equation (2.1) is of interest as it arises in many situations in the study of the Internet of Things (IOT). For example, in some situations a group of agents are asked to achieve a fair allocation of a constrained resource r (e.g. bandwidth), and hence $x_i(k)$ can be modelled as the amount of resources allocated to the agent i at time k , and the feedback function $g(x(k))$ can be regarded as the total amount of resources allocated to all agents x at time k , which is expected to approach to r over time. TCP is an algorithm that strives to achieve

this objective in internet congestion control. Recently, similar ideas have been applied in the context of charging of electric vehicles, smart grid applications, and in the regulation of pollution in an urban context [105, 167, 189]. In the context of EVs, a distributed consensus algorithm of the form of (2.1) has been developed in [105] to provide an optimal fairness solution for the V2G scheme. The fairness of the solution refers to the discharge rates of EVs will achieve consensus when algorithm converges (i.e. $x_i^* = x_j^*$ for all $i, j \in \{1, 2, \dots, n\}$) and the function $g(x)$ was specifically designed such that the optimality of the algorithm achieves when $g(x^*) = r$. In the context of smart grids, power plants can be easily operated, by using such algorithms, to provide a fair generation of power while maintaining the overall emissions of all plants to a certain level. In this model, the power generation of each plant at given time instance k can be modelled as $x_i(k)$ and $g(x(k))$ can be modelled as the overall emissions polluted by generating $x(k)$ amount of power from all plants, where r can refer to a daily emission target that cannot be exceeded. A second application arises when one wishes to optimise an objective function subject to certain privacy constraints. For example, collaborative cruise control systems are emerging in which a group of vehicles on a stretch of road share information to determine an advised speed limit that minimises fuel consumption of the swarm subject to some constraint (traffic flow, pollution constraints) [67]. Since each car is individually optimised for a potentially different speed, the technical challenge is for the group of cars to agree on a common speed without an individual revealing any of its inner workings to other vehicles.

Another example in this direction arises in the context of deploying services from parked cars as part of an IBM Research project. Here, privacy preserving algorithms of the form of (2.1) have been deployed and demonstrated to show great promise in the context of load balancing across batteries from a fleet of parked vehicles [175]. Other examples of this nature abound. For example, in many applications a number of sensing devices are asked to agree on a common value (a consensus problem). Each device is subject to some sensing error. The objective is then to find the common value that is most likely; namely, minimises some group-wide uncertainty without the individual uncertainty functions being revealed to other agents.

The proliferation of such applications is a direct consequence of large scale connectivity of both devices and people. This connectivity has given rise to a new wave of research focussed on addressing societal inefficiencies in a manner that has hitherto been impossible [31, 156]. At the heart of these engineering applications is the idea that individual things (agents) orchestrate their behaviour to achieve a common goal. Typically, these problems have a common property in that one tries either implicitly or explicitly to solve a consensus problem with an input. As we have mentioned, for reasons of privacy, usually one does

not attempt to solve such problems in a fully distributed manner. Neither, for reasons of robustness, scale, and communication overhead, does one attempt to solve them in a centralised manner. Rather, one uses a mix of local communication, and limited broadcast information, to solve these problems in a manner that conceals the private information of each of the individual agents. Implicit and explicit consensus algorithms that exploit local and global communication strategies are proposed and studied in [95]. Equation (2.1) is perhaps the simplest algorithm of the explicit consensus algorithm with inputs, admitting a very simple intuitive understanding, which can be explained as follows. It is easily known from [162] that a row stochastic matrix P operates on a vector $x \in \mathbb{R}^n$ such that

$$\max(x) - \min(x) \geq \max(Px) - \min(Px) \quad (2.3)$$

where $\max(x)$ and $\min(x)$ are defined as the maximum and minimum component in vector x , respectively. Since the addition of $(r - g(x(k)))e$, which is a vector with all same values, does not affect this contraction, intuition suggests that $x_i(k) - x_j(k) \rightarrow 0$ as k increases and eventually, the dynamics of (2.1) will be governed by the following scalar **Lure system**:

$$y(k+1) = y(k) + \mu(r - g(y(k))e), \quad (2.4)$$

with $x_i(k) \approx y(k)$ asymptotically for all i . Intuition further suggests, as long as (2.4) is stable, then so is (2.1). A plausibility argument along these lines, in support of (2.1), is given in [95]. However, no formal stability proof is given in that paper.

Our objective in this chapter is to address this and to establish conditions on the function g for which global uniform asymptotic stability is assured, thereby giving a rigorous proof of convergence in the process.

2.2 Notation, Conventions and Preliminary Results

In this section we give the notation, conventions and present some preliminary results needed to study the dynamics of the systems.

1. Notation. We denote the standard basis in \mathbb{R}^n by the vectors e_1, \dots, e_n . Note that $e = \sum_{i=1}^n e_i$. A matrix $P \in \mathbb{R}^{n \times n}$ is called row stochastic if all its entries are nonnegative and if all its row sums equal one. The row sum condition is equivalent to $Pe = e$, that is, e is an eigenvector of P corresponding to the eigenvalue 1. Hence there is a single transformation which achieves upper block triangularisation of all row stochastic matrices. Let $\{v_2, \dots, v_n\}$ be a basis for the $n - 1$ dimensional subspace $e^\perp := \{x \in \mathbb{R}^n : e^T x = 0\}$. Then $\{e, v_2, \dots, v_n\}$ is a

basis of \mathbb{R}^n . Consider now the transformation matrix $T := [e \ v_2 \ \dots \ v_n]$ which represents a change of basis from the standard basis to the new basis. Under this transformation, a row stochastic matrix P is transformed as follows:

$$T^{-1}PT = \begin{bmatrix} 1 & c^T \\ 0 & Q \end{bmatrix} \quad (2.5)$$

where $c \in \mathbb{R}^{n-1}$ and $Q \in \mathbb{R}^{(n-1) \times (n-1)}$.

2. Facts about consensus. Given a sequence of row stochastic matrices $\{P(k)\}_{k \in \mathbb{N}}$, consider the time-varying linear system

$$x(k+1) = P(k)x(k). \quad (2.6)$$

A solution of (2.6) is represented by the left products of the matrix sequence in the following sense: a sequence $\{x(k)\}_{k \in \mathbb{N}}$ is a solution of (2.6) corresponding to the initial condition $x(0) = x_0$ if and only if for all $k \in \mathbb{N}$,

$$x(k) = \Phi(k)x_0 \quad (2.7)$$

where

$$\Phi(k) := P(k-1) \cdots P(0), \quad \forall k \in \mathbb{N}. \quad (2.8)$$

The sequence $\{P(k)\}_{k \in \mathbb{N}}$ is called *weakly ergodic* if the difference between each pair of rows of $\Phi(k)$ converges to zero, i.e. if for all i, j we have

$$\lim_{k \rightarrow \infty} (e_j^T - e_i^T) \Phi(k) = 0. \quad (2.9)$$

This is equivalent to system (2.6) being a *consensus system*, that is, every solution $\{x(k)\}_{k \in \mathbb{N}}$ of (2.6) satisfies

$$\lim_{k \rightarrow \infty} x_j(k) - x_i(k) = 0 \quad (2.10)$$

for all i, j .

The sequence $\{P(k)\}_{k \in \mathbb{N}}$ is *strongly ergodic* if it is weakly ergodic and, in addition, the limit $\lim_{k \rightarrow \infty} \Phi(k)$ exists. By a result of Chatterjee and Seneta [27] weak and strong ergodicity are equivalent for left products of row stochastic matrices. This is equivalent to every solution of (2.6) satisfying

$$\lim_{k \rightarrow \infty} x(k) \in E \quad (2.11)$$

or, equivalently,

$$\lim_{k \rightarrow \infty} \Phi(k)x_0 \in E \quad (2.12)$$

for all $x_0 \in \mathbb{R}^n$ where $E := \text{span}\{e\}$ is the space of consensus vectors.

We call the sequence $\{P(k)\}_{k \in \mathbb{N}}$ *uniformly strongly ergodic*, if all tail sequences $\{P(k)\}_{k=k_0}^{\infty}$ are strongly ergodic for all $k_0 \in \mathbb{N}$. Note that a sequence can be strongly ergodic and not uniformly strongly ergodic. For instance, if one of the matrices in the sequence has rank 1 and all the subsequent matrices are the identity matrix.

Using the transformation (2.5) a system equivalent to (2.6) is given by

$$\begin{aligned} z(k+1) &= T^{-1}P(k)Tz(k) \\ T^{-1}P(k)T &:= \begin{bmatrix} 1 & c(k)^T \\ 0 & Q(k) \end{bmatrix}. \end{aligned} \quad (2.13)$$

It is then clear that $\{P(k)\}$ is strongly ergodic if and only if

$$\lim_{k \rightarrow \infty} Q(k) \dots Q(0) = 0. \quad (2.14)$$

A useful property in the study of products of row stochastic matrices is the observation that for any row stochastic matrix P

$$\min(x) \leq \min(Px) \leq \max(Px) \leq \max(x) \quad (2.15)$$

for all $x \in \mathbb{R}^n$, where for any vector $y \in \mathbb{R}^n$,

$$\min(y) := \min\{y_1, \dots, y_n\}, \quad \max(y) := \max\{y_1, \dots, y_n\}.$$

Note that details of this property can be referred from [91, 188]. As the associated difference of maximum and minimum plays the role of a Lyapunov function we introduce the notation

$$V(x) := \max(x) - \min(x). \quad (2.16)$$

Clearly, (2.15) implies that $V(Px) \leq V(x)$. Also, the sequence $\{P(k)\}_{k \in \mathbb{N}}$ is strongly ergodic, if and only if

$$\lim_{k \rightarrow \infty} V(\Phi(k)x_0) = 0 \quad (2.17)$$

for all $x_0 \in \mathbb{R}^n$ where $\Phi(k)$ is given by (2.8).

In this chapter the standard norm used is the Euclidean norm $\|x\| = \sqrt{x^T x}$. Note that any vector $x \in \mathbb{R}^n$ can be uniquely decomposed as

$$x = \bar{x}e + x_{\perp}$$

where

$$\bar{x} := (1/n)e^T x \quad (2.18)$$

is the mean of the components of x and

$$x_{\perp} := x - \bar{x}e \in e^{\perp}, \quad (2.19)$$

i.e. $e^T x_{\perp} = 0$. Hence

$$\text{dist}(x, E) = \|x_{\perp}\| \quad (2.20)$$

where

$$\text{dist}(x, E) := \inf\{\|x - z\| : z \in E\}$$

is the distance of a vector $x \in \mathbb{R}^n$ to the consensus set E .

Note also that

$$V(x) = V(x_{\perp}) \quad (2.21)$$

and for any vector $z \in \mathbb{R}^n$ and any row-stochastic matrix $P \in \mathbb{R}^{n \times n}$ we have

$$\|z\|_{\infty} = \max_{1 \leq i \leq n} |z_i| \quad \text{and} \quad \|P\|_{\infty} = \max_{1 \leq i \leq n} \sum_{j=1}^n |P_{ij}| = 1$$

where P_{ij} is the entry in i^{th} row and j^{th} column of the matrix P .

2.3 Consensus under Feedback

Consider a sequence of row stochastic matrices $\{P(k)\}_{k \in \mathbb{N}}$ and a continuous function $G : \mathbb{R}^n \rightarrow \mathbb{R}$. Then, the system,

$$\begin{aligned} x(k+1) &= F(k, x(k)) \\ F(k, x) &:= P(k)x + G(x)e \end{aligned} \quad (2.22)$$

can be regarded as consensus system under feedback.

In later statements, further differentiability assumptions will be imposed on G as required. Associated with (2.22) we consider the one-dimensional system

$$\begin{aligned} y(k+1) &= h(y(k)) \\ h(y) &:= y + G(ye). \end{aligned} \tag{2.23}$$

This is the aforementioned Lure system and, as we shall see, the dynamics of the consensus system (2.22) is strongly related to the dynamics of (2.23). Unless stated otherwise we consider the systems (2.22) and (2.23) with initial time $k_0 = 0$. A few comments on results that hold uniformly with respect to all initial times are made where appropriate.

2.3.1 Local Stability Results

We begin with the following elementary observations.

Lemma 1 *Let $\{P(k)\}_{k \in \mathbb{N}}$ be a sequence of row stochastic matrices and $G : \mathbb{R}^n \rightarrow \mathbb{R}$. If $\{y(k)\}_{k \in \mathbb{N}}$ is a solution of (2.23) then $\{y(k)e\}_{k \in \mathbb{N}}$ is a solution of (2.22).*

Proof: This follows from $P(k)e = e$. □

The next result tells us that the consensus system under feedback (2.22) is also a consensus system.

Lemma 2 *Let $\{P(k)\}_{k \in \mathbb{N}}$ be a sequence of row stochastic matrices which is strongly ergodic. Then for every solution $\{x(k)\}_{k \in \mathbb{N}}$ of (2.22) we have*

$$\lim_{k \rightarrow \infty} \text{dist}(x(k), E) = 0. \tag{2.24}$$

Proof: Consider any solution $\{x(k)\}_{k \in \mathbb{N}}$ of (2.22) and let $x_0 = x(0)$. Since $\{P(k)\}_{k \in \mathbb{N}}$ is strongly ergodic, recalling from (2.17) we have

$$\lim_{k \rightarrow \infty} V(\Phi(k)x_0) = 0,$$

where $\Phi(k)$ is given by (2.8). On the other hand,

$$\begin{aligned} V(x(k+1)) &= V(P(k)x(k) + G(x(k))e) \\ &= V(P(k)x(k)). \end{aligned}$$

This shows by induction that for all $k \in \mathbb{N}$ we have

$$V(x(k)) = V(\Phi(k)x_0).$$

Hence,

$$\lim_{k \rightarrow \infty} V(x(k)) = 0,$$

which is equivalent to

$$\lim_{k \rightarrow \infty} x_j(k) - x_i(k) = 0$$

for all i, j . This is the same as the desired result (2.24). \square

We now consider the local stability of (2.22) and see that it is determined by the stability of the induced system (2.23) on the consensus space. As we have no global concerns no Lipschitz property of G is required. Initially, it is sufficient that G be continuous.

Theorem 3 *Let $\{P(k)\}_{k \in \mathbb{N}}$ be a strongly ergodic sequence of row stochastic matrices and $G : \mathbb{R}^n \rightarrow \mathbb{R}$ be continuous. Suppose that y^* is a locally asymptotically stable fixed point of the one dimensional system (2.23). Then y^*e is a locally asymptotically stable fixed point at time $k = 0$ for (2.22).*

*If the sequence $\{P(k)\}_{k \in \mathbb{N}}$ is uniformly strongly ergodic, then y^*e is asymptotically stable for all initial times $k_0 \in \mathbb{N}$.*

Proof: Suppose that y^* is a locally asymptotically stable fixed point for system (2.23). Let W be a local Lyapunov function which guarantees this stability property. That is, $W(y^*) = 0$ and there is an open neighborhood U of y^* such that $W(y) > 0$ and $W(h(y)) < W(y)$ for all $y \in U \setminus \{y^*\}$. Without loss of generality we may assume U to be a forward invariant set of (2.23). This assumption implies if $y(k) \in U$ then so is $h(y(k)) \in U$ at all times $k \in \mathbb{N}$. Define the arithmetic mean of the entries of $x \in \mathbb{R}^n$ by

$$\bar{x} := (1/n)e^T x. \quad (2.25)$$

For $\varepsilon > 0$ such that $W^{-1}([0, \varepsilon]) \subset U$ is a compact set we may choose $\delta > 0$ sufficiently small, so that

$$W(h(y) + d) < \varepsilon \quad \text{for} \quad W(y) < \varepsilon \quad \text{and} \quad |d| \leq \delta.$$

This is possible by continuity of all the functions involved and by the decay property of the Lyapunov function W .

Now note that for any $x \in \mathbb{R}^n$,

$$Px = P(\bar{x}e + x_{\perp}) = \bar{x}e + Px_{\perp}.$$

Hence

$$\overline{Px} - \bar{x} = \overline{Px_{\perp}} = (1/n)e^T Px_{\perp}. \quad (2.26)$$

Given a sufficiently small $\varepsilon > 0$ and an appropriate δ as above, choose $\eta > 0$ such that $V(x) \leq \eta$ and $W(\bar{x}) \leq \varepsilon$ implies for any row stochastic matrix P that

$$|\overline{Px} - \bar{x}| + |G(x) - G(\bar{x}e)| < \delta.$$

This is possible by uniform continuity of G on a bounded neighborhood of y^*e . Roughly speaking, the uniform continuity of G guarantees that $G(x)$ can be sufficiently close to $G(\bar{x}e)$ if x is sufficiently close to $\bar{x}e$. Consider now the neighborhood of y^*e given by

$$N_\varepsilon := \{x \in \mathbb{R}^n : \bar{x} \in U, W(\bar{x}) < \varepsilon, V(x) < \eta\}.$$

We wish to prove the local stability of y^*e by showing N_ε is forward invariant at all times $k \in \mathbb{N}$. Indeed, if $x(k) \in N_\varepsilon$, then we obtain

$$\begin{aligned} \bar{x}(k+1) &= \overline{P(k)x(k)} + G(x(k)) \\ &= \bar{x}(k) + G(\bar{x}(k)e) + d \\ &= h(\bar{x}(k)) + d \end{aligned}$$

where $d = \overline{P(k)x(k)} - \bar{x}(k) + G(x(k)) - G(\bar{x}(k)e)$. Hence $|d| < \delta$ from which it follows that

$$W(\bar{x}(k+1)) < \varepsilon.$$

Referring to the argument in the proof of Lemma 2

$$V(x(k+1)) = V(P(k)x(k)) \leq V(x(k)) < \eta.$$

As ε, η were arbitrary, this shows stability of y^*e .

To show local attractivity, let $x_0 \in N_\varepsilon$ for $\varepsilon > 0$ sufficiently small so that stability holds. Note that by Lemma 2 and by stability we have that $\omega(x_0) \subset Ue \subset E$ where $\omega(x_0)$ is the ω -limit set of the solution corresponding to x_0 . Suppose that $ye \in \omega(x_0)$ and $y \neq y^*$. Then as the trajectory starting in ye converges to y^*e it follows that $y^*e \in \omega(x_0)$. However, the assumption that y^*e and ye are in the ω -limit set contradicts the stability of y^*e . Hence $\{x(k)\}_{k \in \mathbb{N}}$ converges to y^*e . \square

We now extend the previous result to local exponential stability. To this end we call a sequence of row stochastic matrices $\{P(k)\}_{k \in \mathbb{N}}$ *exponentially ergodic* if it is strongly ergodic

and there exist scalars $M \geq 1$, $0 < r < 1$ such that for all $k \in \mathbb{N}$

$$\|\Phi(k) - \Phi_\infty\| \leq Mr^k.$$

The sequence is called *uniformly exponentially ergodic*, if it is uniformly strongly ergodic and the constants M , r can be chosen such that for all $k, k_0 \in \mathbb{N}$ with $k \geq k_0$ there exists a matrix Φ_∞ such that $\|\tilde{\Phi}(k, k_0) - \Phi_\infty\| \leq Mr^{(k-k_0)}$; where

$$\tilde{\Phi}(k, k_0) := P(k-1) \cdots P(k_0).$$

Theorem 4 *Let $\{P(k)\}_{k \in \mathbb{N}}$ be an exponentially ergodic sequence of row stochastic matrices and $G : \mathbb{R}^n \rightarrow \mathbb{R}$ be continuously differentiable. Suppose that y^* is a locally exponentially stable fixed point of the one dimensional system (2.23). Then, y^*e is a locally exponentially stable fixed point at time $k = 0$ for (2.22). If the sequence $\{P(k)\}_{k \in \mathbb{N}}$ is uniformly exponentially ergodic, then y^*e is locally uniformly exponentially stable.*

Proof: Consider the linearisation of the one-dimensional map defining (2.23). By the assumption of exponential stability its modulus must satisfy

$$|h'(y^*)| < 1 \tag{2.27}$$

where $h'(y^*) = 1 + DG(y^*e)e$ and DG is the derivative of G , which we interpret as a row vector. We now compute the derivative of F with respect to x at $x = y^*e$ and time k to obtain

$$\frac{\partial F}{\partial x}(k, y^*e) = P(k) + eDG(y^*e). \tag{2.28}$$

If we now consider the transformation T which results in (2.13) and using $T^{-1}e = e_1$ we see that

$$T^{-1} \frac{\partial F}{\partial x}(k, y^*e) T = \begin{bmatrix} 1 & c(k)^T \\ 0 & Q(k) \end{bmatrix} + e_1 DG(y^*e) T. \tag{2.29}$$

Two things are noticeable when considering this equation. First the resulting transformed matrix is of the form

$$\begin{bmatrix} \lambda & \tilde{c}(k)^T \\ 0 & Q(k) \end{bmatrix}, \tag{2.30}$$

where only the first row is affected by G and λ is independent of k . Secondly,

$$\lambda = 1 + DG(y^*e)e = h'(y^*). \tag{2.31}$$

Hence $|\lambda| < 1$. By assumption $\|Q(k)Q(k-1)\dots Q(0)\| \leq Mr^k$ for suitable constants $M \geq 1, r \in (0, 1)$. It now follows that the linearised system of (2.22) at the fixed point y^*e is exponentially stable. It follows by standard linearisation theory, that the nonlinear system is locally exponentially stable at y^*e . If the sequence $Q(k)Q(k-1)\dots Q(0)$ converges to zero uniformly exponentially, this shows local uniform exponential stability of y^*e for the nonlinear system. \square

2.3.2 Global Stability Results

To obtain global stability results we first need the following boundedness result.

Lemma 5 *Let $\{P(k)\}_{k \in \mathbb{N}}$ be a strongly ergodic sequence of row stochastic matrices and suppose that $G : \mathbb{R}^n \rightarrow \mathbb{R}$ is continuous and satisfies the following conditions.*

- (i) *There exists an $\varepsilon > 0$ such that G satisfies a Lipschitz condition with constant $L > 0$ on the set*

$$B_\varepsilon(E) := \{x \in \mathbb{R}^n : \text{dist}(x, E) \leq \varepsilon\}.$$

- (ii) *There exists constants $\beta, \gamma > 0$ such that*

$$|h(y)| \leq |y| - \gamma \quad \text{when } |y| \geq \beta$$

where $h(y) = y + G(ye)$.

Then every trajectory of (2.22) is bounded.

Proof: Consider any solution $\{x(k)\}_{k \in \mathbb{N}}$ of (2.22) with $x(0) = x_0$. By Lemma 2 there exists a $k_0 \in \mathbb{N}$ such that $x(k) \in B_\varepsilon(E)$ for all $k \geq k_0$.

We can express $x(k)$ as

$$x(k) = \bar{x}(k)e + x_\perp(k)$$

where $\bar{x}(k) = (1/n)e^T x(k)$ and $x_\perp(k) := x(k) - \bar{x}(k)e$.

It follows from (2.24) that $\lim_{k \rightarrow \infty} \|x_\perp(k)\| = 0$. Hence boundedness of the sequence $\{\bar{x}(k)\}_{k \in \mathbb{N}}$ implies boundedness of $\{x(k)\}_{k \in \mathbb{N}}$. Considering the evolution of $\bar{x}(k)$ we obtain that, for $k \geq k_0$,

$$\begin{aligned}
|\bar{x}(k+1)| &= |\overline{P(k)x(k) + G(\bar{x}(k)e + x_{\perp}(k))}| \\
&\leq |\bar{x}(k) + G(\bar{x}(k)e)| \\
&\quad + |\overline{P(k)x(k)} - \bar{x}(k)| \\
&\quad + |G(\bar{x}(k)e + x_{\perp}(k)) - G(\bar{x}(k)e)| \\
&\leq |h(\bar{x}(k))| + |(1/n)e^T P(k)x_{\perp}(k)| + L\|x_{\perp}(k)\| \\
&\leq |h(\bar{x}(k))| + \tilde{L}\|x_{\perp}(k)\|
\end{aligned}$$

where $l := \sup_{k \in \mathbb{N}} (1/n)\|e^T P(k)\|$ and $\tilde{L} := l + L$. Hence

$$|\bar{x}(k+1)| \leq |h(\bar{x}(k))| + \tilde{L}\|x_{\perp}(k)\|.$$

It now follows from hypothesis (ii) that whenever $|\bar{x}(k)| \geq \beta$, we must have

$$|\bar{x}(k+1)| \leq |\bar{x}(k)| - \gamma + \tilde{L}\|x_{\perp}(k)\|.$$

Since $\lim_{k \rightarrow \infty} \|x_{\perp}(k)\| = 0$, there exists a $k_* \geq k_0$ such that $\tilde{L}\|x_{\perp}(k)\| \leq \gamma$ for all $k > k_*$. Thus,

$$|\bar{x}(k+1)| \leq |\bar{x}(k)| \quad \text{when } k \geq k_* \text{ and } |\bar{x}(k)| \geq \beta.$$

This implies boundedness of $\{\bar{x}(k)\}_{k \in \mathbb{N}}$ and completes the proof. \square

Comment: As an example of a general class of functions which satisfy hypothesis (ii) of Lemma 5, consider any strict contraction mapping h on \mathbb{R} , i.e., for a suitable constant $c \in (0, 1)$,

$$|h(x) - h(y)| \leq c|x - y|, \quad \forall x, y \in \mathbb{R}.$$

By the Banach contraction theorem, there is a unique fixed point y^* such that $h(y^*) = y^*$. Hence,

$$\begin{aligned}
|h(y)| &\leq |h(y) - y^*| + |y^*| \\
&\leq c|y - y^*| + |y^*| \\
&\leq c|y| + (1+c)|y^*| \\
&= |y| - (1-c)|y| + (1+c)|y^*|
\end{aligned}$$

and hypothesis (ii) is assured with $\beta = \frac{1+c}{1-c}|y^*|$.

Finally, we state a global result on asymptotic and exponential stability. In spirit, the following two results are closely related to [121, Theorem 1]. Note that we obtain a global

result and are only concerned with fixed points, not general attractors. Also no assumption on the invertibility of the Jacobian is required.

Theorem 6 *Let $\{P(k)\}_{k \in \mathbb{N}} \subset \mathbb{R}^{n \times n}$ be a strongly ergodic sequence of row stochastic matrices and suppose that G satisfies all conditions of Lemma 5. If y^* is a globally asymptotically stable fixed point of (2.23) then, y^*e is a globally asymptotically stable fixed point for system (2.22).*

Proof: The assumptions of Theorem 3 are met and so it only remains to show global attractivity. Note that, by Lemma 5 all solutions of (2.22) are bounded. By Lemma 2 the ω -limit sets corresponding to all initial conditions lie in E . So consider an ω -limit set $\omega(x_0)$ and assume that $ye \in \omega(x_0)$ but $y \neq y^*$. Let U be a neighborhood of y^*e on which local stability holds according to Theorem 3. We may assume $\text{dist}(ye, U) > 0$. As $ye \in E$ it follows from Lemma 1 that all solutions $x(\cdot; k_0, ye)$ with the initial condition $x(k_0) = ye$ satisfy

$$\lim_{k \rightarrow \infty} x(k; k_0, ye) = y^*e.$$

Note that on E the system is time-invariant, so that there exists a time K , such that for all k_0 we have

$$x(k_0 + K; k_0, ye) \in U.$$

By assumption (i) the maps $x \mapsto P(k)x + G(x)e$ are equicontinuous (i.e., each map is uniformly continuous) on $B_\varepsilon(E)$. Choose $\eta > 0$ such that

$$B_{\eta, \infty}(E) := \{x \in \mathbb{R}^n ; \text{dist}_\infty(x, E) = \min_{r \in \mathbb{R}} \|x - re\|_\infty < \eta\}$$

is contained in $B_\varepsilon(E)$. The set $B_{\eta, \infty}(E)$ is forward invariant under all $F(k, \cdot)$, because if $\text{dist}_\infty(x, E) = \|x - r_x e\|_\infty < \eta$, then as $\|P\|_\infty = 1$ for all row stochastic matrices

$$\text{dist}_\infty(P(k)x + G(x)e, E) = \text{dist}_\infty(P(k)x, E) = \min_{r \in \mathbb{R}} \|P(k)(x - re)\|_\infty \leq \|P(k)(x - r_x e)\|_\infty < \eta.$$

Thus there exists a sufficiently small neighborhood U_2 of ye such that for all $k_0 \in \mathbb{N}$ the solution corresponding to the initial condition $x(k_0) \in U_2$ satisfies $x(k_0 + K; k_0, x(k_0)) \in U$. But then by local stability, it follows that $x(k; k_0, x(k_0)) \in U$ for all $k \geq k_0 + K$. We thus arrive at a contradiction, if $ye \in \omega(x_0)$, then there exists a sequence $k_\ell \rightarrow \infty$ so that $\lim x(k_\ell; 0, x_0) = ye$. But then $x(k_\ell; 0, x_0) \in U_2$ for a sufficiently large ℓ and hence $x(k; 0, x_0) \in U$ for all $k \geq k_\ell + K$. Hence no subsequence of $\{x(k)\}$ converges to ye . This contradiction completes the proof. \square

The previous result can be sharpened, if we assume exponential stability of the fixed point of (2.23). We omit the proof, which uses the same arguments as the proof of Theorem 6.

Theorem 7 *Let $\{P(k)\}_{k \in \mathbb{N}} \subset \mathbb{R}^{n \times n}$ be a uniformly exponentially ergodic sequence of row stochastic matrices and suppose that $G : \mathbb{R}^n \rightarrow \mathbb{R}$ is differentiable and satisfies conditions (i) and (ii) of Lemma 5. Then y^*e is globally uniformly exponentially stable for system (2.22).*

Proof: The proof follows with the same arguments of the proof of Theorem 6 and is omitted. \square

2.3.3 Switched Systems

In previous sections, we study the properties of system (2.22) given a fixed sequence of $\{P(k)\}_{k \in \mathbb{N}} \subset \mathbb{R}^{n \times n}$. In this section, we present some stability results for the system under arbitrary switching in the context of switched systems.

Given a compact set of row stochastic matrices $\mathcal{P} \subset \mathbb{R}^{n \times n}$, we may consider the switched system

$$x(k+1) = P(k)x(k) + G(x(k))e, \quad (2.32)$$

where $P(k) \in \mathcal{P}$. The results obtained so far have some immediate consequences for consensus under feedback with arbitrary switching. It is well-known that all sequences $\{P_k\}_{k \in \mathbb{N}} \in \mathcal{P}^{\mathbb{N}}$ are strongly ergodic if and only if all sequences in $\mathcal{P}^{\mathbb{N}}$ are uniformly exponentially ergodic [121]. In this case we call \mathcal{P} uniformly ergodic. The rate of convergence towards E is in fact given by the projected joint spectral radius [121].

With this in mind the results obtained so far have immediate consequences for switched systems of the form (2.32). We note one of these consequences.

Corollary 8 *Let \mathcal{P} be a compact set of row stochastic matrices that is uniformly ergodic and suppose that $G : \mathbb{R}^n \rightarrow \mathbb{R}$ is differentiable and satisfies conditions (i) and (ii) of Lemma 5. Then y^*e is globally uniformly exponentially stable for the switched system (2.32) under arbitrary switching.*

2.4 Conclusions

In this chapter we present a rigorous proof of stability and convergence of a recently proposed consensus system with feedback. More applications based on this system will be introduced in Chapters 4, 6 and 7.

Part II

Grid Integration with EVs

Chapter 3

EV Charging Strategies in Low-Voltage Distribution Networks

***Abstract:** In this chapter, we discuss a variety of EV charging strategies for achieving both instantaneous and temporal optimisation objectives with practical constraints in Low-Voltage (LV) distribution networks. It is joint work with Paul McNamara, Seán McLoone, Robert Shorten, Sonja Stüdl, Richard Middleton and Julio Braslavsky and has been published in [107–110, 114]. This chapter also presents a review of some recent EV charging literature.*

3.1 Introduction

From a power system perspective, a major concern is that, as increasing numbers of EVs plug into low-voltage distribution networks, e.g., residential areas or Small Medium Enterprise (SME) areas, if charging is not regulated it is likely that coincident uncontrolled charging of EVs will overload local distribution networks and substantially increase power requirements [32, 157]. Not surprisingly, therefore, developing smart grid infrastructure and EV charging strategies to mitigate the impact of the role out of EVs on the grid have been the focus of considerable research effort in recent years [142, 156, 182].

To date, several different strategies have been proposed for charging groups of EVs connected to low-voltage distribution networks [31, 32, 50, 164]. These strategies can be classified from the perspective of the different actors in the power system, which consist of EV consumers, Distribution System Operators (DSOs) and Transmission System Operators (TSOs) [208].

Consumer oriented algorithms typically focus on maximising the amount of charge that can be allocated to a customer in a given time period. It is usually desired to allocate the avail-

able power to EVs in a fair way, providing a satisfactory Quality of Service (QoS), without violating system constraints, and minimising the cost to the customer. Many algorithms have been proposed using a centralised framework, the aim of which is to maximise the amount of charge allocated to customers [163, 164]. Here, centralised implies that all the information in the network is available to a centralised controller, which in turn processes the information and decides the charge each EV will receive. These algorithms are based on linear programming techniques. While centralised coordination gives the best performance possible [88], centralised algorithms require access to global system information, which might not always be accessible to a centralised controller, and centralised algorithms sometimes need to collect private information from customers for decision making. They usually have a significant communication overhead, involve higher complexity computations and typically do not scale well [35, 88, 126, 137]. For these reasons several decentralised strategies have been proposed recently for EV charging [22, 48, 102, 158, 174, 182]. In decentralised charging strategies individual EVs are given a certain level of decision making autonomy. Often individual EV chargers send a limited amount of information to a centralised unit which in turn provides some global coordination of their decisions, to a degree determined by the algorithm in use.

In this context, most recently, Stüdli et al. [189] have proposed EV charging strategies based on Additive-Increase-Multiplicative-Decrease (AIMD) that can be implemented in a decentralised fashion to maximise power utilisation by EVs while achieving a fair allocation of power across customers under certain assumptions. Also, Fan [48] borrowed the concept of congestion pricing in internet traffic control and introduced a Willingness To Pay (WTP) parameter to model the preference of user demand. Based on these ideas, he then developed a novel distributed framework for demand response and verified the convergence and dynamic behaviour of his adaptive algorithm, namely Distributed Price Feedback (DPF). With this framework in place, a novel distributed EV charging method was proposed such that each EV user could adapt their charging rate according to their personal preferences, maximising their own benefits. While it should be noted that most research studies to date, e.g. [48, 163, 164, 189] assume that future charging facilities will be capable of regulating EV charge rates continuously, few works consider the more realistic situation of EV chargers that support only on-off charging functionality. Some recently proposed results on solving this problem can be seen in [23, 167, 187, 192]. In particular, the authors [192] formulated this problem using Markov chain theory and proposed a distributed charging algorithm to maximise the utilisation of the available power via on-off charging control. However, practical power system infrastructure and operating constraints were not considered.

From the perspective of DSOs, charging strategies are usually designed to achieve a grid related objective such as the minimisation of power losses, while satisfying grid constraints,

and providing satisfactory customer service. Several centralised coordination strategies of this nature have been developed [1, 32, 39, 40, 142, 197, 211]. Vehicle-to-Grid (V2G) techniques for grid regulation have also been proposed in the literature. For example, in [211], V2G was used for grid regulation on a daily basis and for peak reduction at times of high demand. Some decentralised optimisation approaches have also been proposed to enhance grid regulation [189, 210].

Charging strategies aligned to TSO priorities include those focused on the scheduling of power supplies in an economic way, and those seeking to maximise the use of renewables on the grid. Centralised TSO based charging strategies include [219], where serial quadratic programming techniques were used to minimise the variance in the U.K. national demand profile, and [128] which examined the use of quadratic programming for load flattening under different penetrations of EVs. A more general study of adapting different centralised optimisation strategies for the coordination of EVs from the perspective of TSOs is presented in [81]. Several decentralised approaches developed from the TSO perspective are given in [3, 21]. In [8, 83, 100, 120] EVs are used for storage and control in order to maximise the utilisation of renewable energy. In [8], Mixed-Integer-Linear-Programming (MILP) was used to schedule EV charging loads in order to reduce charging costs and carbon emissions. In addition to this, EVs have been used to provide ancillary services, such as frequency control [57, 213].

With such a wide variety of algorithms available for EV charging it is desirable to have a common framework under which their performance can be compared. The objective of this chapter is to present such a framework for charging EVs in low-voltage distribution networks, and to consider the aforementioned works by providing a comparative evaluation of a range of EV charging strategies within this framework using a realistic distribution network simulation testbed and representative charging scenarios in both residential and SME areas. To do this, we review the basic mechanisms for several fairness based EV charging strategies, namely AIMD, DPF and on-off based charging. We propose a number of enhancements to these algorithms that take account of the power system structure, mitigate the impact of EVs on the grid from the perspective of transformer loading levels and voltage profiles, and reduce peak power requirements by responding to time-of-day pricing. Further, we also investigate other charging scenarios to provide a comparative evaluation of charging strategies from a different perspective rather than fairness. In particular, we consider those EV charging strategies focused on cost minimisation and valley-filling. Using an custom OpenDSS-Matlab simulation platform, different implementations of the algorithms are evaluated for a typical low-voltage feeder network with 50% EV penetration. With these results, we compare all considered charging strategies according to their different characteristics. Through

this comparison the positive and negative characteristics of each approach are identified. Additionally, we present a hardware design for a wireless AIMD based battery charging testbed to physically illustrate the ease of deployment of the decentralised algorithms. Finally, we conclude the chapter by providing suggestions for applying each charging strategy in practice.

The remainder of the chapter is organised as follows: In Section 3.2, we formulate the EV charging problems. Section 3.3 reviews the mechanisms of uncontrolled charging, AIMD, and DPF algorithms, and also provided a brief introduction to the ideal centralised solution. In the same section, we also introduce the distributed (on-off) and the centralised (on-off) charging algorithms [164]. The enhancements to all algorithms are presented in Section 3.4. In Section 3.5, two valley-filling based charging strategies are introduced. In Section 3.6, we present two cost minimisation based charging strategies. In Section 3.7, we set the simulation platform and evaluate the performance of different continuous EV charging strategies¹ in a residential charging scenario. In Section 3.8 we implement the on-off based EV charging strategies in a SME charging scenario. In Section 3.9, we discuss our results. Section 3.10 describes our hardware testbed designs. Finally, we give an overall assessment of each introduced approach and conclude the chapter in Section 3.11.

3.2 Problem Formulation

3.2.1 Notation

A scenario in which a number of houses incorporating EVs are connected to a power distribution network is shown in Figure 3.1. In this network, S is defined as the number of distribution transformers connected to the Medium-Voltage (MV) substation bus, SubBus. The SubBus is powered by a large rating transformer called $TR(0)$, which connects to an external bulk power system. Let \underline{S}^0 denote the set $\{0, 1, \dots, S\}$ for indexing all transformers.

A number of simplifications are used in the system model. The load power consumption in the network is discretised into M discrete time slots, each of length ΔT . For indexing purposes, let \underline{M} denote the set $\{1, 2, \dots, M\}$. The loads are classified as non-EV loads, and EV loads, in the low-voltage areas. The number of houses across all low-voltage areas is given by N . Each EV charger is connected to a standard household outlet which is regarded as an EV charge point and each house can only have a maximum of one EV connected for charging. Let \underline{N} denote the set $\{1, 2, \dots, N\}$ for houses and all EV charge points. The index set

¹The definition of ‘continuous’ and ‘on-off’ based EV charging strategies will be given in Section 3.3.

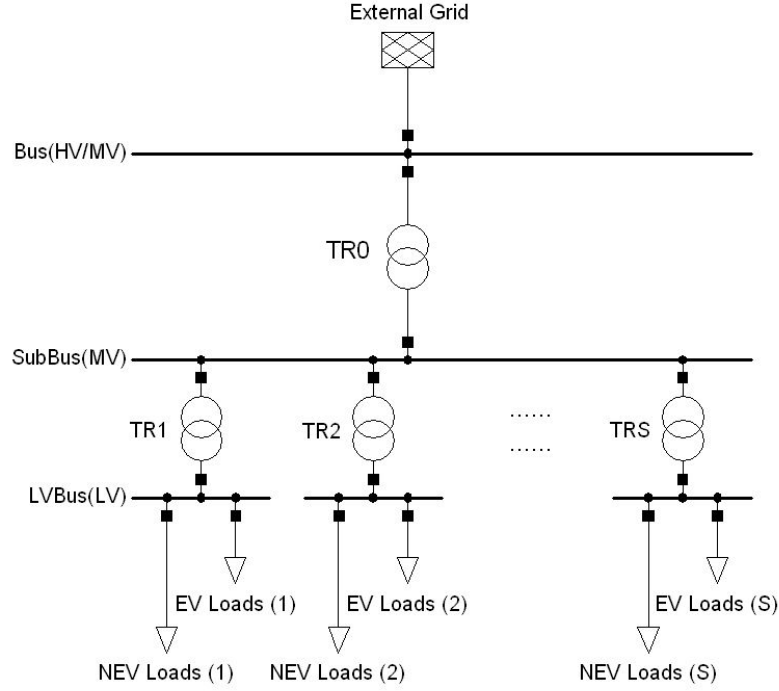


Fig. 3.1 Schematic diagram of the distribution network

of all houses connected to the transformer $TR(r)$ is given by Φ_h^r , and similarly the index set of all EVs connected to the transformer $TR(r)$ is given by Φ_c^r .

The non-EV power consumption for the j^{th} house at time slot k is given by $h_j(k)$, and $c_i(k)$ denotes the charge rate of the i^{th} active EV charge point at time k , for all $k \in \underline{M}$. The electricity price signal at time slot k , denoted $E(k)$, represents the Time-Of-Use (TOU) [169] or real-time pricing. The corresponding electricity price signal vector is given by $E^T := [E(1), E(2), \dots, E(M)]$. The charge rate vector for all EV charge points is given by $c(k)^T := [c_1(k), c_2(k), \dots, c_N(k)]$ for all $k \in \underline{M}$. The charge rate profile for the i^{th} EV is specified by $c_i^T := [c_i(1), c_i(2), \dots, c_i(M)]$. A charge rate matrix is also defined as $C := [c(1), c(2), \dots, c(M)]$. The plug-in time and plug-out time of the i^{th} EV are given by τ_{in}^i and τ_{out}^i , respectively. Therefore, the i^{th} EV must be charged within $[\tau_{\text{in}}^i, \tau_{\text{out}}^i]$. Let $P_{\text{av}}(k)$ denote the maximum available power that can be drawn from the external grid at time slot k . Let $P_{\text{av}}^{\text{ev}}(k)$ denote the maximum available power that can be provided for EV charging. Thus,

$$P_{\text{av}}^{\text{ev}}(k) = \min\left(\sum_{i=1}^N c_{\text{max}}^i, P_{\text{av}}(k) - \sum_{j=1}^N h_j(k)\right). \quad (3.1)$$

Due to the battery specification, each EV may have a different battery size (kWh), and this parameter is denoted as B_i for the i^{th} vehicle. The State-of-Charge (SOC) for the i^{th} EV at time k , $SOC_i(k)$, within $[\tau_{\text{in}}^i, \tau_{\text{out}}^i]$ is given by:

$$SOC_i(k) = SOC_i(\tau_{\text{in}}^i) + \sum_{\tau=\tau_{\text{in}}^i}^{k-1} \frac{c_i(\tau) \cdot \Delta T}{B_i} \quad (3.2)$$

where $SOC_i(\tau_{\text{in}}^i)$ is the initial SOC for the i^{th} EV when it plugs in. The maximum achievable SOC for the i^{th} EV is given by:

$$SOC_{\text{max}}^i = \min \left(1, SOC_i(\tau_{\text{in}}^i) + \frac{c_{\text{max}}^i (\tau_{\text{out}}^i - \tau_{\text{in}}^i) \cdot \Delta T}{B_i} \right) \quad (3.3)$$

where c_{max}^i is the maximum charge rate (kW) of the i^{th} EV charge point. A feasible charging profile is a charging profile which satisfies both plug-in constraints and the state of charge condition, i.e. $SOC_i(M) = SOC_{\text{max}}^i$ [58]. The following are also defined:

1. Aggregate non-EV base load at time k is given by:

$$b(k) := \sum_{j=1}^N h_j(k). \quad (3.4)$$

2. Aggregate non-EV base load profile is defined as:

$$b^T := [b(1), b(2), \dots, b(M)]. \quad (3.5)$$

3.2.2 Plug-in Constraints

The ratings of both the EV charge point and vehicle battery impose constraints on the feasible charge rates which can be drawn from the charging socket by each EV. These are described in the following. For the i^{th} EV, the maximum charge rate is denoted by c_{max}^i . Considering the charging rate over the course of the full M time slots and noting that charging can only take place when the EV is plugged in and not already fully charged, the constraints are given as follows:

$$\text{If } \tau_{\text{in}}^i \leq k \leq \tau_{\text{out}}^i, \quad 0 \leq c_i(k) \leq c_{\text{max}}^i, \quad (3.6)$$

$$\text{If } k \leq \tau_{\text{in}}^i, k \geq \tau_{\text{out}}^i, \text{ or } SOC_i(k) = 100\%, \quad c_i(k) = 0. \quad (3.7)$$

3.2.3 Power System Constraints

Some of the charging scenarios considered in the thesis explicitly take account of constraints on power system transformer loading levels and voltage profiles. The total loading conditions for each transformer $P_{\text{sub}}^r(k)$, $r \in \underline{S}^0$ at each time slot k is inspected, and the voltage for each connected node $V_i(k)$ is used to evaluate the voltage level at each sample step. In this context, the power flow for the r^{th} transformer can be expressed as:

$$P_{\text{sub}}^r(k) = \sum_{j \in \Phi_h^r} h_j(k) + \sum_{i \in \Phi_c^r} c_i(k), \quad \forall r \in \{1, 2, \dots, S\}. \quad (3.8)$$

Accordingly, the total power flow for the main substation is defined as:

$$P_{\text{sub}}^0(k) = \sum_{r=1}^S P_{\text{sub}}^r(k). \quad (3.9)$$

In practice, equations (3.8) and (3.9) would not be evaluated explicitly, rather the relevant power flows would be measured directly at the transformers and would therefore also include distribution system losses. Letting TR_{max}^r denote the maximum power rating for the r^{th} transformer, the power flow constraint can be expressed as:

$$P_{\text{sub}}^r(k) \leq TR_{\text{max}}^r, \quad \forall r \in \underline{S}^0. \quad (3.10)$$

In a similar fashion, defining the minimum acceptable voltage level as V_{min} , the voltage constraint is given by:

$$V_i(k) \geq V_{\text{min}}, \quad \forall i \in \underline{N}. \quad (3.11)$$

While the voltage level can be measured at each charge point, in general for monitoring purposes it only needs to be checked at the end of each phase since this will be the point where voltage violations will occur first.

3.2.4 Types of Optimisation

From a modelling perspective, different desired EV charging behaviours can be expressed as cost functions that need to be optimised. Typically cost functions for EV charging can be divided into two groups. The first are temporally based cost functions $J(C)$ that evaluate actions taken over a period of time. The second are instantaneous cost functions $J(c(k))$ that only consider the current sample step.

In the case of temporal optimisation, which is essentially a scheduling problem, the optimum solution requires a priori knowledge of all relevant parameters over the optimisation

horizon, $k \in \underline{M}$, such that the full charge rate matrix C can be determined, leading to sub-optimal solutions due to the uncertainty surrounding the predicted loads. These problems are typically computationally challenging and do not scale well. Typical temporal optimisation objectives include:

- Minimising the total charging costs for all EVs over the course of all time slots [196].
- Minimising the total energy losses on power transmission lines during EV charging periods [184].
- Minimising the load variance (thereby flattening the load profile) [58],[21].

On the other hand, instantaneous cost functions are defined in terms of the information available at the current sample step, and hence are not subject to the uncertainty associated with load prediction, PEV availability, etc. Also, they are typically more amenable to decentralised implementation than temporal methods. However, as these functions only cater for the conditions at the current sample step, they typically cannot accommodate global or long term objectives. Examples of instantaneous optimisation objectives include:

- Charge rate based fairness [189]. (Here, the objective is to minimise the difference between the charge rates of EVs while distributing the available power among EVs.)
- Price based fairness [48]. (In this case, charging fairness is defined from the perspective of the charging cost. In this problem, we expect the allocated charge rate of each EV to be proportional to the amount of money they would like to pay.)
- Maximising available power utilisation [163]. (Here, utility companies wish to maximise the power delivered to charging EVs.)

3.3 Fairness based EV Charging Strategies

In this section we review the principles of a number of fairness based EV charging algorithms that have been recently proposed in the literature. In Sections 3.3.1 to 3.3.4, we introduce the charging algorithms which are classed as ‘continuous’, that is algorithms that explicitly require that the charge rate of the i^{th} EV can be adjusted continuously to any value in the range $[0, c_{\max}^i]$. The performance of these algorithms will be compared in Section 3.7.2 and 3.7.3. Further, in Section 3.3.5 and 3.3.6 we review the mechanisms of two on-off based EV charging strategies, where we require that the charge rate of the i^{th} EV can only adopt one of two values, 0 or c_{\max}^i . We shall compare the performances of both algorithms in Section 3.8.

3.3.1 Uncontrolled Charging Strategy

Uncontrolled charging, also known as uncoordinated charging or dumb charging, is where each EV begins charging at the maximum rate once it is plugged in, and continues charging at this rate until fully charged. The negative consequences of this approach for grid operation have been highlighted in many studies, see for example [32] and [163]. In the worst case scenario, if all EVs start to charge during peak load hours, then peak power requirements will be increased significantly and local distribution networks will likely be overloaded. This charging strategy can be viewed as the solution to the following temporal optimisation problem:

$$\max_C \sum_{k=1}^M \sum_{i=1}^N SOC_i(k) \quad (3.12)$$

subject to: Plug-in constraints

3.3.2 Decentralised AIMD Algorithm

The basic idea of AIMD was originally applied in the context of network communication for providing a fair congestion control scheme to support best-effort traffic in the Internet [218]. To date, this idea has been greatly explored in the network communication community; for many novel protocols and applications see [19, 33, 99, 104, 176, 178, 179, 212]. The AIMD approach was first proposed in [189] in developing a charging context to distribute available power between customers in a variety of user oriented charging scenarios (e.g. domestic, workplace, motorway service station, shopping mall and parking area charging). In the domestic charging scenario, each active EV charge point executes the basic decentralised AIMD algorithm defined in Algorithm 1.

Comment: In practice some distributed/decentralised algorithms (e.g. AIMD) can be implemented in an iterative fashion with different sampling interval (rather than ΔT) during each time slot k . The interval of each algorithm iteration depends on the computational capabilities of the EV charge points and the technologies of the communication infrastructures. For practical implementation of the algorithms, we could further discretise each time slot k into T same clock periods (each of length Δt), indexed by $t \in \{1, 2, \dots, T\}$. Thus, for these algorithms EV charge rates will be adjusted at every (shorter) time slot t and the EV charging constraints need to be satisfied at time slot t as well. We shall expect that at the end of the iteration of each time slot k , the algorithm could approximately converge (due to numerical approximation) to a solution that equivalents to the optimal solution calculated by a centralised based approach.

Algorithm 1 Basic Decentralised AIMD Charging Algorithm

```

1: while battery not charged, at every time slot  $k$  do
2:   for each  $t \in \{1, 2, \dots, T\}$  do
3:     if capacity event then
4:       generate uniform random number,  $p \in [0, 1]$ 
5:       if  $p < p_i$  then
6:          $c_i(t+1) = \beta^{(1)} c_i(t)$ 
7:       else
8:          $c_i(t+1) = \beta^{(2)} c_i(t)$ 
9:       end if
10:    else
11:       $c_i(t+1) = \min(c_{\max}^i, c_i(t) + \alpha \Delta t)$ 
12:    end if
13:  end for
14: end while

```

In Algorithm 1 α is an additive constant value in kW/s; $\beta^{(1)}$ and $\beta^{(2)}$ are multiplicative constants. During operation each EV charge point additively increases its charge rate until a ‘‘capacity event’’ occurs at which point it applies a multiplicative constant to decrease its charge rate. The multiplicative constants $\beta^{(1)}$ and $\beta^{(2)}$ are chosen by the i^{th} charge point with probability p_i and $1 - p_i$ respectively. A capacity event is deemed to have occurred when the total power demanded by all active EV charger points exceeds the maximum available power that can be provided for charging, that is at each time slot k :

$$\sum_{i=1}^N c_i(t) \geq P_{\text{av}}^{\text{EV}}(k), \forall t \in \{1, 2, \dots, T\} \quad (3.13)$$

In the decentralised AIMD framework proposed in [189] the capacity event condition (3.13) is monitored by a central monitoring station server at the main distribution network substation which broadcasts a message to the charge points when events occur. Thus, the decentralised AIMD approach assumes a simple radial communication topology, as depicted in Figure 3.2, with each EV charge point equipped with a communication device that is able to receive signals broadcast by the central monitoring station.

The key characteristic of the basic AIMD charging algorithm is that it guarantees an equitable ‘average’ distribution of the available power between active EV charge points if each charge point chooses the same α , $\beta^{(1)}$, $\beta^{(2)}$ and p_i parameters [178]. The elegance of the approach is that it achieves this desirable property while requiring a minimum of communication infrastructure and only limited computing capabilities on each EV. In addition, the simple communication topology and minimal communication bandwidth make it a highly

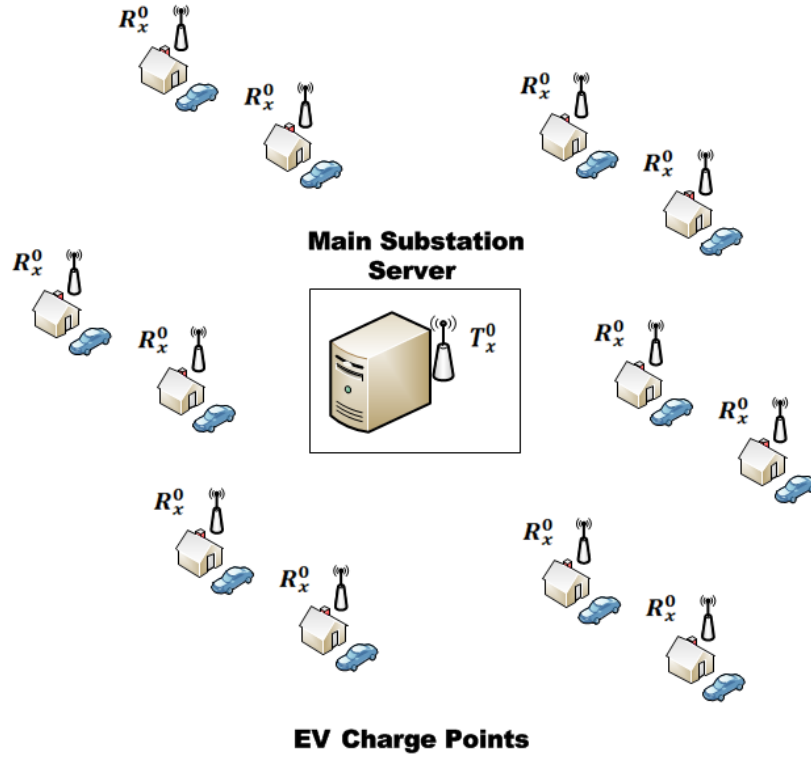


Fig. 3.2 Decentralised AIMD smart charging communication topology

scalable and cost effective solution [99, 116]. In this context, the fair AIMD charging algorithm can be thought of as providing an approximate distributed solution to the following optimisation problem:

$$\begin{aligned}
 & \min_{c(k)} \sum_{i=1}^N [c_i(k) - \frac{1}{N} \sum_{i=1}^N c_i(k)]^2 \\
 & \text{subject to: } \left\{ \begin{array}{l} \sum_{i=1}^N c_i(k) = P_{av}^{ev}(k), \forall k \in \underline{M} \\ \text{Plug-in constraints} \\ \text{Power system constraints (enhanced)} \end{array} \right\} \quad (3.14)
 \end{aligned}$$

3.3.3 Distributed Price Feedback Algorithm

In this section, we introduce the basic idea of the DPF algorithm proposed in [48]. After that we show how the algorithm can be modified to fit the mathematical framework considered in Section 3.2. At the beginning of the EV charging process, each EV owner provides a Willingness To Pay (WTP) parameter, $\omega_i > 0$, that is used to determine their charge rate. In general, the larger ω_i the more charge a vehicle can expect to receive, and in the absence

of power system or plug-in constraints available power is distributed proportionally to ω_i . During every time slot k , the price signal $E(t)$ in this algorithm is then defined as:

$$E(t) = f\left(\sum_{i=1}^N c_i(t)\right), \forall t \in \{1, 2, \dots, T\} \quad (3.15)$$

where $f(x)$ is given by

$$f(x) = a\left(\frac{x}{P_{av}^{ev}(k)}\right)^d \quad (3.16)$$

where a and d are both positive constants.

Each EV i is associated with a utility function $\mu_i(x)$ with respect to the charging demand x at each charging time slot. $\mu_i(x)$ is a non-decreasing function to achieve proportional fair pricing defined as:

$$\mu_i(x) = \omega_i \log(x) \quad (3.17)$$

Hence, our objective is that each EV charge point chooses $c_i(t)$ to maximise its net profit:

$$\mu_i(c_i(t)) - c_i(t)E(t) \quad (3.18)$$

According to [48], the i^{th} EV charge point adapts its charge rate using the following equation to maximise the above utility function:

$$c_i(t+1) = c_i(t) + \gamma_i(\omega_i - c_i(t)E(t)) \quad (3.19)$$

Here γ_i is a parameter that controls the rate of convergence of the algorithm. The charge rate of each EV is updated according to the feedback pricing signal $E(t)$ and its WTP parameter ω_i . The mechanism for implementation of the basic DPF algorithm is illustrated as follows.

Algorithm 2 Distributed Price Feedback Charging Algorithm

```

while battery not charged, at every time slot  $k$  do
  for each  $t \in \{1, 2, \dots, T\}$  do
    Send  $c_i(t)$  to the central infrastructure
    Get  $E(t)$  from the central infrastructure
    Update  $c_i(t)$  using (3.19)
  end for
end while

```

This strategy can be used to provide a distributed solution similar to solving the following optimisation problem:

$$\begin{aligned} \min_{c(k)} \quad & \sum_{i=1}^N \left[\frac{c_i(k)}{\omega_i} - \frac{1}{N} \sum_{i=1}^n \omega_i \cdot c_i(k) \right]^2 \\ \text{subject to:} \quad & \left\{ \begin{array}{l} \sum_{i=1}^N c_i(k) = P_{\text{av}}^{\text{ev}}(k), \forall k \in \underline{\mathbf{M}} \\ \frac{c_i(k)}{c_j(k)} = \frac{\omega_i}{\omega_j}, \quad \forall i \neq j \in \underline{\mathbf{N}}, \forall k \in \underline{\mathbf{M}} \\ \text{Plug-in constraints (enhanced)} \\ \text{Power system constraints (enhanced)} \end{array} \right\} \end{aligned} \quad (3.20)$$

Comment: The constraint $\sum_{i=1}^N c_i(k) = P_{\text{av}}^{\text{ev}}(k)$ in both (3.14) and (3.20) is considered to avoid trivial solutions. In addition, the power system constraint is not considered in the decentralised AIMD algorithm in [189] and both plug-in constraint and power system constraints are not considered in the DPF algorithm in [48]. However, as a necessary option for the grid, we shall consider these constraints in the proposed enhanced algorithms in Section 3.4. Thus, the enhanced AIMD and DPF could provide approximate solutions to optimisation problems in (3.14) and (3.20) with the included constraints depicted by (enhanced).

3.3.4 Ideal Centralised Instantaneous Charging

In this section, we introduce an ideal centralised instantaneous charging (ICIC) solution based on a hierarchical structure. At sample step k , all charging EVs are required to send their charging requests c_{max}^i to their local transformers. Each local transformer calculates the charge rate for each EV i in the r^{th} area, taking into account the current local capacity $TR_{\text{max}}^r - P_{\text{sub}}^r(k)$, and forwards the power requirements to the main substation. If the total amount of requested power exceeds the available power, the main substation $TR(0)$ allocates the available power to each substation in proportion to the requested values. Each substation then updates their EV charge rates accordingly and broadcasts the information to the charge points. This strategy is feasible for solving the following optimisation problem.

$$\begin{aligned} \min_{c(k)} \quad & \sum_{i=1}^N \left[c_i(k) - \frac{1}{N} \sum_{i=1}^N c_i(k) \right]^2 \\ \text{subject to:} \quad & \left\{ \begin{array}{l} \text{Plug-in constraints} \\ \sum_{i=1}^N c_i(k) = P_{\text{av}}^{\text{ev}}(k), \forall k \in \underline{\mathbf{M}} \\ P_{\text{sub}}^r(k) \leq TR_{\text{max}}^r, \forall r \in \underline{\mathbf{S}} \end{array} \right\} \end{aligned} \quad (3.21)$$

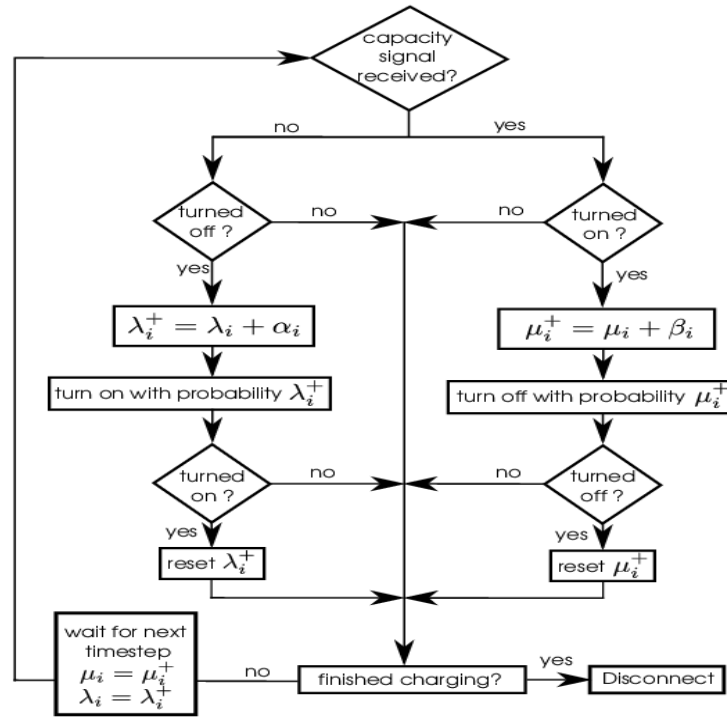


Fig. 3.3 Flow chart of the distributed charging algorithm

Note: Voltage constraints are not considered within this formulation for the sake of simplicity.

3.3.5 Distributed On-Off Charging

In this section, we consider a distributed on-off based EV charging algorithm that has been recently proposed in [192]. The algorithm, based on a learning automation method, is used to control the operation of a fleet of EVs connected to on-off type chargers in order to maximise the utilisation of the available power. To this end, an ergodic Markov Chain based distributed control system is formulated to analyse the charging dynamics of each EV. Depending on whether a congestion signal is received or not, each EV can automatically turn on or turn off its charging according to the determined probability at each time step. This algorithm has been demonstrated to be capable of converging to a fair allocation of available power for EV charging. The flow chart of this distributed charging algorithm is depicted in Figure 3.3. In this algorithm, μ_i , μ_i^+ and β_i are the parameters for the turn-off phase and λ_i , λ_i^+ and α_i are for the turn-on phase. For a detailed description of the algorithm, please refer to [192].

3.3.6 Centralised On-Off Charging

The centralised charging algorithm proposed here is partly inspired by the optimal EV charging algorithm in [164], where a linear programming technique is employed to solve the optimisation problem. Here, a similar framework is applied which is adapted to deal with binary control actions. A technique based on MILP is employed to maximise the available power utilisation while satisfying grid constraints. The voltage deviations at each node are calculated at each time step by using voltage sensitivity analysis. Hence, the voltage constraint for EV charging point i at time step k in (3.11) becomes

$$\mu_i c_i(k) + \sum_{j=1; j \neq i}^N \mu_{ji} c_j(k) + V_i(k) \geq V_{\min}. \quad (3.22)$$

Here, μ_i represents the voltage sensitivity at i^{th} charge point due to an EV charging at charge point i and μ_{ji} is the sensitivity of charge point i to an EV charging at charge point j [164]. Let A be a $N \times N$ voltage constraint matrix containing μ_i in the diagonals and μ_{ji} as off diagonal elements. Then a MILP optimisation problem incorporating the voltage constraint can be defined as [164]:

$$\begin{aligned} \max_x \quad & e^T x \\ \text{subject to:} \quad & Ax \leq d \end{aligned} \quad (3.23)$$

where $x \in \mathbb{R}^N$ is the state of the EVs with entries either 0 or 1 representing the off and on state, respectively, of each EV. $e \in \mathbb{R}^N$ is a coefficient vector with all one entries. $A \in \mathbb{R}^{N \times N}$ is the voltage sensitivity matrix. $d \in \mathbb{R}^N$ is the vector with the maximum voltage deviation from the current node voltage to the corresponding voltage limit. These matrices are then augmented to also include the phase load constraint and transformer loading constraints as specified in (3.10).

3.4 Enhanced Charging Strategies

The distributed EV charging algorithms outlined above do not take into account any power system constraints. However, as previously explained, maintaining these grid constraints is critical to meeting consumer power quality guarantees and ensuring the state and reliable operation of the power grid. Therefore, we adapt the distributed algorithms to react to violations of these constraints in this section. It should be remarked that, due to the similarities in applying the enhancement methods to different distributed algorithms, as an example, we shall only elaborate our enhancement approaches to the basic AIMD algorithm. However,

the enhanced performance of different algorithms other than AIMD, i.e., enhanced DPF (EnDPF) and enhanced distributed on-off Charging, are also summarised in Sections 3.7 and 3.8 respectively.

In addition, we introduce a heuristic method to regulate the available power in response to a varying electricity price to affect a shift in EV loads away from periods of high demand, thereby reducing peak-power capacity requirements and ultimately the costs to the consumer. The overall objective for the enhanced charging strategies is to achieve benefit for both utilities and customers with all EVs sharing the maximum amount of available power fairly while ensuring that the distribution network continues to operate within acceptable limits.

3.4.1 Communication Topology and Infrastructure Requirements

In order to incorporate power system constraints into the decentralized AIMD charging algorithm in a practical and scalable way a hierarchical communication topology paralleling the topology of the grid is proposed, as shown in Figure 3.4. The complexity of the communication and charger infrastructure required depends on the power system constraints that are taken into account.

At its simplest the AIMD algorithm only requires the broadcasting capability of the main substation sever and the receiving capability of each EV charger as envisaged by [189] and depicted in Figure 3.2. However, equivalently, this can be implemented in a cascaded fashion as shown in Figure 3.4 with the central monitoring station at the main distribution substation relaying its generation capacity event broadcasts to the local distribution substations, which in turn relay the broadcast to the EV charge points in their local area.

An advantage of this hierarchical approach is that it reduces transmitter power requirements and can take advantage of existing communication infrastructure that typically exists on the transmission network. More importantly, it offers the possibility of responding to local infrastructure capacity events such as overloading of a substation transformer. To enable this each substation has to have a local monitoring station (substation server) to receive generation capacity event broadcasts from the central monitoring station (main substation server), detect local infrastructure capacity events and broadcast capacity event information to the charge points in its area. It should be noted that since the AIMD algorithm does not distinguish between capacity event types no modifications are required to the EV charge points to accommodate infrastructure capacity events.

However, this is not the case for line voltage events. Since line voltage issues are inherently local to the user, they cannot be detected at the local substation. Instead they have to be sensed by the individual EV charge points and the information relayed back to the local substation. Therefore, in order to respond to voltage events each EV charger needs to

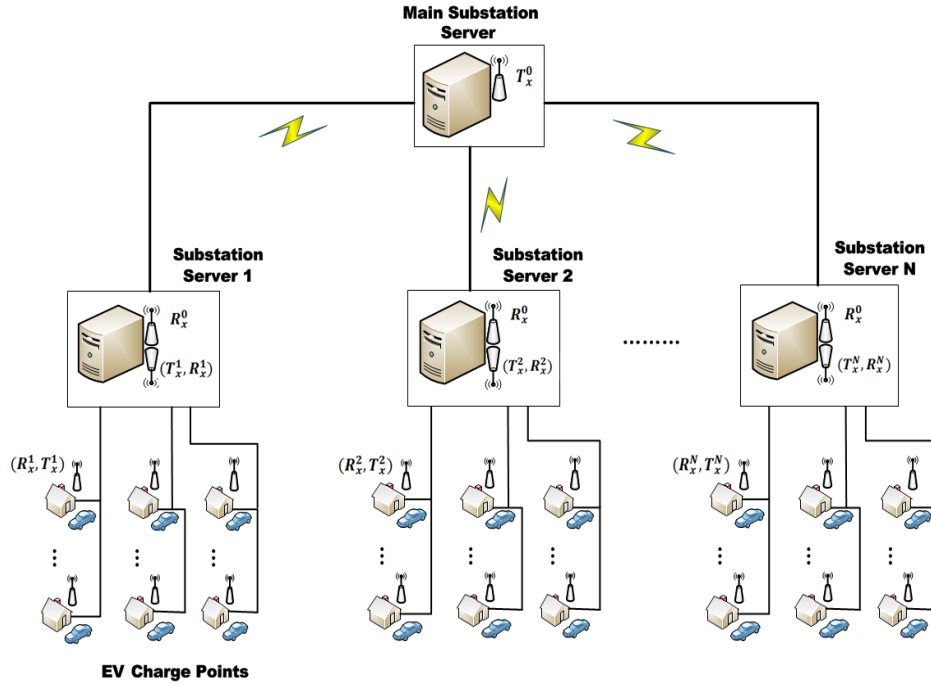


Fig. 3.4 Communication topology for the enhanced AIMD implementation

have the capability to continuously sense its own socket voltage and transmit a voltage event message to its local substation when the voltage drops below an acceptable level.

3.4.2 Enhanced AIMD Charging Strategy

With the appropriate communication and sensing infrastructure in place, as outlined above, the basic AIMD smart charging algorithm running on each charge point can be modified to respond to voltage, infrastructure and generation capacity events as shown in Algorithm 3. Recalling that, $V_i(k)$ is the line voltage of the i^{th} EV charge point at the k^{th} time instant. Here, V_{event} is a threshold voltage level below which a voltage event is triggered and voltage event message transmitted to the local substation server, and $V_{\text{min}} < V_{\text{event}}$ is the minimum acceptable voltage level below which the EV charger enters a protective self regulation mode. The remaining parameters are as defined previously for the basic AIMD implementation.

The local monitoring station for a given area broadcasts a capacity event signal to the active EV charge points in its area if any of the following conditions are satisfied:

- A generation capacity event is broadcast by the main substation.
- A voltage event message is transmitted by any of the charge points in its local area
- A local infrastructure constraint violation is detected (e.g. transformer overload)

Algorithm 3 Enhanced Decentralised AIMD Charging Algorithm

```

while battery not charged, at every time slot k do
  for each  $t \in \{1, 2, \dots, T\}$  do
    if capacity event then
      generate uniform random number,  $p \in [0, 1]$ 
      if  $p < p_i$  then
         $c_i(t+1) = \beta^{(1)} c_i(t)$ 
      else
         $c_i(t+1) = \beta^{(2)} c_i(t)$ 
      end if
    else
       $c_i(t+1) = \min(c_{\max}^i, c_i(t) + \alpha \Delta t)$ 
    end if
    if  $V_i(t) < V_{\text{event}}$  then
      transmits a voltage event message (treated as a local capacity event signal)
    end if
    if  $V_i(t) < V_{\min}$  then (self regulation)
       $c_i(t+1) = 0$ 
    end if
  end for
end while

```

In addition to monitoring infrastructure constraints, the central monitoring station at the main substation is responsible for determining the power available $P_{\text{av}}(k)$ at every time slot k and broadcasting a generation capacity event when $P_{\text{sub}}^0(t) > P_{\text{av}}(k)$, $\forall t \in \{1, 2, \dots, T\}$.

Compared to the basic AIMD EV charging strategy, the enhanced AIMD (EnAIMD) implementation offers greater protection to the grid infrastructure and optimum usage of available power. For example, if one of the local transformers is overloaded but overall generation capacity is not being exceeded at the main substation, the basic AIMD implementation would fail to respond, while the enhanced implementation will decrease only the charge rates of the EVs in the corresponding local area to protect the transformer. The basic AIMD charging solution in these circumstances would require that charge rates of EVs in unaffected areas also be reduced, but this would lead to under utilisation of available generating capacity.

While responding to voltage constraint violations within the AIMD framework adds substantially to the complexity of EV charge point infrastructure the local sensing of voltage at each EV allows a degree of self-regulation/fail-safe mode to be introduced whereby each EV switches off whenever the detected line voltage drops below a minimum acceptable level, V_{\min} , irrespective of whether a capacity event has been received or not. Since severe generation capacity and infrastructure overloading events generally cause significant voltage

issues, this offers a degree of robustness to communication system failures. In practice, this self regulation mode will only rarely be activated provided there is a sufficient margin between V_{\min} and V_{event} .

3.4.3 Price-adjusted Available Power

AIMD is inherently an instantaneous algorithm with no temporal visibility hence it cannot take a longer term view in determining EV charge rates. However, a simple heuristic modification can be introduced to the available power calculation that allows the temporal context to be taken into account in a meaningful way with negligible impact on overall system complexity. The heuristic is to modulate the available power signal $P_{\text{av}}(k)$ with time-of-use pricing information so that an artificial reduction in available power is created at times of high electricity prices, that is,

$$P_{\text{tou}}(k) = P_{\text{av}}(k) - \xi(E(k) - E_{\min}(k)) \quad (3.24)$$

Here ξ is a constant tuning parameter, $E(k)$ (cent/kWh) is the Time-of-Use (TOU) price at time k and E_{\min} is the minimum TOU price during the day. Since the TOU prices reflect the peak demand periods on the grid, this modification essentially drives EV load to off-peak times. To implement price-adjusted AIMD charging the only additional requirement is that TOU pricing be made available to the central monitoring station. Where this information is pre-defined and fixed [169], it can be pre-programmed into the central monitoring station software. Otherwise it can be periodically relayed to the station via a communication link.

3.5 Valley-Filling based Charging Strategies

In this section, we present two typical EV charging strategies, namely optimal decentralised valley-filling charging and centralised load-variance-minimisation charging, aimed at achieving valley-filling for the grid. We give the descriptions of both strategies with regard to our optimisation framework.

3.5.1 Optimal Decentralised Valley-Filling Charging

In [58], Gan *et al.* proposed a novel decentralised temporal optimisation algorithm, namely optimal decentralised valley-filling (ODVF), to optimally schedule EV charging to perform valley filling through an iterative process. It has been shown that the charging profile for each

EV can reach optimality within a few iterations and that the approach provides satisfactory performance and is robust to errors in users' specifications and outdated signals.

In order to minimise the load variance (valley-filling) by the ODVF method, the following is solved:

$$\begin{aligned} \min_C \quad & \sum_{k=1}^M \left[\sum_{i=1}^N c_i(k) + b(k) \right]^2 \\ \text{subject to: } & \left\{ \begin{array}{l} \text{Plug-in constraints} \\ P_{\text{sub}}^0(k) \leq TR_{\text{max}}^0 \\ SOC_i(M) = SOC_{\text{max}}^i, \forall i \in \underline{N} \end{array} \right\} \end{aligned} \quad (3.25)$$

where $b(k)$ denotes the k^{th} element of base load profile b . Please refer to [58] for details of the algorithm implementation.

3.5.2 Centralised Load-Variance-Minimisation Charging

In this case, the optimisation problem is formulated as a quadratic programming problem, the aim of which is to flatten the overall load profile, i.e., valley-filling. Compared to the ODVF method, as defined in Section 3.5.1, this charging strategy, denoted CLVM, gathers all the necessary information from both the grid and EV customers before solving the quadratic optimisation problem, in order to determine the optimal charge rate matrix C before charging commences. Mathematically the optimisation problem is given by equations (3.26) and (3.27) presented below.

$$J(C) = \sum_{k=1}^M (P_{\text{sub}}^0(k) - \overline{P_{\text{sub}}^0})^2 \quad (3.26)$$

where $\overline{P_{\text{sub}}^0}$ is defined as the average power consumption measured at the main transformer over the course of M time slots.

In each case the optimisation problem is defined as

$$\begin{aligned} \min_C \quad & J(C) \\ \text{subject to: } & \left\{ \begin{array}{l} \text{Plug-in constraints} \\ SOC_i(M) = SOC_{\text{max}}^i, \forall i \in \underline{N} \end{array} \right\} \end{aligned} \quad (3.27)$$

where the SOC constraint is necessary to avoid the trivial solution $C = 0$.

3.6 Cost Minimisation based Strategies

In this section, we introduce decentralised and centralised cost minimisation based EV charging strategies for minimising total charging costs of EV customers with respect to a given TOU pricing suggested in [169].

3.6.1 Decentralised Selfish Charging Strategy

In this charging strategy it is assumed that charging is conducted in a decentralised fashion by each EV guided only by TOU pricing information (assumed to be available *a priori*) and plug-in constraints. TOU information motivates EV owners to shift their demands to cheaper price periods. Therefore, in decentralised selfish charging (DSC) each EV optimises its charging schedule in order to meet its charging requirements at the minimum cost with no regard for the impact on the power system. Mathematically the DSC formulation can be viewed as solving the follows optimisation problem:

$$\begin{aligned} \min_{c_i} \quad & \sum_{k=1}^M c_i(k) \cdot \Delta T \cdot E(k), \quad \forall i \in \underline{N} \\ \text{subject to:} \quad & \left\{ \begin{array}{l} \text{Plug-in constraints} \\ SOC_i(M) = SOC_{\max}^i, \forall i \in \underline{N} \end{array} \right\} \end{aligned} \quad (3.28)$$

3.6.2 Centralised Charging Cost Minimisation Strategy

In this section, a centralised charging cost minimisation (CCCM) strategy based on linear programming is proposed to minimise the total cost of charging EVs. Using this method, the charge rate matrix of all EV charge points C is determined at a centralised control centre. Rather than updating the charge rate locally according to some feedback signals (e.g. price signal) at every time slot, centralised approaches are more amenable to fulfilling temporal based objectives (e.g. minimising total charging costs, valley-filling). We assume that at the beginning of the scheduling window, all required information is provided to the optimisation program for computation in the control centre. This information includes the predicted base load b defined in (3.5) and the charging schedule of each EV, i.e., τ_{in}^i and τ_{out}^i .

In this case, the optimisation problem is taken as a centralised scheduling problem to minimise total charging costs. The mathematical formulation can be defined considering the SOC of all EVs, power system constraints and plug-in constraints:

$$\begin{aligned} \min_C \quad & \sum_{k=1}^M \sum_{i=1}^N c_i(k) \cdot \Delta T \cdot E(k) \\ \text{subject to:} \quad & \left\{ \begin{array}{l} \text{Plug-in constraints} \\ \text{Power system constraints} \\ SOC_i(M) = SOC_{\max}^i, \forall i \in \underline{N} \end{array} \right\} \end{aligned} \quad (3.29)$$

Comment: If the power system constraints are omitted, the solution to the optimisation problem defined in (3.29) is mathematically equivalent to the solution of (3.28). Thus, CCCM is an enhancement of DSC since it is not practical to incorporate power system constraints in the DSC method. However, this is at the expense of substantial communication and computation overhead.

3.7 Comparisons of ‘Continuous’ EV Charging Strategies

In this section, the performance of all continuous EV charging strategies are compared in a typical low-voltage distribution network in a residential area. In Section 3.8, the performance of the on-off charging strategies are evaluated in a SME area for another scenario of interest.

3.7.1 Simulation Setup

In order to compare the performance of the different charging strategies in a residential area, a one day simulation was run with ΔT set to 5 minutes and Δt set to 5 seconds. The simulation was conducted on a residential low-voltage distribution network with $S = 3$ and $N = 160$. The houses are distributed evenly across phases with maximum 50% EVs randomly connected in three household areas. The topology of the network is given in Figure 3.1.

This distribution network was modelled and implemented using a custom OpenDSS/ Matlab simulation platform. OpenDSS [44], an open source electric power system Distribution System Simulator, was used to simulate the power system and calculate the instantaneous power flows and voltage profiles for the test network. Matlab was used to simulate typical residential EV connection, SOC and disconnection patterns (randomly generated for each EV) and to create a wrapper programme to simulate the operation of the network over a period of time for varying household and EV loads based on various charging strategies. The main steps performed by the wrapper programme are summarised in Algorithm 4.

Algorithm 4 OpenDSS-Matlab Wrapper Programme for EV Charging Simulation

```

for  $k = 1, 2, \dots, M$  do
  1. Sense the amount of energy available  $P_{av}(k)$ 
  2. Each household generate its current non-EV load,  $h_i(k)$ .
  3. Calculate the available power for EV charging  $P_{av}^{ev}(k)$  (optional)
  for  $t = 1, 2, \dots, T$  do
    4. Determine the set of EVs currently connected to the grid.
    5. For each EV compute its instantaneous charge rate,  $c_i(t)$ , according to the
    selected algorithm.
    6. Generate an updated OpenDSS simulation parameters file.
    7. Call the OpenDSS software to simulate the current state of the distribution
    network.
    8. Record the current values of relevant EV and distribution network states (con-
    nection status, SOC, line voltages, substation power flows etc.)
  end for
end for

```

Comment: The wrapper programme provides an generalised OpenDSS/Matlab simulation platform for implementation of the instantaneous based charging approaches. For instance, the selected algorithms in the fifth step could include AIMD, DPF, ICIC, distributed on-off and their extended versions. Note that temporal based charging approaches (e.g. CCCM and CLVM) are not included here since they require different simulation setups.

Residential power consumption profiles for each scenario were generated based on residential customer smart meter electricity trial data provided by the *Commission for Energy Regulation* (CER) [26] in Ireland. This dataset consists of time series demand data for 4225 residential customers over 536 days, sampled every 30 minutes starting from 15th of July 2009. The non-EV household load profiles for each of the 160 houses in the test network were generated by randomly selecting load profiles from the CER dataset and upsampling them using linear interpolation to the desired sampling interval ΔT . To illustrate this dataset, we consider a typical summer scenario from the period 22nd of July to 24th of July 2009, and a winter scenario from the period 22nd of January to 24th of January 2010. A comparison diagram of the average load consumption for 4225 residential smart meters during both periods is shown in Figure 3.5. As expected this shows that the average power consumption during typical Irish winter days is much higher than during summer days. In particular, the peak power consumption during the three winter days is more than 50% greater than the summer peaks. In our simulation study we consider a typical winter day scenario for better illustration of the performance of the algorithms. The average non-EV household load consumption in each of our charging scenarios is illustrated in Figure 3.6.

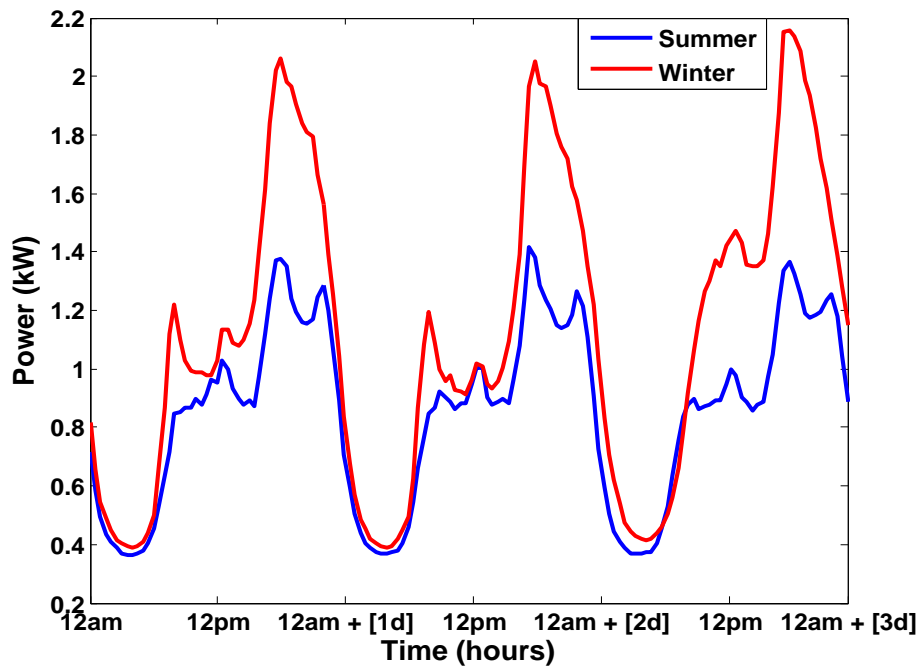


Fig. 3.5 Average summer and winter residential power consumption profiles in Ireland as computed from smart meter trial data of 4225 customers [26]

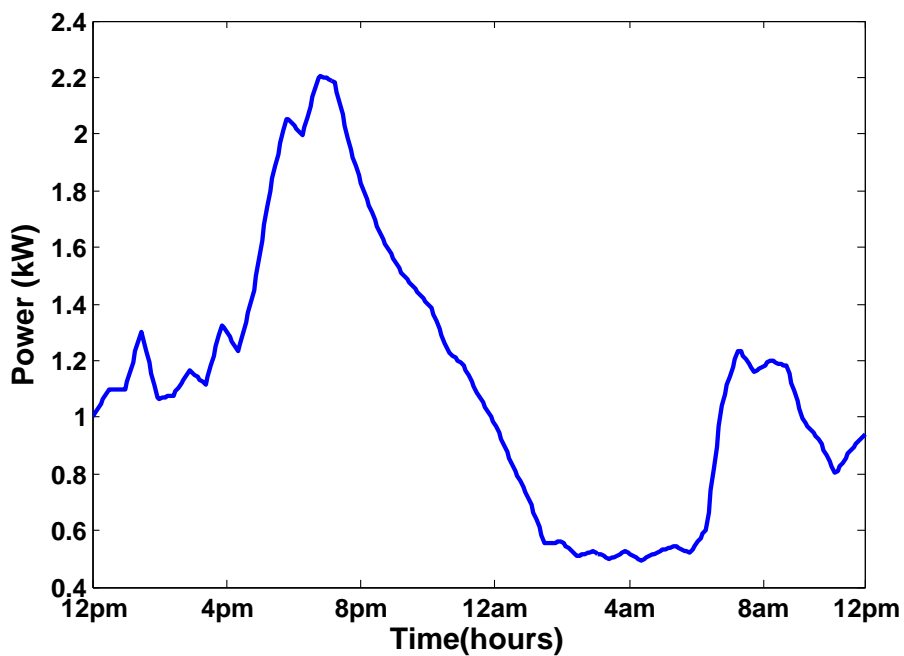


Fig. 3.6 Average residential power consumption profiles for 160 customers on January 23rd 2010 [26]

The assumptions on EV travelling patterns, and hence SOC and plug-in/out probability distributions, were taken from [36]. For EV connection patterns, we assume that EVs arrive home and connect to the charge points between 4pm-7pm (21% of all daily journeys in Irish Urban area) with the following time distribution: 4pm-5pm (33%), 5pm-6pm (38%), 6pm-7pm (29%). Similarly, for EV disconnection patterns, we assume that most of them depart from home between 7am and 10am (19% of all daily journeys in Irish Urban areas) with the following time distribution: 7am-8am (21%), 8am-9am (47%), 9am-10am (32%). The battery capacity for each EV was assumed to be 20kWh and the initial energy required for each EV was normally distributed. The mean of the distribution was set to 10kWh and the standard deviation was chosen as 1.5kWh. This means 99.9% of the EVs require between 5kWh and 15kWh and 81.8% require between 8kWh and 12kWh to fully charge their batteries. For comparison purposes, the same plug-in/out and SOC values were used with each method considered. It was assumed that all EVs charged overnight and that once an EV was plugged in it only physically plugged out at the scheduled plug-out time.

Several assumptions are also made with regard to EVs and residential EV charging infrastructure, which are consistent with previous studies in [164, 189]. The assumptions are as follows.

1. The nominal voltage of each EV charge point is set at 230V.
2. The maximum power output from the EV home charger cannot exceed 3.7kW.
3. The maximum available power can be provided from the grid is 400kVA.
4. Each EV has the ability to adapt its charge rate in real-time and continuously.
5. Power flow for EV charging is unidirectional from grid to vehicle (i.e. vehicle-to-grid is not considered).

We now present a comparison of the listed charging strategies grouped according to their different characteristics as follows:

1. Uncoordinated charging strategy
2. Fairness based (continuous chargers) strategies : AIMD, DPF, EnAIMD, EnDPF and ICIC and their TOU price adjusted extensions
3. Cost minimisation strategies: DSC and CCCM
4. Valley-Filling strategies: ODVF and CLVM

3.7.2 Evaluation of the Uncoordinated Charging Strategy

As already noted in Section 3.3.1, uncontrolled charging is where each EV is charged at its maximum rate once it is plugged in and continues charging at this rate until it is fully charged. In this section, different penetration levels of EVs on the network were examined to evaluate the impact of uncontrolled charging on both the power grid and customers. As shown in Figure 3.7, the minimum non-EV voltage on all buses during the peak-periods was found to be 0.9538pu (219.36Volts). With uncontrolled EV charging coinciding with peak-power several bus voltages drop below 0.95pu (the minimum accepted voltage on the grid), with the minimum voltage found to be 0.9151pu around 7pm.

The power flow at the substation and all local transformers are marginally overloaded during peak times as a result of EV charging in the case of 10% EV penetration, as can be seen in Figure 3.8. In the case of 50% EV penetration, maximum loading occurs around 8pm and exceeds the available power by 43.56%. Thus, for our test distribution network, uncontrolled charging at 50% EV penetration cannot be supported.

3.7.3 Evaluation of Continuous Fairness based Charging Strategies

In this section, the performance of the different fairness based charging strategies is discussed. In the DPF method, the WTP parameter was chosen to be 1, 2 or 3 randomly (with same probability) by each EV. In the case of the ICIC algorithm, results are presented only for the implementation without the voltage limitation condition. For all methods, the utility regulatory factor ξ in equation (3.24) was set to 10 so that only limited available power can be accessed during peak times. The resultant power and voltage profiles, and the profile of the loading of the second transformer are presented in Figures 3.9, 3.10, and 3.11, respectively.

The results show that both AIMD and DPF provide a good approximation to the ideal solution, and as such are competitive alternatives to the ideal solution given the substantially reduced communication overhead associated with their distributed implementation. DPF has the advantage that by using its price-feedback approach it is able to provide users with a charge rate proportional to their WTP in their local area (local fairness is maintained at each given time instance), which is demonstrated in Figure 3.12. The averaged charge rate obtained by DPF method for EVs connected in a given area (TR(2)) was calculated as 0.94kW, 1.42kW and 1.76kW by means of slow (WTP = 1), normal (WTP = 2) and fast charging (WTP = 3), respectively. It should be mentioned that the average charge rate for the different EVs is not necessarily proportional to their WTP parameters, due to the impact of local power system and charging infrastructure constraints. Further results for all scenarios

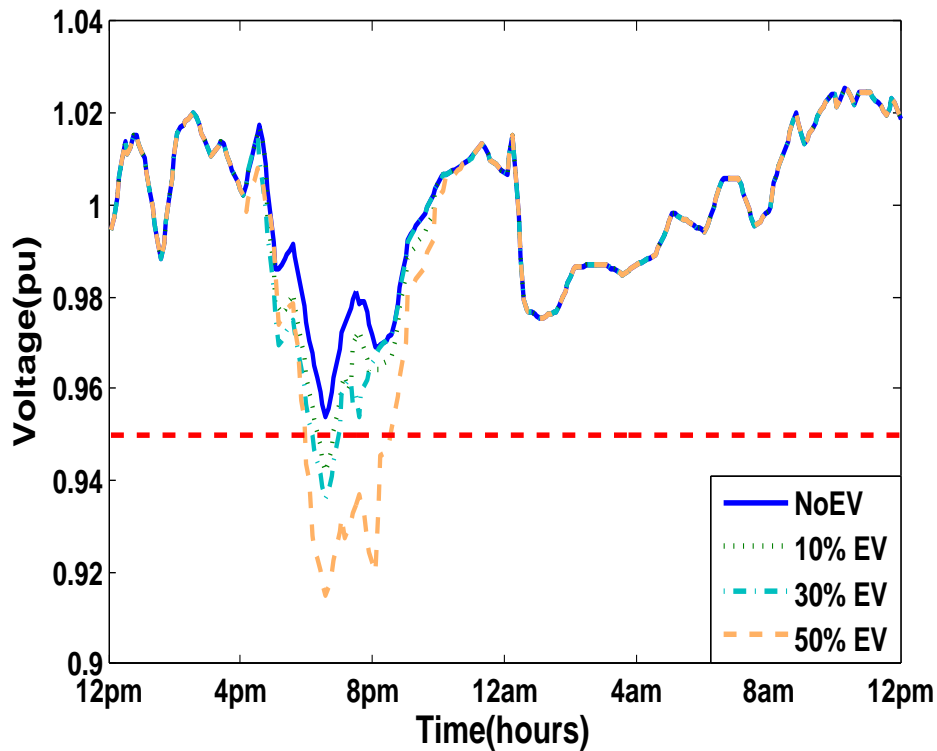


Fig. 3.7 Comparison of the minimum voltage profiles with different levels of EV penetration using uncontrolled charging. Red dashed line marks the minimum acceptable voltage level on the network.

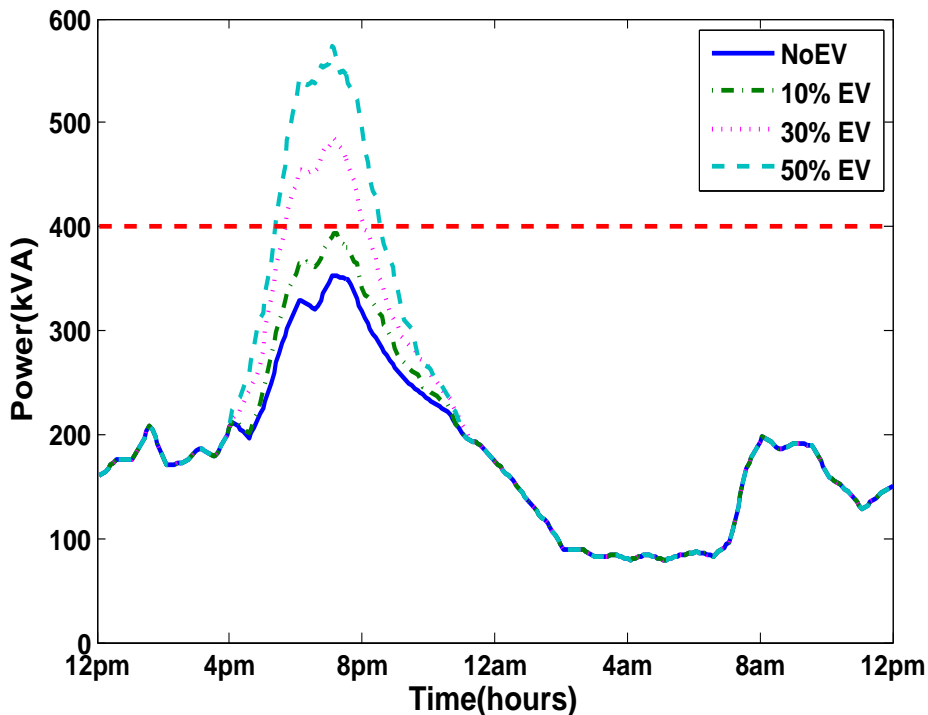


Fig. 3.8 Comparison of the power consumption at the main substation with different levels of EV penetration using uncontrolled charging. Red dashed line marks the maximum available power from the grid.

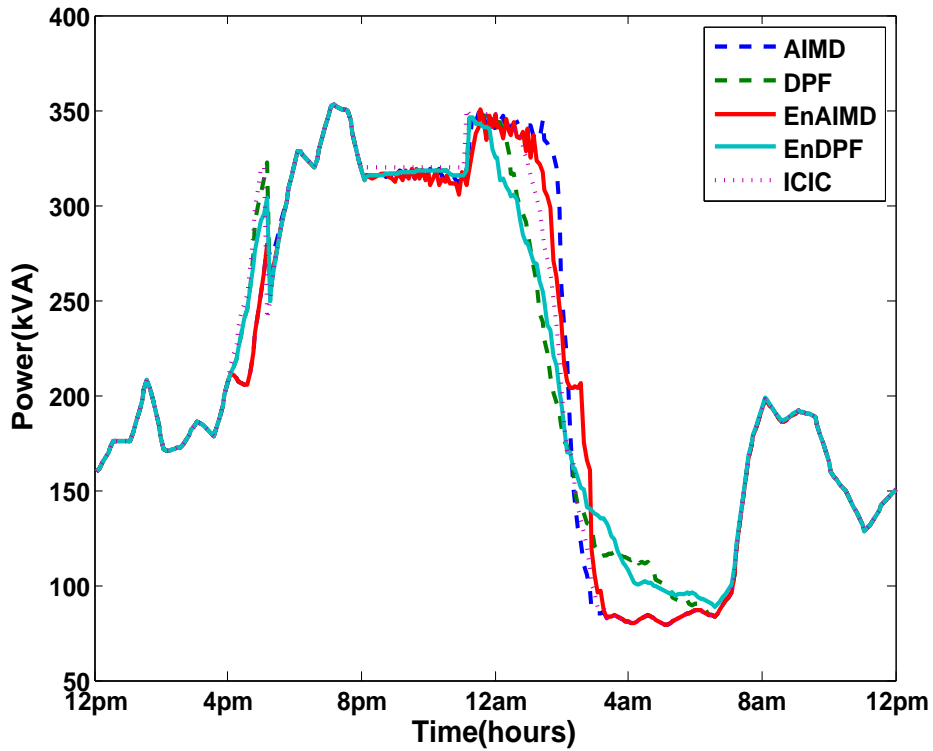


Fig. 3.9 Comparison of the power consumption at the main substation with different charging strategies.

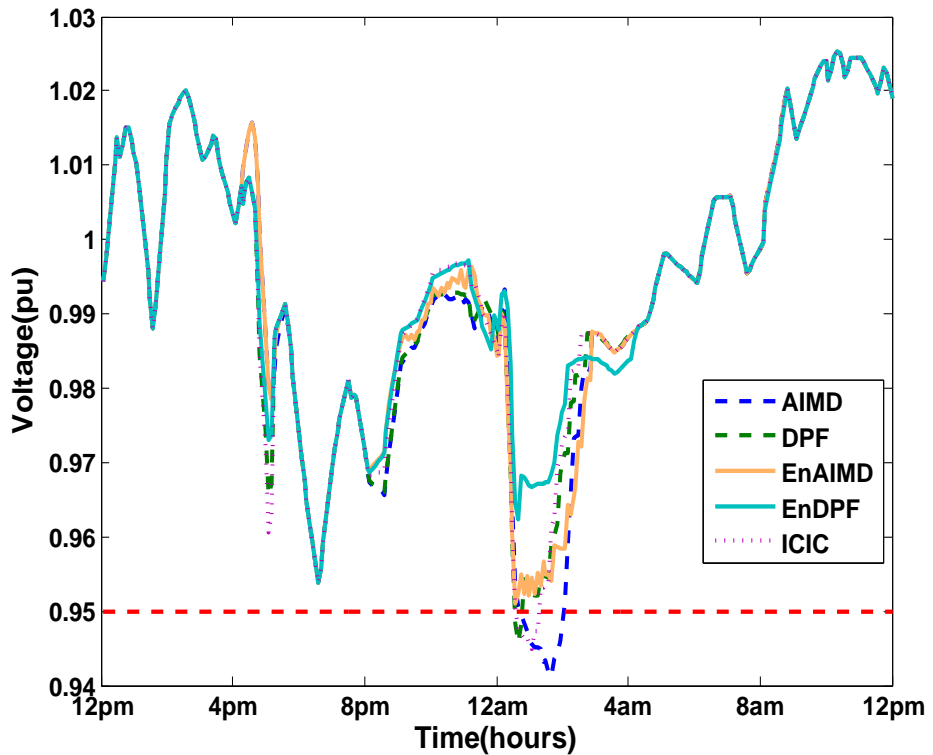


Fig. 3.10 Comparison of the minimum voltage profile with different charging strategies. Red dashed line marks the minimum acceptable voltage level on the network.

considered in this section, including the scenarios without price-adjusted available power, are summarised in Table 3.1. This will be discussed in Section 3.9.

3.7.4 Evaluation of Cost Minimisation Strategies

In this section, the two charging strategies designed to minimise charging costs, namely DSC and CCCM, are applied to the distribution network with 50% EV penetration and TOU pricing as given in Figure 3.13. Simulation results show that DSC, which has no regard for power system constraints, violates local transformer loading constraints even if EV charging is delayed to off-peak times (around 12am), while 50% EV penetration can be comfortably accommodated on the network with CCCM, as shown in Figure 3.14 and the transformer loading indexes reported in Table 3.4. However, CCCM needs to gather information from EVs and also from the power grid, hence it has substantial scalability issues compared to DSC.

3.7.5 Evaluation of Valley-Filling Charging Strategies

For the following simulations, a simplification is made by assuming that all EVs share a common plug-out time of 6am. As can be seen in Figure 3.15 and Table 3.4, the performance of the ODVF method, when it is allowed a number of iterations (e.g. 20 algorithm iterations in this case), is comparable to that of CLVM. Most significantly, the ODVF method gives a significant reduction in computation time compared to the CLVM method as illustrated in Tables 3.2 and 3.3. These times are calculated using quadprog in Matlab using a Dell Computer with a Win7 64bits operation system (RAM: 6GB, CPU: Inter(R) Core(TM) i7-2600, 3.4GHz). Thus it is easy to observe the significant advantages of applying the ODVF method versus the CLVM method from the perspective of computation times.

The performance of the ODVF method was also evaluated from the perspective of the Mean Square Error (MSE) between the iterative load profile and the optimal aggregated load profile using the CLVM method. In particular, Figure 3.16 illustrates that the ODVF method is capable of achieving 90% of the CLVM based optimum within 6 iterations.

3.8 Comparisons of On-Off EV Charging Strategies

In this section, we consider a SME scenario where on-off EV charging strategies are implemented in a low-voltage distribution network. This scenario is attractive since it can be used to represent a typical working area, for instance, a certain number of EVs are charging in

Table 3.1 A comparison of simulation results for various EV charging strategies (50% EV penetration)

Strategies	Ave ^a Time(h)	Std ^b Time(h)	Min ^c Time(h)	Max ^d Time(h)
NoEV	n/a	n/a	n/a	n/a
Uncontrolled	2.80	0.38	1.83	3.83
AIMD	7.53	0.88	5.42	9.17
AIMD(P) ^e	8.34	1.05	5.92	10.08
EnAIMD	7.89	1.63	4.58	10.83
EnAIMD(P)	8.56	1.29	5.83	11.00
DPF	7.86	1.84	4.42	11.42
DPF(P)	8.71	1.81	5.00	12.33
EnDPF	8.00	2.42	3.92	14.50
EnDPF(P)	9.19	2.02	5.83	14.58
ICIC	7.41	1.11	4.67	9.25
ICIC(P)	8.24	1.10	5.67	10.08

^a Average charging time ^b Standard derivation of charging time

^c Minimum charging time ^d Maximum charging time

^e (P) for price-adjusted available power

Strategies	Ave costs ^f (cents/kWh)	Ave rate ^g (kW)	Min Volt ^h (pu)	Max TR ⁱ Loading (%)	Overload ^j Duration(h)
NoEV	n/a	n/a	0.954	112.93	2.25
Uncontrolled	22.32	3.70	0.915	177.68	14.83
AIMD	13.36	1.38	0.940	122.49	9.33
AIMD(P)	11.21	1.25	0.941	113.92	6.58
EnAIMD	12.74	1.36	0.953	112.93	2.75
EnAIMD(P)	11.18	1.23	0.950	112.93	2.25
DPF	13.93	1.36	0.946	122.17	9.33
DPF(P)	11.30	1.22	0.947	113.91	5.83
EnDPF	13.63	1.35	0.953	112.93	5.17
EnDPF(P)	11.22	1.16	0.954	112.93	2.33
ICIC	13.84	1.41	0.951	124.47	9.92
ICIC(P)	11.20	1.27	0.945	116.01	5.75

^f Average EV charging costs ^g Average EV charging rate

^h Minimum voltage on the grid ⁱ Maximum percent of the transformer loading level

^j Duration for transformers overloading

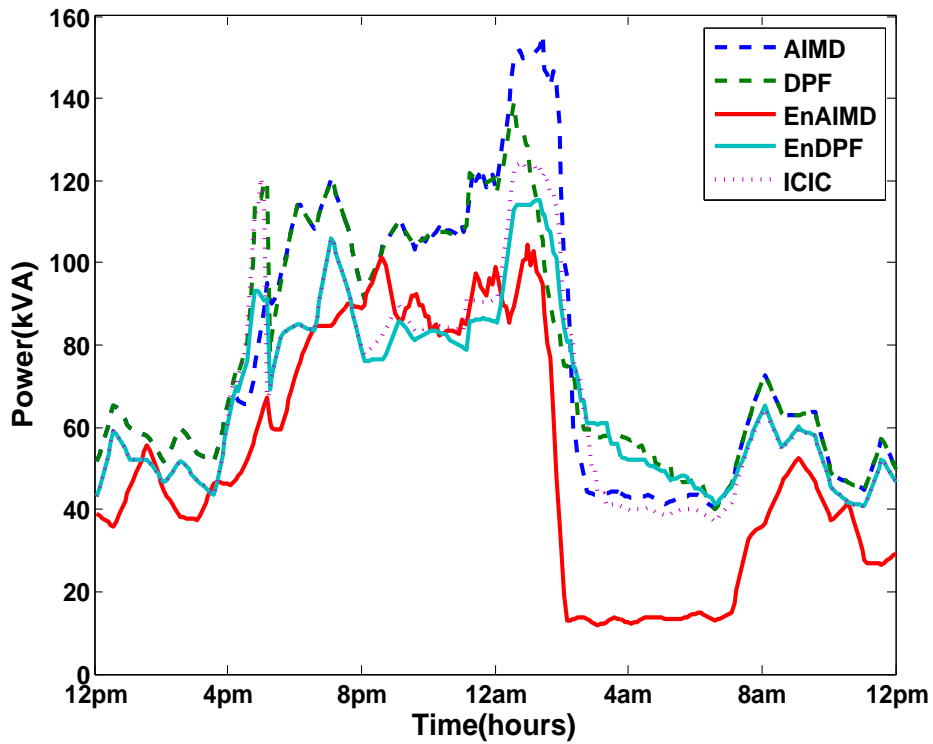


Fig. 3.11 Comparison of the loading conditions on transformer TR(2) with different charging strategies

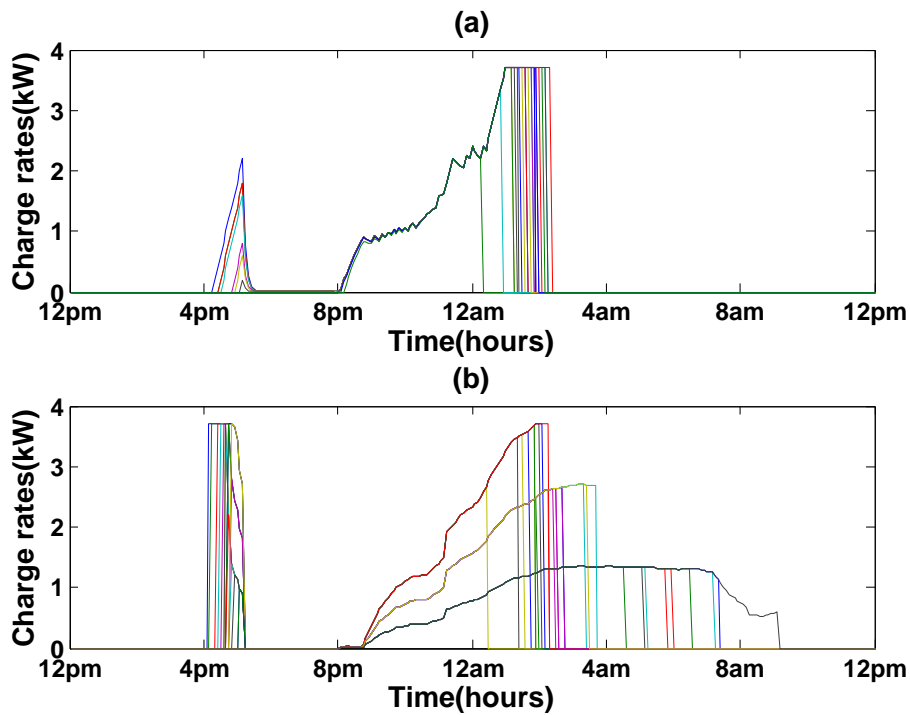


Fig. 3.12 Comparison of the charge rates in the same area [both connected to TR(2)] (a) Enhanced AIMD charging with price adjusted available power (b) Enhanced DPF charging with price adjusted available power

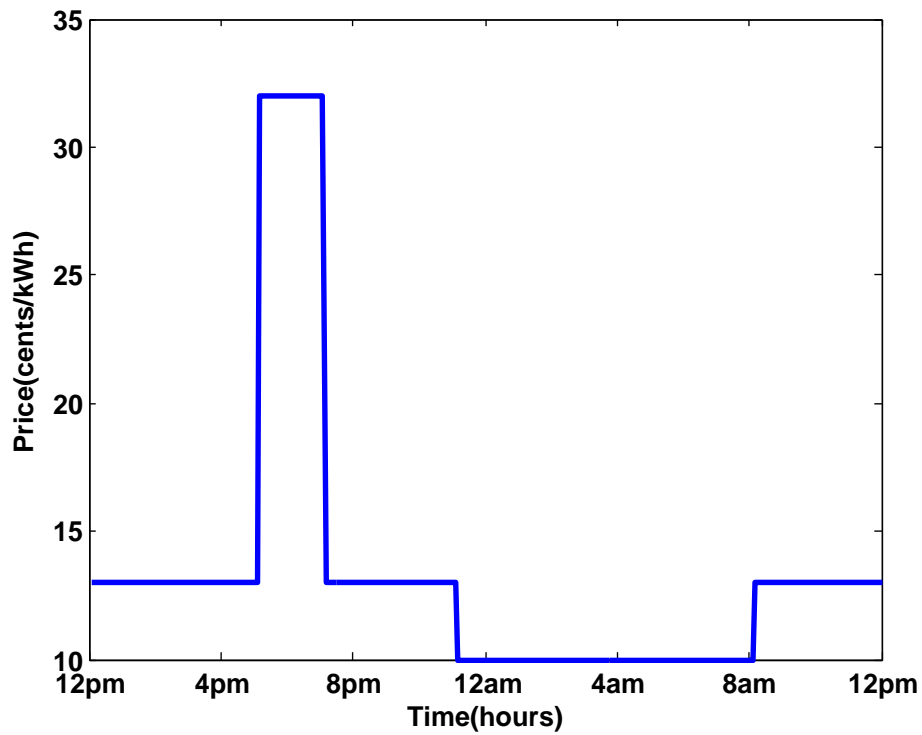


Fig. 3.13 Diagram of the TOU electricity price

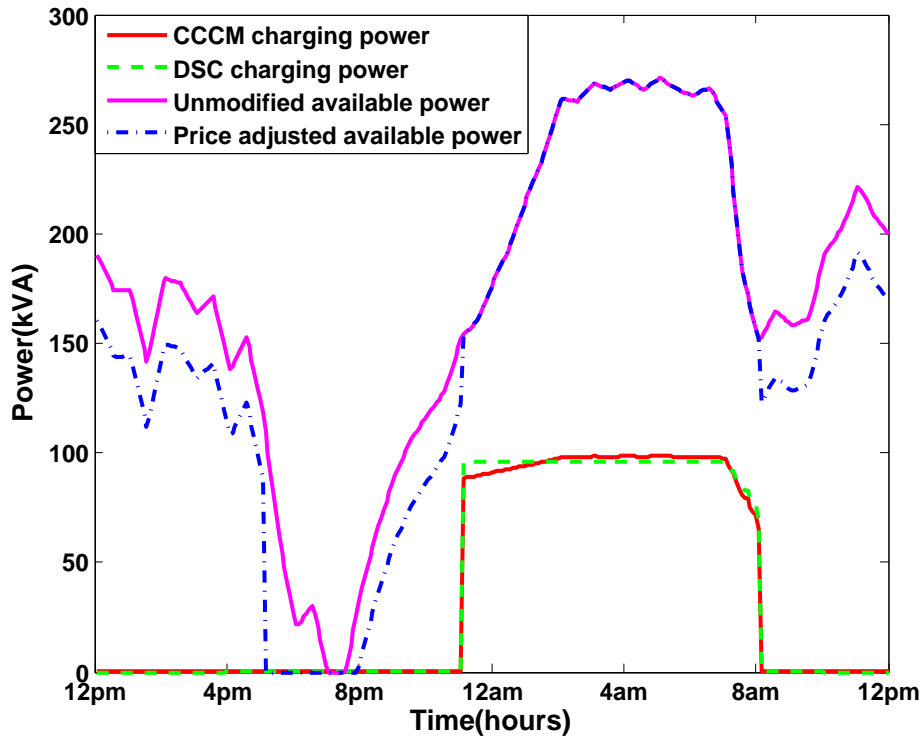


Fig. 3.14 Comparison of the EV load when using CCCM and DSC with the price adjusted available power modification

Table 3.2 ODVF computation time for different iteration counts (50% EV penetration).

ODVF	5	10	15	20
Time(s)	6.08	11.41	16.96	22.79

Table 3.3 CLVM computation times with different levels of EV penetration.

CLVM	10%	20%	30%	40%	50%
Time(s)	20.87	104.72	236.02	789.23	2105.78

Table 3.4 A comparison of simulation results for various temporal based EV charging strategies (50% EV penetration)

Strategies	Ave ^a Time(h)	Std ^b Time(h)	Min ^c Time(h)	Max ^d Time(h)
NoEV	n/a	n/a	n/a	n/a
ODVF	7.31	0.74	5.92	8.58
CLVM	7.31	0.74	5.92	8.58
DSC	8.88	0.26	7.92	9.00
CCCM	8.89	0.27	7.92	9.00

^a Average charging time ^b Standard derivation of charging time

^c Minimum charging time ^d Maximum charging time

Strategies	Ave costs ^e (cents/kWh)	Ave rate ^f (kW)	Min Volt ^g (pu)	Max TR ^h Loading (%)	Overload ⁱ Duration(h)
NoEV	n/a	n/a	0.954	112.93	2.25
ODVF	10.46	1.36	0.958	112.93	2.25
CLVM	10.46	1.36	0.958	112.93	2.25
DSC	10.00	1.13	0.954	112.93	2.61
CCCM	10.00	1.11	0.954	112.93	2.25

^e Average EV charging costs ^f Average EV charging rate

^g Minimum voltage on the grid ^h Maximum percent of the transformer loading level

ⁱ Duration for transformers overloading

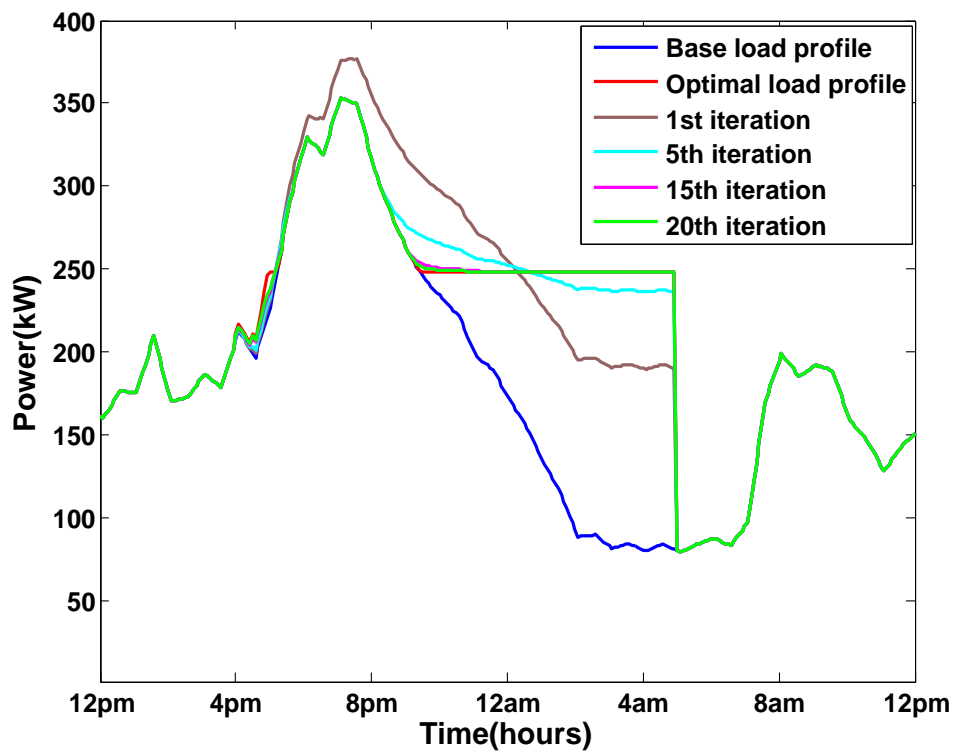


Fig. 3.15 Comparison of the optimal aggregated load profile obtained using CLVM and the iterative ODVF methods

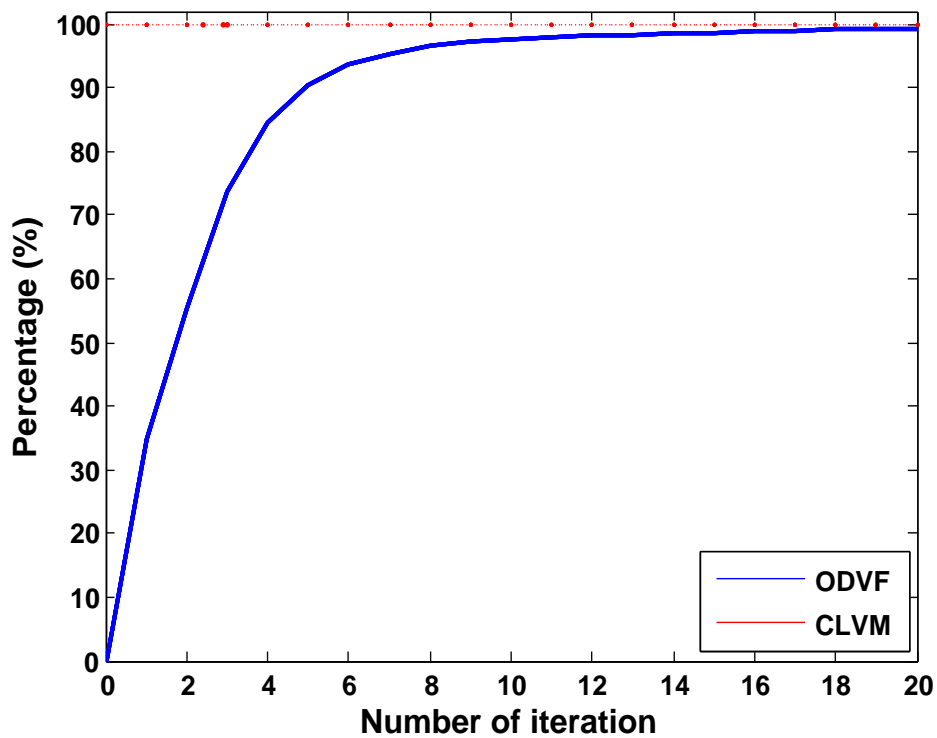


Fig. 3.16 Percentage obtained for CLVM and the iterative ODVF methods (in terms of MSE) with different numbers of iterations

a common parking lot near an office building. Next we introduce the simulation setup and evaluate the charging strategies using power system simulation.

3.8.1 Simulation Setup

In order to compare the performance of different on-off based charging strategies, a low-voltage distribution network with 45 EV charge points and an office building was modelled using the OpenDSS software [44], as illustrated in Figure 3.17. All charge points were evenly distributed on each phase. The distance between each charge point was set to 10 meters. At the source end of the network, a 10kV/400V (400kVA) Δ/Y (grounded) two windings step-down transformer was modelled. The voltage from the external grid was set to 1.05pu and the minimum voltage level that can be tolerated on the grid was set to 0.95pu. In addition, a 50kVA safety margin was reserved for the transformer for secure operation. i.e. the maximum available power that can be drawn from the grid is 350kVA. The distance between each section of the three phase underground cable was set to 100meters. The aggregated load profile for the office building was generated by selecting several winter load profiles from the smart meter electricity trial dataset (SME subset) provided by the CER in Ireland [26]. For simplicity, the power factor for the office building load was assumed to 0.95 lagging over the course of the full M time slots. The time step was set to 1 second for a 14 hour simulation conducted from 6am to 8pm. The load profile for the office building applied in this time period is illustrated in Figure 3.18. Each data point of the load profile was sampled and assumed to be constant during every half an hour.

The maximum charge rate of each EV was set to 3.7kW which corresponds to a nominal charging current of 16A. This means that when the EV charger is required to turn on, the charge rate can only be set to 3.7kW. The assumptions on the SOC, and the travelling patterns for EVs are consistent with the assumptions made in the previous section (i.e., for comparisons of 'continuous' EV charging strategies). However, since we are now modelling a working scenario in which EVs will be charged in a SME area during the day, thus we shall assume that EVs depart for work between 7am and 10am and come back home between 4pm and 7pm with the same probability distribution as specified in the previous section. In addition, we assume that in total 40 EVs connect, which represents 89% of available charging points. Without loss of generality, in our simulation three EVs were assumed to already connect to the parking lot at the beginning of the simulation time (6am). This assumption can be used to model some fixed number of EVs which are normally required to park overnight in the area (e.g. service vehicles).

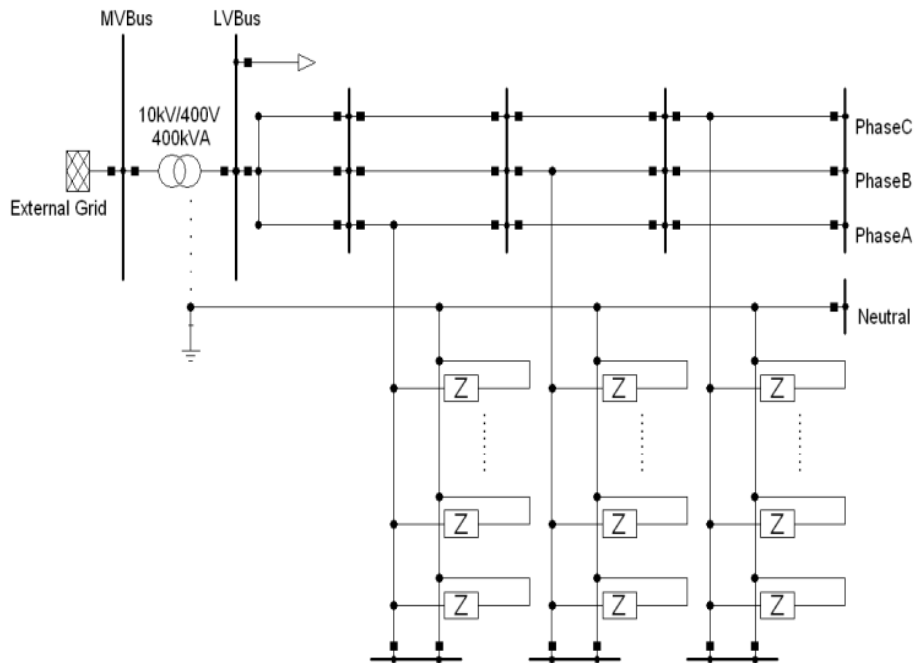


Fig. 3.17 Schematic diagram of the distribution network

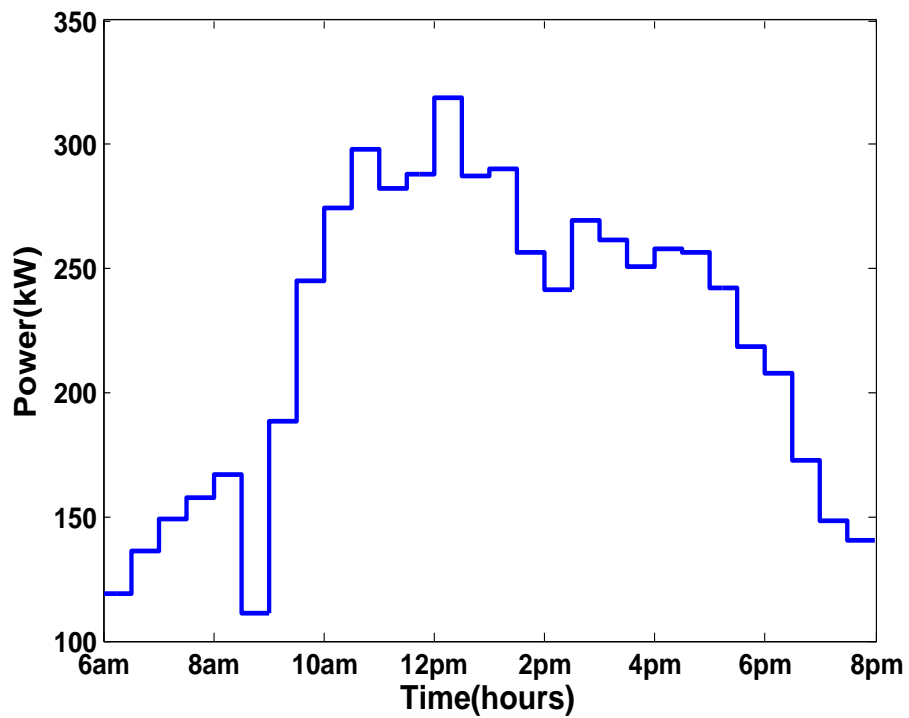


Fig. 3.18 Office building power consumption from 6am to 8pm

3.8.2 Evaluation of On-Off Fairness based Charging Strategies

The simulation results for the on-off charging strategies considered are also compared from the perspective of both the grid operators and customers. Power grid utilities wish to reduce power losses, voltage sag and maximize the energy that can be delivered to customers at all times. Hence, the power utilisation, the power losses in the cables and the voltage sag are investigated, see Figures 3.19 to 3.21. The results show that uncontrolled charging has a severe impact on the grid and could not be tolerated. The basic distributed charging strategy improves the power network performance with regard to power losses and power utilisation. However, the voltage drop is still significant, as shown in Figure 3.21. By using the enhanced distributed algorithm the minimum voltage is substantially improved. It is also noteworthy that the enhanced distributed strategy achieves comparable performance to the centralised solution throughout the simulation in terms of grid operation.

From the customer side, performance is measured in terms of the quality of service that is delivered. This depends on the amount of energy they receive or whether their EV is fully charged before their departure. The best result in this regard is achieved by uncontrolled charging, where all the EVs can finish charging within four hours. When using the enhanced or distributed algorithms all EVs were able to finish charging before departure. In terms of customer wishes, the centralised approach behaved worst with multiple EVs not fully charged at their departure. As expected, the enhanced method is able to provide some fairness to the EVs. In other words, the centralised method provides the best solution from the grid perspective, but ignores fairness from the perspective of the customers. A detailed comparison of the charging time for the EVs can be found in Table 3.5, including the average charging time and the extreme values.

Therefore, the enhanced distributed on-off charging strategy can provide many benefits to both utilities and customers. At the same time the required enhancements to the existing charging infrastructure are small, as it requires only broadcast communication and measurement points at critical locations in the grid. Note that the results presented in this section depend on the investigated power grid. The actual improvements possible can vary when considering other grid structures and need to be investigated in detail.

3.9 Discussion

In general, uncontrolled charging provides the best performance in terms of its objective, i.e., minimising customer charging times. Similarly, by applying the basic AIMD, DPF and distributed on-off based charging strategies, charging fairness can be achieved for each

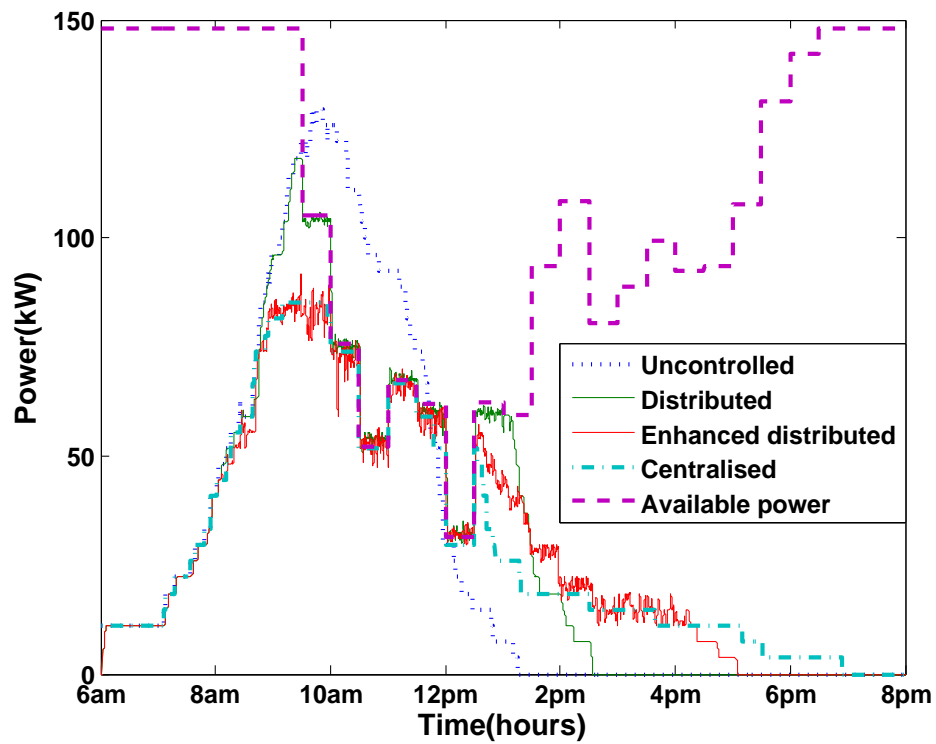


Fig. 3.19 Comparison of the power utilisation

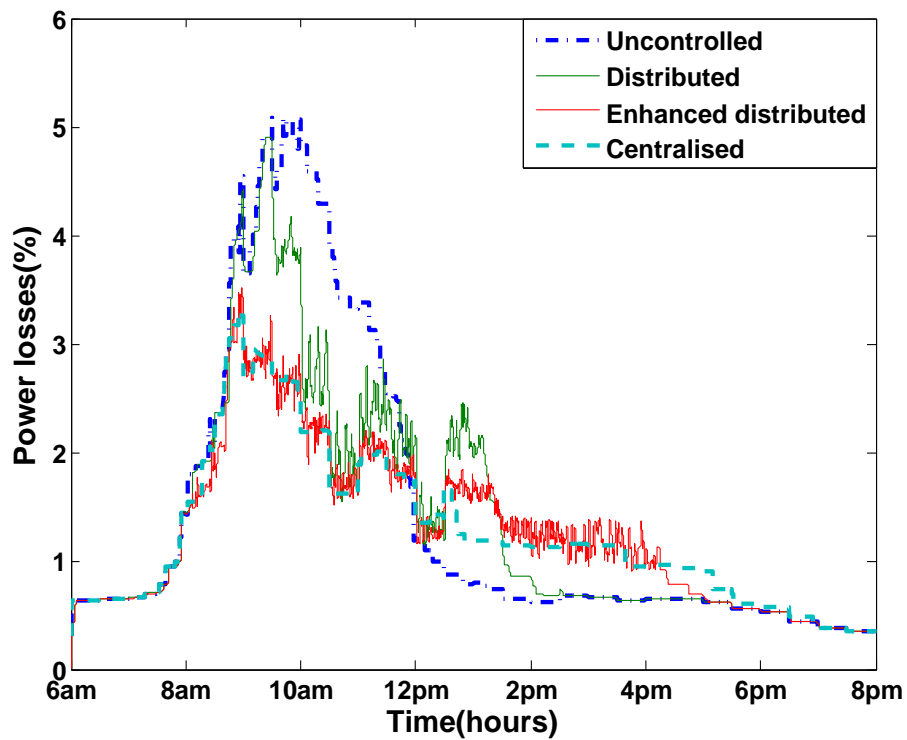


Fig. 3.20 Comparison of the total power losses

Table 3.5 A comparison of simulation results for various on-off type of EV charging strategies (50% EV penetration)

Strategies	Uncontrolled	Distributed ^a	Enhanced ^b	Centralised ^c
Ave Time(h)	2.81	3.74	4.60	4.14
Std Time(h)	0.40	0.76	1.51	1.61
Min Time(h)	1.92	2.16	2.06	1.92
Max Time(h)	3.59	4.90	7.43	7.79
No. not finished ^d	0	0	0	2
Missed (kWh) ^e	0	0	0	5.65
Earliest EV (h:m) ^f	08:26	08:28	08:30	08:26
Last EV (h:m) ^g	13:15	14:33	17:42	n/a

^a Distributed on-off charging

^b Enhanced distributed on-off charging

^c Centralised on-off charging

^d Number of EVs not fully charged

^e Remained energy to be charged to finish charging of all EVs

^f The earliest time that an EV finishes charging ^g The latest time that an EV finished charging

customer under appropriate assumptions, while the basic DPF method can adjust this fairness according to the WTP specified by individual customers.

However, typically these approaches violate grid constraints, as can be seen in Table 3.1 and 3.5 and Figures 3.7 and 3.8. The addition of constraints allows the respective charging goals to be met while respecting grid constraints, as shown in Table 3.1 and 3.5 and Figures 3.9–3.11 and Figures 3.19–3.21. While centralised algorithms achieve the best performance in terms of their stated goals, including satisfying power system constraints, they require global information and also do not scale well, as mentioned previously. For example, here, the CLVM method has the longest simulation times. Decentralised algorithms, like the ODVF algorithm, approach the performance of centralised algorithms and are scalable.

Therefore the modified AIMD,DPF and distributed on-off algorithms show much promise. These algorithms provide a trade off between a small communication overhead and almost optimal performance in terms of their grid objectives, and can be coordinated to approxi-

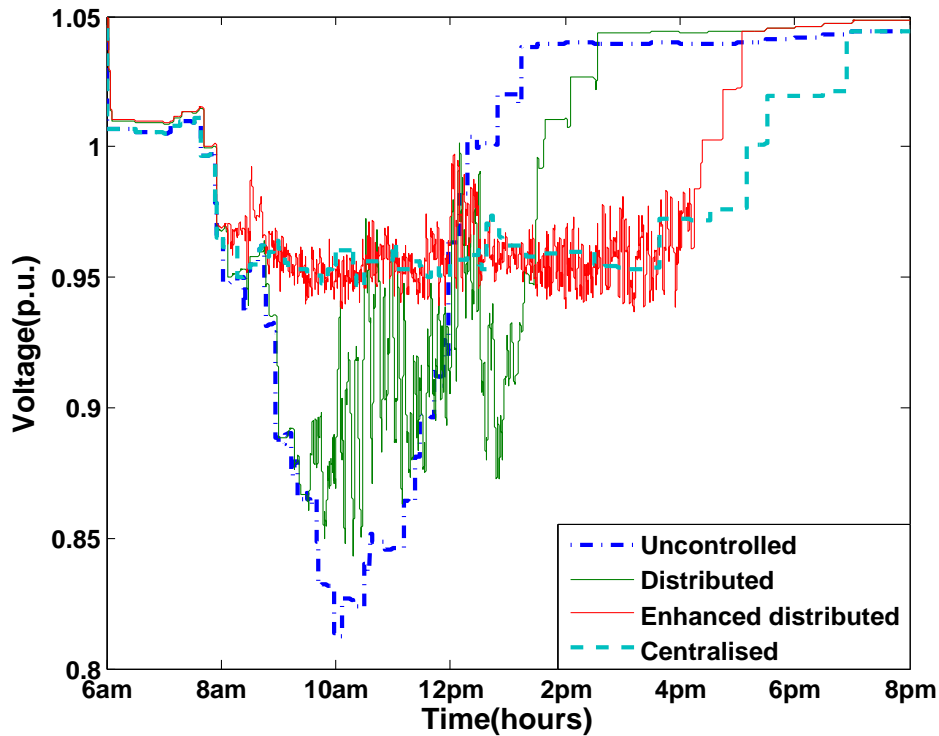


Fig. 3.21 Comparison of the minimum voltage profile

mately achieve some temporal objectives without the necessity of accurate load prediction, i.e. by applying a price-adjusted available power heuristic.

3.10 Testbed Design

To conclude the chapter, we go beyond the simulations and build a hardware testbed using the AIMD algorithm for charging mobile phone batteries as a proxy for EVs.

This project is mainly built on the Arduino electronics platform [10]. The schematic diagram of the project is illustrated in Figure 3.22. Here, the Arduino UNO [38] is acting as a central controller for computing and coordination. For the application at hand, we extend the basic functions of the UNO by including charging and wireless modules. The charging module is used to charge the phone battery and the wireless module is for packet transmission. In particular, we use the Zigbee protocol [47] for short distance communication between devices. However, for longer transmission range, this wireless module can be easily replaced by other available RF options or by enhancing the antennas. Finally, we use the oscilloscope for demonstration and data logging. With these modules in place, the basic decentralised AIMD algorithm can be applied on the testbed.

According to the AIMD algorithm requirements, the wireless transmission system is divided into two parts. We shall denote them as coordinator and router/end user separately. In practice, a coordinator can be regarded as an EV aggregator which provides available power and services for EV charging. The end users are normally regarded as the EV owners which require EV charging services. In Figure 3.22 it is shown that there are two end users and one coordinator. The coordinator is used to broadcast the capacity event signals to the end users. In our experiments, each capacity event signal is triggered manually by pressing a designated button connected to the coordinator. Note that this manual operation can be thought as in a practical scenario when more than two end users are charging simultaneously, where the condition of capacity events depends on the charging status of all end users and the uncertainty of the available power that can be provided. In this case, we can manually trigger the capacity event signals in our design for easy implementations of the algorithm. The end user is used to receive the packet from the coordinator. Each packet consists of one bit of information for coding the capacity event. For instance, if an end user receives a '1' (i.e. rather than '0'), it implies that a capacity event happened just now. On receiving each packet, each UNO (end user) decides whether to linearly increase or multiplicatively decrease the charging current for the next time slot and forwarding this value to the charging module. In this way the charging current through each battery can be adjusted in a decentralised fashion by the AIMD algorithm via wireless coordination.

The charging module is used to adjust the charging current based on the packet forwarded from the UNO (end user). This module is mainly composed of a MOSFET (PNP) and a limiting current component. The voltage applied on the MOSFET (gate) is used to control the current generated on the drain. The input voltage is generated from each UNO (end user) and it is adjustable via the built-in PWM mechanisms. The limiting current component is composed of a diode. The charging current can be measured directly by monitoring the voltage across the resistance in parallel with the diode. Although the PWM signal can be used to control charging current directly, we filter the PWM signal via a simple RC circuit such that the smoothed DC voltage can be clearly shown on the multimeter and the oscilloscope.

With the data logging devices in place, the real-time data from the testbed can be exported. Figure 3.23 shows the comparisons of two filtered PWM signals from two different charging boards. For observation purposes, the yellow curve is offset by 500mV to the blue curve. In this example, a series of capacity event signals were generated between 10 and 70 seconds. Although with a bit delay in wireless transmission between devices, the fairness of charging is shown clearly. With respect to these PWM signals, Figure 3.24 demonstrates the changes in both charging voltage and current obtained from one battery. It is shown that the charging current reduces rapidly after receiving these capacity event signals, and it rises back (approx.)

linearly when the capacity events end. This illustrates that the basic AIMD algorithm has been nicely implemented on our testbed. Further, it is also shown that the maximum charging current that can be provided by the board is 0.2A and the maximum charging voltage can be adjusted to around 3.8V with respect to the open circuit voltage which equals 3.7V. Note that the open circuit voltage can be observed when the charging current equals 0A at the beginning of the charging process. This indicates that our battery is protected effectively from fast and overcharging. Note also that the maximum charging current of the experimental battery is 1.3A and the maximum charging voltage is 4.2V.

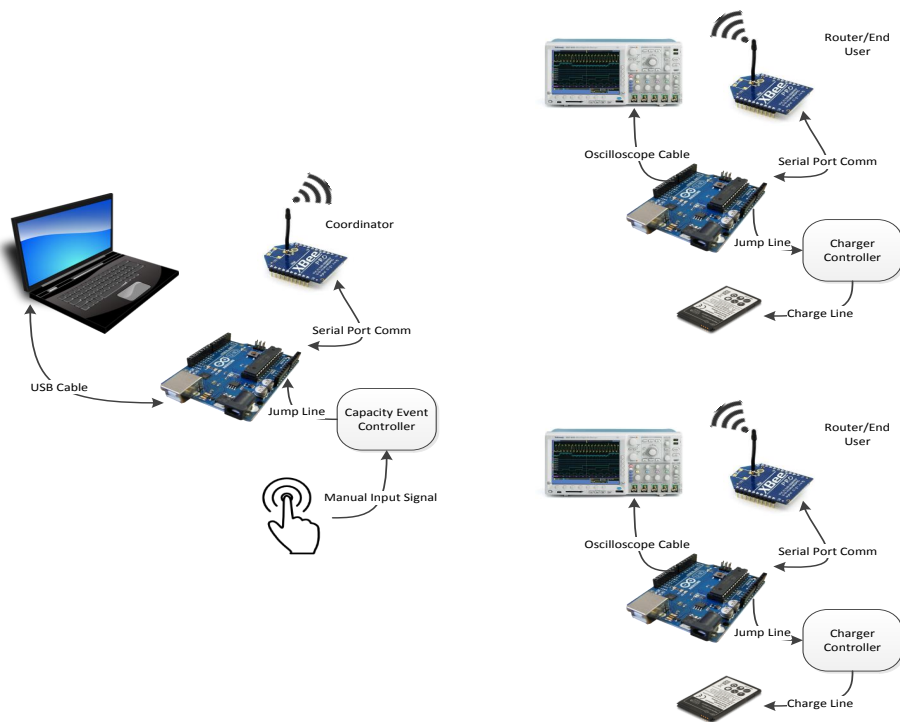


Fig. 3.22 Schematic diagram for the hardware testbed

3.11 Conclusions

In this chapter, we considered a wide variety of EV charging strategies applied in low-voltage distribution networks. To commence the chapter, we have presented a comprehensive review of the literature for charging a fleet of EVs by using different coordination strategies. Our starting point is the observation that with all of these charging strategies available, there is no common framework such that the performance of these strategies can be compared. Motivated by this, a mathematical framework for formulating EV charging problems has been

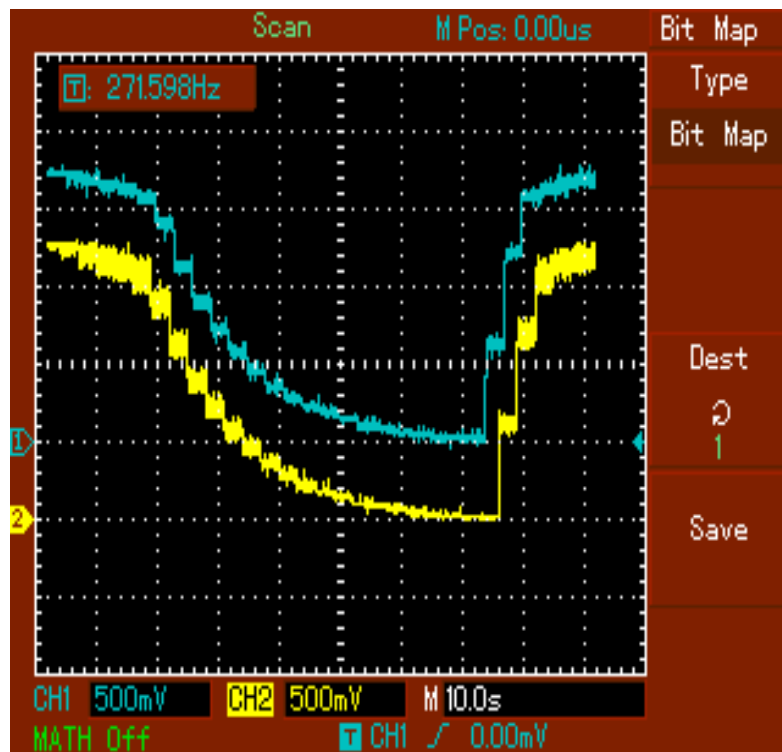


Fig. 3.23 Comparisons of charging fairness on the testbed

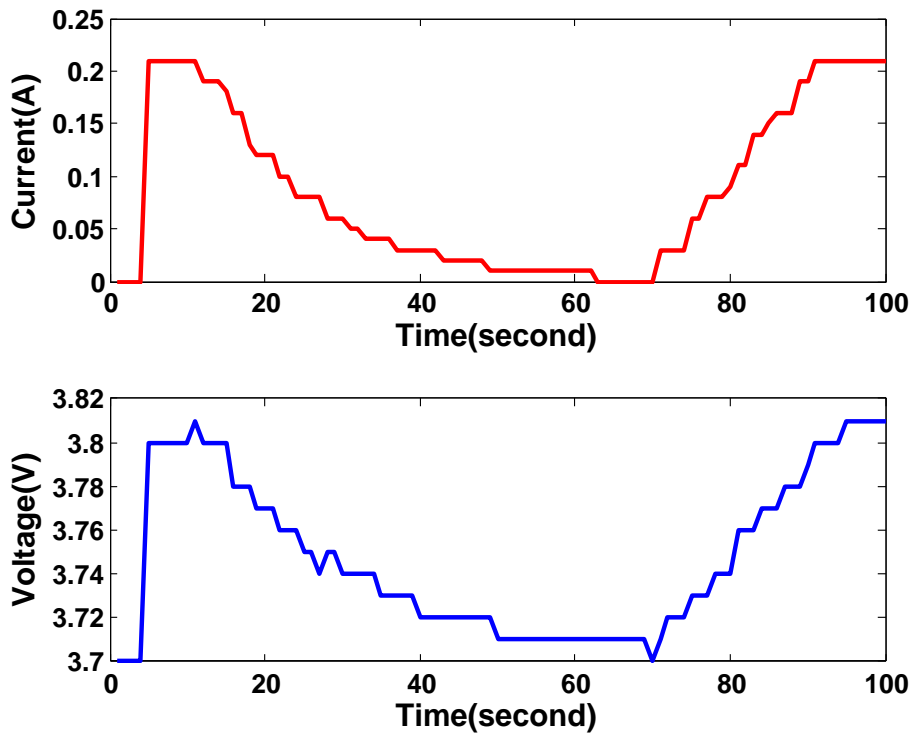


Fig. 3.24 Charging current and voltage of the first battery

presented that incorporates both power system and charging infrastructure constraints and caters for both instantaneous and temporal optimisation objectives. Within this framework, several typical charging strategies were evaluated. These algorithms were further tested on a power system distribution level testbed in both residential and SME scenarios using a hybrid Matlab/OpenDSS platform, and using realistic demand and charging profiles.

To conclude, we give an overall assessment for each approach considered in this chapter. It was found that those algorithms that ignored system constraints, i.e., Uncontrolled, AIMD, AIMD(P), DPF, DPF(P) and distributed on-off, typically violated them for large EV penetrations and thus not suitable for practical implementations. Of the algorithms that considered power system constraints, the modified AIMD, DPF and distributed on-off algorithms provided the best trade off in terms of achieving almost optimal performance in terms of their grid objectives while satisfying constraints and maintaining a small communication overhead are most recommended for practical implementations. While for other communication based optimal algorithms considered, i.e. ICIC, ICIC(P), CLVM, DSC and CCCM, are not scalable well and usually require global information for decision making, and thus they are not suggested for practical implementations.

Chapter 4

Using V2G for Ancillary Services

***Abstract:** This chapter discusses different V2G schemes for providing ancillary services to the grid. In particular, two applications involving groups of EVs are investigated: (1) mitigating the current imbalance in a typical three-phase power network; and (2) providing optimal fairness power dispatch in a microgrid scenario. The research which is joint work with Emanuele Crisostomi, Seán McLoone, and Robert Shorten was published in [105, 111].*

4.1 Introduction

The previous chapter evaluated various strategies for coordinating the charging of EVs and how they impacted on the grid. In all cases the focus was on controlling the power flow from the Grid-to-Vehicle (G2V). Vehicle-to-Grid (V2G) opportunities were not explored.

In this chapter we shall investigate applying different V2G technologies on a group of EVs to provide ancillary services to the grid. In this regard, we consider two applications. In the first application, we harness the power of V2G to reduce the current imbalance on a three-phase distribution network. Current and voltage imbalance are intrinsically linked, however, the issue of balancing currents is less complex than that of balancing voltages. This is because the current magnitudes and angles along phases can easily be measured at the transformer, and current demand can then potentially be altered to balance phases. The voltage on the other hand is related to the distribution of individual loads along the phases, and it is more difficult to determine where the controllable loads, e.g. EVs, are located. In the case of current balancing, it is more advantageous to use a distributed algorithm rather than a centralised solution because global knowledge of the system may not be available to a centralised controller, and a distributed approach allows flexibility in terms of what EVs are controlled at a given time, i.e., it allows a more “plug and play” type approach. With this in mind, a distributed EV charging strategy, based on techniques from the cooperative control

literature, is developed. To date, many cooperative control algorithms have been employed in power system applications [74, 215], and our work uses the distributed consensus method developed in [94] (Note that this method is based on Lemma 4.1 of Chapter 4 [94] and is theoretically the same as Lemma 2 of Chapter 2 of this thesis). The proposed solution seeks to regulate EV charging in order to prevent overloading of the grid, while at the same time coordinating charging/discharging activity across phases so as to reduce current imbalance and power losses.

In the second application, we study the power dispatch problem in a microgrid scenario with EVs and renewable energy generation. In this scenario, EVs are connected to the grid and managed by an aggregator such that EV owners can sell their own energy to the grid when they do not need to travel, and the power grid can store energy by charging the EVs if it is required. This framework is attractive for all participants since EV owners see in this process the possibility of earning money by selling V2G services, and the grid company see in this process the feasibility of regulating the fluctuating energy produced from renewable sources or to improve grid stability at critical times. On this basis, we model the V2G problem as an optimisation problem that aims to achieve an optimal trade-off between the economic benefit of using energy from renewables instead of energy from other more expensive power plants, and the inconveniences caused to the owner in terms of residual energy remaining in the EV. Also, we are interested in computing a “fair” solution, where fairness is related to the fact that the same energy should be taken from all EVs participating in the V2G programme (i.e. some EVs’ owners might decide not to participate in such a programme to preserve the level of energy in their EVs for future use).

Note that the challenge with such an optimisation problem is that the utility functions associated with each EV are personal, and should not be revealed to others. Also, we are interested in computing the optimal solution in a distributed fashion, to avoid increasing computation load on the central infrastructure (e.g. base stations) and to improve flexibility, privacy and robustness from a system perspective. We shall illustrate a distributed consensus algorithm that solves this V2G problem in a fair manner, trying to achieve an optimal trade-off between power generation costs and inconvenience to the vehicle owner. Note that our proposed solution is largely based on the results obtained in Chapter 2.

The remainder of the chapter is organised as follows. In Section 4.2, the application of V2G to current imbalance reduction is presented. In Section 4.3, the V2G problem is formulated and the proposed algorithm is applied to achieve optimal V2G power dispatch in a microgrid. Section 4.4 concludes the chapter.

4.2 Current Imbalance Reduction

4.2.1 Current Unbalance Factor

The Voltage Unbalance Factor (VUF) is proposed as a metric for quantifying the degree of voltage imbalance in a network. To date, there have been many different definitions proposed for VUF, such as the *IEEE* and *NEMA* standards [129, 154]. However, in practice VUF is not always sufficient for a complete analysis of the power network. In this regard, Standards for the Current Unbalance Factor (SCUF) are proposed, which help to calculate the VUF and support better understanding of the power grid. In this chapter it is assumed that the maximum acceptable SCUF on the grid is 10% [51]. The SCUF is given as follows [156]:

$$\%SCUF = \left(\frac{|i_n|}{|i_p|} \right) \times 100\%, \quad (4.1)$$

where i_n and i_p are the negative sequence and positive sequence components of the current i . If we denote the zero sequence current as i_0 , and the current in the individual phases as i_a , i_b , and i_c then:

$$\begin{bmatrix} i_0 \\ i_p \\ i_n \end{bmatrix} = \frac{1}{3} \begin{bmatrix} 1 & 1 & 1 \\ 1 & \alpha & \alpha^2 \\ 1 & \alpha^2 & \alpha \end{bmatrix} \begin{bmatrix} i_a \\ i_b \\ i_c \end{bmatrix}, \quad (4.2)$$

where α is defined as follows:

$$\alpha = e^{j\frac{2}{3}\pi}. \quad (4.3)$$

With (4.2), we can easily calculate the current unbalance factor using the measured current on each phase.

4.2.2 Current Balance Equation

The current balance equation can be formulated in a general framework by considering the EV charging loads on each phase [51]. The balance equations are given as follows:

$$\begin{aligned} i_n &= i_{nr} + i_{ni}i, \\ i_p &= i_{pr} + i_{pi}i, \end{aligned} \quad (4.4)$$

where

$$\begin{aligned}
i_{pr} &= \frac{1}{3}(i_{d1} + i_{d2} + i_{d3}) \\
i_{pi} &= -\frac{1}{3}(i_{q1} + i_{q2} + i_{q3}) \\
i_{nr} &= \frac{1}{3}i_{d1} - \frac{1}{6}(i_{d2} + i_{d3}) + \frac{\sqrt{3}}{6}(i_{q2} - i_{q3}) \\
i_{ni} &= \frac{1}{3}i_{q1} - \frac{1}{6}(i_{q2} + i_{q3}) - \frac{\sqrt{3}}{6}(i_{d2} - i_{d3})
\end{aligned} \tag{4.5}$$

and also with:

$$\begin{bmatrix} i_{d1} \\ i_{d2} \\ i_{d3} \end{bmatrix} = \begin{bmatrix} \frac{P_{L1}+P_{EV1}}{V_{s1}} \\ \frac{P_{L2}+P_{EV2}}{V_{s2}} \\ \frac{P_{L3}+P_{EV3}}{V_{s3}} \end{bmatrix}, \begin{bmatrix} i_{q1} \\ i_{q2} \\ i_{q3} \end{bmatrix} = \begin{bmatrix} \frac{Q_{L1}+Q_{EV1}}{V_{s1}} \\ \frac{Q_{L2}+Q_{EV2}}{V_{s2}} \\ \frac{Q_{L3}+Q_{EV3}}{V_{s3}} \end{bmatrix}. \tag{4.6}$$

In (4.6), the variables P_{EVj} and Q_{EVj} denote the total active and reactive powers consumed by the EV loads on the j^{th} phase. Similarly, the variables P_{Lj} and Q_{Lj} are used to represent the total active and reactive powers consumed by all household loads on the j^{th} phase. In addition, V_{sj} is used to represent the voltage at the transformer on the j^{th} phase. In (4.4), i_{nr} and i_{ni} denote the real and imaginary components of the negative sequence current. Similarly, i_{pr} and i_{pi} are used to represent the real and imaginary components of the positive sequence current. In (4.5), i_{dj} and i_{qj} represent the in-phase and quadrature component on the j^{th} phase of current i . It is worth noting that in a balanced system, zero sequence component i_0 should always equals to zero. Since the zero sequence component is not related to the SCUF defined in (4.1), this expression is not considered in the context of this chapter.

According to the definition in (4.1), the SCUF can be set to 0 if the value of i_n can be manipulated to 0. With this in mind, referring to (4.5), if the following holds:

$$i_{d1} = i_{d2} = i_{d3} > 0 \tag{4.7}$$

$$i_{q1} = i_{q2} = i_{q3} = 0 \tag{4.8}$$

then both i_{nr} and i_{ni} will be equal to 0 while i_p will still be a positive value. Therefore, $|i_n| = \sqrt{i_{nr}^2 + i_{ni}^2}$ will be 0. Referring to (4.6), the active power flow on each phase can be made the same via manipulation of P_{EVj} , for $j = 1, 2, 3$ (ignoring the small differences between phase voltages at the head of transformer V_s), so as to satisfy (4.7), and (4.8) is satisfied by letting:

$$Q_{Lj} = -Q_{EVj}, \text{ for } j = 1, 2, 3. \tag{4.9}$$

It is possible to achieve this goal using a V2G framework where each EV has the flexibility to adjust their charge rates as required [170]. Based on this idea, a distributed control framework can be designed as in the following section.

4.2.3 Distributed Consensus Algorithm

Let us consider a scenario in which there are N number of EVs connected to the grid. It is assumed that each EV charger has a maximum allowable apparent power s_{\max}^i , a maximum active power draw, c_{\max}^i , and a maximum reactive power draw, r_{\max}^i , such that:

$$s_{\max}^i = \sqrt{c_{\max}^i{}^2 + r_{\max}^i{}^2}. \quad (4.10)$$

The load power consumption in the network is discretised, with a sample time ΔT . The measured active and reactive power consumptions on the j^{th} phase of the transformer at sample step k are denoted by $T_a^j(k)$ and $T_r^j(k)$, respectively. The index set of all EVs connected at the j^{th} phase at sample step k is denoted by $\Theta_j(k)$. To protect the transmission line from overloading, the maximum power flow that can be tolerated at each phase is defined as P_{\max} . The active and reactive charge rates for the i^{th} EV at sample step k are denoted by $c_i(k)$ and $r_i(k)$, respectively. Here, $r_i(k) > 0$, such that the i^{th} EV can inject the same amount of reactive power as the reactive power consumed by the houses. The variables $G_a^j(k)$ and $G_r^j(k)$, which denote the total chargeable capacity of active and reactive powers on the j^{th} phase, are given as follows:

$$\begin{aligned} G_a^j(k) &= \sum_{i \in \Theta_j(k)} (c_{\max}^i - c_i(k)), \text{ for } j = 1, 2, 3, \\ G_r^j(k) &= \sum_{i \in \Theta_j(k)} (r_{\max}^i - r_i(k)), \text{ for } j = 1, 2, 3. \end{aligned} \quad (4.11)$$

Now the result in Lemma 2 can be applied to the EV charging strategy outlined above.

Lemma 2 Let $\{P(k)\}_{k \in \mathbb{N}}$ be a sequence of row stochastic matrices which is strongly ergodic. Then for every solution $\{x(k)\}_{k \in \mathbb{N}}$ of (2.22) we have

$$\lim_{k \rightarrow \infty} \text{dist}(x(k), E) = 0. \quad (4.12)$$

To apply the above Lemma we proceed as follows. For each k we define the $P(k)$ as

$$P_{\tilde{i}, \tilde{j}}(k) = \begin{cases} 1 - \sum_{\tilde{j} \in N_k^{\tilde{i}}} \eta_{\tilde{j}}, & \text{if } \tilde{j} = \tilde{i}, \\ \eta_{\tilde{j}}, & \text{if } \tilde{j} \in N_k^{\tilde{i}}, \\ 0, & \text{otherwise.} \end{cases}, \quad (4.13)$$

where \tilde{i}, \tilde{j} are the indices of the entries of the matrix $P(k)$, $\eta_{\tilde{j}} \in \mathbb{R}$ is a weighting factor, and $N_k^{\tilde{i}}$ represents the set of neighbour agents communicating to the i^{th} EV. For example, a convenient choice for $\eta_{\tilde{j}}$ can be $\frac{1}{|N_k^{\tilde{i}}|+1} \in (0, \frac{1}{N-1})$, where $|\bullet|$ denotes cardinality, giving rise to an equal weight factor for all elements in $x(k)$. This leads to the following distributed consensus algorithm for the charging of EVs on the individual phases:

Algorithm 5 Distributed Consensus Algorithm

```

1: while Battery not charged do
2:   for each  $i \in \Theta_j(k)$  do
3:     Get  $E_a^j(k)$  from the server at the main transformer.
4:     Get  $c_h(k)$  from all neighbours  $h \in N_k^i$ .
5:     Do  $\delta_i(k) = \eta_a^i \sum_{h \in N_k^i} (c_h(k) - c_i(k)) + \mu_a \cdot E_a^j(k)$ .
6:     Do  $c_i(k+1) = \min(c_{\max}^i, c_i(k) + \delta_i(k))$ .
7:   end for
8: end while
9:
10: while Charger is active do
11:   for each  $i \in \Theta_j(k)$  do
12:     Get  $E_r^j(k)$  from the server at the main transformer.
13:     Get  $r_h(k)$  from all neighbours  $h \in N_k^i$ .
14:     Do  $\lambda_i(k) = \eta_r^i \sum_{h \in N_k^i} (r_h(k) - r_i(k)) + \mu_r \cdot E_r^j(k)$ .
15:     Do  $r_i(k+1) = \min(r_{\max}^i, r_i(k) + \lambda_i(k))$ .
16:   end for
17: end while

```

Comment: As an example to illustrate the matrix $P(k)$, let us consider a simple network with three EVs at a given time step k . We assume the followings: the first EV is able to receive the info only from the second EV; the second EV is not able to receive any info from its neighbours; the third EV is able to receive info from all EVs; then the corresponding matrix $P(k)$ can be shaped as:

$$P(k) = \begin{bmatrix} \frac{1}{2} & \frac{1}{2} & 0 \\ 0 & 1 & 0 \\ \frac{1}{3} & \frac{1}{3} & \frac{1}{3} \end{bmatrix}$$

The variables η_a^i and η_r^i are weighting factors of the i^{th} EV determining the convergence rate for active and reactive power and μ_a and μ_r affect the stability of the algorithm. With a proper choice of parameters, consensus will be approximately achieved (due to numerical quantisation) for the both active and reactive charge rates for each EV connected on the same phase. The variable $E_a^j(k)$ is the difference between the allowable power on phase j and the current power being drawn on phase j . Effectively this is the amount of extra power that can be absorbed by the available EVs along each phase j . A similar definition applies to $E_r^j(k)$ as regards the reactive power, where it is only required to compensate for the reactive power consumed on each phase j by the household loads.

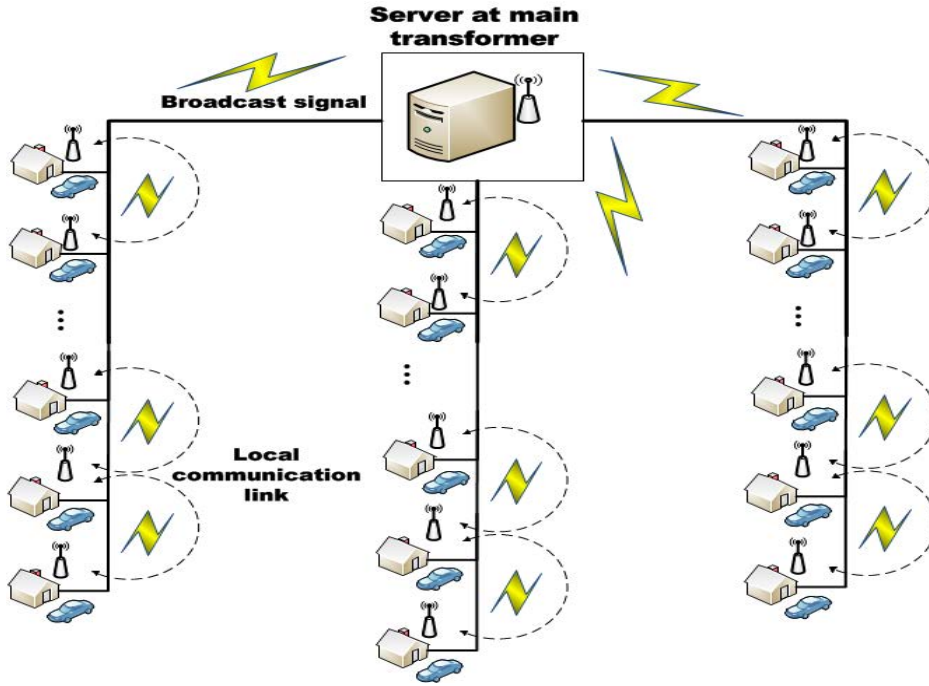


Fig. 4.1 Schematic diagram of the communication topology

To apply this theory, it is also assumed that each EV has the ability to exchange information about its charge rate with its connected neighbours. This constructed communication graph can be time-varying (e.g. due to uncertain communication issues) and it is assumed that this communication always exist unless only one or zero EVs are in the network. Beyond that, it is also required that each EV has the ability to receive a broadcast signal from the transformer. This signal is used to coordinate the charge rates of EVs and achieve some common goal (e.g. current balancing). A schematic diagram for the required communication topology is illustrated in Figure 4.1.

It should be noted that, for the algorithm presented here, it is not necessarily required to know the number of connected EVs at each time slot. The values of $G_a^j(k)$ and $G_r^j(k)$ in (4.11) are communicated in a similar fashion to the charge rates, but the result is accumulated as it is transmitted along the communication nodes. In practice, this process is performed before the broadcast signals are updated each time step on the transformer side. It is also required that at least one of the EVs connected to the j^{th} phase is able to send the $G_a^j(k)$ and $G_r^j(k)$ signals back to the transformer.

It is then necessary for the transformer to recalculate both the reactive power required for compensation at each sample step, and also the active power charge rates required for the maximisation of EV charging whilst maintaining balanced phases. To this end, the signals

related to the active, $E_a^j(k)$, and reactive power, $E_r^j(k)$, broadcast from the transformer to each EV connected to the j^{th} phase, are formulated as follows:

$$\begin{aligned} P_{\text{tot}}^j(k) &= \min(P_{\text{max}}, G_a^j(k) + T_a^j(k)), \\ P_{\text{min}}(k) &= \min(P_{\text{tot}}^1(k), P_{\text{tot}}^2(k), P_{\text{tot}}^3(k)), \\ E_a^j(k) &= P_{\text{min}}(k) - T_a^j(k), \\ E_r^j(k) &= \min(G_r^j(k), T_r^j(k)). \end{aligned} \quad (4.14)$$

Here $P_{\text{tot}}^j(k)$ is the total potential power that could be drawn by phase j at sample step k . The variable $P_{\text{min}}(k)$ is defined as the minimum of the $P_{\text{tot}}^j(k)$ values that can be drawn amongst the three phases at sample step k . This is then the setpoint for the total power to be drawn in each of the individual phases. The allowable power to be drawn in phase j , $E_a^j(k)$, is then given by the difference between the total power phase j can draw and the current power being drawn in phase j . The reactive power, $E_r^j(k)$, is chosen on each phase to equal the reactive power being drawn by household loads at sample step k .

4.2.4 Simulations

In this section a distribution level simulation is developed. We adopted a similar topology to a distribution network modelled in Section 3.8.1.

As illustrated in Figure 4.2, a 10kV/400V(400kVA) Δ/Y (grounded) transformer was connected at the head of the feeder. The voltage from the external grid was set to 1.05pu. The distribution network was modelled with the TN-C-S earthing system, where the three-phase transmission line was split clearly with a neutral line connected back to the neutral point. The variable Z denotes the total power consumption at the location to which it is connected, which includes both household loads and EV charging loads. Each load Z was modelled as a constant current load and each household load was associated with a power factor. For simplicity, we assumed this factor was equal to 0.95 lagging for each house during the day. The load profile for each house was randomly chosen from the dataset given in [26]. Then each load profile was resampled every minute such that the load consumption was constant within each one minute interval. In addition, the sampling time for the charging algorithm was set to one second. In other words, it was assumed that each EV was able to finish exchanging charge rate information with their neighbours in this one second interval.

It was assumed that there were 20 houses located evenly on each phase. The distance between each house was 10 meters. The power limit P_{max} for each phase line was defined as 80kW. The maximum apparent power s_{max}^i for i^{th} EV was set to 4kW, and the maximum active charge rate c_{max}^i was set to 3.7kW. Thus, the maximum reactive charge rate r_{max}^i was

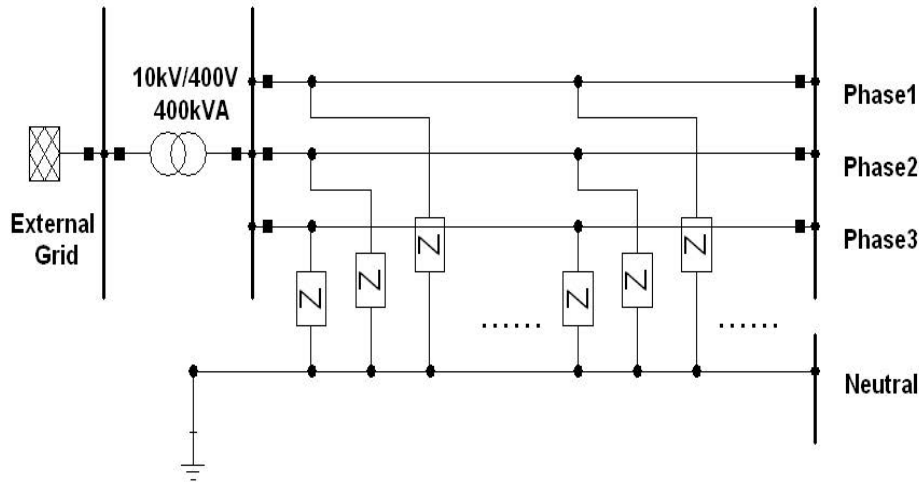


Fig. 4.2 Schematic diagram of the distribution network.

calculated as 1.52kvar, which corresponds to a maximum of 6.6A quadrature component of charging current under a nominal single phase voltage of 230V. The battery capacity for each EV was assumed to be 20kWh and the initial energy required by each EV was normally distributed with a mean of 10kWh and a standard deviation of 1.5kWh. EV arrival times were also based on a normal time distribution with mean 6pm and a standard deviation of 1 hour, and EVs left between 7am and 10am with the following time distribution: 7am-8am (21%), 8am-9am (47%) and 9am-10am (32%) based on [36]. These consumption patterns are consistent with the assumptions made in Section 3.7.

4.2.5 Results and Discussion

To demonstrate the algorithm, a simple Matlab based simulation was devised. In this simulation 10 EVs are connected to each phase and each was given a random initial charge rate. The maximum number of sample steps was set to 100. In this example, we assume that EVs only sought to balance the active power flow on each phase. At the initial time step, the total measured power flow on each phase was 50kW, 40kW and 60kW in phases 1, 2 and 3, respectively, and the maximum active charge rate for each EV was 4kW. The simulation was run and the results are given in Figures 4.3-4.6.

The results show that the EVs on each phase coordinate their actions and achieve consensus on their charge rates within 50 time steps. By adjusting η , the convergence speed can be made faster, as illustrated in Figure 4.4. On the other hand, it is also shown that improper selection of μ , can result in instability, as illustrated in Figure 4.6. Therefore, a suitable choice of both parameters is essential to maintain stable and fast control of the system [94].

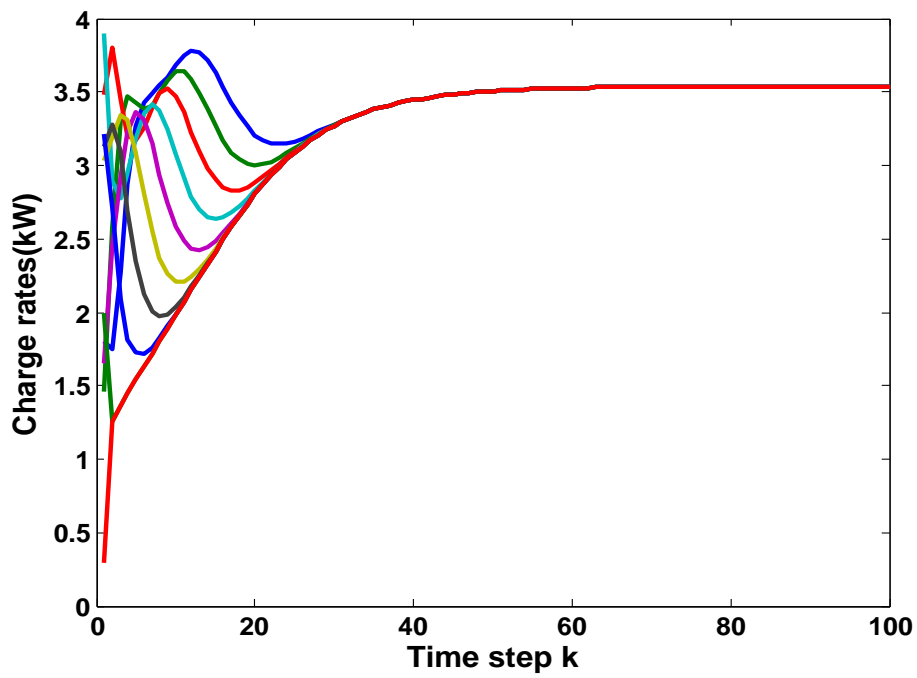


Fig. 4.3 Active charge rates for EVs connected to phase one with $\eta = 0.5$ and $\mu = 0.01$.

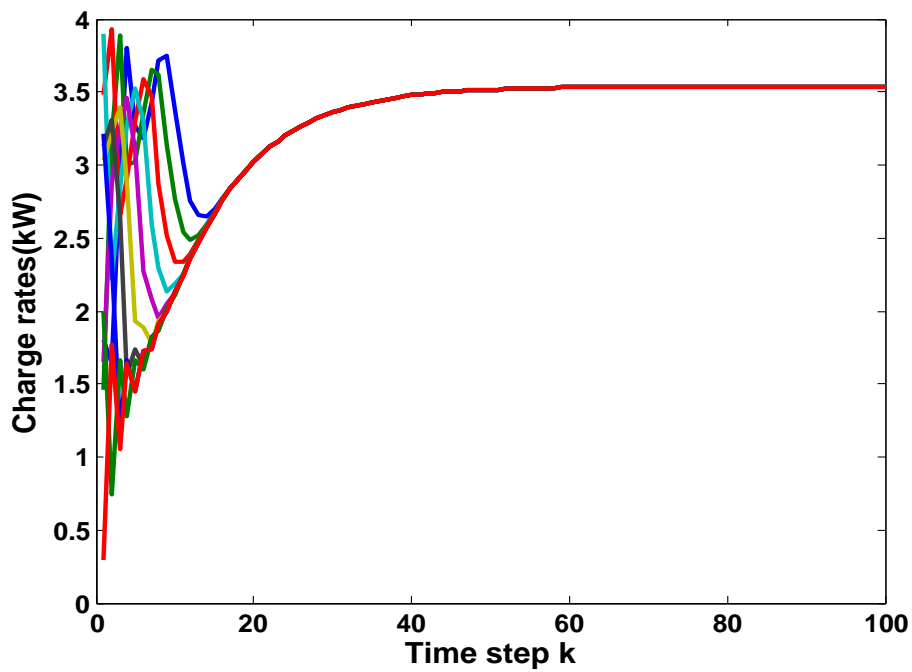


Fig. 4.4 Active charge rates for EVs connected to phase one with $\eta = 0.8$ and $\mu = 0.01$.

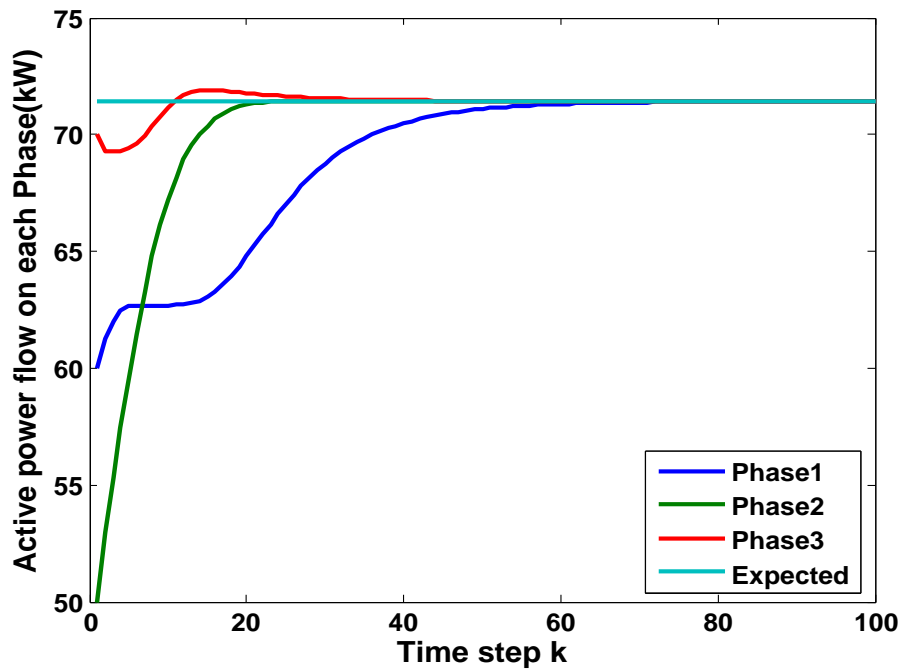


Fig. 4.5 Total power consumptions on each phase compared with desired result with $\eta = 0.5$ and $\mu = 0.01$.

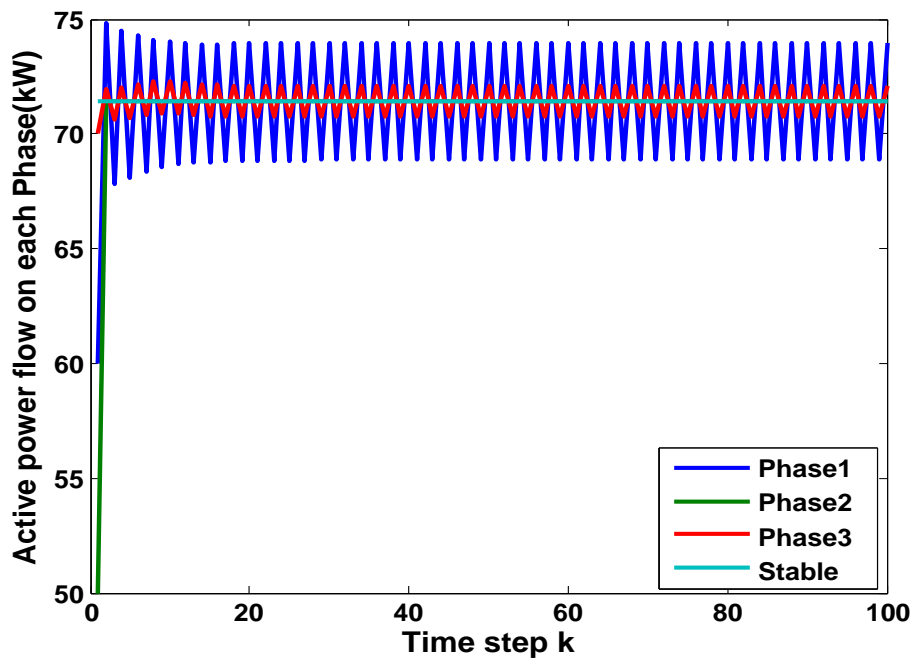


Fig. 4.6 Active charge rates for EVs connected to phase one with $\eta = 0.5$ and $\mu = 0.2$.

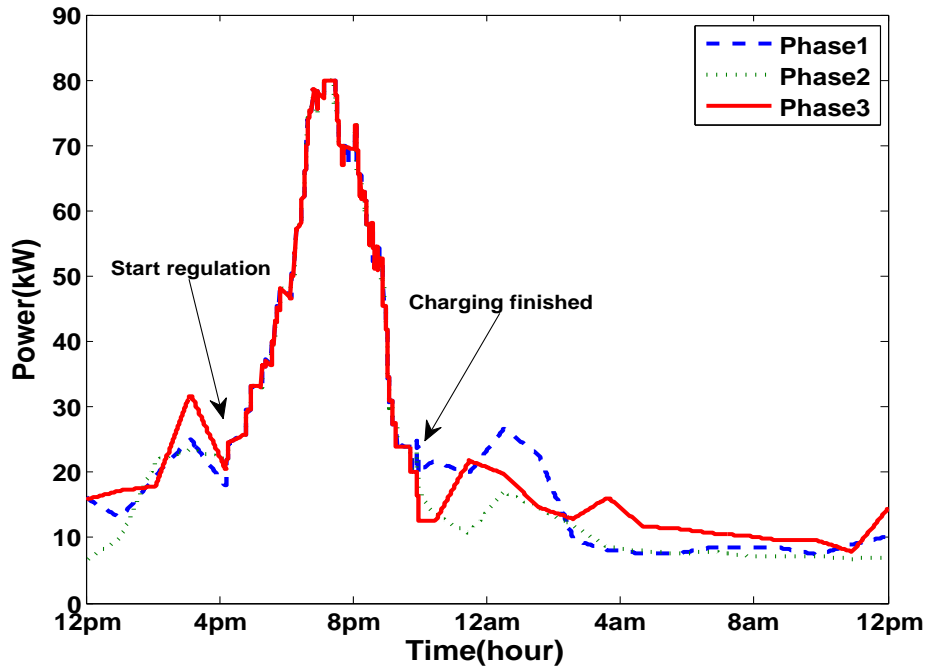


Fig. 4.7 Active power consumption on each phase with distributed consensus algorithm.

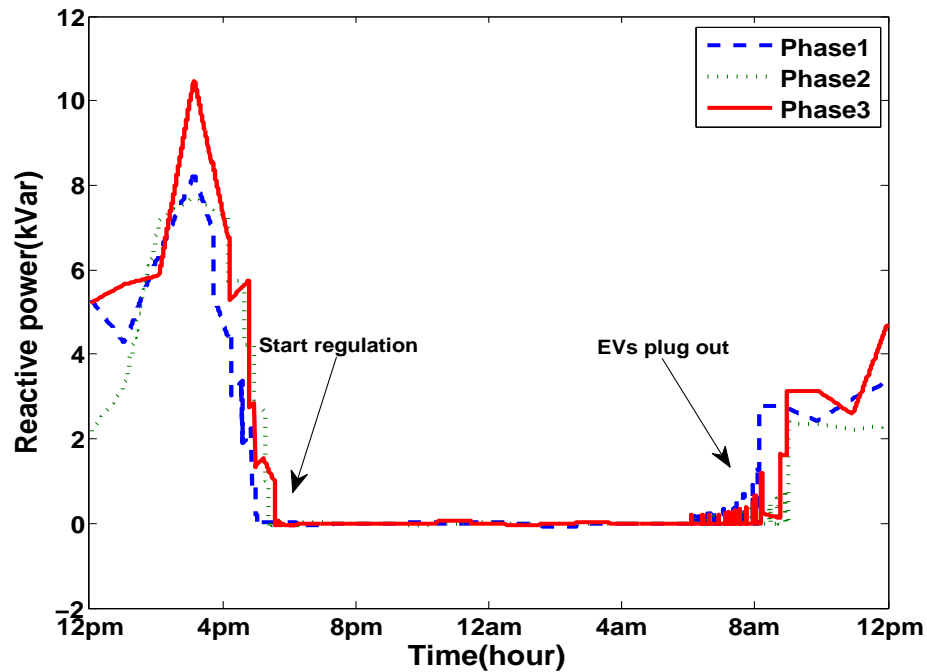


Fig. 4.8 Reactive power consumption on each phase with distributed consensus algorithm.

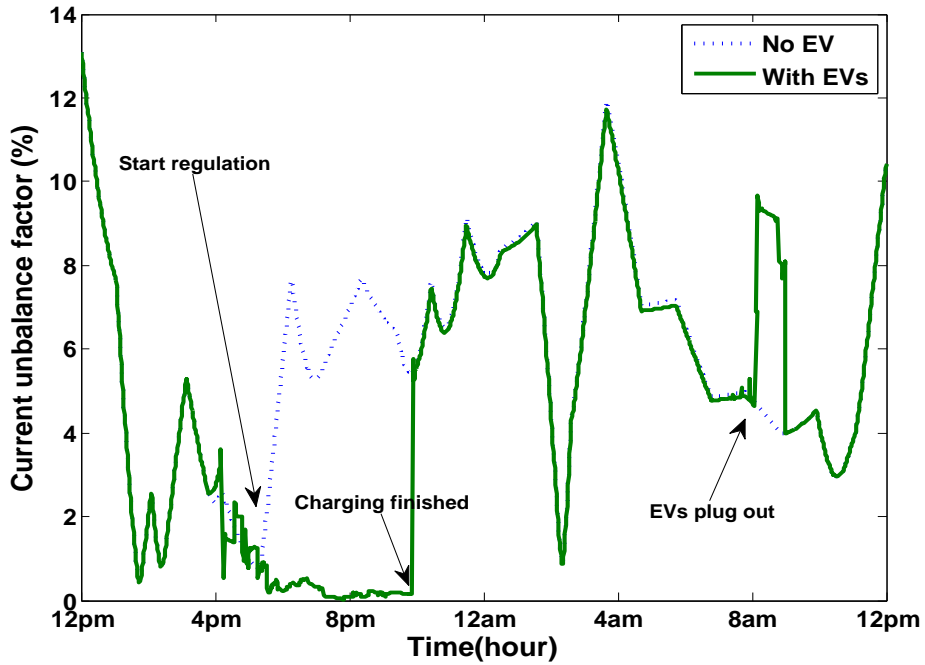


Fig. 4.9 Comparison of current balance factor

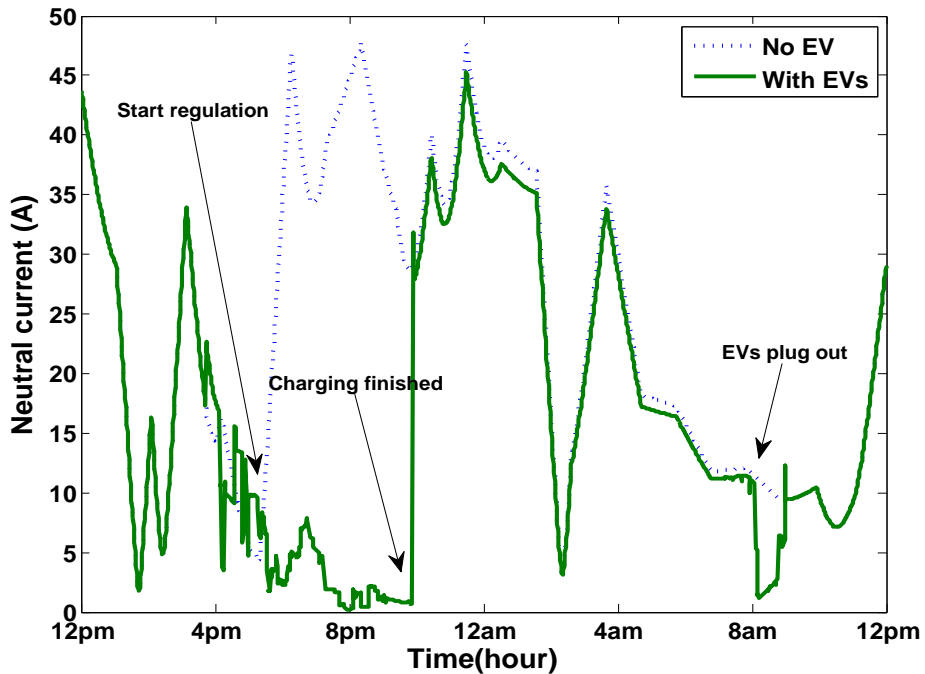


Fig. 4.10 Comparison of neutral current magnitude

The results for the power system simulations are illustrated in Figures 4.7-4.10. It can be seen in Figures 4.7 and 4.8 that by using the distributed consensus technique both active power and reactive power consumptions were balanced on each phase. The active power flow is well balanced until around 10pm, when most of the EVs have finished charging. The reactive power remains balanced while most of the EVs remain plugged in. As a result, the neutral current and current unbalance factor were minimised during EV charging times (the SCUF is almost zero in this case). While the EVs are connected both the active and reactive powers are well balanced as desired across the 3 phases. This is dependent on there being critical levels of EVs in place on the grid. Outside of the times when there are critical levels of EV penetration on the grid, it may not be possible to provide active power phase balancing using the available EVs alone. Thus, it may also be necessary to have other sources which could provide this ancillary service.

4.3 Optimal V2G Power Dispatch

4.3.1 Model and Algorithm

In this section we consider a scenario in which a number of EVs are plugged-in in a large parking lot (e.g., a parking lot in a city airport) in a microgrid. Some of these EVs decide to participate in a V2G programme: during their parking period, they can be discharged/recharged within some given limits in order to improve the economic operation of the grid. The EVs participate on the basis of getting a financial reward. The discharge should thus occur in a fair way to avoid having some EVs getting more money than others.

The EVs are coordinated by an EV aggregator in the microgrid. In this scenario, the optimal power discharge rate is computed by taking into account economic factors and some Quality of Service (QoS) to customers. We assume that the grid will charge the EV batteries with excess energy produced from renewable sources in the microgrid. This implies that in the future, when needed, the grid will consider the possibility of taking energy from EVs back to the grid if the load exceeds the energy currently produced from renewables (e.g., peak-time hours). Without EVs connected, the grid would have to use the power generated from conventional sources, thus incurring high generation costs (e.g., fuel consumption costs) and increased harmful pollution (e.g., CO and NO_x). Thus, the economic benefit of using EVs relies on recovering energy from the EVs rather than producing new energy from conventional plant. The QoS aspect of the utility functions takes into account the concerns of EV owners with regard to having a reduced mobility range if too much energy is taken from their EV batteries.

We mathematically formulate the previous problem as follows. Let N denote the maximum number of EVs participating into the scheme. Define the set $\underline{N} := \{1, 2, \dots, N\}$ as the index set for all EVs and the set $\Phi(k)$ as the index set for the EVs available at time k , i.e., the EVs with enough SOC to participate in discharge cycles in the scheme. Let $|\Phi(k)|$ denote the number of elements in the set $\Phi(k)$. Let $c_i(k)$ denote the discharge rate of the i^{th} EV in set \underline{N} . Further, let c_{\max}^i represent the maximum discharge rate that can be injected to the grid. Both values are assumed to be positive in the V2G mode. The corresponding discharge rate vector for all EVs at time k is defined as $c(k)^T := [c_1(k), c_2(k), \dots, c_N(k)]$. In our study, V2G power dispatch to the grid is discretised into M time slots (indexed as $1, 2, \dots, M$) each of length ΔT . Each EV connects to the grid during a certain time slot, which is represented by the range $[a_i, b_i]$. Due to technical diversity of batteries and chargers, each EV may have a different battery capacity (kWh) and a different energy transferring efficiency. The parameters for both factors are denoted as B_i and η_i respectively. Furthermore, to protect the EVs from over-discharging, the minimum SOC for the i^{th} EV is defined as SOC_{\min}^i . This parameter defines the drop out criteria for the EV. Thus, if $SOC_i(k) \leq SOC_{\min}^i$, then $c_i(k) = 0$. Finally, given the initial V2G regulation time k_0 , the SOC for the i^{th} EV at time k is given by:

$$SOC_i(k) = SOC_i(k_0) - \sum_{j=k_0}^{k-1} \frac{c_i(j) \cdot \Delta T}{B_i}, \quad \forall i \in \underline{N} \quad (4.15)$$

4.3.2 Utility Functions

In addition to the basic model parameters, each EV i is also associated with a utility function $f_i : \mathbb{R} \mapsto \mathbb{R}$, which models both economic and QoS factors associated with the energy delivered from the i^{th} EV. This function will be modelled as a convex function arising from combining the two terms. In addition, we will denote the first derivative of the utility function f_i as f'_i .

Now we model the utility functions in detail. As already mentioned, each function f_i is composed of two different terms that take into account the economic and the QoS aspects, respectively. A diagram is illustrated in Figure 4.11 demonstrating the basic function relation of both terms related to the EV discharge rate.

Note that in Figure 4.11 the notation f_e and f_q refer to the economic term and the inconvenience term of discharge rate (i.e., $c_i(k)$) respectively. The maximum discharge rate is assumed to be 4kW corresponding to the parameter c_{\max}^i in the model. According to this diagram, the economic term f_e implies that the less energy delivered from EVs, the greater expense for the grid due to the need to employ more expensive power generation, e.g., conventional power plants. In fact, power generation costs in the literature are typically modelled as a quadratic function of the energy produced in a unit of time [7, 207]. On the

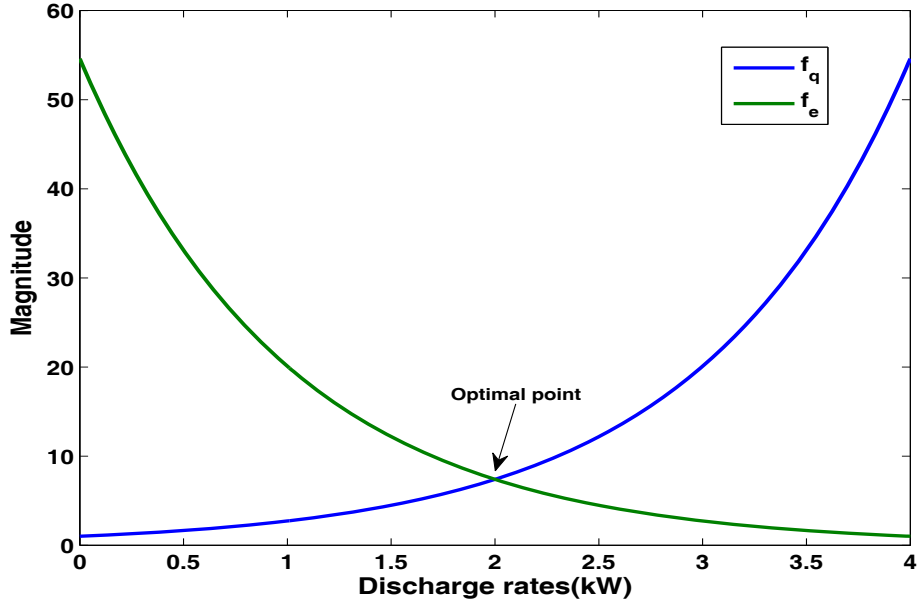


Fig. 4.11 Schematic diagram of the utility function

other hand, the inconvenience term f_q indicates that the more energy delivered from EVs, the greater the inconvenience for EV owners. With this idea, we approximately model the overall utility function taking account of both terms as a quadratic function. Considering the variation in the inconvenience term among users, we perturbed each function with a factor according to the SOC of each EV. To this end, the overall expression of the utility function of the i^{th} EV is modelled as follows:

$$f_i(c_i(k)) = f_q^i(c_i(k)) + f_e^i(c_i(k)) = \alpha_i \cdot c_i(k)^2 + \beta_i \cdot c_i(k) + \left[1 - (SOC_i(k_0) - SOC_{\min}^i)\right] \cdot c_i(k) + \gamma_i, \forall i \in \Phi(k). \quad (4.16)$$

Comment: In (4.16), parameters α_i , β_i and γ_i refer to the pricing function adopted by the grid to give revenues to the EVs participating to the programme. Each perturbed function f_i is associated with an increasing affine function with positive parameter $\left[1 - (SOC_i(k_0) - SOC_{\min}^i)\right]$. Thus, the closer an EV is to its safety level of energy SOC_{\min}^i required to get back home, the greater the inconvenience to the owner. In practice, the EV owners can indicate a bigger SOC_{\min}^i than the one truly needed, if they are particularly anxious to have enough energy for their next journey. In addition, they can always set the parameter SOC_{\min}^i to 1 to be automatically excluded from the V2G programme.

Now the overall optimisation problem can be defined as follows:

$$\begin{aligned} & \min_{c(k)} \sum_{i \in \Phi(k)} f_i(c_i(k)) \\ & \text{subject to: } \begin{cases} c_i(k) = c_j(k), \forall i \neq j \in \Phi(k) \\ 0 \leq c_i(k) \leq c_{\max}^i \\ SOC_{\min}^i \leq SOC_i(k) \leq 1 \end{cases} \end{aligned} \quad (4.17)$$

4.3.3 Optimal Solution

In this section, we show how to apply the previous results in Chapter 2 to solve a class of optimisation problem¹ similar to the form of (4.17).

For a general model setup, we consider a scenario in which there are N vehicles connected in a network through communication links and let \underline{N} denote the set $\{1, 2, \dots, N\}$ for indexing the vehicles. We assume that each vehicle is able to receive/transmit messages from/to either nearby vehicles or available centralised infrastructure (e.g. base station). We assume that each vehicle can communicate a limited amount of information with the infrastructure, and that the infrastructure can broadcast information to the entire network of vehicles, and each vehicle can send a broadcast signal to its neighbours.

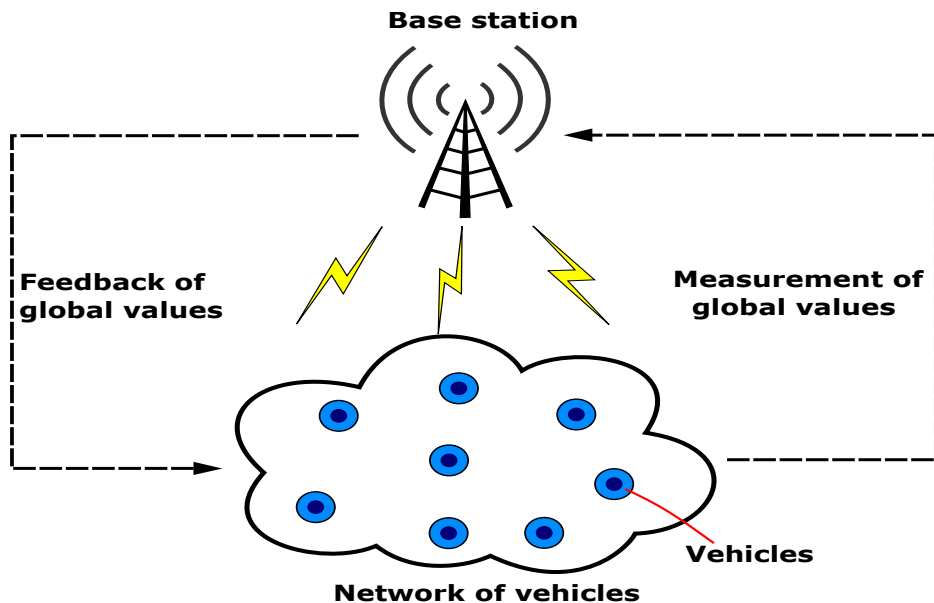


Fig. 4.12 Schematic diagram of the optimisation framework [94]

¹The proposed solution presented in this section can also be used to solve other similar problems in different scenarios (e.g. intelligent transportation scenarios in Chapters 6 and 7).

The problem we wish to solve is to find an optimal consensus point satisfying $x^* = y^*e$ such that the following optimisation problem is solved:

$$\min_{x \in \mathbb{R}^N} \sum_{i=1}^N f_i(x_i) \quad (4.18)$$

subject to: $x_i = x_j, \forall i \neq j \in \underline{N}$.

We wish to use an iterative feedback scheme of the form (2.22) to solve the optimisation problem (4.18). We will require that (4.18) has a unique solution and derive the specific form for function G in (2.22) from first order optimality conditions. To this end, it follows from elementary optimisation theory that when the f_i 's are strictly convex, the optimisation problem (4.18) will be solved if and only if there exists a unique $y^* \in \mathbb{R}$ satisfying

$$\sum_{i=1}^N f'_i(y^*) = 0, \quad (4.19)$$

where f' denotes the first derivative of the utility function f . With this in mind we apply a feedback signal

$$G(x) = -\mu \sum_{i=1}^N f'_i(x_i) \quad (4.20)$$

where $\mu \in \mathbb{R}$ is a parameter to be determined. This gives rise to the following dynamical system

$$x(k+1) = P(k)x(k) - \mu \sum_{i=1}^N f'_i(x_i(k))e \quad (4.21)$$

where we assume that the sequence $\{P(k)\}_{k \in \mathbb{N}}$ satisfies the conditions of uniform strong ergodicity as specified in Section 2.2, and recalling that $e \in \mathbb{R}^N$ is a vector with all entries equal to 1. As we assume that the f_i are strictly convex, their derivatives are strictly increasing. We assume that each f'_i has a strictly positive and bounded growth, i.e., there exist constants d_{\min}^i and d_{\max}^i ; such that for any $a \neq b$

$$0 < d_{\min}^i \leq \frac{f'_i(a) - f'_i(b)}{a - b} \leq d_{\max}^i \quad \forall i \in \underline{N}. \quad (4.22)$$

We claim that provided μ is chosen according to

$$0 < \mu < 2 \left(\sum_{i=1}^N d_{\max}^i \right)^{-1} \quad (4.23)$$

then (4.21) is uniformly globally asymptotically stable at the unique optimal point x^*e of the optimisation problem (4.18). First, we consider the scalar system of (4.21) which is given by

$$y(k+1) = y(k) - \mu \sum_{i=1}^N f'_i(y(k)). \quad (4.24)$$

Note first that the fixed point condition for (4.24) is $\sum_{i=1}^N f'_i(y^*) = 0$. So that a fixed point y^* of (4.24), gives rise, by Lemma 1 to a fixed point of (4.21), which satisfies the necessary and sufficient conditions for optimality (4.19). Now, we wish to use Theorem 6 to show global asymptotic stability. To this end, we need to verify the system (4.21) satisfies all the conditions required in Theorem 6. The condition (4.23) ensures in fact that the right hand side of (4.24) is in fact a strict contraction on \mathbb{R} . It follows from our comments after Lemma 5 that the assumption (ii) of Lemma 5 is satisfied. To show the Lipschitz condition (i) note that by (4.22) each f'_i is globally Lipschitz. As the coordinate functions are globally Lipschitz and sums of globally Lipschitz functions retain that property we obtain condition (ii).

For completeness, we formally state the above arguments as a theorem. In Theorem 9, we refer to a one-dimensional Lure system (2.23) associated to (2.22). The Lure system is used to demonstrate the stability of system (2.22).

Theorem 9 ([94, 115]) *Consider the optimisation problem (4.18), the optimisation algorithm (2.22), and the associated Lure system (2.23). If G is defined by (4.20) and the condition (4.23) holds, then the following assertions hold:*

- (i) *There exists a unique, globally asymptotically stable fixed point $y^* \in \mathbb{R}$ of the Lure system (2.23).*
- (ii) *The fixed point y^* of (i) satisfies the optimality condition (4.19) and thus $y^*e \in \mathbb{R}^N$ is the unique optimal point for the optimisation problem (4.18).*
- (iii) *If, in addition, $\{P(k)\}_{k \in \mathbb{N}} \subset \mathbb{R}^{N \times N}$ is a strongly ergodic sequence of row-stochastic matrices, then y^*e is a globally asymptotically stable fixed point for system (2.22).*

4.3.4 Optimal Decentralised Consensus Algorithm for V2G

We now describe an optimal decentralised consensus (ODC) algorithm that is consistent with Theorem 9 and applies to the practical scenario of interest. The Algorithm 6 follows from the principles defined in Theorem 9 and takes into account practical grid constraints.

For practical implementations of the algorithm, we assume that each EV is able to receive/transmit messages from/to either nearby EVs or available infrastructure (e.g. a base station provided by the aggregator) via a specific communication device (e.g. a mobile phone with access to WiFi/3G networks) facilitated on the EV. In addition, we assume that each EV i can communicate $f'_i(c_i(k))$ with the infrastructure at every time step k , and that the infrastructure can broadcast the feedback signal $\sum_{j \in \Phi(k)} f'_j(c_j(k))$ to the entire network of EVs, and each EV i can send a broadcast signal $c_i(k)$ to its nearby EVs at every time step k .

In Algorithm 6, N_k^i represents the set of neighbours of the i^{th} EV at time k , satisfying $N_k^i \subset \Phi(k)$, which can send their discharge rate signals to the i^{th} EV. We assume that the communications among EVs subject to a variety of distributions such that the corresponding graphs for EV connections are time-varying. However, we require that the communication graphs for EVs are strongly connected at most time instances. Note that this assumption holds if there are sufficient EVs parking in a given area in the airport. To this end, we adopt the same definition of $P(k)$ as specified in (4.13) for modelling the time-varying communication topology of the connected EVs. For convergence of the algorithm, the parameter μ is chosen in the range defined in (4.23) and η_i is chosen in $(0, \frac{1}{N-1})$.

4.3.5 Simulations

To evaluate the performance of the proposed ODC algorithm in a realistic microgrid scenario, a specific microgrid model was constructed through the OpenDSS simulation platform. A schematic diagram is illustrated in Figure 4.14 to demonstrate the structure of the microgrid.

The power topology diagram of this microgrid is shown in Figure 4.13. In the simulation, we assumed that several Distributed Generators (DGs) were installed in the Medium-Voltage (MV) network with voltage level equal to 10kV. This network included three wind plants, two Photovoltaic (PV) plants and one Combined Heat and Power (CHP) plant. The DGs associated with the V2G power inverted from EV batteries are connected through three phase 400V/10kV step-up transformers to the MV network. The DGs were modelled as constant P-Q generators with the same power factor (i.e., 1.0) to generate pure active power for the loads. The capacity of the wind plants, the PV plants and the CHP were chosen as 600kW, 184kW and 800kW. The maximum wind power output for each wind DG was randomly chosen from real wind turbine data according to [141]. In addition, the maximum solar power generation profile of each PV was computed according to a quadratic function with non-zero values from 6am to 6pm, randomly perturbed to simulate cloud disturbances, as in [4]. We assumed that total demand in the microgrid was composed of 20 basic loads

Algorithm 6 Optimal Decentralised Consensus algorithm for V2G

```

1: for  $k = k_0, k_0 + 1, k_0 + 2, \dots$  do
2:   if  $k = k_0$  then
3:     Initialise  $c(k) = 0$ 
4:     Determine the set of available EVs  $\Phi(k)$ 
5:     Each EV  $i$  evaluates  $f'_i(c_i(k))$ 
6:   else
7:     for each  $i \in \underline{N}$  do
8:        $SOC_i(k) = SOC_i(k-1) - c_i(k-1) \cdot \frac{\Delta T}{B_i}$ 
9:       if  $a_i \leq k < b_i$  then
10:        if  $SOC_i(k) \leq SOC_{\min}^i$  then
11:           $\Phi(k) \leftarrow \Phi(k-1) - \{i\}$ 
12:           $c_i(k) = 0$ 
13:        else
14:           $\Phi(k) \leftarrow \Phi(k-1) + \{i\}$ 
15:        end if
16:      else
17:         $\Phi(k) \leftarrow \Phi(k-1) - \{i\}$ 
18:         $c_i(k) = 0$ 
19:      end if
20:    end for
21:
22:    for each  $i \in \Phi(k)$  do
23:      Get  $c_j(k-1)$  from all neighbours  $j \in N_{k-1}^i$ .
24:      Get  $\tilde{F}(k-1) = \sum_{j \in \Phi(k)} f'_j(c_j(k-1))$  from the base station.
25:      Do  $q_i(k-1) = \eta_i \sum_{j \in N_{k-1}^i} (c_j(k-1) - c_i(k-1))$ .
26:      Do  $c_i(k) = \min(c_{\max}^i, c_i(k-1) + q_i(k-1) - \mu \cdot \tilde{F}(k-1))$ 
27:    end for
28:  end if
29: end for

```

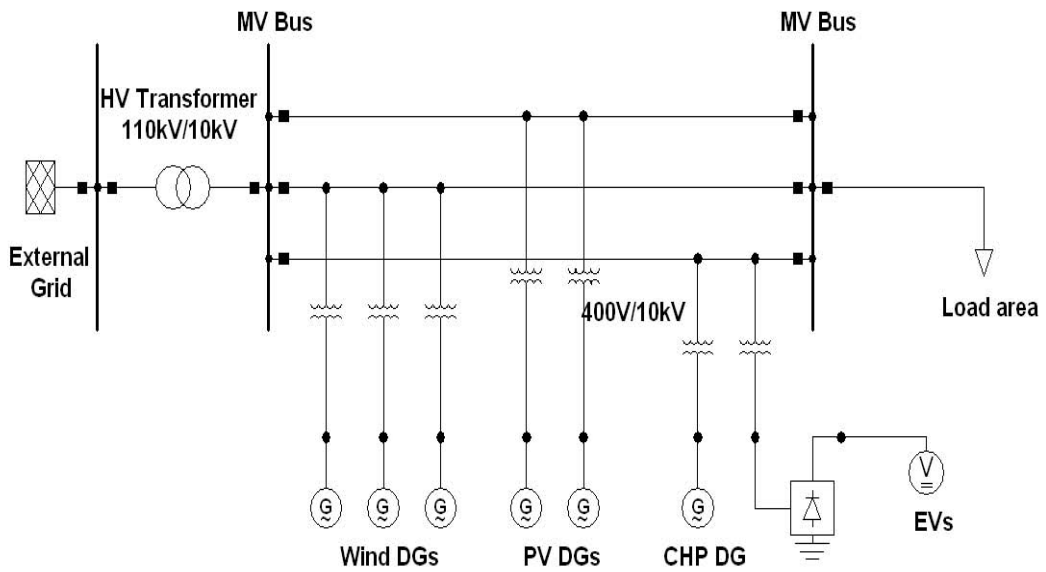


Fig. 4.13 Power topology of the microgrid network

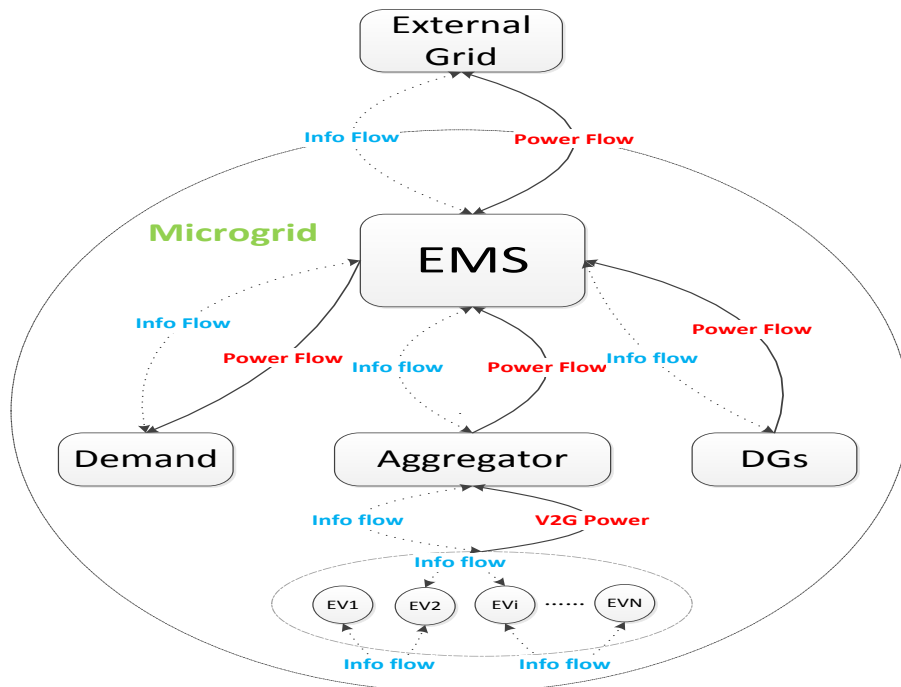


Fig. 4.14 Schematic diagram of the microgrid

connected randomly in the load area, each of which had the nominal power consumption of 100kW. The load profiles were randomly chosen for a period of 24 hours according to [165].

Although microgrids can be also operated in island mode, we assumed in our example that it could still exchange a bidirectional power flow with the external grid supplier, if needed. The V2G programme is activated when the EMS sends the signal to the aggregator that power dispatch from the EVs is required. As long as the signal is not received, the EVs are idle or charged and used as a virtual battery storage device. Finally, we assumed that the CHP is used to balance the power management within the microgrid, if required.

4.3.6 Results and Discussion

We assumed that at the beginning of the simulation, 50 EVs are participating in the V2G scheme. Then, we simulated the arrival process of new EVs as a stochastic process where every minute a new EV arrives with probability 5% until the airport car park is full. The EVs arrive with an initial random SOC greater than 10%, and with a desired SOC_{min} , which corresponds to the minimum level of the battery that is strictly required to return home from the airport at the end of the journey. If SOC_{min} is smaller or equal to the initial SOC, the EV immediately starts participating in the V2G programme, and as illustrated in the algorithm, its SOC will never drop below SOC_{min} . If SOC_{min} is greater than the initial SOC, then the grid treats the EV as a normal load, and only when the SOC reaches the level of SOC_{min} does the EV start to participate in the V2G programme. We assumed that the efficiency parameter of the batteries was different for each EV, and varied it between 80% to 90% uniformly.

We assumed that the cost of generating power with the CHP was a quadratic function with parameters $\alpha = 2$, $\beta = -3$ and $\gamma = 8$. Then, we assumed that the grid would give revenues to the EVs according to another quadratic function with parameters $\alpha_i = 1$, $\beta_i = -5$ and $\gamma_i = 8$. With such values, it is always more cost effective for the grid to take energy from the EVs rather than from the CHP (though, obviously, other pricing functions could be chosen to obtain the same result). In addition, we set the iterative update time ΔT to 1 minute, which corresponds to the sampling rate of the base load, and the optimisation parameters η_i and μ were set to 0.001.

We now first illustrate the dynamics of the ODC algorithm and analyse the performance of the algorithm from the perspective of fair discharging of EV batteries. Then, we show the benefits for the microgrid of introducing the V2G regulation service by simulation studies.

Comment: Figure 4.15 illustrates the discharge rates of all available EVs during the V2G power dispatch. It can be seen that the discharge rates are approximately the same for all the EVs. To better appreciate such a result, we now use the fairness index introduced in [46],

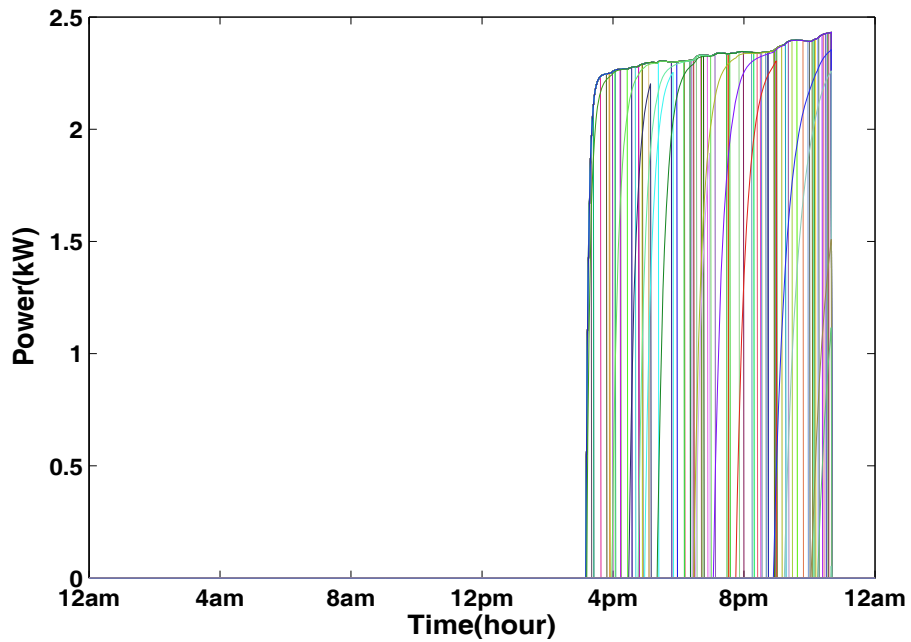


Fig. 4.15 Discharge rates of the EVs with V2G in operation

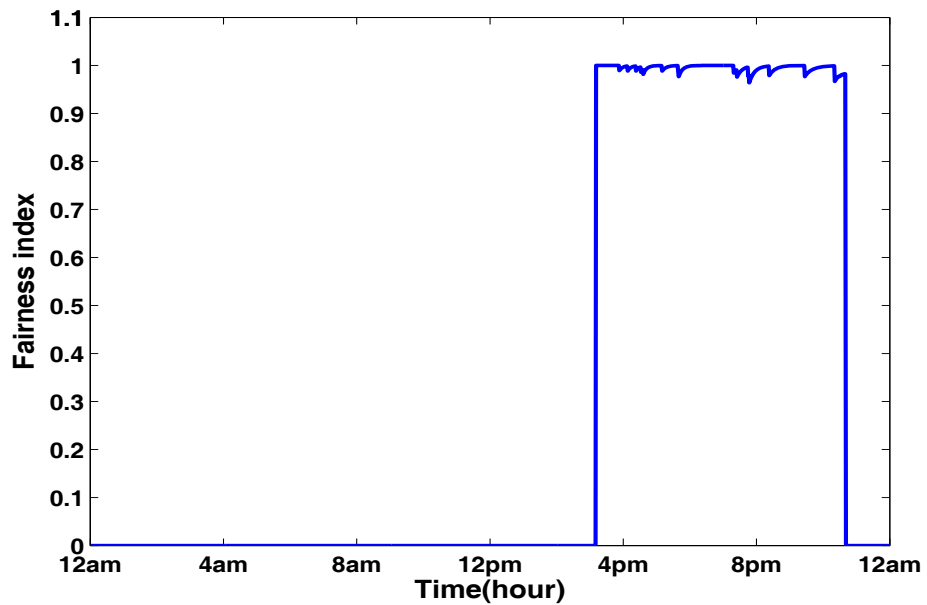


Fig. 4.16 Fairness index of the ODC algorithm with V2G in operation

which is given by:

$$FI(k) = \frac{\left(\sum_{i \in \Phi(k)} c_i(k) \right)^2}{|\Phi(k)| \cdot \sum_{i \in \Phi(k)} c_i(k)^2}, \forall k \in \{1, 2, \dots, M\} \quad (4.25)$$

where $|\Phi(k)|$ denotes the total number of elements in the set $\Phi(k)$. Figure 4.16 shows that the V2G procedure is fair, apart for some transitory time intervals when a new EV starts participating in the scheme. However, fairness is restored in a very short time. The maximum power that can be generated by each of the DGs is depicted in Figure 4.17.

The power generated by the DGs is shown in Figure 4.18. In Figure 4.18, *Totaldemand* refers to the power required by the *Baseload* plus that required by the EVs that are being charged until they reach the required level SOC_{min} . *DGmax* denotes the maximum power that can be generated by all DGs, *DGnoCHP* indicates the total maximum power generation by all DGs without considering the CHP, which corresponds to the power generated by renewable sources, and *DGnoCHP + V2G* corresponds to the power generated by renewable sources plus that stored in EVs. In practice, when the total power generated by renewables sources is smaller than the base load, then the EVs with high SOC are discharged. Vice versa, when the total power generated by renewables sources is greater than the base load, then the EVs participating to the V2G programme are recharged.

The economic benefits for all stakeholders participating in the V2G scheme are illustrated in Figures 4.19-4.22. The economic benefits for EV owners are demonstrated in Figures 4.19-4.20. Further, it is shown clearly from Figures 4.21-4.22 that both the grid company and EV owners benefit from adopting the proposed V2G scheme (Note: the “magnitude” on the y-axis of these figures only illustrates numerical results (i.e. dimensionless) under specified setup for comparison purposes). Hence, both stakeholders are incentivised to participate in the V2G scheme resulting in better utilisation of EVs and renewable energy sources.

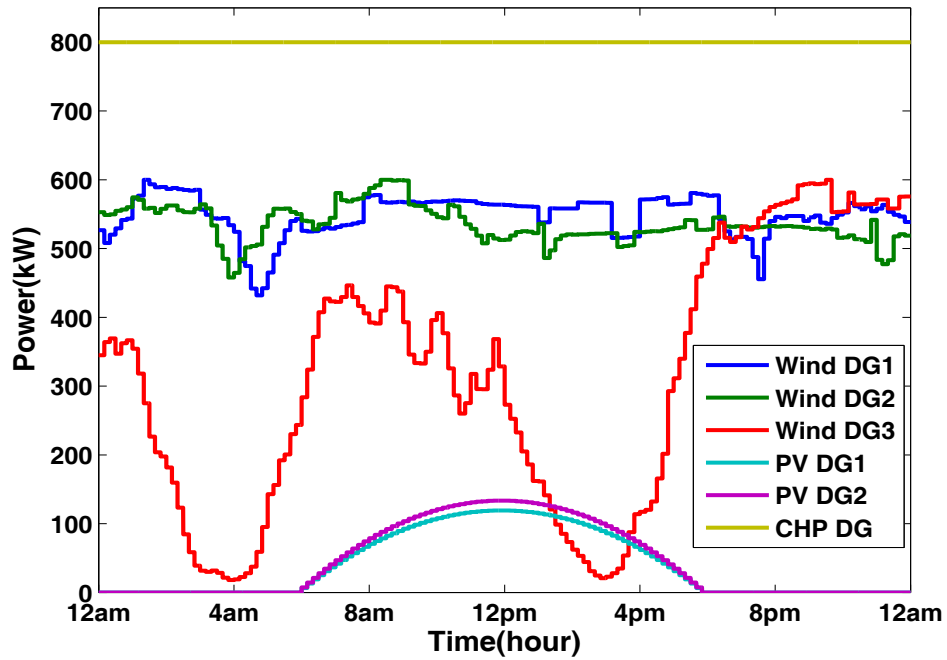


Fig. 4.17 Power generation profiles of DGs

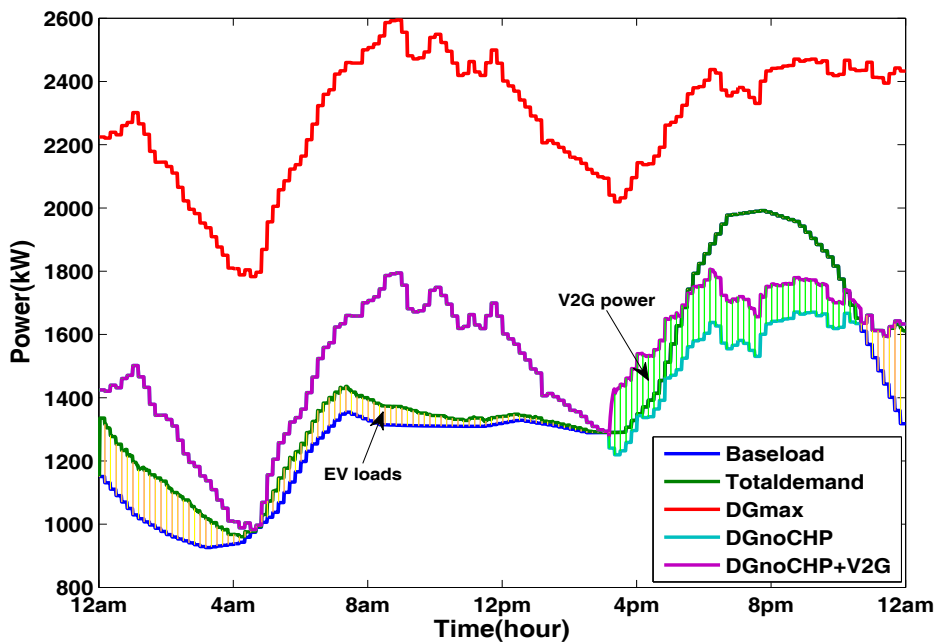


Fig. 4.18 Comparison of demand and power generation with V2G and EV loads

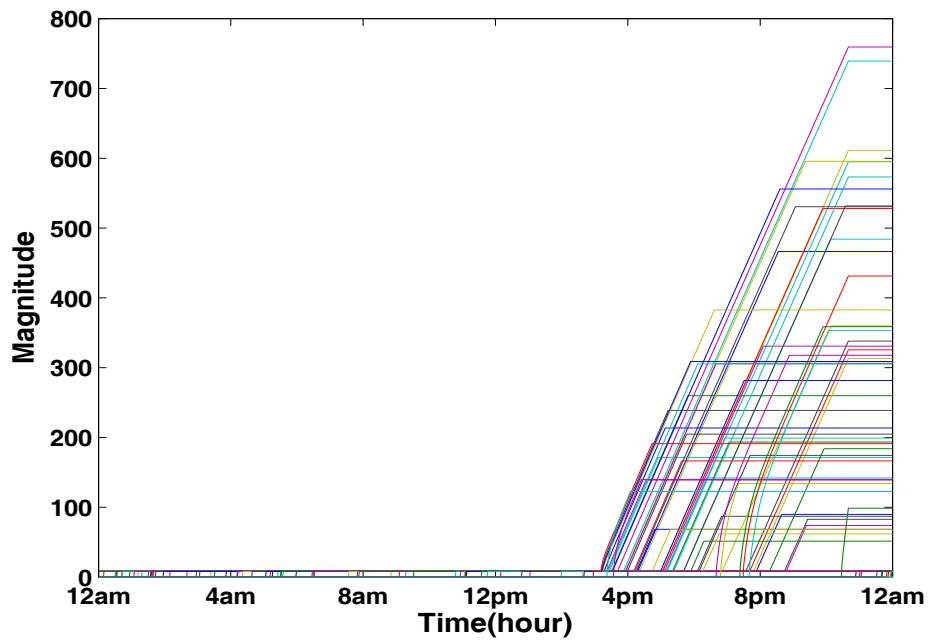


Fig. 4.19 Accumulative economical benefits for each EV in the scheme

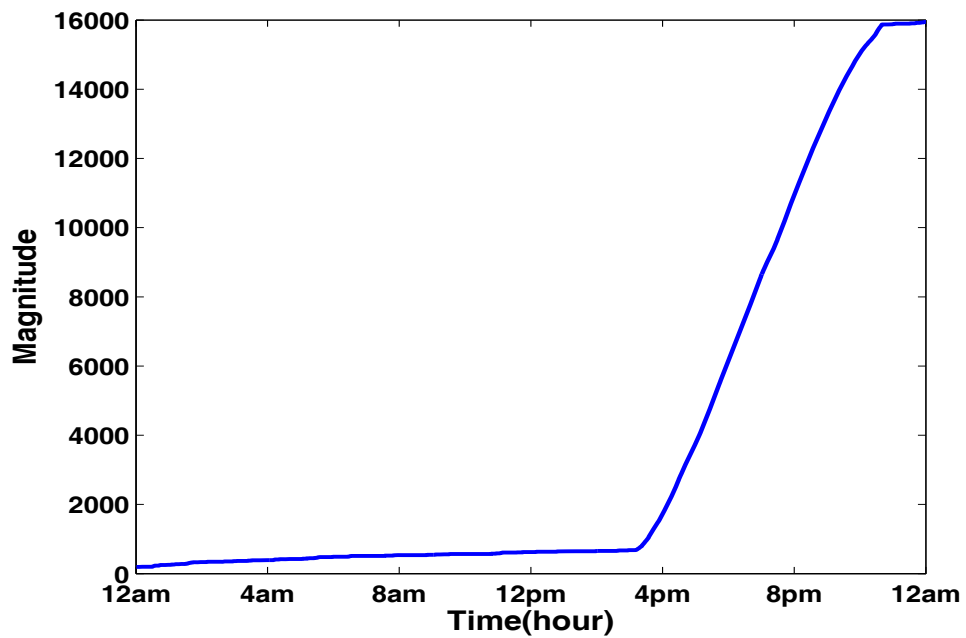


Fig. 4.20 Accumulative economical benefits for all EVs in the scheme

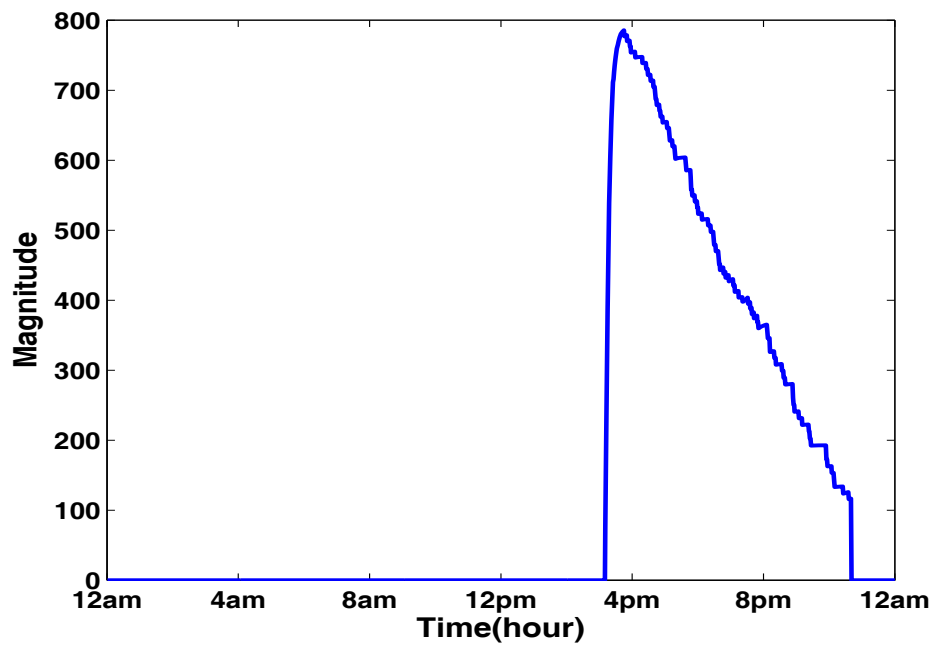


Fig. 4.21 Economical benefits for the grid at each time slot

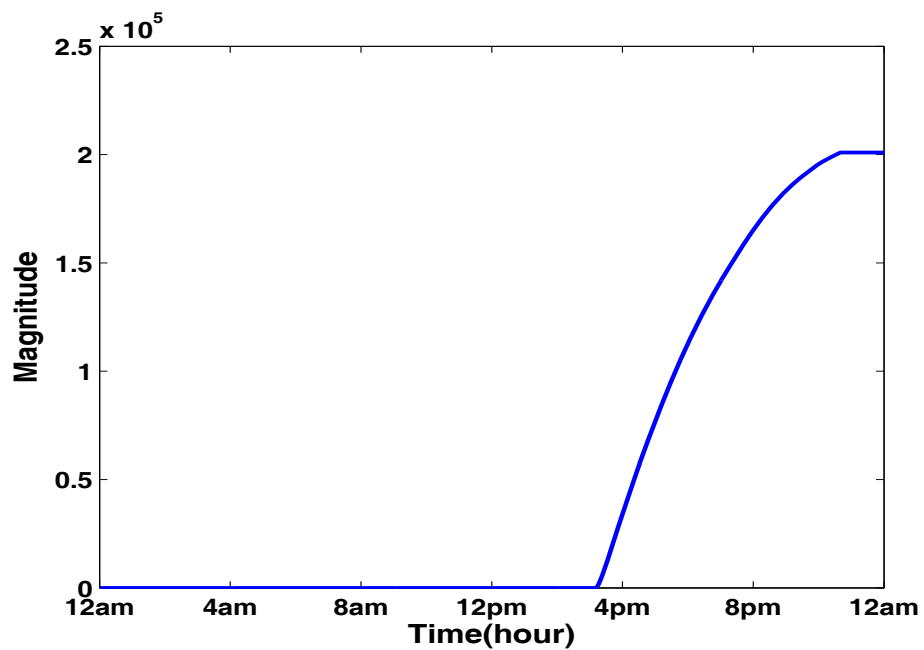


Fig. 4.22 Accumulative economical benefits for the grid

4.4 Conclusions

In this chapter we have shown that by harnessing the power of V2G technologies, groups of EVs can be used to provide effective ancillary services to the grid. Specifically, we investigate two V2G applications in different scenarios.

In the first scenario, we applied a recently proposed distributed consensus algorithm in [94] to a group of EVs to design an EV charging strategy which minimises the current imbalance on a three phase distribution network. Matlab simulations were presented to illustrate the consensus characteristics and rate of convergence of the algorithm. Realistic power system simulations were implemented on a dedicated testbed to demonstrate the effectiveness of the algorithm in terms of the reductions in power losses and current imbalance.

In the second scenario, we applied an optimal decentralised consensus algorithm to design a fair V2G programme. In this programme, a microgrid stores the surplus energy generated by renewable sources in EV batteries, and takes it back when needed. The optimality of the V2G strategy is with respect to utility functions that contain an economic term (the more energy taken from the EVs, the better for the grid), and a QoS term (the energy taken from the EV batteries must be limited to avoid getting close to the minimum level of SOC required to complete the journey home when the owner takes his/her EV). Then, we formulated the fair power dispatch problem of EVs as an optimisation problem with consensus constraints.

The chapter also derived a specific form of function G in system (2.22) based on first order optimality conditions and demonstrated that such a system can be used to solve a class of optimisation problem with consensus constraints. We further applied this result to solve our specific optimisation problem by including realistic grid constraints and we illustrated the resulting optimal decentralised consensus algorithm. To evaluate this strategy, we simulated the ODC algorithm on a Matlab/OpenDSS testbed, and demonstrated its performance both in terms of fairness and in terms of economic convenience for the grid.

As a conclusion, the overall objective in this chapter was to apply consensus based algorithms to solve two specific application problems by using V2G techniques. The consensus algorithm in the first application was used to regulate active and reactive power consumption on each phase of the grid network such that the current imbalance can be minimised. In contrast, in the second application, the consensus algorithm was applied in an optimisation framework, where the consensus of the algorithm refers to the “fairness” in terms of the amount of power dispatch from EVs. The optimality of the algorithm was achieved by adding a common feedback term to the basic consensus algorithm, and a specific form was later derived which guarantees the first order optimality condition. Finally, note that the proposed optimisation framework is useful to solve other problems in different scenarios as we shall see later in Chapters 6 and 7.

Part III

Optimal Energy Management Strategies in Smart Grid

Chapter 5

Optimal Algorithms for Energy Management

***Abstract:** In this chapter, we adapt the distributed AIMD algorithm to optimally share the power generation tasks for distributed energy resources in a microgrid scenario. This idea is further extended to incorporate thermal constraints for double power balancing requirements. The work in this chapter was undertaken in cooperation with Emanuele Crisostomi, Marco Raugi, and Robert Shorten, and published in [35, 106].*

5.1 Introduction

One of the most interesting and challenging objectives of the smart grid is to enable situational awareness of the grid, and to allow for fast-acting changes in power production and power routing, thus altering the stream of electrical supply and demand on a moment-by-moment basis. However, balancing the energy demand and the energy offer is a challenging problem due to a number of effects, e.g., the uncertain demand and the energy that can be offered.

- **The uncertain demand.** This refers to the uncertain energy consumption of both industries and single users. Many authors have addressed this problem using techniques from machine learning and time series analysis in an attempt to accurately forecast the power load [131, 132, 148, 193].
- **The uncertain energy offer.** As the penetration level of energy being produced from renewable sources is constantly increasing, the availability of energy is highly affected by weather conditions (i.e., availability of sun/wind). More accurate weather forecast services, together with an extensive use of storage systems, are currently used to mitigate such uncertainties [206].

In addition, such an ambitious objective (i.e. real-time power balancing) also poses difficult issues for the Energy Management System (EMS) of the power network in terms of communication and control. In fact, in order to optimally share the power generation task among the DERs, the EMS is required to solve an optimal scheduling problem at fixed time steps, typically chosen between 5 and 30 minutes. To solve this problem, it is usually necessary to apply a centralised based optimisation to determine the optimal solution at every fixed time step. However, this centralised solution has the main drawback of a significant communication overhead, as every single DER must communicate to the EMS how much power can be provided. Then, the EMS must gather all this information, and the energy needed by all users, to solve an optimisation problem, and communicate back to each DER its correct allocation of energy. See for instance [4, 149, 150] for examples of this approach to optimal power scheduling. In the future, when considering a larger energy system framework with heating devices (e.g. CHPs), the communication and control of power generation will become even more difficult since the amount of electrical power generation is associated with the amount of thermal power generation.

To overcome these issues, some authors have designed day-ahead thermal and electrical scheduling algorithms for large-scale VPPs (LSVPPs) [62, 101, 159] where the day-ahead unit commitment problem is solved in a distributed fashion. In [194] the day-ahead solution is then corrected in a centralised framework, considering latest available measurements. In fact, in the afternoon prior to the scheduled energy delivery, the hourly prices for the following day (set by electricity spot markets) are already known, and at the same time, quite accurate weather and load forecasts are also available [62]. This approach is for the most part effective. However, it does not consider real-time information, such as the error between the available power and that predicted on the basis of weather forecast, that could be important to fully exploit renewable resources. In addition, this solution is not robust, and problems in the EMS will have consequences for the entire network in terms of grid stability. Therefore, it is desirable to design an algorithm that automatically shares the power generation tasks among the available DERs satisfying the energy demand and to reduce the increasing requirements in terms of communication overhead and complex control of the conventional EMS.

In the last chapter, we investigated the optimal V2G power dispatch of EVs in a low-voltage microgrid using the proposed optimised distributed consensus algorithm. The idea of this distributed algorithm arises from the convergence and optimality of the dynamical system introduced in Chapters 2 and 4. In this chapter, we consider the optimal power dispatch problem of DGs in a VPP scenario. We show that by adapting an AIMD algorithm [33, 189], which has been introduced in Section 3.3.2, a cost utility function of interest can be minimised in a distributed manner. To show the efficacy of the algorithm, we implement

the proposed strategies in a realistic power network simulation with a few DERs and a total load of the order of a few MW. With these results we show that the achievable performance is very close to the full communication centralised case. In addition, we also demonstrate that the idea of the algorithm can be further extended to include thermal balancing requirements and provide supporting simulation studies.

The remainder of this chapter is organised as follows. Section 5.2 describes the power generation problem and the financial cost function of a microgrid. Section 5.3 reviews the basic AIMD algorithm and explains how it can be adapted to minimise power generation costs in a distributed manner. In the same section we also explain how the proposed algorithm can be adapted to optimise both thermal and electrical scheduling. Section 5.4 introduces the simulation setup using a Matlab/OpenDSS environment, and compares the performance of the proposed algorithm with that of a fully centralised solution in two scenarios, i.e., one scenario considers the electrical scheduling and the other considers the scheduling for both electrical and thermal power generation. Finally, Section 5.5 concludes the chapter.

5.2 Problem Statement and Preliminaries

We consider the scenario depicted in Figure 5.1, and assume that at a given time k , each one of N DERs provides an amount of power denoted as $p_i(k)$, where the index i refers to the i^{th} DER. In addition, we define the set $\underline{N} := \{1, 2, \dots, N\}$ for indexing all DERs. Our main

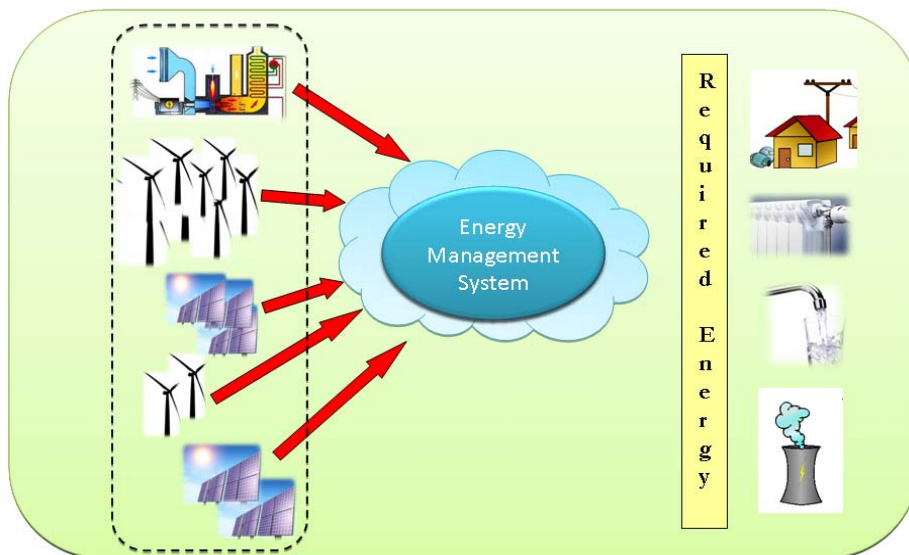


Fig. 5.1 DERs (on the left) must provide enough energy to satisfy the demand coming from the users (e.g., from industries and residential areas).

assumption is that at every time step k , the overall set of DERs is always able to provide the total power $d(k)$ required by the users. Therefore, the EMS has the ability to choose which of the DERs will be used, and in which proportion, to provide the requested power.

Remark: Note that the assumption that the power requested by the users is smaller or equal to the capacity of the DERs is not a strong assumption. In fact, if this is not true, then the EMS can either take more energy from storage systems, or buy it from other VPPs or from the external grid. It may also decide to disconnect some of the loads, thus reducing the demanded power. After completing any of the previous actions, the condition that the energy produced by the DERs is enough to satisfy the (residual) demand holds. Many papers in the literature have tackled the problem of which of these actions is more convenient from the EMS point of view; see for instance [4], [149] and [150] that propose optimal scheduling solutions. However, this problem is not of interest here. In this work it is more convenient to simply assume that the demand is smaller than the power deliverable from the DERs; otherwise, the load is provided in a best effort fashion.

As the DERs provide more or equal power than is required by the users, the purpose of this chapter is to automatically allocate power generation tasks among DERs in a decentralised manner such that some utility function of interest is minimised; namely, the financial cost associated with power generation.

5.2.1 Utility Minimisation

In principle, the EMS has many ways of sharing the power demand among the available DERs. We are interested in the power share that minimises the financial cost of producing the desired power. To solve this problem, we associate each DER with a quadratic utility function, as is common in the VPP literature, see [20] and [149].

$$C(P_g) = a \cdot P_g^2 + b \cdot P_g + c, \quad (5.1)$$

where C is the hourly cost in Currency Unit (C.U.) per hour, P_g is the generated power in MW, and a , b and c are coefficients of appropriate measurement unit that depend on the technology of the power plant (e.g., fuel cost, efficiency, etc). In particular, b includes operation and maintenance costs (O&M) costs, and fuel and carbon costs, which are usually expressed in €/MWh (or in /kWh). The coefficient c takes into account the expenses that are incurred even if no energy is produced at all. Quadratic cost functions have been used in many references in the literature, see for instance the classic reference [151], or the more recent references

[20] and [149] in the context of VPPs. Due to the fact that the coefficients a are usually quite small, and because of the difficulty of handling nonlinear (though quadratic) cost functions, many authors in the literature simply neglect the quadratic term, and use affine functions in the optimisation; see for instance [4]. Also note that in the literature it is very simple to find databases containing values of coefficients b and c for several examples of DERs all over the world, for the computation of the Levelised Costs of Electricity (LCOE) [180].

In this work we use the complete quadratic cost function (5.1) to minimise total financial costs of the DERs. Note that the quadratic cost functions can also be used to model an environmentally friendly utility function (e.g., CO_2 or SO_2 emissions in terms of active power generation of a traditional power plant) to stimulate the penetration of renewables [41, 63]. However, the study can be extended for minimisation of other convex utility functions of interest, which is the subject of our current work.

5.3 AIMD based Utility Optimisation Algorithms

The problems that we described are very close to those encountered in Internet congestion control. In Internet congestion control, one tries to allocate bandwidth such that certain objectives are realised [186]. A wide variety of work has been published in this area and it can be shown that TCP Reno and TCP Vegas both correspond to different utility maximisation solutions [186]. In AIMD an individual agent (e.g., a computer sending packets) gently increases its transmission rate, during the Additive Increase (AI) phase, until a packet loss signal is received. This is called a congestion event, and indicates that the sum of individual bandwidths has exceeded the total capacity. Upon detecting congestion, the agents instantaneously decrease their transmission rate in a multiplicative fashion. This is the Multiplicative Decrease (MD) phase of the algorithm [28].

Note that the congestion control problem in the Internet exhibits similar characteristics to the power generation scenario considered here. The quantities of interest are positive (bandwidth/power), locally bounded (local maximum transmission rate/available power), the available capacity/required energy may vary over time, and the system of interconnected agents (Internet/Smart Grid) is very large scale. We refer the reader to Section 3.3.2 for the application of AIMD algorithms in an EV charging context and references [28, 33, 34, 177, 178] for a detailed discussion on convergence properties of the AIMD algorithms.

5.3.1 AIMD

In this section we recall the basic AIMD algorithm introduced in Section 3.3.2 and adapt the AIMD algorithm to the new scenario of interest here.

Algorithm 7 Basic AIMD Algorithm (p_i)

```

 $p_i(0) = p_{i0}$ 
while simulation not ended do
  if  $\sum_{i=1}^N p_i(k) < d(k)$  then
     $p_i(k+1) = \min(p_i(k) + \alpha_i, \bar{p}_i(k)), \forall i \in \underline{N}$  (AI)
  else
     $p_i(k+1) = \max(\beta_i p_i(k), \underline{p}_i(k)), \forall i \in \underline{N}$  (MD)
  end if
   $k = k + 1$ 
end while

```

In Algorithm 7, the parameter α_i is the positive additive parameter associated with the additive increase phase of the algorithm (AI) (expressed in kW or MW), and $0 < \beta_i \leq 1$ is the multiplicative parameter used in the decrease phase (MD). The quantities $\underline{p}_i(k)$ and $\bar{p}_i(k)$ denote the minimum and maximum bound on the power respectively. $p_i(k)$ represents the real power output from the i^{th} DER at time k . In fact, the values of p_i cannot take arbitrary values due to: (i) the limited sizes of the DERs; (ii) the availability of renewables (sun/wind); (iii) the power network constraints (e.g., transformer tap settings, security constraints, minimum voltages at load buses and transmission lines); and (iv) due to the physical constraints on the DER ramp rate. Note also that such bounds are time varying.

Remark: The main feature that makes the AIMD algorithm particularly convenient to apply in large-scale systems, is that the algorithm can be easily implemented in a truly distributed manner. In fact, Algorithm 7 only requires the EMS to send a “congestion notification” to the DERs when the produced power equals the demanded power, which can be coded in a single bit of information. In the context of power balancing, such a notification will be denoted as *balancing notification* in the remainder of the chapter. This implies that the DERs do not have to exchange information among themselves, do not have to communicate the available sun/wind to the EMS, and also do not even have to communicate when they stop or start contributing to the power generation task. Furthermore, the EMS itself does not have to communicate to the DERs how much power they must provide. Note that in Algorithm 1 (Section 3.3.2) the MD phase consists of two multiplicative parameters selected randomly where in Algorithm 7 only one multiplicative parameter is chosen. Having two (or more)

multiplicative parameters gives more flexibility for implementation of the AIMD algorithm. For instance, in the EV charging scenario, one could design a larger multiplicative parameter to increase power utilisation and a smaller multiplicative parameter to reduce the number of congestions events. For the applications considered in this chapter, the more complex multi-parameter implementation of the algorithm is not required.

In order to illustrate in a simple fashion the mechanism of the basic AIMD algorithm (Algorithm 7), Figures 5.2 to 5.5 illustrate the output of the algorithm in a simple toy example, which corresponds to the VPP scenario investigated in [4]. Therefore, we assume that three DERs are available: a PV plant; a wind plant; and a CHP. It is assumed that the PV plant has a net capacity of 6 MW and a capacity factor of 6%; the wind plant has a net capacity of 45 MW and a capacity factor of 27%; the CHP plant has a net electrical capacity of 40 MW and a capacity factor of 85%. We assume that all DERs have the same α_i and β_i parameters equal to 0.01 MW and 0.95 respectively. Figure 5.2 illustrates the case without constraints (i.e., without even considering the sizes of the power plants), when the power demand is constant and equal to 35 MW. Note that in this case AIMD gives rise to the fair solution where each single DER produces exactly the same quantity of energy. When the smaller sizes of the renewable energy sources, together with renewable availability (e.g., no sun at night time) are introduced, the AIMD solution provides completely different results as depicted in Figure 5.3. The case study scenario is further complicated, if a more realistic non-constant power demand is associated. The corresponding results are shown in Figure 5.4 (the time-varying demanded power profile is taken again from [4]). In the same scenario, Figure 5.5 compares the associated power demand and power generation. Note that power generated by the individual DER is now summed, and, as expected, demand and offer are perfectly balanced.

Remark: Algorithm 7 illustrated in this section gives rise to saw-tooth signals. Note that not all equipment may be capable of handling such signals. Thus, typical methods that are already used to handle oscillating power generated from renewable sources might be required (e.g., PI-smoothing of the output power, pre-filtering of the AIMD signal, use of batteries for primary frequency and voltage control).

5.3.2 Utility Optimisation via Synchronised AIMD

The basic AIMD algorithm is designed to share the required energy among the available DERs in some manner. For instance, if there were no constraints, then each DER would provide the same quantity of energy as illustrated in Figure 5.2. In this section we show

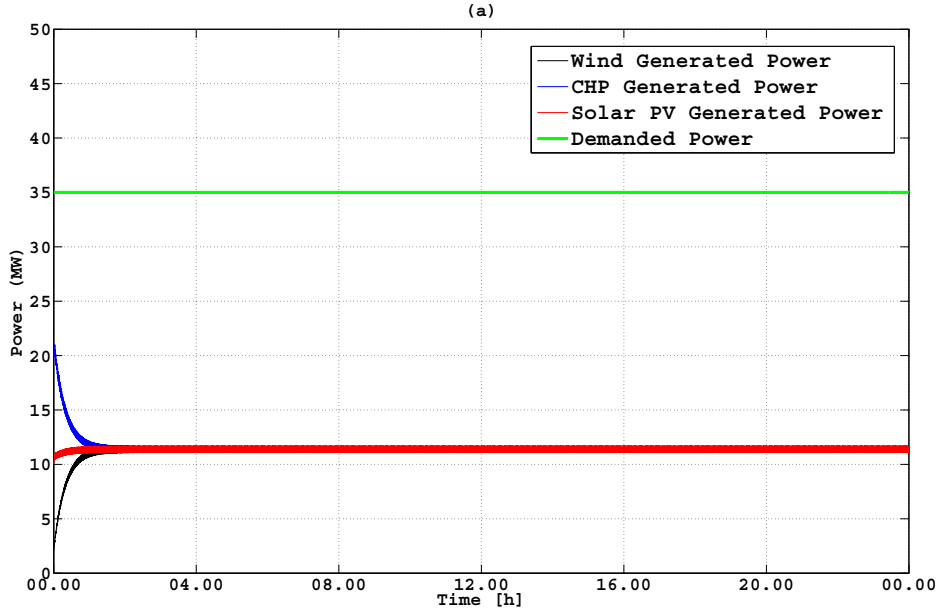


Fig. 5.2 A scenario where a PhotoVoltaic (PV) plant, a wind plant and a CHP are required to provide a (static) power of 35 MW. The fair sharing solution is that all plants provide the same power.

that by appropriately modifying the basic AIMD algorithm, it is possible to minimise the financial cost of generating the required power, according to the cost functions introduced in Section 5.2.1. Similar work in this direction can be found in [34, 84, 189]. The optimisation problem can be formally stated as

$$\begin{aligned} \min_{p_i(k)} \quad & \sum_{i=1}^N f_i(p_i(k)) \\ \text{subject to:} \quad & \sum_{i=1}^N p_i(k) = d(k) \end{aligned} \quad (5.2)$$

i.e., at every time step k we want to find the combination of $p_i(k)$ such that the generated power is equal to the requested power, and it minimises the sum of the cost functions. Further, we assume that the optimal solution of $p_i(k)$ is in the interior of the polytope, constructed by the constraints, as a feasible region [16]. Each utility function has the form $f_i(p_i(k)) = a_i \cdot p_i(k)^2 + b_i \cdot p_i(k) + c_i$, as was described in Section 5.2.1. Note that in this section we do not consider the constraints on the single $p_i(k)$, as the AIMD algorithm will automatically satisfy them as described in Section 5.3.1. This minimisation problem can then

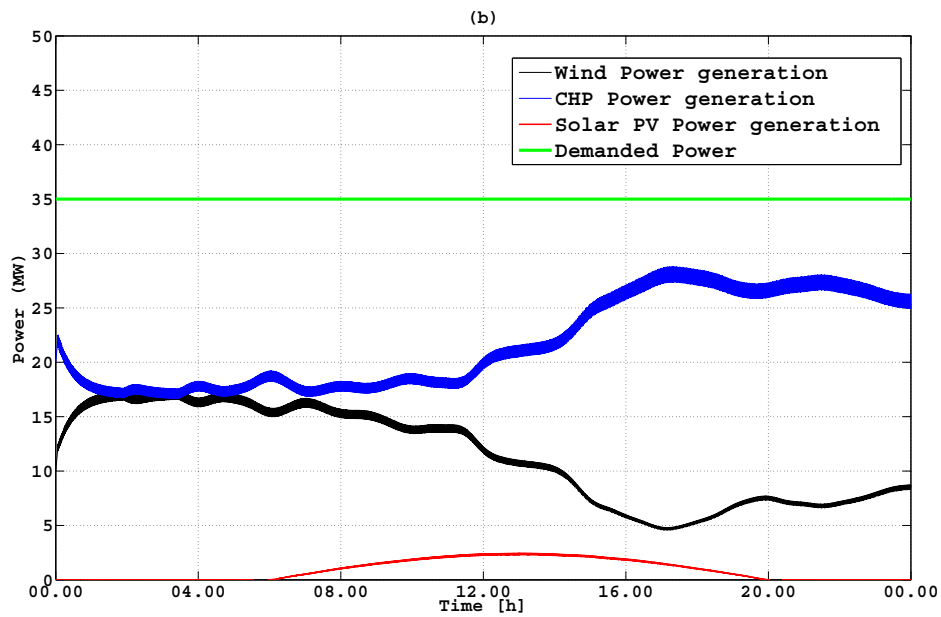


Fig. 5.3 Constraints on the plant sizes and availability of solar / wind.

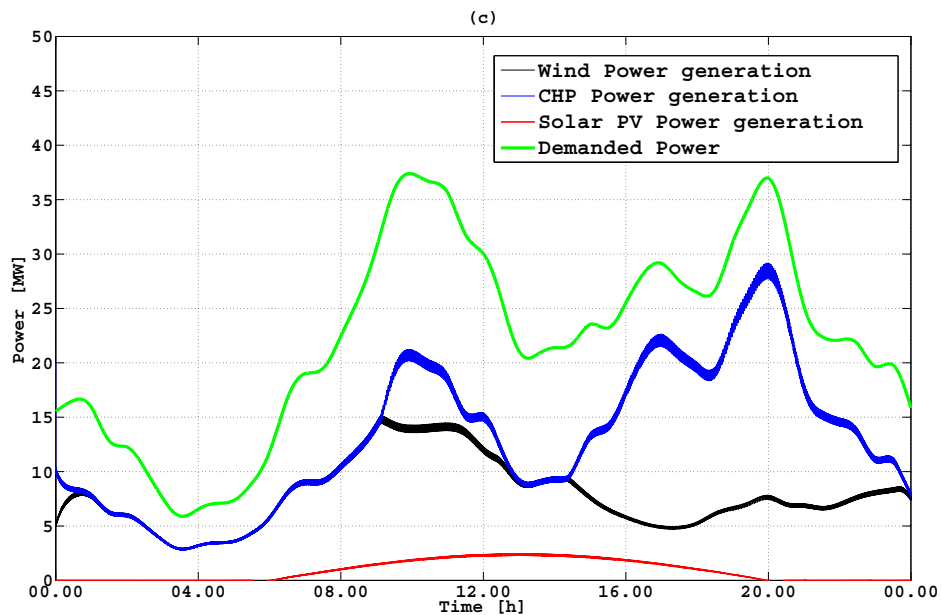


Fig. 5.4 A typical non-constant energy requirement.

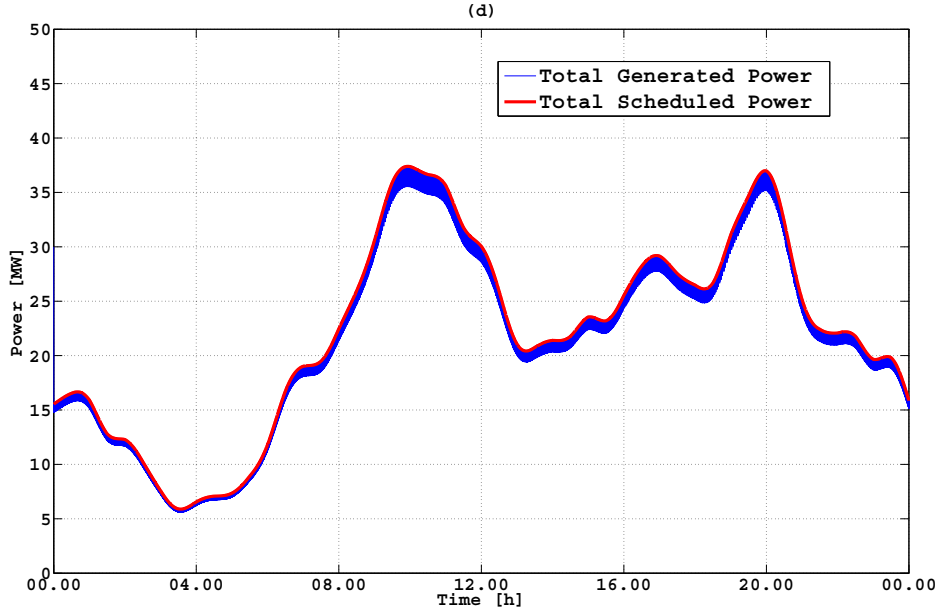


Fig. 5.5 Required and provided power (summing contributions of single plants) of scenario in Fig. 5.4.

be conveniently solved at each time step k with the aid of Lagrange multipliers. With this in mind, the optimal solution $p_i^*(k)$ can be obtained by solving the following equations:

$$\frac{\partial \left[\sum_{i=1}^N f_i(p_i(k)) + \lambda(k) \left(d(k) - \sum_{i=1}^N p_i(k) \right) \right]}{\partial p_i(k)} = 0, \forall i \in \underline{N} \quad (5.3)$$

where $\lambda(k)$ represents the Lagrange multiplier for the linear constraint $\sum_{i=1}^N p_i(k) = d(k)$. By substituting $f_i(p_i(k)) = a_i \cdot p_i(k)^2 + b_i \cdot p_i(k) + c_i$, we obtain

$$p_i^*(k) = \frac{\lambda^*(k) - b_i}{2a_i}, \quad (5.4)$$

where

$$\lambda^*(k) = \frac{d(k) + \sum_{i=1}^N \frac{b_i}{2a_i}}{\sum_{i=1}^N \frac{1}{2a_i}} \quad (5.5)$$

subject to the linear constraint being satisfied, and where the uniqueness of the solution follows from the convexity of the quadratic functions. Note that the Karush-Kuhn-Tucker (KKT) conditions (5.3) are necessary for optimality [16]. By placing extra conditions (i.e., the convexity) on the utility functions they are also sufficient. Our approach is similar, but

we solve the minimisation problem by achieving consensus on the value of the function $\lambda_i(k) := \partial f_i(p_i(k))/\partial p_i(k)$, i.e., $\lambda_i(k) = \lambda_j(k)$, $\forall i, j \in \underline{N}$, subject to the linear constraint. Note that the consensus condition can be derived from (5.3). To this end, the basic AIMD algorithm can be adapted for utility optimisation purposes as follows:

Algorithm 8 AIMD Utility Optimisation (λ_i)

```

 $p_i(0) = p_{i0}$ 
while simulation not ended do
  if  $\sum_{i=1}^n p_i(k) < d(k)$  then
     $\lambda_i(k+1) = \lambda_i(k) + \alpha_\lambda$ ,  $\forall i \in \underline{N}$  (AI)
  else
     $\lambda_i(k+1) = \beta_\lambda \lambda_i(k)$ ,  $\forall i \in \underline{N}$  (MD)
  end if
   $k = k + 1$ 
end while

```

In Algorithm 8, the multiplicative step is performed when the sum of delivered power exceeds the requested power. All DERs have the same parameters α_λ and β_λ , so called to denote that they refer to an AIMD algorithm applied to the variable λ . Therefore, AIMD makes all λ_i converge to a unique value which is λ^* . Note that each DER has to update its own variable λ_i , and the only communication requirement is the balancing notification from the EMS.

5.3.3 Practical Implementation

The utility optimisation problem can be theoretically solved by simply running an AIMD consensus problem on λ_i , as when all DERs have the same value of λ_i , then this value has to be λ^* . However, $\lambda_i(k) = \partial f_i(p_i(k))/\partial p_i(k)$ is only an abstract quantity which, for the choice of utility functions considered here, is $2a_i p_i(k) + b_i$; it is not straightforward to compute how a DER can change its own value of $\lambda_i(k)$ by adjusting its power generation, and also how to express the power constraints in terms of $\lambda_i(k)$. Therefore, we now remap the AIMD algorithm in terms of $p_i(k)$ instead of $\lambda_i(k)$. By simply exploiting the fact that $\lambda_i(k) = 2a_i p_i(k) + b_i$, we can rewrite Algorithm 8 as Algorithm 9.

Note that this algorithm provides the same solution as Algorithm 8 with parameters α_λ and β_λ , and is formally identical to Algorithm 7 when the parameters for each DER are defined as

Algorithm 9 AIMD Utility Optimisation (p_i)

```

 $p_i(0) = p_{i0}$ 
while simulation not ended do
  if  $\sum_{i=1}^N p_i(k) < d(k)$  then
     $p_i(k+1) = \min(p_i(k) + \frac{\alpha_\lambda}{2a_i}, \bar{p}_i(k)), \forall i \in \underline{N}$  (AI)
  else
     $p_i(k+1) = \max((\beta_\lambda + b_i \frac{\beta_\lambda - 1}{2a_i p_i(k)})p_i(k), \underline{p}_i(k)), \forall i \in \underline{N}$  (MD)
  end if
   $k = k + 1$ 
end while

```

$$\alpha_i = \frac{\alpha_\lambda}{2a_i}$$

$$\beta_i(k) = \beta_\lambda + b_i \cdot \frac{\beta_\lambda - 1}{2a_i p_i(k)}. \quad (5.6)$$

Algorithm 9 solves the utility optimisation problem, while retaining the convenient feature of AIMD that the only required communication is the notification of the balancing event, broadcasted by the EMS to all the DERs. The only required assumption is that each DER knows its own cost function (i.e., parameters a_i , b_i and c_i that associate their own generated power with the financial costs) as this information is needed to tune the personal AIMD parameters α_i and β_i .

5.3.4 Extensions for Thermal and Electrical Scheduling

In this section, we shall demonstrate how to extend the idea in Algorithm 9 to include thermal balancing requirements. To this end, we describe the optimisation problem and develop a full AIMD algorithm for solving the problem.

To be consistent with the previous sections, we still adopt quadratic utility functions for the total financial costs from DGs. However, the objective of the new AIMD algorithm is to compute the optimal instantaneous $p_i^{\text{et}}(k)$ and $p_i^{\text{th}}(k)$ (i.e. electrical and thermal power

generated by the i^{th} DER) that minimise the total cost of power generation, while satisfying the power demand by the users; mathematically this optimisation problem is given as:

$$\begin{aligned} \min_{p_i^{\text{el}}(k), p_i^{\text{th}}(k)} \quad & \sum_{i=1}^N f_i^{\text{el}}(p_i^{\text{el}}(k)) + f_i^{\text{th}}(p_i^{\text{th}}(k)) \\ \text{subject to:} \quad & \left\{ \begin{array}{l} \sum_{i=1}^N p_i^{\text{el}}(k) = d^{\text{el}}(k) \\ \sum_{i=1}^N p_i^{\text{th}}(k) = d^{\text{th}}(k) \end{array} \right\} \end{aligned} \quad (5.7)$$

In optimisation problem (5.7), the electrical and thermal power flows of the i^{th} DER are denoted by p_i^{el} and p_i^{th} , respectively. The formulation problem (5.7) is a general one, as we are assuming that each DER could in principle generate both thermal and electric power. Also, we are assuming that the cost functions for producing thermal or electrical power could be different. This general formulation allows us to consider indirect thermal power production, e.g., a PV plant could be connected to a boiler and be simultaneously used to provide thermal power. In this section, utility functions for both the electrical (f_i^{el}) and the thermal (f_i^{th}) are modelled as quadratic functions.

To solve (5.7), we need to suitably tailor the AIMD algorithms in order to achieve a second balancing objective, related to the thermal power flows. Thus, we design the Algorithm 10 which alternatively performs an AIMD step on the electrical power, and one on the thermal power; also, as the two steps are strongly related (e.g. the electrical power production of a CHP is coupled with its thermal production), we give priority to one of the two power balancing loops, namely, the thermal loop. The motivation to do so is that most power plants have the ability to generate electrical power, while usually only a subset of them can also directly provide thermal power.

Note that in Algorithm 10, the electrical AIMD step is performed by a subset of all DERs \underline{N} denoted as \underline{M} ; in particular, the DERs in the set \underline{M} are not involved in the thermal power balancing loop. This strategy has been used to deal with the case where the thermal AIMD algorithm requires some DERs to increase their thermal power generation (i.e. because the thermal demand is greater than the supply), while the electrical AIMD algorithm requires some DERs to decrease their electrical power generation (i.e., because the electrical demand is lower than supply). As the quantity of electrical power provided by a DER is usually related to the provided thermal power, such a conflicting situation is not simple to handle. A possible way to solve it is to appropriately choose the value of α_i^{th} , α_i^{el} , β_i^{th} and β_i^{el} to give more importance to the thermal balancing loop; alternatively, which is the solution implemented here in Algorithm 10, we assume that a subset of DERs is used only to accommodate the residual electrical power request.

Algorithm 10 Full AIMD Algorithm ($p_i^{\text{th}}(k), p_i^{\text{el}}(k)$)

```

 $p_i^{\text{th}}(0) = p_{i0}^{\text{th}}, p_i^{\text{el}}(0) = p_{i0}^{\text{el}}$ 
while simulation not ended do
  if  $\sum_{i=1}^N p_i^{\text{th}}(k) < d^{\text{th}}(k)$  then
     $p_i^{\text{th}}(k+1) = \min(p_i^{\text{th}}(k) + \alpha_i^{\text{th}}, \bar{p}_i^{\text{th}}(k)), \forall i \in \underline{N}$  (AI)
  else
     $p_i^{\text{th}}(k+1) = \max(\beta_i^{\text{th}} p_i^{\text{th}}(k), \underline{p}_i^{\text{th}}(k)), \forall i \in \underline{N}$  (MD)
  end if
  if  $\sum_{i=1}^N p_i^{\text{el}}(k) < d^{\text{el}}(k)$  then
     $p_i^{\text{el}}(k+1) = \min(p_i^{\text{el}}(k) + \alpha_i^{\text{el}}, \bar{p}_i^{\text{el}}(k)), \forall i \in \underline{M}$  (AI)
  else
     $p_i^{\text{el}}(k+1) = \max(\beta_i^{\text{el}} p_i^{\text{el}}(k), \underline{p}_i^{\text{el}}(k)), \forall i \in \underline{M}$  (MD)
  end if
   $k = k + 1$ 
end while

```

Comment: Similar to (5.2), the optimisation problem (5.7) can be easily solved by appropriately choosing the AIMD parameters; in particular, the optimal choice is

$$\alpha_i^{\text{th,el}} = \frac{\alpha_\lambda^{\text{th,el}}}{2a_i^{\text{th,el}}}$$

$$\beta_i^{\text{th,el}}(k) = \beta_\lambda^{\text{th,el}} + b_i^{\text{th,el}} \cdot \frac{\beta_\lambda^{\text{th,el}} - 1}{2a_i^{\text{th,el}} p_i^{\text{th,el}}(k)}. \quad (5.8)$$

where the superscripts “th,el” mean that the same equation can either refer to the thermal loop parameters, or to the electrical loop parameters. Parameters $\alpha_i^{\text{th}}, \alpha_i^{\text{el}}, \beta_i^{\text{th}}$ and β_i^{el} are the utility function parameters, as from (5.1). Also, $0 < \beta_\lambda^{\text{th,el}} < 1$ and $\alpha_\lambda^{\text{th,el}}$ are two arbitrary parameters that can be used to adjust the AIMD speed of convergence properties.

5.4 Case Studies

5.4.1 Simulations for the Electrical Scheduling

In order to evaluate the performance of our proposed AIMD utility optimisation strategy in a more realistic fashion, we tested our algorithms on a revised version of the distribution power system based on the IEEE 37 bus test feeder [87]. This test network incorporates a

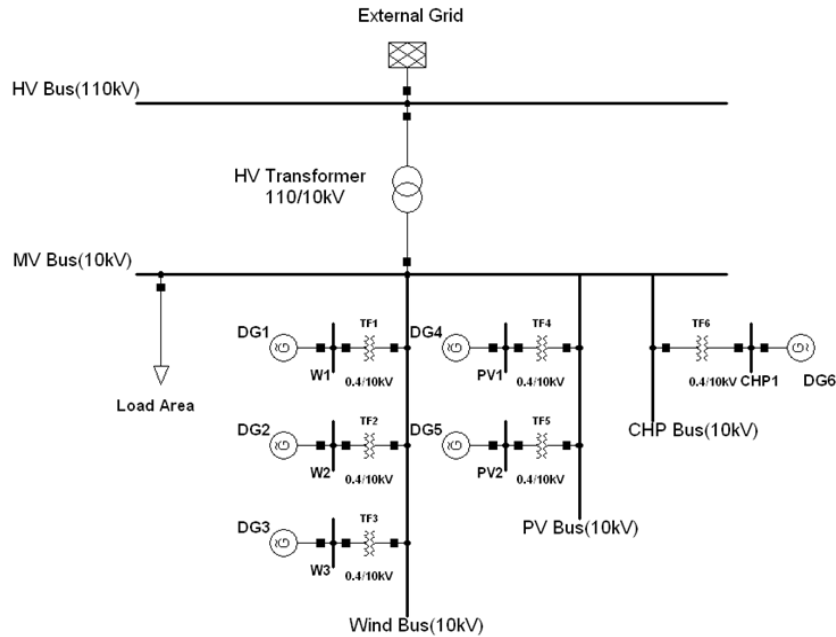


Fig. 5.6 Schematic topology of the tested network.

certain amount of loads, is served by several DERs, and connects to the microgrid (or VPP). Figure 5.6 illustrates the topology of our test network.

In our simulations, the base voltage of the High-Voltage (HV) network was set to 110kV (1.0 pu) at the source-end of the external grid. A 2.5MVA distribution substation was connected to the external grid to bring the voltage level down to 10kV, which is a typical Medium-Voltage (MV) level in European power systems. We considered three wind DERs, two PV DERs, and a CHP. Each DER is able to produce power to the MV substation via a connected transformer. To simplify our model, we assumed that the same type of DERs had the same level of generation capacity. However, the real power output from each DER was dependent on the available resource (e.g., wind speed/solar intensity) and the requested power from the load area at each time slot. In addition to this, all the DERs were modeled as constant P-Q generators with the same power factors equal to 1.0 to generate pure active power for the loads. It is clearly not realistic to assume that DERs produce pure active power and to model the loads without reactive power consumption. However, we did so as an example of this chapter to illustrate the algorithm works effectively from the perspective of active power generation. In practice, this corresponds to assuming that the reactive power is provided by some ancillary services in the power network (e.g., capacitance tanks, reactive V2G and G2V services), or bought from the external grid. Note that the AIMD algorithm could be further extended through a double prioritised algorithm to accomplish reactive

Table 5.1 Parameters of the utility functions

Plant	a_i	b_i	c_i
Wind Plant 1	0.0027	17.83	4.46
Wind Plant 2	0.0028	17.54	4.45
Wind Plant 3	0.0026	17.23	4.44
Solar PV 1	0.0055	29.30	4.45
Solar PV 2	0.0055	29.58	4.46
CHP	0.0083	75.73	5.21

power management, as shown in the recent reference [190] in the context of EV charging, and is not shown here in the interest of conciseness.

We also assumed that the wind plants, the PV plants and the CHP had a capacity of 750 kW, 200 kW and 1 MW respectively. Such values typically allow the microgrid to work in island mode, i.e., the required power is less than the power provided by the DERs, as assumed in Section 5.2. We assumed that each load had a power factor of 0.95 lagging, and load profiles were randomly chosen for a period of 24 hours, according to reference [165]. The maximum wind power output for each wind DER was randomly chosen from real wind turbine data from the National Renewable Energy Laboratory (NREL) [141]. The maximum solar power generation profile of each PV was computed according to a quadratic function with non-zero values from 6am to 6pm, randomly perturbed to simulate cloud disturbances, as in [4]. The parameters of the utility functions were taken from [149] and [180] and are summarised in Table 5.1. Note that in the current model the unit of the utility functions is represented by US dollars, but it can be easily converted to Euro or other units of interest by simply multiplying the currency exchange rate. We decided to sample the load profiles and the maximum output of the DERs every 5 minutes, and assumed that they would be constant during such a time lapse. The whole scenario was simulated using a customised OpenDSS-Matlab simulation platform [43]. In particular, Matlab was used to generate the power dispatch data for each DER, and a day power system simulation was implemented by OpenDSS to evaluate the state of the network, e.g., line voltage, substation power flow, power losses, for each time slot.

Now we illustrate the simulation results obtained by implementing the proposed AIMD utility optimisation algorithm in the network described in the previous section. To better evaluate the performance of the proposed algorithm, we compared our distributed solution with the optimal one obtained in a centralised fashion which relies on a full exchange of information among DERs and the EMS. The centralised solution is computed every 5

minutes, assuming that the EMS is informed of the maximum power that each DER can provide (depending on wind/sun availability) and also by the power required by the users. Then we assumed that the EMS had the ability to solve instantaneously the constrained optimisation problem (i.e., considering the power network constraints) and to schedule the optimal power flows to the DERs. As for the AIMD case, each step of the algorithm implementation was iterated every 5 seconds.

The simulation results obtained are summarised in Figures 5.7 to 5.10. Figure 5.7 depicts that both the centralised algorithm and the proposed distributed one manage to balance the generated power with that required by the users. We also show the maximum power that could be generated by all the DERs working at full capacity. Figure 5.8 illustrates how much power was generated by each single DER. As can be noted, the CHP is mainly used to back-up the energy production from the renewable plants, as it is less economical from the point of view of the cost function being considered here (i.e., due to its fuel and carbon costs). Figure 5.9 shows that the value of the utility function is almost the same as would have been obtained by implementing a fully centralised approach. Finally, Figure 5.10 shows that the communication requirement of the AIMD performed every 5 seconds is similar to that of the centralised solution performed every 5 minutes. However, even in the simple scenario adopted for this comparison, as can be seen from the same figure, the centralised solution can not be used at faster time scales and if we use the same step size for both approaches, then the communication requirement of the centralised approach becomes about 100 times larger than that of AIMD. Clearly, as the operation of smart grids is heading towards real-time fully automated practices, AIMD-like techniques are much more desirable than a centralised solution from a communication perspective.

5.4.2 Simulations for Thermal and Electrical Scheduling

In this section, we evaluate the performance of the proposed double priority AIMD utility optimisation implementation in a similar microgrid scenario as described in Section 5.4.1. The topology of the tested network is illustrated in Figure 5.11. In this network, we assume that several DERs are installed and that they collectively have sufficient capacity to participate in the electricity market and serve both thermal and electrical demand in the load area. In our simulation, the base voltage of the HV network was set to 110kV (1.0pu) at the source-end of the external grid. Two HV/MV transformers were applied to step down the voltage from 110kV to 10kV in the load area. In addition, several 110/10kV transformers were used to step up the voltage generated from the DERs to the HV power network. We considered three wind plants, two PV plants, and two CHPs. We assume that the generation capacity of each CHP is sufficient to serve its local fixed electrical load. Also, CHPs must have the ability to

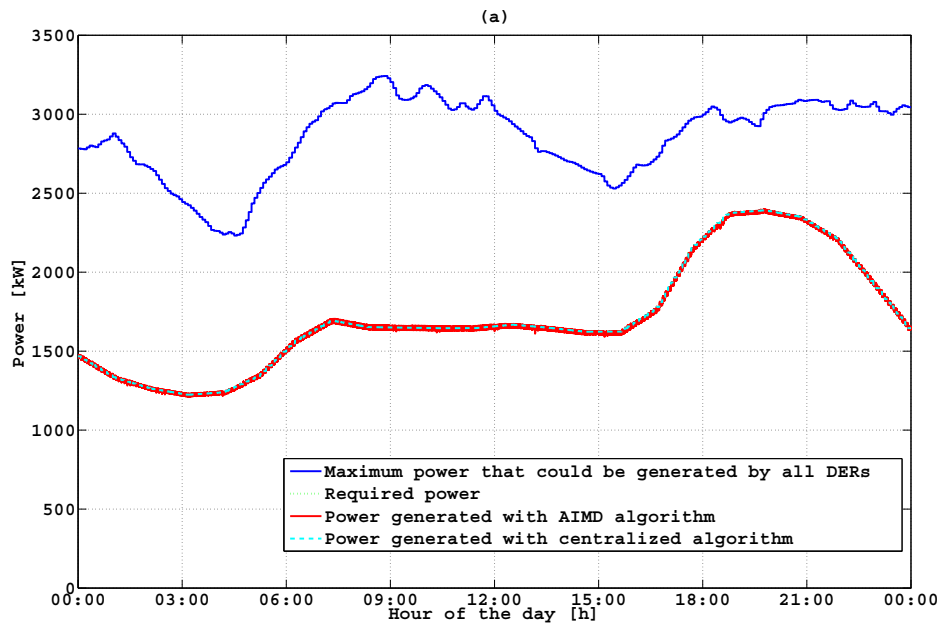


Fig. 5.7 Comparisons of the distributed AIMD solution and the optimal centralised solution on electrical power balancing during the whole day

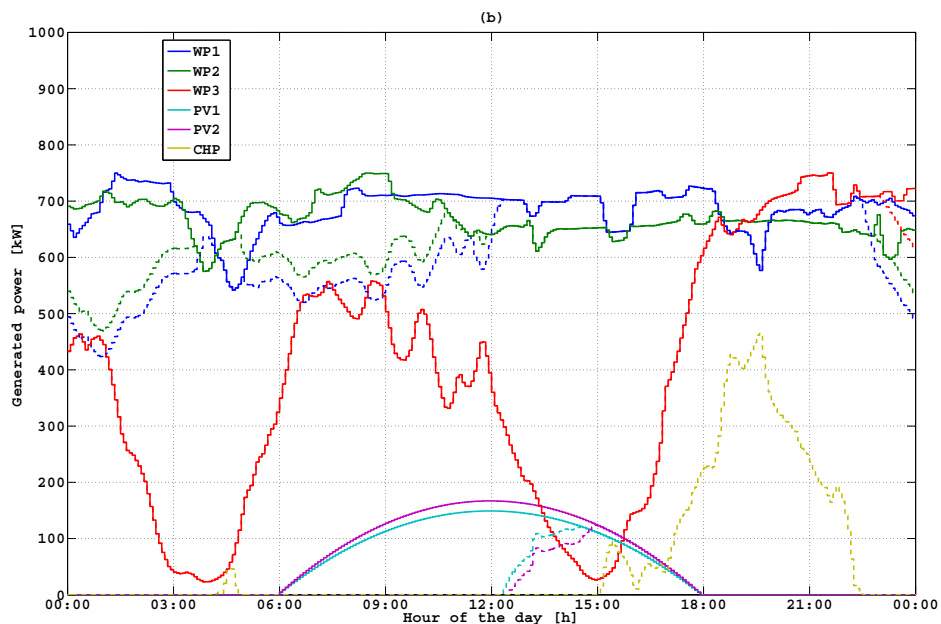


Fig. 5.8 The detail of how AIMD shares the energy production.

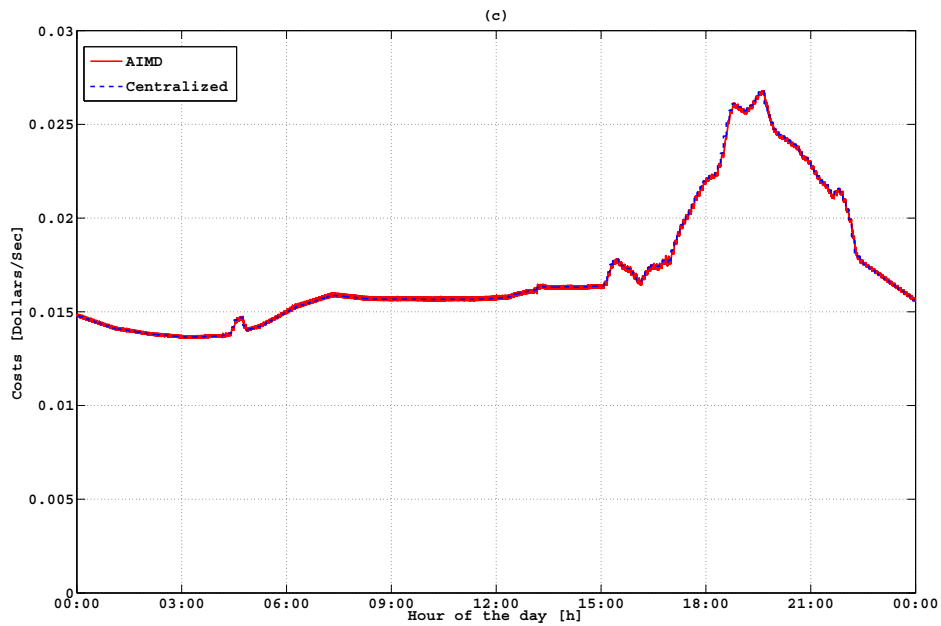


Fig. 5.9 Comparisons on the costs of the two algorithms

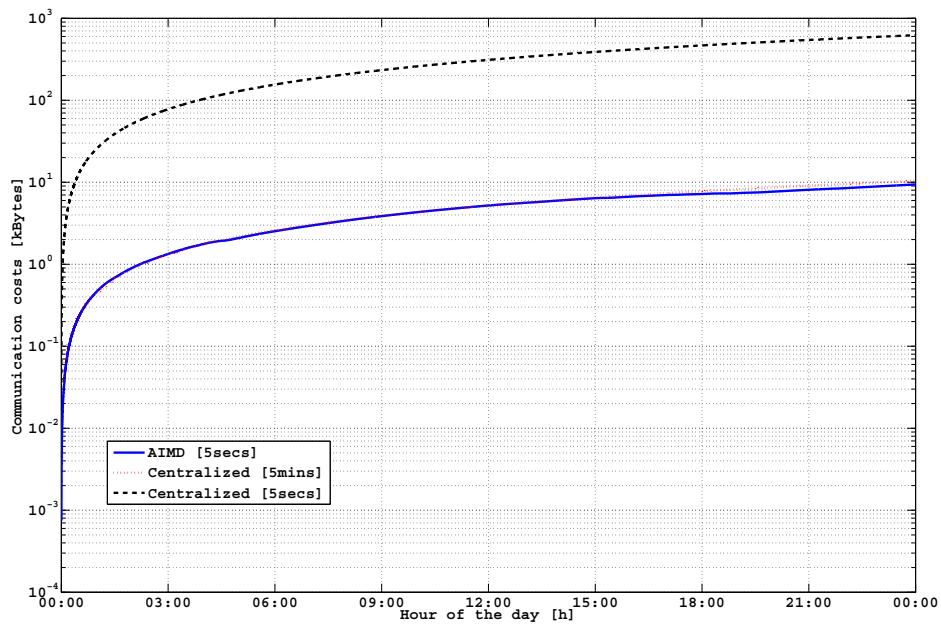


Fig. 5.10 Comparisons on the communication costs of the two algorithms: with same step size, AIMD clearly outperforms the centralised approach.

generate enough thermal energy. All of the DERs in the network were modelled as constant P-Q generators with the same power factors equal to 1.0 to generate pure active power for the loads. We chose the capacity of each DER according to existing plants for which parameters were available from [180]. In particular, the capacities of the wind plants were chosen as 12.15MW, 13.5MW and 7.7MW, respectively. The capacities for the PV plants were selected as 1.8MW and 2.1MW and the capacities for the CHPs were chosen as 24MW and 14MW. The fixed loads located around the CHPs were taken as 10MW and 5MW, respectively. We assumed that the CHP were the only DERs able to produce thermal power, with a heat to power ratio equal to 1.0. In particular, the microgrid was sized to satisfy both the electrical and the thermal demand at any moment during the simulation.

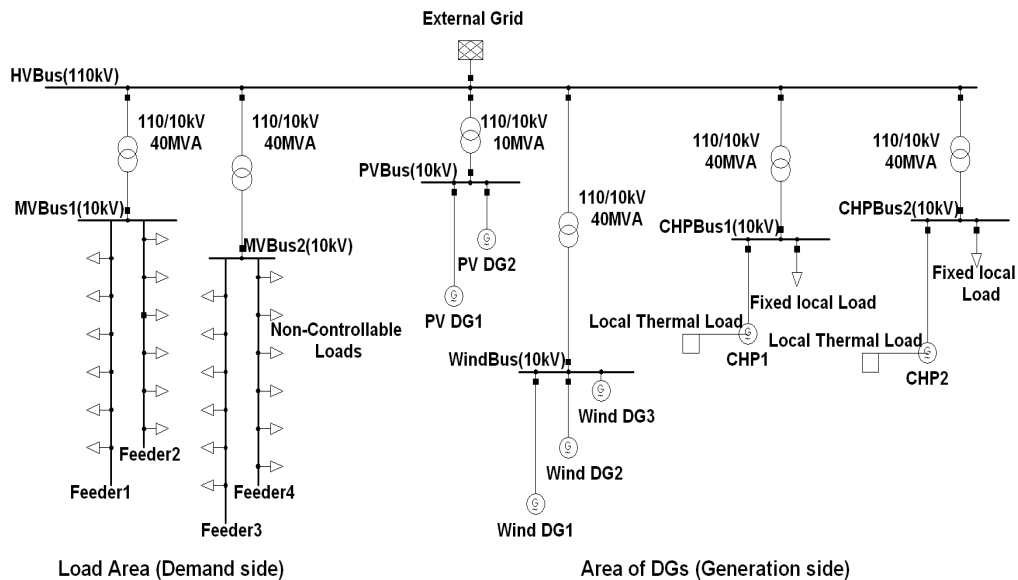


Fig. 5.11 Schematic topology of the tested network.

In the simulation, we further assumed that each load has a power factor of 0.98 lagging, and load profiles were randomly chosen for a period of 24 hours from reference [165]. Loads are located in the microgrid area at a random distance (uniformly distributed between 0.5km and 1km) between each other. The maximum wind power output for each wind DER was also randomly chosen from real onshore wind turbine data from the National Renewable Energy Laboratory (NREL) [141]. The maximum solar power generation profile of each PV was computed according to a quadratic function with non-zero values from 6am to 6pm, randomly perturbed to simulate cloud disturbance, as described in Section 5.4.1. The real thermal power profile was referred from [152] and applied to the total thermal power demand in our simulation, proportionally to a maximum thermal peak of 18MW during the day. The parameters of the utility functions were taken from [180] and [149] and are summarised in

Table 5.2 Parameters of the utility functions

Plant	a_i^{el}	b_i^{el}	c_i^{el}	a_i^{th}	b_i^{th}	c_i^{th}
Wind Plant 1	0.0021	20.59	3.438	-	-	-
Wind Plant 2	0.0021	19.54	3.440	-	-	-
Wind Plant 3	0.0020	25.33	3.418	-	-	-
Solar PV 1	0.0042	23.73	3.428	-	-	-
Solar PV 2	0.0042	15.88	3.435	-	-	-
CHP1	0.0064	39.22	4.011	0.0064	39.22	4.011
CHP2	0.0062	33.84	4.024	0.0064	39.22	4.011

Table 5.2. In particular, as the CHPs provide revenues due to thermal power generation, a heat credit is subtracted from total unit costs to establish an equivalent of the levelised costs of producing only electricity [180]. We sampled the load profiles and the maximum output of the DERs every 10 minutes, so that the values of $\bar{p}_i^{\text{th}}(k)$, $\underline{p}_i^{\text{th}}(k)$, $\bar{p}_i^{\text{el}}(k)$, $\underline{p}_i^{\text{el}}(k)$, $d^{\text{th}}(k)$, $d^{\text{el}}(k)$ did actually change every 10 minutes.

In this part we report the simulation results obtained by implementing the proposed double priority AIMD utility optimisation algorithm in the network described in Section 5.4.2. We compared the distributed solution to the optimal centralised based solution for better evaluation of the performance of the proposed algorithm. The centralised solution is computed every 10 minutes, assuming that the EMS is informed of the maximum power that each DER can provide and also of the power required by the users. We assumed that the EMS had the ability to solve the optimisation problem instantaneously and to schedule the optimal power flows to the DERs. These are the same assumptions as we made in Section 5.4.1. As for the AIMD implementation, each step of the algorithm iteration was set to 1 second for a more accurate observation of the results. Figure 5.12 depicts the optimal share of electrical power generated by each available DER. Figure 5.13 shows that both a centralised full-communication and the proposed distributed algorithm manage to match supply and demand of both electrical and thermal power. Figure 5.14 shows that both algorithms achieve the same minimum cost result. Finally, Figure 5.15 depicts the minimum and the maximum per-unit voltage in the network, as computed from the OpenDSS simulation environment. It should be noted that we assumed that all the DGs were allocated outside of the load centre and produced a large aggregated available power. For the sake of simplicity, we assumed that the required reactive power was taken from the external grid, and the figure only illustrates the voltage impact on the grid in case no voltage control actions are taken.

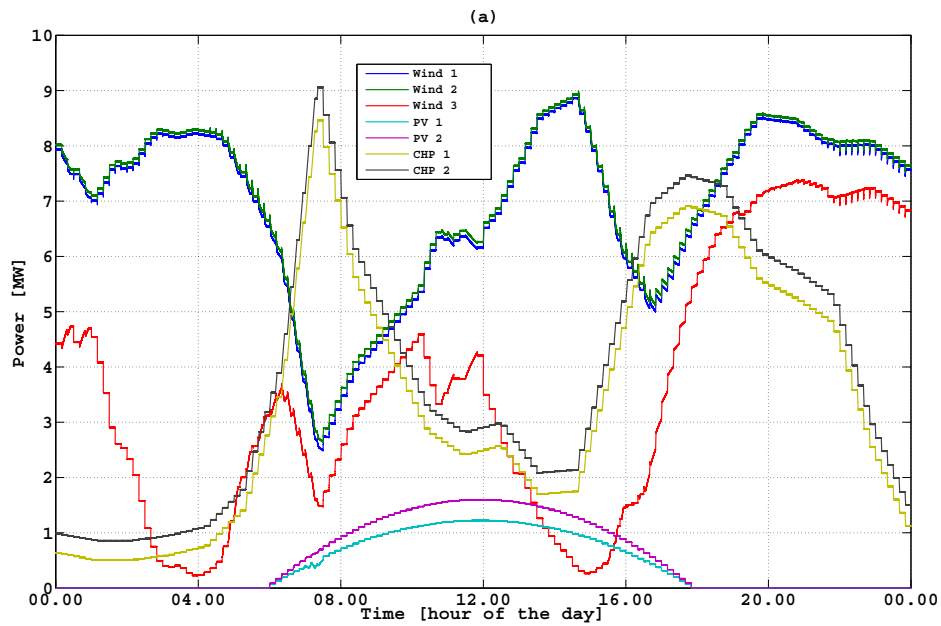


Fig. 5.12 Electrical power generation by each DER.

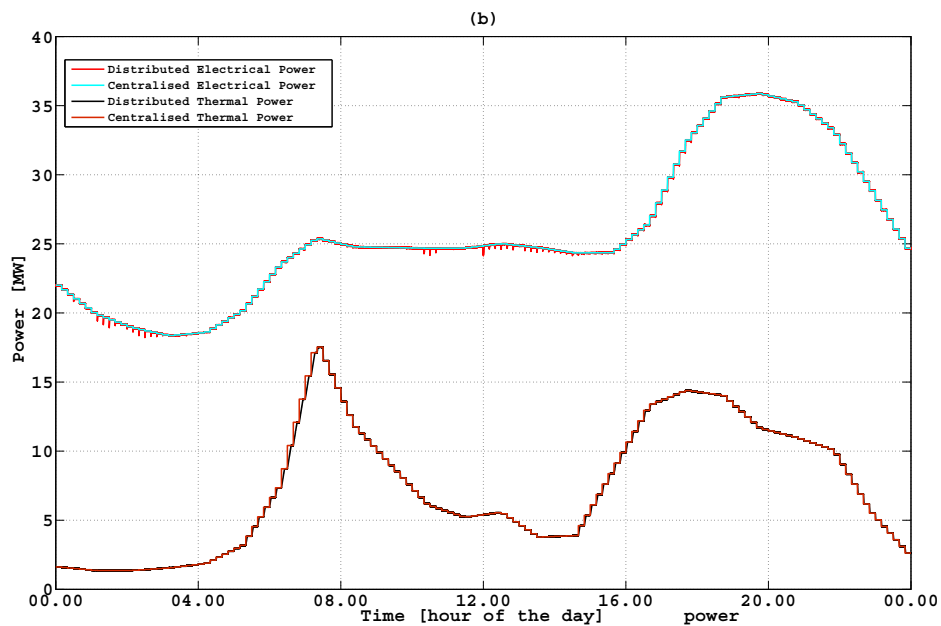


Fig. 5.13 Comparisons of the total power generation profile (both electrical and thermal) by applying different algorithms.

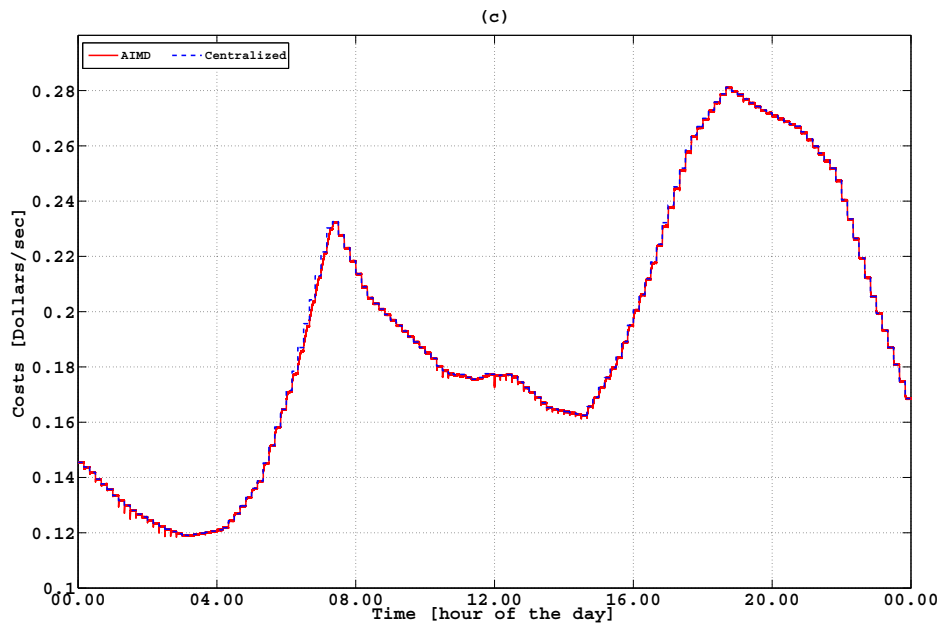


Fig. 5.14 Comparisons of the costs by using the two algorithms.

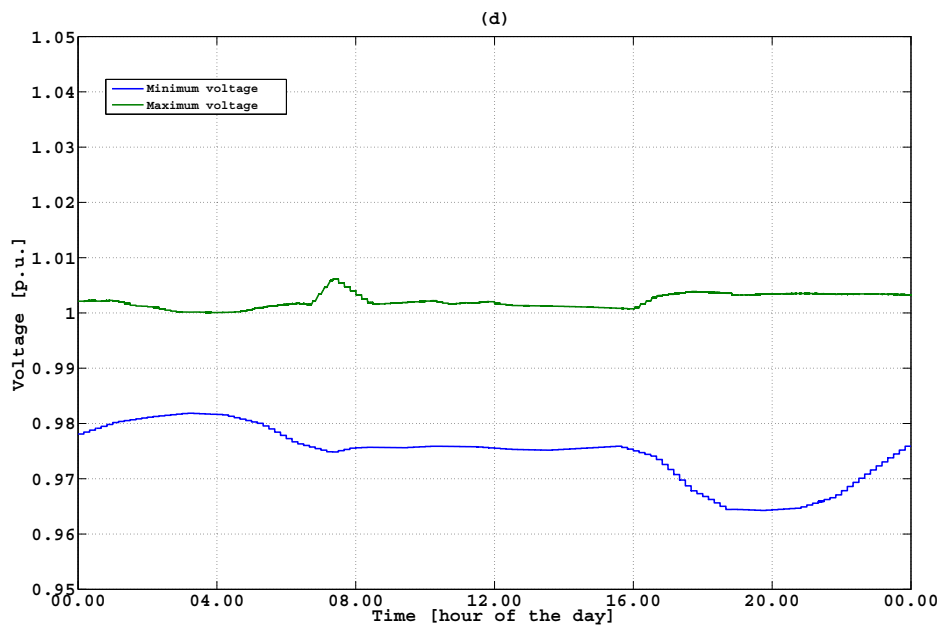


Fig. 5.15 Minimum and maximum voltage profiles in the network obtained with the two algorithms.

5.5 Conclusions

In this chapter, we demonstrate a methodology for adapting the AIMD algorithm to solve a utility optimisation problem in a microgrid scenario with DGs. The objective is to achieve real-time power balancing of DGs and the demand, and to decide how much energy should be generated from the DGs, in a distributed manner, such that the total cost of energy production from the DGs can be minimised. We show that our proposed distributed algorithms can successfully solve the power generation problem in an optimal fashion, greatly reducing the communication overhead required by centralised algorithms, even in the presence of a second thermal constraint. In particular, power balancing is achieved without having to communicate real-time power availability from renewable resources (sun/wind), or the power required by the users, but by simply notifying the DERs with a single bit of information every time the provided power equals the required power.

Part IV

Distributed and Privacy-Aware Speed Advisory Systems

Chapter 6

Intelligent Speed Advisory System for Electric Vehicles

***Abstract:** In this chapter, we introduce a new application of the speed advisory system, using ideas from Chapter 2, for minimising energy consumption of a group of EVs in a city centre scenario. The performance of the system was evaluated through Matlab simulations. It is joint work with Rodrigo Ordóñez-Hurtado, Fabian Wirth, Yingqi Gu, Emanuele Crisostomi, and Robert Shorten. The original work presented in this chapter was submitted for publication in [112, 113].*

6.1 Introduction

At present, Intelligent Speed Advisory (ISA) systems, which are a component of Advanced Driver Assistance Systems (ADASs), have become a fundamental part of Intelligent Transportation Systems (ITS). Such systems offer many potential benefits, including improved vehicle and pedestrian safety, better utilisation of the road network, and reduced emissions. Recently, many papers have appeared on this topic reflecting the problem from the viewpoint of road operators, infrastructure providers, and transportation solution providers [2, 11, 18, 24, 61, 80, 202, 216].

In this chapter we consider the design of a Speed Advisory System (SAS) making use of vehicle-to-vehicle/infrastructure (V2X) technologies. In particular, we are interested in solving the speed advisory problem in the case that the fleet of vehicles is only composed of EVs. Such a situation might occur in some sensitive areas in city centres that are closed to conventional traffic, and only allow transit to specific categories of low (or zero) polluting vehicles, see for instance the case of *umweltzonen* [37] in Germany; or a similar problem

might occur for a fleet of urban electric buses. The use of electric buses to decrease harmful emissions and noise pollution is becoming widespread in different cities of the world, see for instance the recent cases of São Paulo [140], Louisville in the US [82], or Wien in Europe [53].

Our starting point is the observation that different EVs are designed to operate optimally (e.g., in terms of energy efficiency) at different vehicle speeds and at different loading conditions. Thus, a recommended speed, or speed limit may be optimal for one vehicle and not for others. Our objective in this chapter is to develop a SAS which allows groups of EVs to collaborate in order to find the optimal speed that should be recommended to all vehicles belonging to the fleet of EVs, in order to minimise the overall energy consumption of the fleet; or similarly, to extend their range. We shall assume that EVs are equipped with V2X technologies, and can exchange information with their neighbours and can exchange limited information with the infrastructure.

Clearly, this task is performed provided that some basic safety and Quality of Service (QoS) requirements are guaranteed (i.e., the optimal recommended speed should be within a reasonable realistic range). As we shall see later, the optimal speed heavily depends on how single EVs travel in traffic (e.g., whether air conditioning is on/off and how many people are on-board). Since people might not be interested in sharing such private pieces of information (i.e. privacy-preserving), we are interested in obtaining the optimal solution without requiring single vehicles to communicate personal information to other vehicles or even to central infrastructure. We shall show that one can design, using simple ideas from cooperative control techniques¹, an effective SAS in a manner that preserves the privacy of individual vehicles. Matlab simulations are given to demonstrate the effectiveness of our approach.

This chapter is organised as follows: Section 6.2 gives a brief review of some related work in literature; Section 6.3 describes the mathematical model and proposes the algorithm for solving the optimisation problem; Section 6.4 evaluates the performance of the algorithms using Matlab simulations; Section 6.5 concludes the chapter.

6.2 Related Work

In this section, we give a brief review of some related work. First note that a detailed review of this topic is given in [147]. Conventional systems are described in [2, 56, 80, 134, 202]. These papers describe various aspects of the ISA design process. This includes the design of driver

¹A similar approach was proposed in Section 4.3 for solving the optimal fair V2G power dispatch problem in a microgrid scenario. In this chapter, we adapt the previously proposed methods for minimising the energy consumption of group of EVs in an ITS scenario (e.g. short distances travelling in city centres). In the next chapter, we explore the application of the approach to fleets of conventional vehicles in a highway scenario.

display systems, the incorporation of external environmental information, and the algorithmic aspects of speed and distance recommendations. Recently, there has been a strong trend to also include traffic density information. References [59, 146, 147, 166, 203, 209] describe work in this direction. In these works density information is included in the procedure via loop detectors or via explicit density estimation via Vehicle-to-Vehicle (V2V) technology. The differentiating feature of the approach followed in this thesis is that density and composition of the vehicle fleet is also used, but in an implicit manner as part of the optimisation algorithm. Finally, we note that there is a huge body of work on cooperative control of vehicles and its connection to consensus algorithms [30, 52, 85, 134]. It is important to note that we are designing a SAS and not a cooperative control system. This distinction is important as it allows us to ignore string stability effects which are a fundamental limitation of many cooperative control architectures [77, 93, 96, 198].

6.3 Model and Algorithm

In this section, we describe the cost functions to represent energy consumption in EVs. After that, we present the problem statement and give the mathematical model for the scenario of interest. Finally, we propose an algorithm to solve the optimisation problem.

6.3.1 Cost Functions

We illustrate a basic model of power consumption in EVs. Such a model will be required to formulate a cost function that relates the travelling speed with the energy efficiency in the later problem statement section. Most of the discussion here follows the reference [204], where the ranges of EVs are reported for different brands and under different driving cycles. Power consumption in an EV driving at a steady-state speed (along a flat road) is caused mainly by four sources:

- **Aerodynamics power losses:** they are proportional to the cube of the speed of the EV, and depend on other parameters typical of a single vehicle such as its frontal area and the drag coefficient (which in turn, depends on the shape of the vehicle).
- **Drivetrain losses:** they result from the process of converting energy in the battery into torque at the wheels of the car. Their computation is not simple, as losses might occur at different levels (in the inverter, in the induction motor, gears, etc); in some cases, these power losses have been modelled as a third-order polynomial of speed, whose parameters have been obtained by fitting experimental data (see [204]).

- **Tires:** the power required to overcome the rolling distance depends on the weight of the vehicle (and thus, on the number of passengers as well), and is proportional to the speed of the vehicle.
- **Ancillary systems:** this category includes all other electrical loads in the vehicle, such as Heating, Ventilation and Air Conditioning (HVAC) systems, external lights, audio system, battery cooling systems, etc. Here, the power consumption does not depend on the speed of the vehicle and can be represented by a constant term that depends on external factors (e.g., weather conditions) and personal choices (desired indoor temperature, volume of the radio, etc). According to experimental evaluations [204], the power losses due to ancillary services usually vary between 0.2 and 2.2 kW.

Thus, by summing up all the previous terms, the power consumption P_{cons} can be represented as a function of the speed v as

$$\frac{P_{\text{cons}}}{v} = \frac{\alpha_0}{v} + \alpha_1 + \alpha_2 v + \alpha_3 v^2, \quad (6.1)$$

where the left hand side is divided by the speed in order to obtain an indication of energy consumption per km, expressed in kWh/km. Such a unit of measurement is usually employed in energy-efficiency evaluations, and we shall assume that each EV i will use (6.1) as its personal cost function, denoted by $f_i(v_i) = \frac{\alpha_{i0}}{v_i} + \alpha_{i1} + \alpha_{i2} v_i + \alpha_{i3} v_i^2$. Accordingly, Figure 6.1 shows a possible relationship between speed and power consumption, obtained using data from the Tesla Roadster and assuming a low power consumption for ancillary services of 0.56 kW (i.e., assuming air conditioning switched off). As can be noted from Figure 6.1, there is large energy consumption at large speeds due to the fact that power increases with the cube of the speed for aerodynamic reasons; however, it is also large for low speeds, due to the fact that travel times increase and, accordingly, constant power required by ancillary services demands more energy than the same services delivered with high speeds.

6.3.2 Problem Statement

We consider a scenario in which a number of EVs are travelling in a city centre. Let N denote the total number of EVs driving on the road where the ISA broadcast signal can be received. Each EV is equipped with a specific communication device (e.g. a mobile phone with access to WiFi/3G networks) so that it is able to receive/transmit messages from/to either nearby EVs or available road infrastructure (e.g. a base station). We assume that each EV can communicate a limited amount of information with the infrastructure, and that the

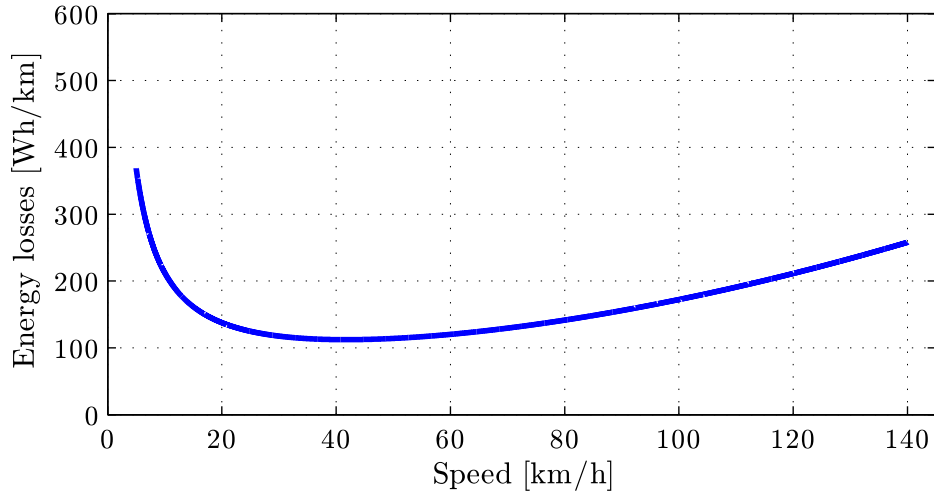


Fig. 6.1 A typical individual cost function.

infrastructure can broadcast information to the entire network of EVs, and each EV can send a broadcast signal to its neighbours.

For convenience, we assume that all EVs have access to a common clock (for example, a GPS clock). Let $k \in \{1, 2, 3, \dots\}$ be a discrete time instant in which new information from EVs is collected and new speed recommendations are made. Let $s_i(k)$ be the recommended speed of the EV $i \in \underline{N} := \{1, 2, \dots, N\}$ calculated at time instant k . Thus, the vector of recommended speeds for all EVs is given by $s(k)^T := [s_1(k), s_2(k), \dots, s_N(k)]$, where the superscript T represents the transposition of the vector. Note that between two consecutive time instants $(k, k+1)$, the recommended speeds are constant while the driving speeds are time-varying real-valued variables. We denote by N_k^i the set of neighbours of EV i at time instant k , i.e. those EVs which can successfully broadcast their recommended speeds to EV i .

In addition, we assume that each EV i can evaluate a function f_i that determines its average energy consumption, were it to be travelling at the recommended speed $s_i(k)$, according to (6.1). Note that in order to achieve this, it is necessary that the vehicle both knows its parameters in the function, and also monitors the functioning of some electric appliances on board (e.g., the intensity of the HVAC system or whether the radio is switched on or not). We further assume that these functions are strictly convex, continuously differentiable and with a Lipschitz continuous first derivative f'_i which is assumed with positive bounded growth rate in the domain of interest D . We assume that the recommended speed can vary within the domain $D = [5, \dots, 130]$, which is a realistic range of speeds, expressed in km/h. Then the requirement on the derivative can be expressed as

$$0 < d_{\min}^i \leq \frac{f'_i(a) - f'_i(b)}{a - b} \leq d_{\max}^i, \quad (6.2)$$

for all $a, b \in D$ (i.e. for reasonable steady-state speeds) such that $a \neq b$, and suitable positive constants d_{\min}^i, d_{\max}^i . Notice that (6.1) fulfils all the previous requirements, and thus, the previous assumptions are usually satisfied in the application of interest here. In this context, we consider the following problem.

Problem 1: *Design an ISA system for a fleet of EVs, following a common speed such as a speed limit, connected via V2X communication systems, such that the total energy consumption from all EVs can be minimised by all of them following the same reference speed.*

The optimisation problem that needs to be solved in order to address Problem 1 can be formulated as follows:

$$\begin{aligned} \min_{s \in \mathbb{R}^N} \quad & \sum_{j \in \underline{N}} f_j(s_j), \\ \text{s.t.} \quad & s_i = s_j, \forall i \neq j \in \underline{N}. \end{aligned} \tag{6.3}$$

This problem is an optimised consensus problem and can be solved in a variety of ways (for example using Alternating Direction Method of Multipliers (ADMM) [15, 45, 173]). Our focus in this work is not to construct a fully distributed solution to this problem, but rather to construct a partially distributed solution which allows rapid convergence to the optimum, without requiring the vehicles to exchange information that reveals individual cost functions to other EVs. This is the privacy preserving component of our problem statement.

Comment: Note that in addressing Problem 1 we are not trying to calculate the recommended speed for all the EVs in one step. Rather we propose an iterative algorithm that in each step yields individual recommended speeds that will eventually converge to the same value on the consensus constraints. Thus, our objective for the minimisation problem (6.3) is to seek the optimal solution of the recommended speeds under a consensus constraint. In doing this, we shall assume that the EVs will be compliant with the recommended speed (this might be more realistic for public transportation rather than single EVs, but non-compliance with the recommended speed is not investigated here and left for future work).

To solve (6.3) we recall the previously discussed optimisation problem (4.18) and Theorem 9 in Section 4.3.3. In a similar way to (4.21), we use the iterative feedback scheme

$$s(k+1) = P(k)s(k) + G(s(k))e, \tag{6.4}$$

for finding the optimal solution s^* of the problem (6.3). To apply Theorem 9 to solve (6.3), we adopt the same definition of $P(k)$, as suggested in (4.13), for modelling the time-varying and strongly connected communication topology.

Comment: The assumption of uniform strong ergodicity holds if the neighbourhood graph associated to the problem has suitable connectedness properties. If sufficiently many cars travel in the city centre area, it is reasonable to expect that this graph is strongly connected at most time instances. Weaker assumptions are possible but we do not discuss them here in this chapter; see [133] for possible assumptions in this context. In any case, note that the time-varying communication graph makes the dynamic system (6.4) a switching system.

Now, we propose the Optimal Decentralised Consensus Algorithm for solving (6.3) as shown in Algorithm 11. The underlying assumption here is that at all time instants all EVs communicate their value $f'_j(s_j(k))$ to the base station, which reports the aggregate sum back to all EVs. This is precisely the privacy preserving aspect of the algorithm, as EVs do not have to reveal their cost functions to the base station, nor to other EVs. Some implicit information (i.e., the derivatives of the cost function at certain speeds) is indeed revealed to the base station but not to any other EVs involved in the fleet.

Algorithm 11 Optimal Decentralised Consensus Algorithm for SAS

```

1: for  $k = 1, 2, 3, \dots$  do
2:   for each  $i \in \underline{N}$  do
3:     Get  $\tilde{F}(k) = \sum_{j \in \underline{N}} f'_j(s_j(k))$  from the base station.
4:     Get  $s_j(k)$  from all neighbours  $j \in N_k^i$ .
5:     Do  $q_i(k) = \eta_i \cdot \sum_{j \in N_k^i} (s_j(k) - s_i(k))$ .
6:     Do  $s_i(k+1) = s_i(k) + q_i(k) - \mu \cdot \tilde{F}(k)$ .
7:   end for
8: end for

```

Comment: We note that in any real implementation in a city centre scenario the recommended speed may be bounded above and below by the road operator.

6.4 Experimental Results

We now give some preliminary results obtained in Matlab simulations. Our objective in this section is to show that the recommended speed is in fact more energy efficient than some

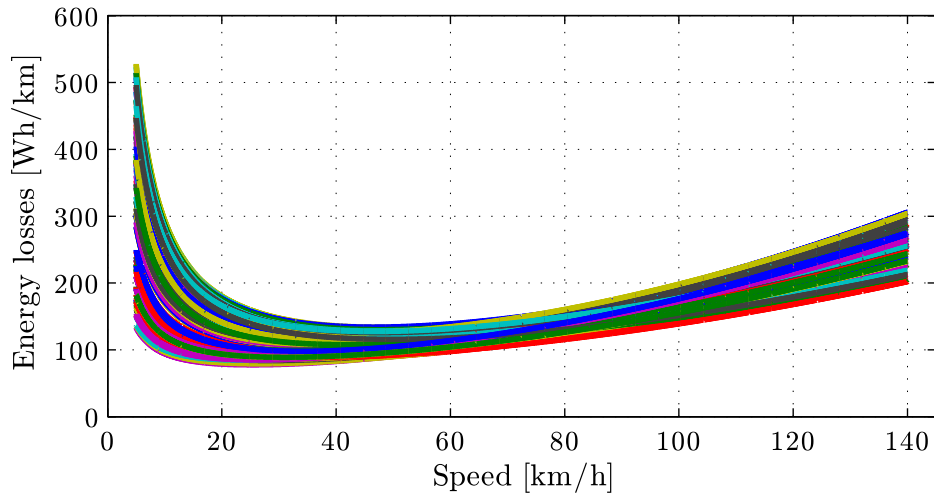


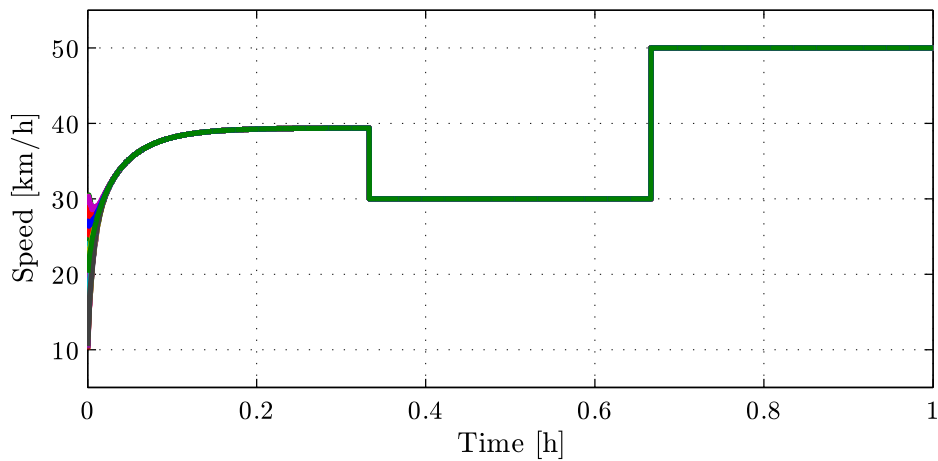
Fig. 6.2 The cost functions for the 100 EVs.

other speeds. For this purpose, we assume that a fleet of 100 EVs travels in the city centre for an hour, and adopt the following driving profiles:

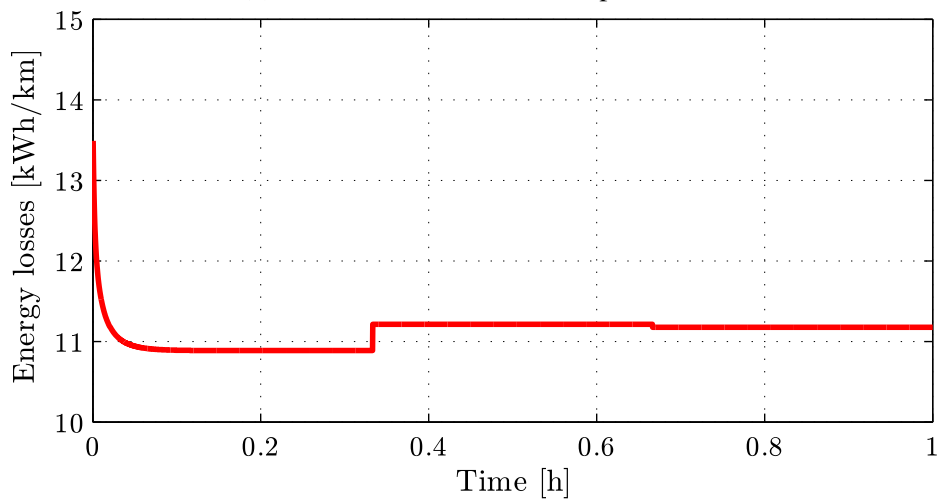
- In the first 20 minutes, the vehicles travel at the optimal speed calculated from Algorithm 11.
- In the second 20 minutes, they travel at a speed lower than the optimal speed.
- In the last 20 minutes, they travel at a speed higher than the optimal speed.

In the first stage we assume that the communication graph among the EVs changes in a random way, i.e., at each time step an EV receives information from a subset of vehicles belonging to the fleet. This is a simplifying assumption that can be justified by assuming that in principle all EVs might communicate to all the other EVs (i.e., they are relatively close), but some communications might fail due to obstacles, shadowing effects, external noise, or other. For this purpose, the time-varying communication graph at each time step in our simulation was modelled by a sequence of strongly ergodic row-stochastic matrices. Besides, in the two last stages we assume that the change of speed occurs instantaneously, since there is no requirement to iteratively compute an optimal speed.

We tuned our parameters in Algorithm 11 as $\eta = \mu = 0.001$, and we simulate different cost functions for each EV by assuming a random number of people inside each car (between 1 and 5 people) with an average weight of 80 kg, and by assuming a different consumption from ancillary services within the typical range of $[0.2, 2.2]$ kW. The curves of the cost functions used in our experiment are shown in Figure 6.2. The evolution of the speeds of the EVs are shown in Figure 6.3a and the average energy consumption is shown in Figure 6.3b.



(a) Evolution of the vehicles' speeds.



(b) Evolution of the overall energy loss..

Fig. 6.3 Simulation results for the network of EVs: Algorithm 11 is applied until time 0.33 h, and then two different speeds (below and above the optimal one) are suggested in [0.33,0.66] h and [0.66, 1] h, respectively.

As is shown in Figure 6.3a, the proposed ISA system converges quickly to consensus and the optimal solution. This solution indeed minimises the group energy consumption of a fleet of EVs effectively as can be seen from Figure 6.3b.

6.5 Conclusions

In this chapter we present a new ISA system. The system is based on a solution to an optimisation consensus problem as we previously discussed in Section 4.3.3. We show that the ISA can be designed, in a privacy-preserving manner, to improve the overall energy efficiency of EVs or, in other words, to collaboratively extend the travelling range of EVs. From the grid perspective, this system also provides benefits by reducing the power loading due to an increasing number of EVs charging on the grid.

Preliminary results have been presented in the chapter through Matlab simulations. In the next chapter, we shall demonstrate that, by using the same ideas, one can design an effective ISA system to minimise emissions for conventional vehicles networks. Extensive simulations, using the realistic traffic simulator software package SUMO, and a dedicated hardware-in-the-loop (HIL) testing platform, are given to illustrate the effectiveness of deploying our proposed framework.

Chapter 7

Intelligent Speed Advisory System for Conventional Vehicles

***Abstract:** In this chapter, we extend our previous discussion in Chapter 6 to the case of a fleet of conventional vehicles¹. We show that, by using the ideas developed in Chapter 6, group emissions of vehicles can be minimised. The performance of the system was evaluated through a variety of simulations. It is joint work with Rodrigo Ordóñez-Hurtado, Fabian Wirth, Yingqi Gu, Emanuele Crisostomi, and Robert Shorten. The work presented in this chapter has been submitted for publication in [67, 112].*

7.1 Introduction

In this chapter we are interested in solving the speed advisory problem in the case that the fleet of vehicles is composed of conventional vehicles. Our starting point is the observation that different vehicle classes (e.g., in terms of emission levels) are designed to operate optimally at different vehicle speeds and at different loading conditions. Thus, as we previously mentioned, a recommended speed, or speed limit may be optimal for one vehicle and not for others. Given a stretch of road network, the group emissions (CO, CO₂, NO_x, O₃, PM10, PM2.5) may or may not be close to the theoretically minimum possible. This of course depends on the composition of traffic on a given road, and the average speed at which vehicles are travelling.

Clearly, the previously designed Algorithm 11 needs to be adapted when applied to a fleet of conventional vehicles. First, in terms of field of application, conventional vehicles

¹We consider conventional vehicles as those vehicles using diesel or petrol engines that can generate pollutant emissions through exhaust pipes. In the following context, we shall use the word “vehicles”, unless otherwise noted, for describing “conventional vehicles”.

can be used for longer travelling distances while EVs are typically used for short distances due to their reduced driving ranges, and thus EVs are most likely deployed in city centres or short-distance commuting areas while conventional vehicles are usually applied for long-distance travelling purposes (e.g. highway scenario); second, the emissions caused by EVs are usually little and can be considered equal to zero (if the batteries can be completely charged by renewable energy resources), while conventional vehicles have different emission levels according to their vehicle types, weights, forms of fuel, engine sizes etc. Accordingly, in the following we shall show how the previous framework can be adapted to the case of a fleet of conventional vehicles, with the objective of minimising the group emission on a given stretch of road in a highway scenario. Another contribution of this chapter is to evaluate the algorithm through extensive simulation studies. In particular, SUMO simulations are given to illustrate the efficacy of the algorithm in a more realistic traffic scenario (compared to Matlab simulations), and Hardware-In-the-Loop (HIL) tests involving real vehicles are given to illustrate user acceptability and ease of the algorithm deployment.

The remainder of the chapter is organised as follows: Section 7.2 briefly describes the problem statement and presents the cost functions for modelling the emission generation of vehicles. Section 7.3 illustrates the simulation results. Section 7.4 concludes the chapter.

7.2 Problem Statement

We consider a scenario in which a number of vehicles are driving along a given stretch of highway with several lanes in the same direction. Note that the assumption on different lanes of the highway allows vehicles to overtake whenever it is appropriate. We wish to find a common recommended speed, by using the same ISA system or, Algorithm 11, suggested in Chapter 6, to minimise the total emissions from all vehicles taking account of the composition of the vehicles (individual vehicle types) and the number of vehicles. We assume that vehicles are connected via V2X communication systems, and are able to evaluate its personal cost function in terms of speed and emission generation, such that the total emissions from all vehicles can be minimised by all of them following the same recommended speed.

To apply the algorithm in this new scenario, we shall adapt the average-speed model proposed in [14] to model each cost function f_i as a function of the average speed s_i as

$$f_i = k \left(\frac{a + bs_i + cs_i^2 + ds_i^3 + es_i^4 + fs_i^5 + gs_i^6}{s_i} \right), \quad (7.1)$$

where $a, b, c, d, e, f, g, k \in \mathbb{R}$ are used to specify different levels of emissions by different classes of vehicles.

7.3 Evaluation using SUMO Simulations

We now evaluate the algorithm for the scenario of interest here using the SUMO simulator [12], and by implementing it in a real vehicle. We conduct the following experiments:

1. First, we compare, for a given scenario, the optimal speed with a non-optimum speed limit. In this simulation, for illustration purposes, we force all vehicles to travel at the recommended speeds, subject to implementation constraints coming from the SUMO simulation (e.g. acceleration/deceleration profiles).
2. We then make the first scenario more realistic by allowing vehicles to travel in a small range around the recommended speed.
3. We then give a simulation which is dynamic in nature. Cars enter/leave the simulation dynamically and over a long stretch of road we allow vehicles to travel as they wish with a broad range of constant speeds. For example, this may represent a highway situation where the traffic flow is moving better in one lane than in another.
4. We then give a hardware-in-the-loop simulation with a real target vehicle travelling on a road and an emulated network with a fixed number of simulated vehicles.

The idea in all situations is to show the benefits of Algorithm 11. In the simulations we use the emission profiles from [14] shown in Table 7.1 and Figure 7.1, corresponding to petrol cars/minibuses with up to 2.5 tons of gross vehicle mass. Besides, we also use the following vehicle types:

- Type 1: accel. 2.15 m/s^2 , decel. 5.5 m/s^2 , length 4.54 m.
- Type 2: accel. 1.22 m/s^2 , decel. 5.0 m/s^2 , length 4.51 m.
- Type 3: accel. 1.75 m/s^2 , decel. 6.1 m/s^2 , length 4.45 m.
- Type 4: accel. 2.45 m/s^2 , decel. 6.1 m/s^2 , length 4.48 m.

7.3.1 SUMO Simulations with a Fixed Number of Vehicles

In this experiment we consider 40 vehicles travelling along a highway. The set-up for this set of experiments is as follows.

- Road: A straight 5 km long highway with 4 lanes in the same direction.
- Duration of the simulation: 1000 s.

- Algorithm sampling interval: $\Delta T = 1$ s.
- Switch-on time: the algorithm is activated at time 500 s.

The results of the experiments are given in Figure 7.2 and Figure 7.3. As can we see from Figure 7.2a, making a small change in the recommended speed yields an about 3% improvement in CO₂ emissions. We then repeat the experiment and allow vehicles to travel in a range around the recommended speed, and the results of this are given in Figure 7.2b. As can we see from Figure 7.2b, also in this case a significant reduction in CO₂ emission can be observed. Finally to conclude, we applied the algorithm to a situation where the cars have a different range of emission profiles and with a different range of speeds. The results are given in Figure 7.3. In this case, as can be seen in Figure 7.3, a reduction of up to 8.07% can be obtained by following the recommended speed. To illustrate what this means in terms of grams of carbon, SUMO predicts that these forty vehicles emit an average of 9407 g/km compared with 8816 g/km when travelling at an optimised speed. This represents a saving of about 591 g/km which integrates over a day into a significant carbon saving.

Table 7.1 Emission factors for some CO₂ emission profiles reported in [14].

Profile Codes	a	b	c	d	e,f,g	k
R007	2.2606E+3	3.1583E+1	2.9263E-1	3.0199E-3	0	1
R016	3.7473E+3	1.9576E+2	-8.5270E-1	1.0318E-2	0	1
R017	3.7473E+3	1.8600E+2	-8.5270E-1	1.0318E-2	0	1
R018	3.7473E+3	1.6774E+2	-8.5270E-1	1.0318E-2	0	1
R019	3.7473E+3	1.5599E+2	-8.5270E-1	1.0318E-2	0	1
R021	3.7473E+3	1.0571E+2	-8.5270E-1	1.0318E-2	0	1

7.3.2 SUMO Simulations with a Dynamic Number of Vehicles

We now consider a dynamic scenario. To do this we partitioned the highway into three consecutive sections L1, L2 and L3. We then proceed as follows. First, vehicles enter the uncontrolled section L1, with constant speed (randomly chosen in a given range); after completing L1, vehicles enter the section L2. On section L2 vehicles calculate and follow a recommended speed. After completing L2 they enter section L3 and on this section they travel freely (the same speeds as they were on L1). The experiments are setup as follows.

- Road: three consecutive straight edges:
 - L1: 5 km long highway with 4 lanes, uncontrolled;

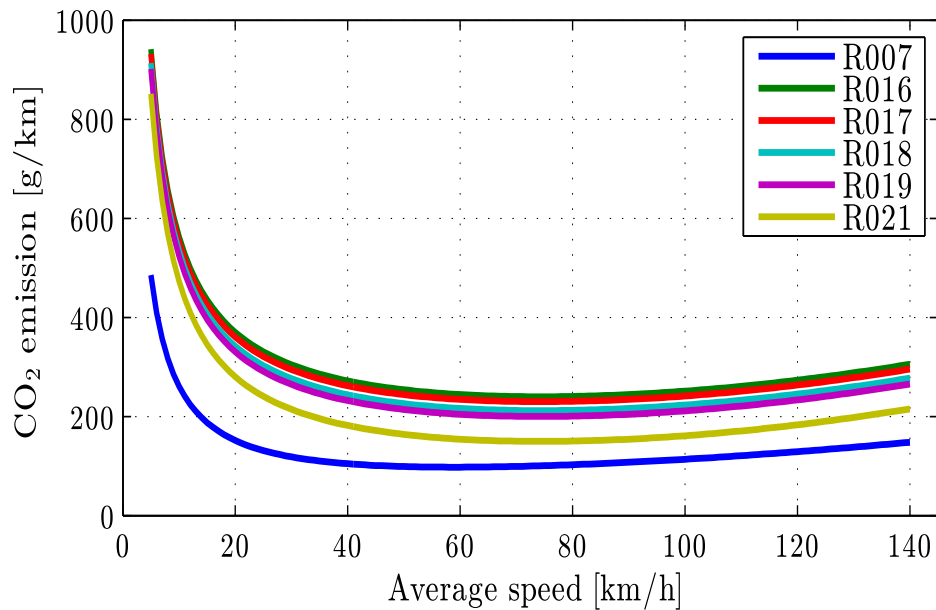
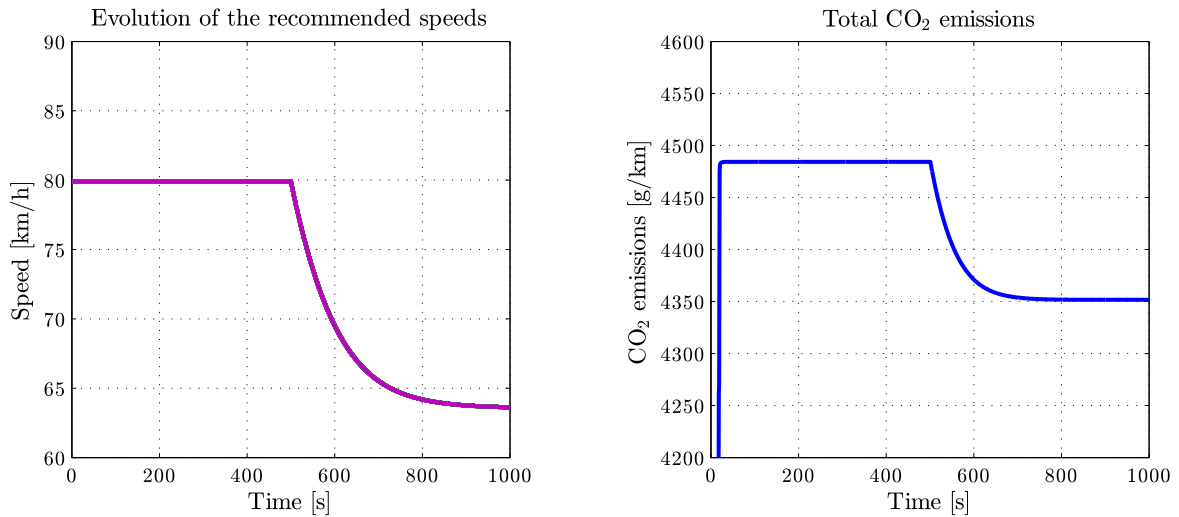
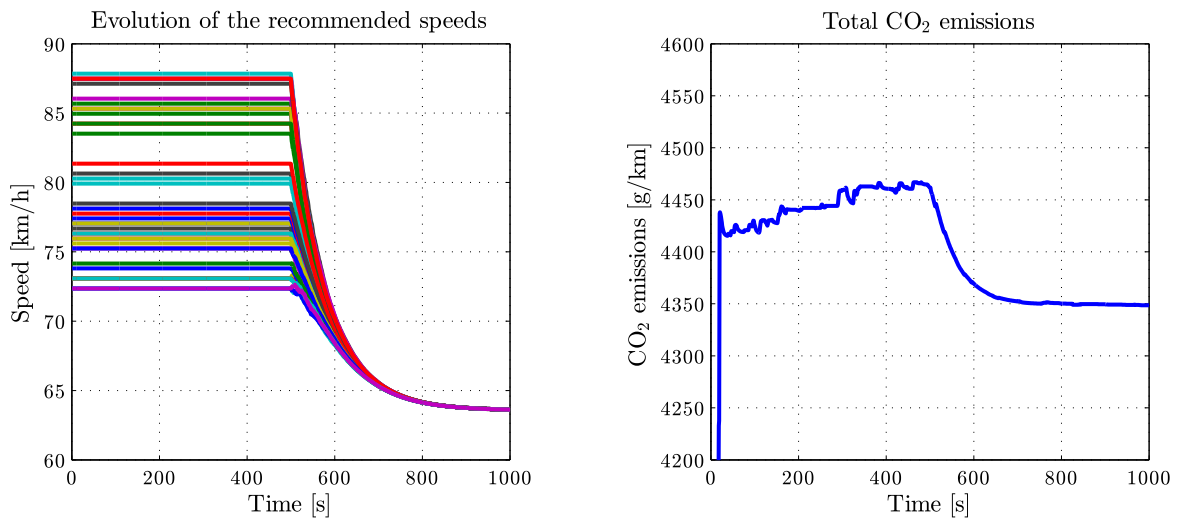


Fig. 7.1 Curves for the CO₂ emission profiles in Table 7.1.

- L2: 5 km long highway with 4 lanes, ISA controlled;
- L3: 5 km long highway with 4 lanes, uncontrolled.
- Total number of cars: 650, with uniform distribution of both emission profiles among R016, R017, R018 and R019, and uniform distribution of types of vehicles.
- Vehicular flow entering L1: one new car every 2 seconds until simulation time 1300 s.
- Length of simulation: 3010 s.
- Window size for the calculation of the moving average (MA) of CO₂ emissions for visualisation purposes: 500 time steps.
- Travelling speeds for cars on L1 are randomly chosen with uniform distribution in 3 scenarios:
 - Case 1, constant speeds in (80, 100) km/h.
 - Case 2, constant speeds in (60, 80) km/h.
 - Case 3, constant speeds in (40, 60) km/h.



(a) All vehicles with constant speed 80 km/h until time 500 s, and following the recommended speed precisely after time 500 s.



(b) All vehicles with constant speed in the range (72, 88) km/h until time 500 s, and following the recommended speed with a maximum variation tolerance of 10% after time 500 s.

Fig. 7.2 Results of the SUMO simulation for the static case, before and after the activation of the algorithm at time step 500 s. Setup: 40 vehicles, of which 32 are of emission type R007 and 8 are of emission profile R021, and uniform distribution of types of vehicles.

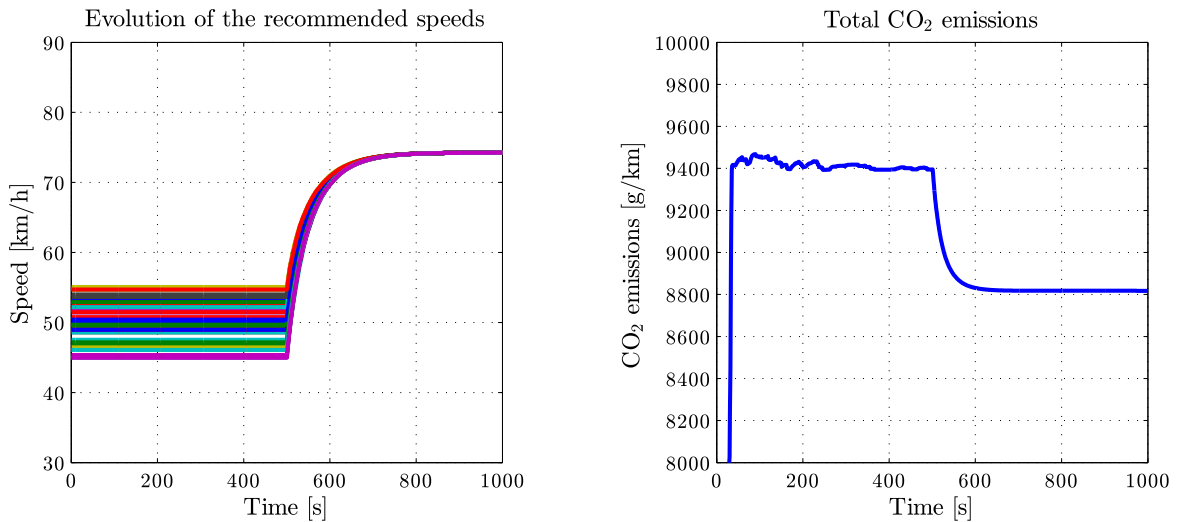


Fig. 7.3 Results of the SUMO simulation for the static case, before and after the activation of the algorithm at time step 500 s. Setup: 40 vehicles, with uniform distribution of emission profile among R016, R017, R018 and R019, and uniform distribution of types of vehicles.

Note that even though this is a dynamic situation, the vehicle density on each part of the road becomes constant after a certain time. A sample of simulation results is given in Figure 7.4, which reveals what might be expected from the initial experiments, namely, the further vehicles are away from the optimal speed, the more that is gained by deploying the ISA.

To complete the section, we conducted one hundred random experiments for each of the three cases described above. In each experiment, we collected the simulation data of the total CO₂ emission generation on each section of the highway from SUMO. Table 7.2 summarises the aggregated results of this exercise, and clearly demonstrate the benefits of the ISA.

Table 7.2 General results: total emissions per lane.

Case	Total Emissions of CO ₂ * [grams]					
	L1 (Uncontrolled)		L2 (Controlled)		Improvement	
	Mean	σ	Mean	σ	Mean	σ
1	2639012.7	1498.38	2587629.4	268.2	1.95%	0.05%
2	2600710.6	606.87	2583472.8	178.3	0.66%	0.02%
3	2787810.6	4200.36	2586943.9	169.9	7.20%	0.14%

* Sum of emissions at every time step (i.e. time integration).

Mean: average of 100 different measurements.

σ : standard deviation.

Comment: Note that it is clearly the case that parameters of the algorithm have the potential to affect emission savings. For example, the speed of convergence of the algorithm affects the rate of which the emissions are saved.

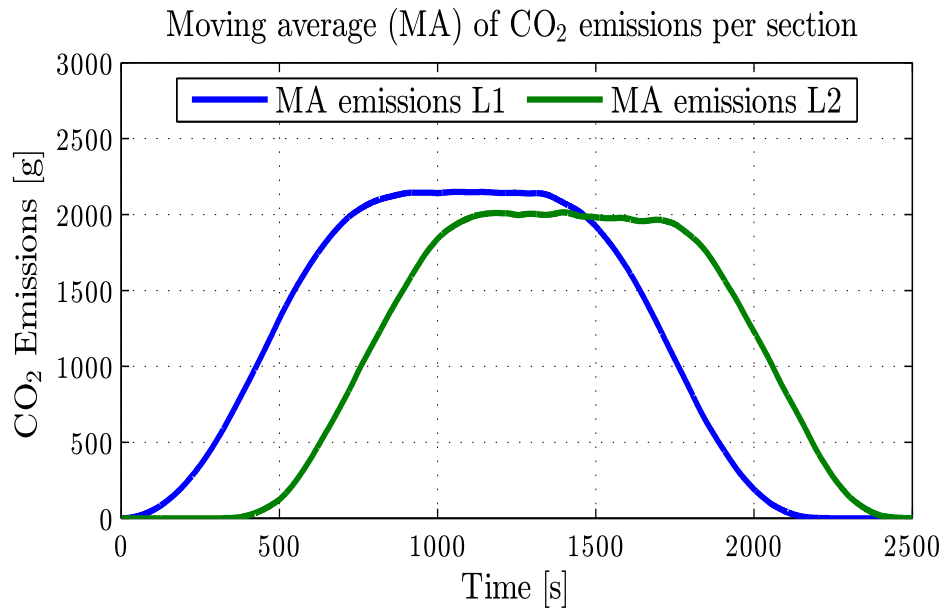


Fig. 7.4 Example for case 3: 500 time-step MA of CO₂ emissions for a set of initial speeds in the range (40, 60) [km/h].

Comment: Note that the solution that we have obtained is optimal for the environment and for the collective, e.g., in terms of overall reduced emissions. However, the solution might be unfair for some single users who would be recommended to drive at a different speed than originally desired. One way to improve fairness could be to decrease road taxes for virtuous vehicles, to compensate them for the inconvenience caused by the dirty vehicles in terms of recommended average speeds.

7.3.3 Hardware-In-the-Loop (HIL) Emulation

Finally, to provide a sense of how this system might function from a driver's perspective we now describe a hardware-in-the-loop implementation of the algorithm. Specifically, we use a SUMO-based Hardware-In-the-Loop (HIL) emulation platform that was developed at the Hamilton Institute [64, 65]. This emulation platform uses the open source road traffic simulator to emulate a real environment and generate virtual cars, along with a dedicated communication architecture supported by TraCI (a Python script implementing a TPC-based client/server architecture) to provide on-line access to SUMO, a smartphone connected to the 3G network and running the plug-in *SumoEmbed* (designed for use with Torque Pro [75]), and a OBD-II adaptor [155] to embed a real car into the simulation, as shown in Figure 7.5. The idea then is to allow the driver, driving a real vehicle on real streets, to experience

being connected to a network of emulated vehicles driving along the same road network. Specifically, we performed this experiment by driving a Toyota Prius on a single-lane street circuit in the North Campus of the Maynooth University, while the Prius is embedded into a HIL emulation and represented by an avatar which interacts with the avatars of 29 other virtual (simulated) vehicles driving along the same stretch of (emulated) road.

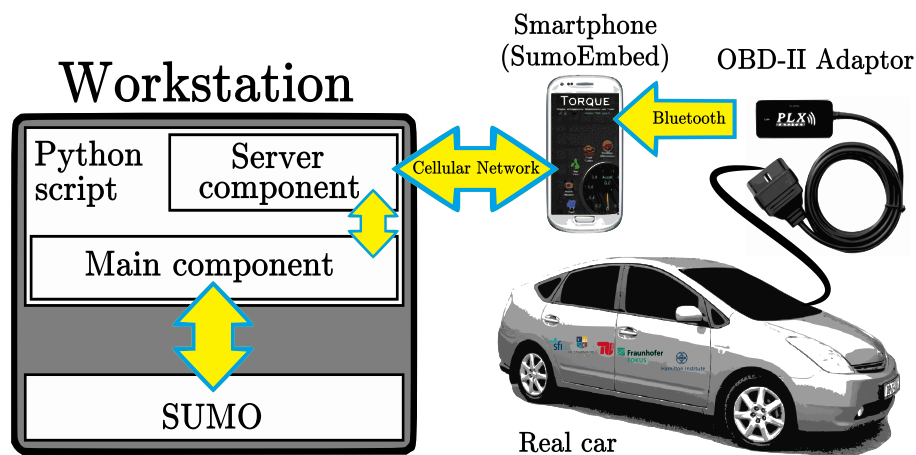


Fig. 7.5 Schematic of the HIL emulation platform.

The experiment begins when the simulation is started on the workstation and the server component of the Python script waits for a call from the OBD-II connected smartphone in the real vehicle. Since the selected street circuit only has one lane, the vehicles are released sequentially from the same starting point. The avatar representing the Prius departs in the sixth position. Once the connection between the Prius and the workstation is established, the position and speed of the Prius' avatar are updated using real-time information from the Prius via the OBD-II adaptor. From the point of view of the ISA algorithm, the Prius is regarded as a normal agent in the SUMO simulation, i.e. treated just like any other simulated vehicle.

The consensus algorithm for the proposed ISA system is embedded in the main component Python script. Thus, once the respective recommended speeds are calculated, they are sent to the vehicles via the server component and the cellular network to the smartphone in the case of the Prius, and via TraCI commands in the case of the other vehicles in the simulation. Note here that the driver behaviour is different for a simulated car compared to the case of the Prius: while we force each simulated vehicle to follow the recommended speed as far as possible², the Prius' driver is allowed to either follow or ignore the speed recommendation (displayed on the smartphone's screen) as desired.

²Concerning mainly the interaction between vehicles and the design parameters for the simulated cars such as acceleration, deceleration, car following model or driver information.

The HIL experiment is setup as follows.

- Length of the experiment: 600 s, of which the ISA algorithm is only engaged at around time 300 s;
- Total number of cars: 30, with uniform distribution of emission profiles among R016, R017, R018 and R019, and uniform distribution of types of vehicles, with a maximum speed of 100 km/h.
- The sampling time interval ΔT for collecting new information and updating the recommendations is 1 s.

Results of the experiment are depicted in Figure 7.6 and Figure 7.7. Figure 7.6 shows that in the turned-off stage of the ISA system (i.e. the first 300 seconds), the overall CO₂ emissions increase almost linearly until all 30 vehicles are added to the emulation (at around 130 s). From this point, it can be observed that the total emissions oscillate around an average peak value of 713 g/km. Again from Figure 7.6, we can observe that the overall CO₂ emissions reduce significantly once the the ISA algorithm is switched on, to an average of 475 g/km. In Figure 7.7 (top), a comparison between the evolution of the Prius' driving and recommended speeds is presented. As can be observed, the recommended speed can be easily followed by the driver.

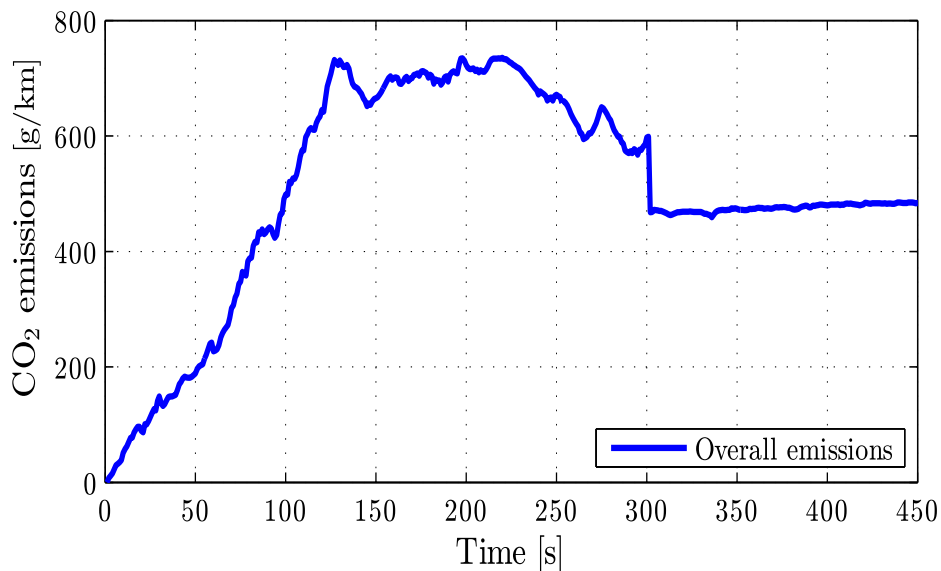


Fig. 7.6 Evolution of the overall CO₂ emissions. The algorithm was turned on around time 300 s.

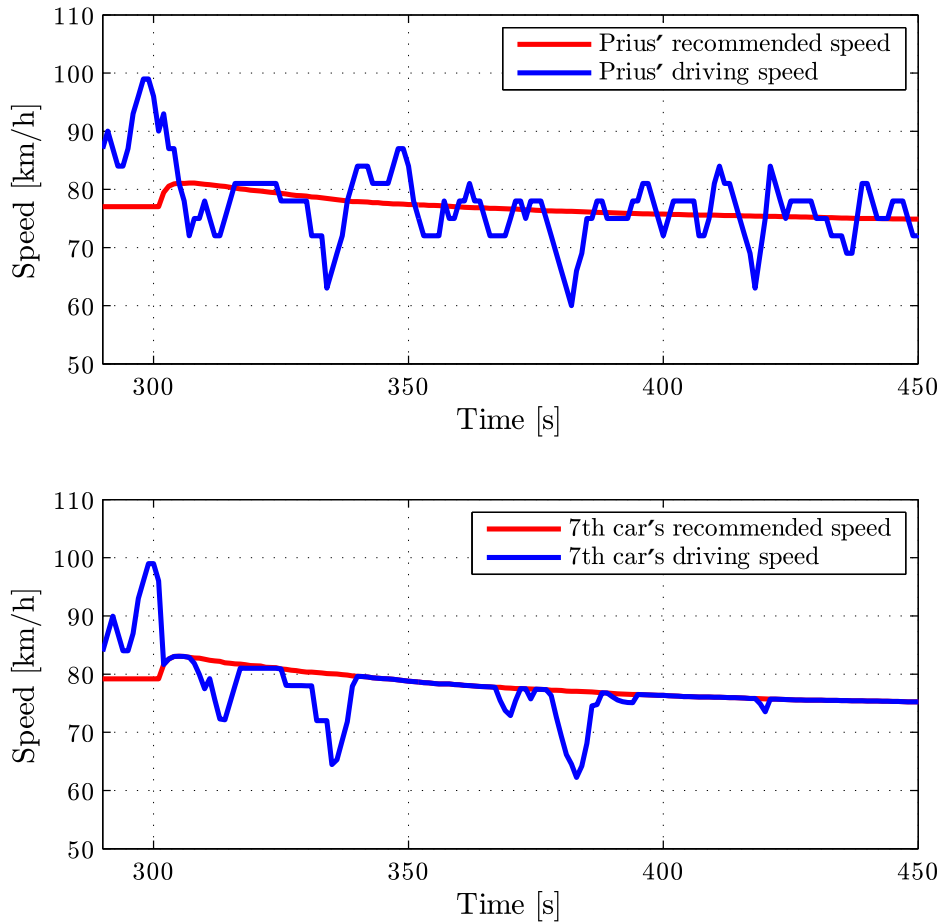


Fig. 7.7 Evolution of some variables along the whole HIL simulation. Top: related speeds for the Prius (the 6th car), and Bottom: the related speeds for the 7th car (just behind the Prius). The algorithm was turned on around time 300 s.

7.4 Conclusions

In this chapter, we extended our previous discussions in Chapter 6 to determining the optimal speeds that should be followed by a fleet of conventional vehicles working to collaboratively reduce their emission generation. This idea has been implemented by adopting Algorithm 11 in Chapter 6, for the new cost functions of interest here. We show that the previously proposed ISA system can be implemented in a manner that accounts for vehicle density and composition, and that it is provably convergent (Theorem 9).

SUMO simulations and HIL emulations are given to illustrate the efficacy and acceptability of the algorithm. Finally, the algorithm has been implemented in a real production vehicle using nothing more than a smartphone and a commercially available OBD-II plug-in.

Chapter 8

Conclusions and Future Work

Abstract: In this chapter, we summarise our work in each chapter of the thesis. We also give some suggestions for potential directions for future research.

8.1 Summary

This thesis discusses the theoretical and application aspects of several distributed control techniques in the context of EVs, smart grid and smart transportation systems. We have provided a rigorous proof of the stability properties of a recently proposed consensus system with feedback, developed customised decentralised algorithms for a variety of practical applications and evaluated their performance with the aid of detailed simulation studies.

To motivate our discussion, we presented the background information on several related topics, arising from the deployment of EVs and the construction of the smart grid and smart transportation systems, in Chapter 1. These topics were classified into four main parts. In the first part, we introduced a useful mathematical algorithm that forms the basis for a number of control algorithms developed in other chapters. In the second and third parts, we considered EV related problems in the context of the smart grid. In the final part, we considered the applications of EVs interacting with a smart transportation system. In each part presented, we pointed out the challenges of the problems and highlighted the objectives and contributions of our work.

8.1.1 A Consensus Algorithm with Feedback

In Part I we discussed a class of recently proposed consensus algorithm with nonlinear feedback. The distributed algorithm is attractive since it has been widely used for solving

many application problems which require collaborative behaviours among agents to achieve some common goals. However, a rigorous analysis of the stability and convergence properties of the system has not been presented to date in the literature. In Chapter 2 we further studied the algorithm by establishing its relations with a Lure system, and explored certain conditions on the feedback functions so that the global convergence of the system can be assured. This is the main mathematical contributions of the thesis.

8.1.2 Grid Integration with EVs

In Part II we discussed topics related to grid integration with EVs. In Chapter 3 we investigated a variety of charging strategies to achieve coordination among EVs for different goals. The charging strategies were implemented on EVs, assuming no V2G capabilities, in typical low-voltage distribution networks (residential and SME areas). We began the chapter by presenting a comprehensive literature review on different EV charging strategies from the view point of EV consumers, DSOs and TSOs. Motivated by these wide variety of algorithms available for EV charging, we presented a common mathematical framework for formulating different EV charging problems that incorporates both power system and charging infrastructure constraints and caters for both instantaneous and temporal optimisation objectives. With this framework in place, different EV charging algorithms including decentralised and centralised and continuously and on-off based implementations, have been evaluated and compared using a realistic distribution network simulation. The results demonstrate that the enhanced AIMD, DPF, and distributed on-off charging algorithms, which cater for both grid constraints and communication overhead problems, provide an effective solution for charging of EVs offering significant benefits to both EV owners and utility companies. At the end of the chapter, we have also presented the design of a distributed wireless testbed for charging mobile phone batteries to physically evaluate the performance of the proposed distributed algorithms.

In Chapter 4 we investigated two V2G applications for providing effective ancillary services to the grid in different scenarios. In the first application we showed that by harnessing the power of V2G technologies, group of EVs could be used to balance both active and reactive power across the 3 phases, thus reducing current imbalance. To do this, we proposed a distributed consensus control framework and algorithms to deliver the required coordination in an efficient manner via EV charging/discharging. The proposed solution seeks to regulate EV charging in order to achieve equalised active power consumption across phases, while at the same time preventing overloading of the grid, and coordinating discharging activities of EVs so as to cancel out the reactive power consumption on the grid. Simulation results using realistic power system simulations have confirmed the efficacy of the consensus control

algorithm and have demonstrated, in particular, that provided a sufficient number of EVs are connected to the grid a substantial positive impact can be achieved. To the best of our knowledge, this is the first time that a distributed consensus algorithm has been employed with EVs to address current imbalance issues.

In the second application, we considered a scenario in which a group of EVs were connecting to the grid providing fair and optimal power dispatch in a microgrid. Our starting point in this application is the observation that the surplus renewable energy generated from the microgrid can be used to charge the EVs when they are not in use, and that the energy can be returned to the grid if the battery charge is maintained above a minimum threshold. With this in mind, we modelled this problem in an optimisation framework where utility functions are used to take account of economic term and QoS trade-offs, and formulated this problem with consensus constraints in terms of fair power dispatch of EVs. This optimisation problem has been solved using an iterative feedback algorithm derived from the system discussed in Chapter 2, taking account of practical grid constraints. Finally, we demonstrated the performance of the proposed algorithm, considering practical grid constraints, through realistic grid simulations. In this application, we have shown that the proposed iterative consensus algorithm can be used to solve optimisation consensus problems if certain conditions on the feedback signal can be satisfied. This is one of the main contributions of the thesis.

8.1.3 Optimal Energy Management Strategies

In Part III we discussed optimal energy management strategies in the context of the smart grid. In Chapter 5 we started the discussion by considering a fundamental power balancing problem in a microgrid connected with DERs. We have shown that the balancing objective is challenging due to a number of factors, e.g., the uncertain power supply, the uncertain energy offer, and the difficulties with designing an effective algorithm for real-time implementation in the EMS. In contrast to many conventional centralised based energy management strategies, our objective was to design an algorithm that automatically shares the power generation task among the available DERs in a way that is fair and distributed. To this end, we showed that one can design, using simple ideas based on AIMD, an effective distributed energy management system to achieve the above objective, without having to communicate real-time power availability from renewable resources, or the power required by the users, but by simply notifying the DERs with a single bit of information every time the provided power equals the required power. We have shown the proposed AIMD-like algorithm performs in practice as well as a centralised full-communication algorithm in simulations. In addition, we also showed that thermal energy requirements can be further included in the microgrid

operation by simply extending the algorithm for double power balancing requirements, and we presented simulation studies to validate the proposed method.

To conclude this part, we have demonstrated that the basic ideas of AIMD can be easily extended to solve optimisation problems with linear capacity constraints. Our approach was based on achieving consensus on the first derivatives of the utility functions (with convexity). The power balancing constraint was satisfied by applying the basic congestion solving mechanisms based on synchronised AIMD (i.e. broadcasting balancing notifications to the entire network). We have shown that the proposed AIMD-like approach can be implemented in a distributed manner with little communication overhead and control requirements for the EMS. This is the main contribution in Part III.

8.1.4 Distributed and Privacy-Aware Speed Advisory Systems

In the final part of the thesis we proposed a consensus based distributed speed advisory system that optimally determines a recommended common speed for a given area in order that the total emissions, or total battery energy consumptions of a group of EVs is minimised.

In Chapter 6 we showed how to design a distributed speed advisory system to minimise battery energy consumptions of a group of EVs in a city centre scenario. We formulated this design problem in a similar fashion to the optimisation problem introduced in Chapter 4. We showed that by adapting mathematical algorithms from Chapter 2, an effective SAS can be designed to maximise the energy efficiency of a group of EVs in a privacy-preserving manner. The proposed SAS provides an effective solution for EV owners, transportation system operators, and the grid companies. From the perspective of EV owners, the SAS maximises the energy efficiency of the group of EVs, thus extending their total travelling range. From the perspective of the transportation system, the consensus recommended speed signal would be helpful in smoothing traffic flow and thus reducing traffic congestion. From the perspective of the grid companies, the proposed SAS would effectively reduce the increasing energy requirements associated with EV charging, which helps to mitigate the heavy loading situation on the grid.

The proposed SAS concept was extended in Chapter 7 to support minimisation of emission generation of conventional vehicles in a highway scenario. We have demonstrated that by adapting the methodology developed in Chapter 6, the SAS can be implemented in a similar fashion, while taking account of vehicle density and composition. The performance of the system was further validated through a variety of simulation studies including SUMO and HIL tests involving real vehicles.

8.2 Future Work

This section outlines some potential directions for future research.

8.2.1 Grid Integration with EVs

The comparative framework presented in Chapter 3 was designed to evaluate the performance of different EV charging strategies applied in distribution networks focusing on the power flow and voltage issues arising from the interaction between the grid and EVs. This work can be extended in a number of directions. It would of interest to include the impact of EV charging on transient grid stability as reflected by frequency variations on the grid and to investigate how decentralised/distributed algorithms (e.g. AIMD and DPF) can be modified to improve grid stability. It would also be interesting to evaluate the practical performance of each introduced method from the perspectives of communication overhead, delays and protocols, by developing an effective communication channel model using realistic network simulators (e.g. NS3 [78] and OMNeT++ [205]). Developing a more complex network scenario, e.g., city scale distribution networks, to validate the performance of the charging strategies on a large scale would also be desirable.

In the context of V2G applications, the proposed consensus algorithms were applied to minimise current imbalance and optimise the power dispatch of EVs in Chapter 4. For the first V2G application, it would be of interest to investigate how to apply the consensus ideas on EVs to address voltage imbalance issues and frequency regulation problems in future research. However, as we mentioned previously in Chapter 4, addressing voltage imbalance issues using EVs will be more challenging since the voltages along phases depend on the distribution of the individual loads, which we did not need to consider in the study of the current imbalance problem. For frequency regulation services, some recent work [70, 71, 201] has demonstrated the potential of V2G in this regard. As an extension for the second V2G application, it would be desirable to explore suitable business models to support the practical (commercial) implementation of the proposed V2G programme.

8.2.2 Optimal Energy Management Strategies

In Chapter 5 our proposed approach was tested on a simple microgrid scenario with a few DERs and a total load of the order of a few MW. In future work the scenario could be further extended by considering the presence of large scale storage systems in addition to the distributed dynamic storage provided by EVs. This would provide more flexibility for power regulation in the microgrid, however it also poses challenges for optimal algorithm

design. Reference [190] shows in a different context, how AIMD algorithms can be modified to further include reactive power management. It would be interesting to explore this idea in the context of the microgrid scenario and coordination framework presented here, and in particular, how multiple, potentially competing optimisation objectives can be incorporated.

8.2.3 Distributed and Privacy-Aware Speed Advisory Systems

In Chapters 6 and 7 we proposed an effective SAS for optimising both electric and conventional vehicles networks. There are a variety of ways this work can be extended, for example: recommended speeds can be communicated, for instance, by establishing a speed limit in the area of interest. However, the speed indicated in the speed limit, and the true steady-state of vehicles are clearly different. Realistic transportation simulations will allow us to identify the most convenient speed limit that in turn would result in an average speed close to the optimal one. Clearly, such an analysis is affected by the specific characteristics of the city centre of interest.

In the simulation studies presented in the thesis the true communication network underlying the fleet of vehicles has not been modelled. We simply assumed that communications can occur in a random fashion. In future work, we shall further include realistic communication networks in the mobility network simulator (e.g., VanetMobiSim [72]) to validate the effectiveness of the SAS algorithm for specific applications of interest (e.g., in terms of convergence speed).

References

- [1] Acha, S., Green, T. C., and Shah, N. (2010). Effects of optimised plug-in hybrid vehicle charging strategies on electric distribution network losses. In *Transmission and Distribution Conference and Exposition, 2010 IEEE PES*, pages 1–6. IEEE.
- [2] Adell, E., Varhelyi, A., Alonso, M., and Plaza, J. (2008). Developing human–machine interaction components for a driver assistance system for safe speed and safe distance. *IET Intelligent Transport Systems*, 2(1):1–14.
- [3] Ahn, C., Li, C.-T., and Peng, H. (2011). Decentralized charging algorithm for electrified vehicles connected to smart grid. In *American Control Conference (ACC), 2011*, pages 3924–3929. IEEE.
- [4] Aloini, D., Crisostomi, E., Raugi, M., and Rizzo, R. (2011). Optimal power scheduling in a virtual power plant. In *Innovative Smart Grid Technologies (ISGT Europe), 2011 2nd IEEE PES International Conference and Exhibition on*, pages 1–7. IEEE.
- [5] Amin, S. M. and Wollenberg, B. F. (2005). Toward a smart grid: power delivery for the 21st century. *Power and Energy Magazine, IEEE*, 3(5):34–41.
- [6] Ancillotti, E., Bruno, R., and Conti, M. (2014). Smoothing peak demands through aggregate control of background electrical loads. In *Innovative Smart Grid Technologies Conference (ISGT), 2014 IEEE PES*, pages 1–5. IEEE.
- [7] Asimakopoulou, G. E., Dimeas, A. L., and Hatziargyriou, N. D. (2013). Leader-follower strategies for energy management of multi-microgrids. *Smart Grid, IEEE Transactions on*, 4(4):1909–1916.
- [8] Aunedi, M. and Strbac, G. (2013). Efficient system integration of wind generation through smart charging of electric vehicles. In *Ecological Vehicles and Renewable Energies (EVER), 2013 8th International Conference and Exhibition on*, pages 1–12. IEEE.
- [9] Bakari, K. and Kling, W. L. (2010). Virtual power plants: An answer to increasing distributed generation. In *Innovative Smart Grid Technologies Conference Europe (ISGT Europe), 2010 IEEE PES*, pages 1–6. IEEE.
- [10] Banzi, M. (2008). *Getting Started with Arduino*. Make Books - Imprint of: O'Reilly Media, Sebastopol, CA, ill edition.
- [11] Barth, M. and Boriboonsomsin, K. (2010). "Intelligent" ways to cut transportation's CO₂ emissions, available online at url: <http://www.uctc.net/research/briefs/PB-2010-03.pdf>.

- [12] Behrisch, M., Bieker, L., Erdmann, J., and Krajzewicz, D. (2011). Sumo-simulation of urban mobility-an overview. In *SIMUL 2011, The Third International Conference on Advances in System Simulation*, pages 55–60.
- [13] Beil, I. and Hiskens, I. (2012). A distributed wireless testbed for plug-in hybrid electric vehicle control algorithms. In *North American Power Symposium (NAPS), 2012*, pages 1–5. IEEE.
- [14] Boulter, P., Barlow, T. J., and McCrae, I. S. (2009). Emission factors 2009: Report 3-exhaust emission factors for road vehicles in the United Kingdom. *TRL Published Project Report*.
- [15] Boyd, S., Parikh, N., Chu, E., Peleato, B., and Eckstein, J. (2011). Distributed optimization and statistical learning via the alternating direction method of multipliers. *Foundations and Trends in Machine Learning*, 3(1):1–122.
- [16] Boyd, S. and Vandenberghe, L. (2004). *Convex optimization*. Cambridge university press.
- [17] Brooks, A. N. (2002). *Vehicle-to-grid demonstration project: Grid regulation ancillary service with a battery electric vehicle*. California Environmental Protection Agency, Air Resources Board, Research Division.
- [18] Buchenscheit, A., Schaub, F., Kargl, F., and Weber, M. (2009). A VANET-based emergency vehicle warning system. In *Vehicular Networking Conference (VNC), 2009 IEEE*, pages 1–8. IEEE.
- [19] Budzisz, L., Stanojevic, R., Shorten, R., and Baker, F. (2009). A strategy for fair coexistence of loss and delay-based congestion control algorithms. *Communications Letters, IEEE*, 13(7):555–557.
- [20] Caldon, R., Patria, A. R., and Turri, R. (2004). Optimal control of a distribution system with a virtual power plant. *Bulk Power System Dynamics and Control, Cortina. d’Ampezzo, Italy*.
- [21] Callaway, Z. M. and Hiskens, I. (2010). Decentralized charging control for large populations of plug-in electric vehicles: application of the nash certainty equivalence principle. In *Control Applications (CCA), 2010 IEEE International Conference on. Control Applications (CCA), 2010 IEEE International Conference on*.
- [22] Cao, Y., Tang, S., Li, C., Zhang, P., Tan, Y., Zhang, Z., and Li, J. (2012). An optimized ev charging model considering tou price and soc curve. *Smart Grid, IEEE Transactions on*, 3(1):388–393.
- [23] Caramanis, M. and Foster, J. M. (2009). Management of electric vehicle charging to mitigate renewable generation intermittency and distribution network congestion. In *Decision and Control, 2009 held jointly with the 2009 28th Chinese Control Conference. CDC/CCC 2009. Proceedings of the 48th IEEE Conference on*, pages 4717–4722. Ieee.
- [24] Carsten, O., Lai, F., Chorlton, K., Goodman, P., Carslaw, D., and Hess, S. (2008). Speed limit adherence and its effect on road safety and climate change-final report. *tech. rep., University of Leeds - Institute for Transport Studies*.

- [25] Carsten, O. M. and Tate, F. (2005). Intelligent speed adaptation: accident savings and cost–benefit analysis. *Accident Analysis & Prevention*, 37(3):407–416.
- [26] CER (2012). Electricity customer behaviour trial, available online at url: <http://www.ucd.ie/issda/data/commissionforenergyregulationcer/>.
- [27] Chatterjee, S. and Seneta, E. (1977). Towards consensus: some convergence theorems on repeated averaging. *Journal of Applied Probability*, 14(1):89–97.
- [28] Chiu, D.-M. and Jain, R. (1989). Analysis of the increase and decrease algorithms for congestion avoidance in computer networks. *Computer Networks and ISDN systems*, 17(1):1–14.
- [29] Chowdhury, S. and Crossley, P. (2009). *Microgrids and active distribution networks*. IET renewable energy series. The Institution of Engineering and Technology, Stevenage.
- [30] Choy, M. C., Srinivasan, D., and Cheu, R. L. (2003). Cooperative, hybrid agent architecture for real-time traffic signal control. *Systems, Man and Cybernetics, Part A: Systems and Humans, IEEE Transactions on*, 33(5):597–607.
- [31] Clement, K., Haesen, E., and Driesen, J. (2009). Coordinated charging of multiple plug-in hybrid electric vehicles in residential distribution grids. In *Power Systems Conference and Exposition, 2009. PSCE'09. IEEE/PES*, pages 1–7. IEEE.
- [32] Clement-Nyns, K., Haesen, E., and Driesen, J. (2010). The impact of charging plug-in hybrid electric vehicles on a residential distribution grid. *Power Systems, IEEE Transactions on*, 25(1):371–380.
- [33] Corless, M. and Shorten, R. (2012). An ergodic aimd algorithm with application to high-speed networks. *International Journal of Control*, 85(6):746–764.
- [34] Corless, M. and Shorten, R. (2014). Analysis of a general nonlinear increase-decrease resource allocation algorithm with application to network utility maximization. *submitted to Automatica*.
- [35] Crisostomi, E., Liu, M., Raugi, M., and Shorten, R. (2014). Plug-and-play distributed algorithms for optimized power generation in a microgrid. *Smart Grid, IEEE Transactions on*, 5(4):2145–2154.
- [36] CSO (2013). National travel survey 2009, available online at url: <http://www.cso.ie/en/media/csoie/releasespublications/documents/transport/2009/natravel09.pdf>.
- [37] Cyrus, J., Peters, A., and Wichmann, H.-E. (2009). Umweltzone münchen—eine erste bilanz. *Umweltmedizin in Forschung und Praxis*, 14(3):127–132.
- [38] D’Ausilio, A. (2012). Arduino: A low-cost multipurpose lab equipment. *Behavior research methods*, 44(2):305–313.
- [39] Deilami, S., Masoum, A., Moses, P., and Masoum, M. A. (2011a). Real-time coordination of plug-in electric vehicle charging in smart grids to minimize power losses and improve voltage profile. *Smart Grid, IEEE Transactions on*, 2(3):456–467.

- [40] Deilami, S., Masoum, A. S., Moses, P. S., and Masoum, M. A. (2011b). Real-time coordination of plug-in electric vehicle charging in smart grids to minimize power losses and improve voltage profile. *Smart Grid, IEEE Transactions on*, 2(3):456–467.
- [41] Dhillon, J., Parti, S., and Kothari, D. (2002). Fuzzy decision-making in stochastic multi-objective short-term hydrothermal scheduling. *IEE Proceedings-Generation, Transmission and Distribution*, 149(2):191–200.
- [42] Dincer, I. (2000). Renewable energy and sustainable development: a crucial review. *Renewable and Sustainable Energy Reviews*, 4(2):157–175.
- [43] Dugan, R. C. (2012). Reference guide: The open distribution system simulator (opendss). *Electric Power Research Institute, Inc.*
- [44] EPRI (2012). Opendss manual, available online at url: <http://sourceforge.net/projects/electricdss/>.
- [45] Erseghe, T., Zennaro, D., Dall’Anese, E., and Vangelista, L. (2011). Fast consensus by the alternating direction multipliers method. *Signal Processing, IEEE Transactions on*, 59(11):5523–5537.
- [46] Escudero-Garzás, J. J., García-Armada, A., and Seco-Granados, G. (2012). Fair design of plug-in electric vehicles aggregator for v2g regulation. *Vehicular Technology, IEEE Transactions on*, 61(8):3406–3419.
- [47] Faludi, R. (2010). *Building Wireless Sensor Networks: With ZigBee, XBee, Arduino, and Processing*. O’Reilly Media, Inc., 1st edition.
- [48] Fan, Z. (2012). A distributed demand response algorithm and its application to phev charging in smart grids. *Smart Grid, IEEE Transactions on*, 3(3):1280–1290.
- [49] Farhangi, H. (2010). The path of the smart grid. *Power and Energy Magazine, IEEE*, 8(1):18–28.
- [50] Farkas, C., Szabo, K. I., and Prikler, L. (2011). Impact assessment of electric vehicle charging on a lv distribution system. In *Energetics (IYCE), Proceedings of the 2011 3rd International Youth Conference on*, pages 1–8. IEEE.
- [51] Fernandez, J., Bacha, S., Riu, D., Turker, H., and Paupert, M. (2013). Current unbalance reduction in three-phase systems using single phase phev chargers. In *Industrial Technology (ICIT), 2013 IEEE International Conference on*, pages 1940–1945. IEEE.
- [52] Flemisch, F., Kelsch, J., Löper, C., Schieben, A., Schindler, J., and Heesen, M. (2008). Cooperative control and active interfaces for vehicle assistance and automation. In *FISITA World automotive congress*.
- [53] Florian, F. (2014). Electric buses: Rapid charging in vienna, available online at url: <http://www.siemens.com/innovation/en/home/pictures-of-the-future/mobility-and-motors/electric-mobility-electric-buses.html>.
- [54] Foley, A., Tyther, B., Calnan, P., and Gallachóir, B. Ó. (2013). Impacts of electric vehicle charging under electricity market operations. *Applied Energy*, 101:93–102.

- [55] Fox-Penner, P. (2014). *Smart Power Anniversary Edition: Climate Change, the Smart Grid, and the Future of Electric Utilities*. Island Press.
- [56] Gallen, R., Hautiere, N., Cord, A., and Glaser, S. (2013). Supporting drivers in keeping safe speed in adverse weather conditions by mitigating the risk level. *Intelligent Transportation Systems, IEEE Transactions on*, 14(4):1558–1571.
- [57] Galus, M. D., Koch, S., and Andersson, G. (2011). Provision of load frequency control by phev, controllable loads, and a cogeneration unit. *Industrial Electronics, IEEE Transactions on*, 58(10):4568–4582.
- [58] Gan, L., Topcu, U., and Low, S. (2011). Optimal decentralized protocol for electric vehicle charging. In *Decision and Control and European Control Conference (CDC-ECC), 2011 50th IEEE Conference on*, pages 5798–5804. IEEE.
- [59] Garelli, L., Casetti, C., Chiasserini, C., and Fiore, M. (2011). Mobsampling: V2V communications for traffic density estimation. In *Vehicular Technology Conference (VTC Spring), 2011 IEEE 73rd*, pages 1–5. IEEE.
- [60] Gerkenmeyer, C., Kintner-Meyer, M. C., and DeSteese, J. G. (2010). *Technical challenges of plug-in hybrid electric vehicles and impacts to the US power system: Distribution system analysis*. Pacific Northwest National Laboratory.
- [61] Giordano, E., Frank, R., Pau, G., and Gerla, M. (2010). CORNER: a realistic urban propagation model for VANET. In *Wireless On-demand Network Systems and Services (WONS), 2010 Seventh International Conference on*, pages 57–60. IEEE.
- [62] Giuntoli, M. and Poli, D. (2013). Optimized thermal and electrical scheduling of a large scale virtual power plant in the presence of energy storages. *IEEE Transactions on Smart Grid*, 4(2):942–955.
- [63] Gjengedal, T. (1996). Emission constrained unit-commitment (ecuc). *Energy Conversion, IEEE Transactions on*, 11(1):132–138.
- [64] Griggs, W. M., Ordóñez-Hurtado, R. H., Crisostomi, E., Häusler, F., Massow, K., and Shorten, R. N. (2014). A Large-Scale SUMO-Based Emulation Platform. Submitted to the *IEEE Transactions on Intelligent Transportation Systems*.
- [65] Griggs, W. M. and Shorten, R. N. (2013). Embedding real vehicles in SUMO for large-scale ITS scenario emulation. In *Connected Vehicles and Expo (ICCVE), 2013 International Conference on*, pages 962–963. IEEE.
- [66] Gruz, T. M. (1990). A survey of neutral currents in three-phase computer power systems. *Industry Applications, IEEE Transactions on*, 26(4):719–725.
- [67] Gu, Y., Liu, M., Crisostomi, E., and Shorten, R. (2014). Optimised consensus for highway speed limits via intelligent speed advisory systems. In *Connected Vehicles and Expo (ICCVE), 2014 International Conference on*. IEEE.
- [68] Guille, C. and Gross, G. (2009). A conceptual framework for the vehicle-to-grid (v2g) implementation. *Energy policy*, 37(11):4379–4390.

- [69] Gyugyi, L., Schauder, C., Williams, S., Rietman, T., Torgerson, D., and Edris, A. (1995). The unified power flow controller: a new approach to power transmission control. *Power Delivery, IEEE Transactions on*, 10(2):1085–1097.
- [70] Han, S., Han, S., and Sezaki, K. (2010). Development of an optimal vehicle-to-grid aggregator for frequency regulation. *Smart Grid, IEEE Transactions on*, 1(1):65–72.
- [71] Han, S., Han, S., and Sezaki, K. (2011). Estimation of achievable power capacity from plug-in electric vehicles for v2g frequency regulation: Case studies for market participation. *Smart Grid, IEEE Transactions on*, 2(4):632–641.
- [72] Härri, J., Filali, F., Bonnet, C., and Fiore, M. (2006). Vanetmobisim: generating realistic mobility patterns for vanets. In *Proceedings of the 3rd international workshop on Vehicular ad hoc networks*, pages 96–97. ACM.
- [73] Hartenstein, H. and Laberteaux, K. (2010). *VANET: vehicular applications and inter-networking technologies*. Wiley Online Library.
- [74] Hatta, H., Uemura, S., and Kobayashi, H. (2010). Cooperative control of distribution system with customer equipments to reduce reverse power flow from distributed generation. In *Power and Energy Society General Meeting, 2010 IEEE*, pages 1–6.
- [75] Hawkins, I. (2013). Torque pro, available online at url: <https://play.google.com/store/apps/details?id=org.prowl.torque>.
- [76] He, Y., Venkatesh, B., and Guan, L. (2012). Optimal scheduling for charging and discharging of electric vehicles. *Smart Grid, IEEE Transactions on*, 3(3):1095–1105.
- [77] Hedrick, J., Tomizuka, M., and Varaiya, P. (1994). Control issues in automated highway systems. *Control Systems, IEEE*, 14(6):21–32.
- [78] Henderson, T. R., Lacage, M., Riley, G. F., Dowell, C., and Kopena, J. (2008). Network simulations with the ns-3 simulator. *SIGCOMM demonstration*, 15:17.
- [79] Hochgraf, C. and Lasseter, R. H. (1998). Statcom controls for operation with unbalanced voltages. *Power Delivery, IEEE Transactions on*, 13(2):538–544.
- [80] Hounsell, N., Shrestha, B., Piao, J., and McDonald, M. (2009). Review of urban traffic management and the impacts of new vehicle technologies. *Intelligent Transport Systems, IET*, 3(4):419–428.
- [81] Hu, J., You, S., Si, C., Lind, M., and Østergaard, J. (2014). Optimization and control methods for smart charging of electric vehicles facilitated by fleet operator: Review and classification. *International Journal of Distributed Energy Resources*, 10(1):383–397.
- [82] James, A. (2015). Louisville gets its first fully-electric, zero-emissions city buses, available online at url: <http://cleantechnica.com/2015/01/16/louisville-gets-first-fully-electric-zero-emissions-city-buses/>.
- [83] Jin, C., Sheng, X., and Ghosh, P. (2013). Energy efficient algorithms for electric vehicle charging with intermittent renewable energy sources. In *Power and Energy Society General Meeting (PES), 2013 IEEE*, pages 1–5. IEEE.

- [84] Kar, K., Sarkar, S., and Tassiulas, L. (2001). A simple rate control algorithm for max total user utility. In *INFOCOM 2001. Twentieth Annual Joint Conference of the IEEE Computer and Communications Societies. Proceedings. IEEE*, volume 1, pages 133–141. IEEE.
- [85] Kato, S., Tsugawa, S., Tokuda, K., Matsui, T., and Fujii, H. (2002). Vehicle control algorithms for cooperative driving with automated vehicles and intervehicle communications. *Intelligent Transportation Systems, IEEE Transactions on*, 3(3):155–161.
- [86] Kempton, W., Udo, V., Huber, K., Komara, K., Letendre, S., Baker, S., Brunner, D., and Pearre, N. (2008). A test of vehicle-to-grid (v2g) for energy storage and frequency regulation in the pjm system. *Results from an Industry-University Research Partnership*, page 32.
- [87] Kersting, W. H. (2001). Radial distribution test feeders. In *Power Engineering Society Winter Meeting, 2001. IEEE*, volume 2, pages 908–912. IEEE.
- [88] Kersting, W. H. (2012). *Distribution system modeling and analysis*. CRC press.
- [89] Khaligh, A. and Li, Z. (2010). Battery, ultracapacitor, fuel cell, and hybrid energy storage systems for electric, hybrid electric, fuel cell, and plug-in hybrid electric vehicles: State of the art. *Vehicular Technology, IEEE Transactions on*, 59(6):2806–2814.
- [90] Khan, M. and Kockelman, K. M. (2012). Predicting the market potential of plug-in electric vehicles using multiday gps data. *Energy Policy*, 46:225–233.
- [91] King, C., Shorten, R. N., Wirth, F. R., and Akar, M. (2008). Growth conditions for the global stability of high-speed communication networks with a single congested link. *Automatic Control, IEEE Transactions on*, 53(7):1770–1774.
- [92] Kisacikoglu, M. C., Ozpineci, B., and Tolbert, L. M. (2010). Examination of a phev bidirectional charger system for v2g reactive power compensation. In *Applied Power Electronics Conference and Exposition (APEC), 2010 Twenty-Fifth Annual IEEE*, pages 458–465. IEEE.
- [93] Klinge, S. and Middleton, R. (2009). Time headway requirements for string stability of homogeneous linear unidirectionally connected systems. In *Decision and Control, 2009 held jointly with the 2009 28th Chinese Control Conference. CDC/CCC 2009. Proceedings of the 48th IEEE Conference on*, pages 1992–1997.
- [94] Knorn, F. (2011). *Topics in cooperative control*. PhD thesis, National University of Ireland, Maynooth.
- [95] Knorn, F., Stanojevic, R., Corless, M., and Shorten, R. (2009). A framework for decentralised feedback connectivity control with application to sensor networks. *International Journal of Control*, 82(11):2095–2114.
- [96] Knorn, S. and Middleton, R. (2013). Stability of two-dimensional linear systems with singularities on the stability boundary using lmis. *Automatic Control, IEEE Transactions on*, 58(10):2579–2590.

- [97] Kutt, L., Saarijarvi, E., Lehtonen, M., Molder, H., and Niitsoo, J. (2013). A review of the harmonic and unbalance effects in electrical distribution networks due to ev charging. In *Environment and Electrical Engineering (EEEIC), 2013 12th International Conference on*, pages 556–561. IEEE.
- [98] Lee, C.-Y. (1999). Effects of unbalanced voltage on the operation performance of a three-phase induction motor. *Energy Conversion, IEEE Transactions on*, 14(2):202–208.
- [99] Leith, D. and Shorten, R. (2004). H-tcp: Tcp for high-speed and long-distance networks. In *Proceedings of PFLDnet*, volume 2004.
- [100] Li, C.-T., Ahn, C., Peng, H., and Sun, J. (2012). Integration of plug-in electric vehicle charging and wind energy scheduling on electricity grid. In *Innovative Smart Grid Technologies (ISGT), 2012 IEEE PES*, pages 1–7. IEEE.
- [101] Li, M. and Luh, P. (2013). A decentralized framework of unit commitment for future power markets. In *Power and Energy Society General Meeting (PES), 2013 IEEE*, pages 1–5.
- [102] Li, N., Chen, L., and Low, S. H. (2011). Optimal demand response based on utility maximization in power networks. In *Power and Energy Society General Meeting, 2011 IEEE*, pages 1–8. IEEE.
- [103] Li, T. and Zhang, J.-F. (2010). Consensus conditions of multi-agent systems with time-varying topologies and stochastic communication noises. *Automatic Control, IEEE Transactions on*, 55(9):2043–2057.
- [104] Li, Y.-T., Leith, D., and Shorten, R. N. (2007). Experimental evaluation of tcp protocols for high-speed networks. *Networking, IEEE/ACM Transactions on*, 15(5):1109–1122.
- [105] Liu, M., Crisostomi, E., Gu, Y., and Shorten, R. (2014a). Optimal distributed consensus algorithm for fair v2g power dispatch in a microgrid. In *Electric Vehicle Conference (IEVC), 2014 IEEE International*. IEEE.
- [106] Liu, M., Crisostomi, E., Raugi, M., and Shorten, R. (2013a). Optimal distributed power generation for thermal and electrical scheduling in a microgrid. In *Innovative Smart Grid Technologies Europe (ISGT EUROPE), 2013 4th IEEE/PES*, pages 1–5. IEEE.
- [107] Liu, M. and McLoone, S. (2013a). Enhanced aimd-based decentralized residential charging of evs. *Transactions of the Institute of Measurement and Control*, page 0142331213494100.
- [108] Liu, M. and McLoone, S. (2013b). Investigation of aimd based charging strategies for evs connected to a low-voltage distribution network. In *Intelligent Computing for Sustainable Energy and Environment*, pages 433–441. Springer.
- [109] Liu, M., McNamara, P., and McLoone, S. (2013b). Fair charging strategies for evs connected to a low-voltage distribution network. In *Innovative Smart Grid Technologies Europe (ISGT EUROPE), 2013 4th IEEE/PES*, pages 1–5. IEEE.

- [110] Liu, M., McNamara, P., McLoone, S., and Shorten, R. (2014b). Residential electrical vehicle charging strategies - the good, the bad and the ugly. *to appear in Special Issue on Electric Vehicles and Their Integration with Power Grid, Journal of Modern Power Systems and Clean Energy*.
- [111] Liu, M., McNamara, P., Shorten, R., and McLoone, S. (2014c). Distributed consensus charging for current unbalance reduction. In *18th IFAC World Congress*.
- [112] Liu, M., Ordóñez-Hurtado, R. H., Wirth, F., Gu, Y., Crisostomi, E., and Shorten, R. (2015a). A distributed and privacy-aware speed advisory system for optimising conventional and electric vehicles networks. *submitted to IEEE transactions on intelligent transportation systems*.
- [113] Liu, M., Ordóñez-Hurtado, R. H., Wirth, F., Gu, Y., and Crisostomi, Emanuele Shorten, R. (2015b). Intelligent speed advisory system for electric vehicles. *submitted to 5th IFAC Conference on Analysis and Design of Hybrid Systems*.
- [114] Liu, M., Stüdl, S., Middleton, R., McLoone, S., Shorten, R., and Braslavsky, J. (2013c). On-off based charging strategies for evs connected to a low voltage distributon network. In *Power and Energy Engineering Conference (APPEEC), 2013 IEEE PES Asia-Pacific*.
- [115] Liu, M., Wirth, F., Corless, M., and Shorten, R. (2015c). On global convergence of consensus with nonlinear feedback, the lure problem, and some applications. *submitted to IEEE transactions on automatic control*.
- [116] Loguinov, D. and Radha, H. (2003). End-to-end rate-based congestion control: convergence properties and scalability analysis. *Networking, IEEE/ACM Transactions on*, 11(4):564–577.
- [117] Lombardi, P., Powalko, M., and Rudion, K. (2009). Optimal operation of a virtual power plant. In *Power & Energy Society General Meeting, 2009. PES'09. IEEE*, pages 1–6. IEEE.
- [118] Lopes, J. A. P., Soares, F. J., and Almeida, P. M. R. (2011a). Integration of electric vehicles in the electric power system. *Proceedings of the IEEE*, 99(1):168–183.
- [119] Lopes, J. A. P., Soares, F. J., and Almeida, P. M. R. (2011b). Integration of electric vehicles in the electric power system. *Proceedings of the IEEE*, 99(1):168–183.
- [120] Lopes, J. P., Soares, F. J., Almeida, P., and da Silva, M. M. (2009). Smart charging strategies for electric vehicles: Enhancing grid performance and maximizing the use of variable renewable energy resources. In *EVS24 Intenational Battery, Hybrid and Fuell Cell Electric Vehicle Symposium, Stavanger, Norveška*.
- [121] Lu, W., Atay, F. M., and Jost, J. (2007). Synchronization of discrete-time dynamical networks with time-varying couplings. *SIAM Journal on Mathematical Analysis*, 39(4):1231–1259.
- [122] Lynch, N. A. (1996). *Distributed algorithms*. Morgan Kaufmann.

- [123] Marinelli, M., Sossan, F., Costanzo, G. T., and Bindner, H. W. (2014). Testing of a predictive control strategy for balancing renewable sources in a microgrid. *IEEE Transactions on Sustainable Energy*, 5(4):1426–1433.
- [124] Masters, G. M. (2013). *Renewable and efficient electric power systems*. John Wiley & Sons.
- [125] Matrose, C., Helmschrott, T., Godde, M., Szczechowicz, E., and Schnettler, A. (2012). Impact of different electric vehicle charging strategies onto required distribution grid reinforcement. In *Transportation Electrification Conference and Expo (ITEC), 2012 IEEE*, pages 1–5. IEEE.
- [126] McDaniel, P. and McLaughlin, S. (2009). Security and privacy challenges in the smart grid. *IEEE Security and Privacy*, 7(3):75–77.
- [127] Meibom, P., Hilger, K. B., Madsen, H., and Vinther, D. (2013). Energy comes together in denmark: The key to a future fossil-free danish power system. *Power and Energy Magazine, IEEE*, 11(5):46–55.
- [128] Mets, K., Verschueren, T., Haerick, W., Develder, C., and De Turck, F. (2010). Optimizing smart energy control strategies for plug-in hybrid electric vehicle charging. In *Network Operations and Management Symposium Workshops (NOMS Wksp), 2010 IEEE/IFIP*, pages 293–299. Ieee.
- [129] Meyer, J., Hahle, S., Schegner, P., and Wald, C. (2011). Impact of electrical car charging on unbalance in public low voltage grids. In *Electrical Power Quality and Utilisation (EPQU), 2011 11th International Conference on*, pages 1–6. IEEE.
- [130] Mohamed, Y.-R. and Radwan, A. A. (2011). Hierarchical control system for robust microgrid operation and seamless mode transfer in active distribution systems. *Smart Grid, IEEE Transactions on*, 2(2):352–362.
- [131] Mohsenian-Rad, A.-H. and Leon-Garcia, A. (2010). Optimal residential load control with price prediction in real-time electricity pricing environments. *Smart Grid, IEEE Transactions on*, 1(2):120–133.
- [132] Molderink, A., Bakker, V., Bosman, M. G., Hurink, J. L., and Smit, G. J. (2010). Management and control of domestic smart grid technology. *Smart grid, IEEE transactions on*, 1(2):109–119.
- [133] Moreau, L. (2005). Stability of multiagent systems with time-dependent communication links. *Automatic Control, IEEE Transactions on*, 50(2):169–182.
- [134] Murray, R. M. (2007). Recent research in cooperative control of multivehicle systems. *Journal of Dynamic Systems, Measurement, and Control*, 129(5):571–583.
- [135] Nedić, A. and Ozdaglar, A. (2009). Distributed subgradient methods for multi-agent optimization. *Automatic Control, IEEE Transactions on*, 54(1):48–61.
- [136] Nedić, A., Ozdaglar, A., Parrilo, P., et al. (2010). Constrained consensus and optimization in multi-agent networks. *Automatic Control, IEEE Transactions on*, 55(4):922–938.

- [137] Negenborn, R. R., De Schutter, B., and Hellendoorn, J. (2008). Multi-agent model predictive control for transportation networks: Serial versus parallel schemes. *Engineering Applications of Artificial Intelligence*, 21(3):353–366.
- [138] New, E. (2003). for electricity in europe—distributed generation: key issues, challenges and proposed solutions. *Luxembourg: Office for Official Publications of the European Communities*.
- [139] Ni, W. and Cheng, D. (2010). Leader-following consensus of multi-agent systems under fixed and switching topologies. *Systems & Control Letters*, 59(3):209–217.
- [140] Nick, M. (2014). São Paulo to introduce its first fleet of fully electric buses, available online at url: <http://cities-today.com/2014/01/sao-paulo-to-introduce-its-first-fleet-of-fully-electric-buses/>.
- [141] NREL (2013). available online at url: <https://pfs.nrel.gov/main.html>.
- [142] O’Connell, A., Flynn, D., Richardson, P., and Keane, A. (2012). Controlled charging of electric vehicles in residential distribution networks. In *Innovative Smart Grid Technologies (ISGT Europe), 2012 3rd IEEE PES International Conference and Exhibition on*, pages 1–7. IEEE.
- [143] Olariu, S. and Weigle, M. C. (2010). *Vehicular networks: from theory to practice*. CRC Press.
- [144] Olfati-Saber, R. (2006). Flocking for multi-agent dynamic systems: Algorithms and theory. *Automatic Control, IEEE Transactions on*, 51(3):401–420.
- [145] Olfati-Saber, R., Fax, A., and Murray, R. M. (2007). Consensus and cooperation in networked multi-agent systems. *Proceedings of the IEEE*, 95(1):215–233.
- [146] Ordonez-Hurtado, R., Griggs, W., Massow, K., and Shorten, R. (2013). Evaluation of a new intelligent speed advisory system using hardware-in-the-loop simulation. In *Connected Vehicles and Expo (ICCVE), 2013 International Conference on*, pages 945–946.
- [147] Ordóñez-Hurtado, R. H., Griggs, W. M., Massow, K., and Shorten, R. N. (2014). Intelligent speed advising based on cooperative traffic scenario determination. In *Optimization and Optimal Control in Automotive Systems*, pages 77–92. Springer.
- [148] Palensky, P. and Dietrich, D. (2011). Demand side management: Demand response, intelligent energy systems, and smart loads. *Industrial Informatics, IEEE Transactions on*, 7(3):381–388.
- [149] Parisio, A. and Glielmo, L. (2011). A mixed integer linear formulation for microgrid economic scheduling. In *Smart Grid Communications (SmartGridComm), 2011 IEEE International Conference on*, pages 505–510. IEEE.
- [150] Parisio, A. and Glielmo, L. (2013). Stochastic model predictive control for economic/environmental operation management of microgrids. In *Control Conference (ECC), 2013 European*, pages 2014–2019. IEEE.

- [151] Park, J., Kim, Y., Eom, I., and Lee, K. (1993). Economic load dispatch for piecewise quadratic cost function using hopfield neural network. *Power Systems, IEEE Transactions on*, 8(3):1030–1038.
- [152] Peacock, A. and Newborough, M. (2007). Controlling micro-chp systems to modulate electrical load profiles. *Energy*, 32(7):1093–1103.
- [153] Pieltain Fernández, L., Roman, T., Cossent, R., Domingo, C. M., and Frias, P. (2011). Assessment of the impact of plug-in electric vehicles on distribution networks. *Power Systems, IEEE Transactions on*, 26(1):206–213.
- [154] Pillay, P. and Manyage, M. (2001). Definitions of voltage unbalance. *IEEE Power Engineering Review*, 21(5):50–51.
- [155] PLX (2015). Obd-ii adaptor, available online at url: <http://www.plxdevices.com>.
- [156] Putrus, G., Suwanapingkarl, P., Johnston, D., Bentley, E., and Narayana, M. (2009). Impact of electric vehicles on power distribution networks. In *Vehicle Power and Propulsion Conference, 2009. VPPC'09. IEEE*, pages 827–831. IEEE.
- [157] Qian, K., Zhou, C., Allan, M., and Yuan, Y. (2011). Modeling of load demand due to ev battery charging in distribution systems. *Power Systems, IEEE Transactions on*, 26(2):802–810.
- [158] Ramchurn, S. D., Vytelingum, P., Rogers, A., and Jennings, N. (2011). Agent-based control for decentralised demand side management in the smart grid. In *The 10th International Conference on Autonomous Agents and Multiagent Systems-Volume 1*, pages 5–12. International Foundation for Autonomous Agents and Multiagent Systems.
- [159] Ramsay, C. and Aunedi, M. (2009). Characterisation of lsvpps. *Fenix project, Del. D*, 1.
- [160] Ren, W. (2007). Consensus strategies for cooperative control of vehicle formations. *Control Theory & Applications, IET*, 1(2):505–512.
- [161] Ren, W. and Atkins, E. (2007). Distributed multi-vehicle coordinated control via local information exchange. *International Journal of Robust and Nonlinear Control*, 17(10-11):1002–1033.
- [162] Ren, W., Beard, R. W., and Atkins, E. M. (2005). A survey of consensus problems in multi-agent coordination. In *American Control Conference, 2005. Proceedings of the 2005*, pages 1859–1864. IEEE.
- [163] Richardson, P., Flynn, D., and Keane, A. (2012a). Local versus centralized charging strategies for electric vehicles in low voltage distribution systems. *Smart Grid, IEEE Transactions on*, 3(2):1020–1028.
- [164] Richardson, P., Flynn, D., and Keane, A. (2012b). Optimal charging of electric vehicles in low-voltage distribution systems. *Power Systems, IEEE Transactions on*, 27(1):268–279.

- [165] SCE (2013). available online at url: http://www.sce.com/005_regul_info/eca/DOMSM11.DLP.
- [166] Schakel, W. J. and van Arem, B. (2014). Improving traffic flow efficiency by in-car advice on lane, speed, and headway. *Intelligent Transportation Systems, IEEE Transactions on*, 15(4):1597–1606.
- [167] Schlote, A., Häusler, F., Hecker, T., Bergmann, A., Crisostomi, E., Radusch, I., and Shorten, R. (2013). Cooperative regulation and trading of emissions using plug-in hybrid vehicles. *IEEE Transactions on Intelligent Transportation Systems*, 14(4):1572–1585.
- [168] Schoch, E., Kargl, F., Weber, M., and Leinmuller, T. (2008). Communication patterns in VANETs. *Communications Magazine, IEEE*, 46(11):119–125.
- [169] SEAI (2012). Time-varying electricity price, sustainable energy authority of ireland, available online at url: http://www.seai.ie/Renewables/Smart_Grids/The_Smart_Grid_for_the_Consumer/Home_Consumer/Smart_Meter/Time_varying_electricity_price/.
- [170] Shahnia, F., Ghosh, A., Ledwich, G., and Zare, F. (2011). Voltage unbalance sensitivity analysis of plug-in electric vehicles in distribution networks. In *Universities Power Engineering Conference (AUPEC), 2011 21st Australasian*, pages 1–6. IEEE.
- [171] Shao, S., Pipattanasomporn, M., and Rahman, S. (2009a). Challenges of phev penetration to the residential distribution network. In *Power & Energy Society General Meeting, 2009. PES'09. IEEE*, pages 1–8. IEEE.
- [172] Shao, S., Pipattanasomporn, M., and Rahman, S. (2009b). Challenges of phev penetration to the residential distribution network. In *Power & Energy Society General Meeting, 2009. PES'09. IEEE*, pages 1–8. IEEE.
- [173] Shi, W., Ling, Q., Yuan, K., Wu, G., and Yin, W. (2014). On the linear convergence of the admm in decentralized consensus optimization. *IEEE TRANSACTIONS ON SIGNAL PROCESSING*, 62(7).
- [174] Shi, W. and Wong, V. W. (2011). Real-time vehicle-to-grid control algorithm under price uncertainty. In *Smart Grid Communications (SmartGridComm), 2011 IEEE International Conference on*, pages 261–266. IEEE.
- [175] Shorten, R., Griggs, W., Ordonez-Hurtado, R., Wirth, F., Rufli, M., Zhuk, S., Gally, O., Verago, R., Nabi, Z., Lee, C., Cogill, R., and Tchrakian, T. (2014). Parked cars as a service delivery platform. in *Proceedings of the 3rd International Conference on Connected Vehicles and Expo (ICCVE)*.
- [176] Shorten, R., King, C., Wirth, F., and Leith, D. (2007). Modelling tcp congestion control dynamics in drop-tail environments. *Automatica*, 43(3):441–449.
- [177] Shorten, R., Leith, D. J., Foy, J., and Kilduff, R. (2005). Analysis and design of aimd congestion control algorithms in communication networks. *Automatica*, 41(4):725–730.
- [178] Shorten, R., Wirth, F., and Leith, D. (2006). A positive systems model of tcp-like congestion control: asymptotic results. *Networking, IEEE/ACM Transactions on*, 14(3):616–629.

- [179] Shorten, R. N. and Leith, D. J. (2007). On queue provisioning, network efficiency and the transmission control protocol. *IEEE/ACM Transactions on Networking (TON)*, 15(4):866–877.
- [180] Sicilia, M. and Keppler, J. (2010). Projected costs of generating electricity. *International Energy Agency, Paris*.
- [181] Singh, B., Saha, R., Chandra, A., and Al-Haddad, K. (2009). Static synchronous compensators (statcom): a review. *Power Electronics, IET*, 2(4):297–324.
- [182] Sortomme, E. and El-Sharkawi, M. A. (2011). Optimal charging strategies for unidirectional vehicle-to-grid. *Smart Grid, IEEE Transactions on*, 2(1):131–138.
- [183] Sortomme, E. and El-Sharkawi, M. A. (2012). Optimal scheduling of vehicle-to-grid energy and ancillary services. *Smart Grid, IEEE Transactions on*, 3(1):351–359.
- [184] Sortomme, E., Hindi, M. M., MacPherson, S. J., and Venkata, S. (2011). Coordinated charging of plug-in hybrid electric vehicles to minimize distribution system losses. *Smart Grid, IEEE Transactions on*, 2(1):198–205.
- [185] Soto-Sanchez, D. E. and Green, T. C. (2001). Voltage balance and control in a multi-level unified power flow controller. *Power Delivery, IEEE Transactions on*, 16(4):732–738.
- [186] Srikant, R. (2004). *The mathematics of Internet congestion control*. Springer Science & Business Media.
- [187] Stanojević, R. (2007). *Router-based algorithms for improving internet quality of service*. PhD thesis, National University of Ireland Maynooth.
- [188] Stanojevic, R. and Shorten, R. (2009). Load balancing vs. distributed rate limiting: an unifying framework for cloud control. In *Communications, 2009. ICC'09. IEEE International Conference on*, pages 1–6. IEEE.
- [189] Stüdli, S., Crisostomi, E., Middleton, R., and Shorten, R. (2012). A flexible distributed framework for realising electric and plug-in hybrid vehicle charging policies. *International Journal of Control*, 85(8):1130–1145.
- [190] Stüdli, S., Crisostomi, E., Middleton, R., and Shorten, R. (2014). Optimal real-time distributed v2g and g2v management of electric vehicles. *International Journal of Control*, 87(6):1153–1162.
- [191] Stüdli, S., Griggs, W., Crisostomi, E., and Shorten, R. (2014). On optimality criteria for reverse charging of electric vehicles. *Intelligent Transportation Systems, IEEE Transactions on*, 15(1):451–456.
- [192] Stüdli, S., Middleton, R., and Braslavsky, J. (2013). A fixed-structure automation for load management of electric vehicles. In *Control Conference (ECC), 2013 European*, pages 3566–3571.
- [193] Su, W., Eichi, H., Zeng, W., and Chow, M.-Y. (2012). A survey on the electrification of transportation in a smart grid environment. *Industrial Informatics, IEEE Transactions on*, 8(1):1–10.

- [194] Su, W., Wang, J., and Roh, J. (2014). Stochastic energy scheduling in microgrids with intermittent renewable energy resources. *Smart Grid, IEEE Transactions on*, 5(4):1876–1883.
- [195] Sun, Y. G., Wang, L., and Xie, G. (2008). Average consensus in networks of dynamic agents with switching topologies and multiple time-varying delays. *Systems & Control Letters*, 57(2):175–183.
- [196] Sundström, O. and Binding, C. (2010). Optimization methods to plan the charging of electric vehicle fleets. In *Proceedings of the International Conference on Control, Communication and Power Engineering*, pages 28–29.
- [197] Sundstrom, O. and Binding, C. (2012). Flexible charging optimization for electric vehicles considering distribution grid constraints. *Smart Grid, IEEE Transactions on*, 3(1):26–37.
- [198] Swaroop, D. and Hedrick, J. (1996). String stability of interconnected systems. *Automatic Control, IEEE Transactions on*, 41(3):349–357.
- [199] Takagi, M., Yamaji, K., and Yamamoto, H. (2009). Power system stabilization by charging power management of plug-in hybrid electric vehicles with lfc signal. In *Vehicle Power and Propulsion Conference, 2009. VPPC'09. IEEE*, pages 822–826. IEEE.
- [200] Taylor, J., Maitra, A., Alexander, M., Brooks, D., and Duvall, M. (2010). Evaluations of plug-in electric vehicle distribution system impacts. In *Power and Energy Society General Meeting, 2010 IEEE*, pages 1–6. IEEE.
- [201] Tomić, J. and Kempton, W. (2007). Using fleets of electric-drive vehicles for grid support. *Journal of Power Sources*, 168(2):459–468.
- [202] Tradisauskas, N., Juhl, J., Lahrmann, H., and Jensen, C. S. (2009). Map matching for intelligent speed adaptation. *Intelligent Transport Systems, IET*, 3(1):57–66.
- [203] Tyagi, V., Kalyanaraman, S., and Krishnapuram, R. (2012). Vehicular traffic density state estimation based on cumulative road acoustics. *Intelligent Transportation Systems, IEEE Transactions on*, 13(3):1156–1166.
- [204] Van Haaren, R. (2011). Assessment of electric cars' range requirements and usage patterns based on driving behavior recorded in the national household travel survey of 2009. In *A Study conducted as part of the Solar Journey USA project*.
- [205] Varga, A. et al. (2001). The omnet++ discrete event simulation system. In *Proceedings of the European simulation multiconference (ESM'2001)*. sn.
- [206] Venayagamoorthy, G. K. and Mitra, P. (2011). Smartpark shock absorbers for wind farms. *Energy Conversion, IEEE Transactions on*, 26(3):990–992.
- [207] Venkatesh, P., Gnanadass, R., and Padhy, N. P. (2003). Comparison and application of evolutionary programming techniques to combined economic emission dispatch with line flow constraints. *Power Systems, IEEE Transactions on*, 18(2):688–697.

- [208] Verzijlbergh, R., Lukszo, Z., and Ilic, M. (2012). Comparing different ev charging strategies in liberalized power systems. In *European Energy Market (EEM), 2012 9th International Conference on the*, pages 1–8. IEEE.
- [209] Wang, F.-Y. (2010). Parallel control and management for intelligent transportation systems: Concepts, architectures, and applications. *Intelligent Transportation Systems, IEEE Transactions on*, 11(3):630–638.
- [210] Wen, C.-K., Chen, J.-C., Teng, J.-H., and Ting, P. (2012). Decentralized plug-in electric vehicle charging selection algorithm in power systems. *Smart Grid, IEEE Transactions on*, 3(4):1779–1789.
- [211] White, C. D. and Zhang, K. M. (2011). Using vehicle-to-grid technology for frequency regulation and peak-load reduction. *Journal of Power Sources*, 196(8):3972–3980.
- [212] Wirth, F., Stanojevic, R., Shorten, R., and Leith, D. (2006). Stochastic equilibria of aimed communication networks. *SIAM Journal on Matrix Analysis and Applications*, 28(3):703–723.
- [213] Wu, C., Mohsenian-Rad, H., and Huang, J. (2012). Vehicle-to-aggregator interaction game. *Smart Grid, IEEE Transactions on*, 3(1):434–442.
- [214] Xiao, F. and Wang, L. (2008). Asynchronous consensus in continuous-time multi-agent systems with switching topology and time-varying delays. *Automatic Control, IEEE Transactions on*, 53(8):1804–1816.
- [215] Xin, H., Lu, Z., Qu, Z., Gan, D., and Qi, D. (2011). Cooperative control strategy for multiple photovoltaic generators in distribution networks. *Control Theory & Applications, IET*, 5(14):1617–1629.
- [216] Yan, G., Olariu, S., and Weigle, M. C. (2008). Providing VANET security through active position detection. *Computer Communications*, 31(12):2883–2897.
- [217] Yan, Y., Qian, Y., Sharif, H., and Tipper, D. (2013). A survey on smart grid communication infrastructures: Motivations, requirements and challenges. *Communications Surveys & Tutorials, IEEE*, 15(1):5–20.
- [218] Yang, Y. R. and Lam, S. S. (2000). General aimed congestion control. In *Network Protocols, 2000. Proceedings. 2000 International Conference on*, pages 187–198. IEEE.
- [219] Zhang, P., Qian, K., Zhou, C., Stewart, B. G., and Hepburn, D. M. (2012). Demand response for optimisation of power systems demand due to ev charging load. In *Power and Energy Engineering Conference (APPEEC), 2012 Asia-Pacific*, pages 1–4. IEEE.
- [220] Zhang, Z. and Chow, M.-Y. (2012). Convergence analysis of the incremental cost consensus algorithm under different communication network topologies in a smart grid. *Power Systems, IEEE Transactions on*, 27(4):1761–1768.